Speleothem Climate Capture – A Holocene Reconstruction of Northern Iberian Climate and Environmental Change

Andrew Christopher Smith

Lancaster Environment Centre

Lancaster University

April 2014

This thesis is submitted in partial fulfilment of the requirements for the degree of Doctor of Philosophy

ProQuest LLC.
789 East Eisenhower Parkway
P.O. Box 1346
Ann Arbor, MI 48106 – 1346

ABSTRACT

An extensive 4 year cave monitoring program has been undertaken at Asiul Cave, a previously unstudied site in Cantabria (Spain). Monitoring indicates that speleothem forming drip waters are sourced from winter rainfall and that the isotopic composition of these waters is influenced by the amount of rainfall. Modern carbonate deposits accurately preserve the isotopic composition of the karst water from which they have formed, indicating that older speleothem deposits should be ideal for the reconstruction of palaeoclimatic conditions, including importantly palaeorainfall amount reconstruction. Two speleothem samples were therefore removed from the cave and analysed for a suite of geochemical proxies. Coeval oxygen isotope records from Asiul Cave indicate that northern Iberia has experienced considerable deviations in rainfall during the last 12,500 years. These high resolution records are strongly coupled with changes in other regionally important climate archives, helping to add to our understanding of northern Iberian climate evolution. The Asiul speleothem records however, go beyond explaining local changes in environmental conditions by exhibiting a strong coupling between atmospheric conditions, in the form of the North Atlantic Oscillation (NAO) and North Atlantic Ocean circulation. These speleothem archives indicate that the NAO controls not only the positioning of atmospheric storm tracks throughout Europe; but through interactions with the surface layer of the ocean can cause major changes in oceanic circulation. These NAO controlled changes in North Atlantic Ocean circulation have been shown to cause significant cooling within the northern North Atlantic and the southerly transport of ice rafted debris, with a millennial periodicity of ~1500 years. The Asiul cave speleothem record is one of the first convincing archives of a millennial scale NAO system which has the capacity to force changes in oceanic circulation. These speleothems also act to extend existing archives of the NAO back into the Younger Dryas; by doing so the Asiul records challenge our current understanding of NAO dynamics and the exact timing of initial NAO development.

LIST OF CONTENTS

LIST OF FIGURES

LIST OF TABLES

ACKNOWLEDGMENTS

I would like to extend my thanks to a great number of people who have helped and supported me throughout this project.

Firstly, I would like to thank my supervisors at Lancaster University: Peter Wynn for his suggestion that I apply for the project and his continued support and encouragement during the last three and a half years and Philip Barker for his guidance, which has always kept the project moving forwards. Without both of you this experience would not have been so enjoyable. Additionally, I would like to thank Andy Stott and the Centre for Ecology and Hydrology (CEH) for the analytical support they have provided.

My great thanks must also go to Melanie Leng my CASE supervisor at the British Geological Survey (BGS) and to Steve Noble, who has undertaken all of the U/Th analysis. Your support and dedication within all aspects of the analytical work has advanced this project beyond where we first thought possible and the personal encouragement I have received has ensured that I always enjoyed my visits to Keyworth. I would also like to extend my thanks to many other members of the BGS staff who have helped this project develop including: Hilary Sloane, Carol Arrowsmith, Tim Heaton and Beatrice Bullock von Moos.

Alongside the academic support I have received, I would like to thank all those who have been involved in fieldwork associated with this project. Without the support and guidance of the Matienzo Caves Expedition team including Juan Corrin, Peter Smith and Andy Quin the project would not have got started; Pete's continued dedication to cave and climate monitoring in valley has led to the production of some fantastic cave monitoring records. My time spent in Matienzo has made me understand why so many people are drawn back to this place each year; I can only hope that this work has helped to further our understanding of the Matienzo valley and its caves.

On a more personal note, I would like to thank my parents and my friends, who have as always been there to offer me guidance and support. I am especially grateful to Hulda, without whom the last three and a half years would not have been as enjoyable.

Finally, my gratitude is expressed to the Cantabrian government for permission to work within the Matienzo Valley and to the Natural Environment Research Council for financial support through the funding of a British Geological Survey CASE award and a NERC Isotope Geosciences Facilities Steering Committee (NIGFSC) grant.

1. INTRODUCTION AND AIMS

1.1 Introduction

The accurate prediction and effective mitigation of modern climate change relies upon a robust understanding of global climate systems and how they operate. Of greatest importance when trying to contextualise modern climatic change is to understand our most recent history. For this reason, the Holocene is a critical period of time where climatic amelioration in many regions has led to favourable changes in environmental conditions and the rapid expansion of human populations. However, to fully understand Holocene climate more records of natural climate change are required, especially those which aim to expand our understanding with regards to the long term interconnectivity between components of the climate system.

Of particular interest is the interaction between the Earth's atmosphere and the global oceans. These two systems are fundamental to the regulation of our current climate, acting to store and transfer energy around the globe. Current palaeorecords from the North Atlantic region have identified that important natural cycles of ocean warming and cooling are often coupled to changes in terrestrial moisture availability, with a pacing of 1500 ± 500 years (O'Brien et al., 1995, Bond et al., 1997, Björk et al., 2006). Coupled changes in the climate system have been linked to atmospheric restructuring (Moros et al., 2004, Giraudeau et al., 2010), solar cycles (Bond et al., 2001, Morley et al., 2011, Sejrup et al., 2012) and changes in North Atlantic Ocean circulation (Debret et al., 2007, Thornalley et al., 2009, Sorrel et al., 2012). Whilst numerous theories have been put forward, no coherent explanation currently exists as to why Europe has been dominated by climate cycles with a 1500 year periodicity throughout the Holocene.

To understand the mechanisms which may drive the Holocene 1500 year climate cycle, palaeoclimate archives must originate from regions sensitive to both oceanic and atmospheric systems. One such region is Northern Spain. The northern Iberian coastline lies within an atmospheric and geographic boundary in the centre of Europe and is therefore sensitive to fluctuations in both atmospheric moisture delivery and changing oceanic conditions (Allen et al., 1996, Pena et al., 2010). To date, terrestrial records from this region have been predominately based upon near shore ocean (Pena et al., 2010, Mojtahid et al., 2013) and lake sediment cores (Morellón et al., 2009, Morellón et al., 2012). However, these archives are occasionally interrupted by human development and few provide complete

records of climate and environmental evolution throughout the Holocene. To combat the problem of human interference and to increase the resolution of existing climate records, more work is required using cave speleothems which act as proxies of past environmental conditions (Stoll et al., 2013, Martinez-Pillado et al., 2014).

Under ideal conditions, speleothems are known to offer rapidly depositing, long duration archives of climate and environmental change through the incorporation of trace element and stable isotope chemistry into the carbonate crystal lattice (McDermott 2004). Speleothem chemistry is ultimately derived from incoming rainfall, soil and vegetation processes and bedrock weathering; by analysing changes to this chemistry we can start to develop an understanding about how environmental conditions have evolved (Fairchild and Baker 2012). Whilst speleothems offer a real alternative to more traditional, often interrupted palaeoclimate archives, it is now well established that *all* cave and speleothem systems operate differently, and therefore require detailed monitoring, before speleothem samples are analysed for palaeoclimatic proxies.

Changes in karst water availability (Baker et al., 1997), speleothem drip water chemistry (Fairchild et al., 2006, Miorandi et al., 2010) and cave carbon dioxide concentrations (Spötl et al., 2005) can all regulate speleothem development and the incorporation of chemical proxies. Therefore modern studies which use speleothems for palaeoclimate reconstruction should first aim to robustly characterise the cave environment; ensuring that ancient carbonate chemistry is interpreted in an appropriate, site specific manner. However, the interpretation of old carbonates based on modern growth conditions relies on the assumption that the driving forces behind speleothem development and elemental or isotopic incorporation into carbonate remain stable over long time periods.

The following thesis presents the findings of climatic reconstruction using speleothem deposits form a previously unstudied cave site in Northern Iberia. The goal of this work has been to further our understanding about cave systems through intensive monitoring and to search for an answer as to how oceanic and atmospheric systems have become so closely coupled during the Holocene.

1.2 Research Aims

Therefore the aims of this PhD thesis are:

1. To set up and undertake high resolution cave monitoring to assess modern karst, cave and speleothem systems; enabling the accurate interpretation of chemical records from ancient carbonate deposits found in Asiul Cave (N. Spain).

2. To use Holocene duration speleothem records to identify and characterise regionally important periods of climatic or environmental change.

3. To link changes in local climate to the global climate system, helping to further our understanding of atmospheric and oceanic coupling throughout the Holocene.

The following thesis is therefore split into two sections, preceeded by a literature review and short methodology. The first section deals with aim one; within this, two chapters present the results and discussion surrounding four years of high resolution cave monitoring in Asiul Cave (N. Spain). The first chapter deals with cave and karst hydrology, whilst the second focusses on cave atmospherics. Both chapters aim to characterise modern cave conditions and speleothem growth dynamics. This section of the thesis therefore acts to produce a modern analogue from which ancient speleothem carbonate can be interpreted.

The second section of the thesis is broken down into two further chapters. The first acts as a results section, presenting in-depth trace element and stable isotope data from two coeval, Holocene duration speleothem deposits. The second chapter draws upon our understanding of speleothem development in Asiul Cave, to produce palaeoclimate records of local and global change. These archives are then compared to previously published palaeoclimate records for validation. Speleothem archives from this cave system offer evidence of millennial scale climatic cycles which have persisted throughout the Younger Dryas (YD) and Holocene. These cycles are derived from changes in the global atmospheric system and show a close connectivity with periods of oceanic cooling (Bond et al., 1997). Speleothem archives from Asiul identify for the first time a solely atmospheric control over North Atlantic Ocean temperature and circulation patterns which extends throughout the YD and Holocene.

2. LITERATURE REVIEW

2.1 From Climate to Calcite

Cave speleothems contain isotopic and trace element signatures related to external climate. This overview section outlines the basic processes by which external climate signals are encapsulated (Figure 2.1).

Regional rainfall contains chemical signatures related to the source and trajectory of the parent air mass and the amount of rainfall. Upon deposition, this rainfall infiltrates into the soil zone and acquires carbon dioxide generated by microbial respiration (Equation 2.1).

$$H_2O + CO_2 \longrightarrow H_2CO_3 \qquad (2.1)$$

The acquisition of soil CO_2 produces a weak carbonic acid. This solution also acts to leach trace elements, and transport small particulates out of the soil.

Carbonic acid dissolves the underlying karst bedrock, producing a solution supersaturated in carbonate (Equation 2.2). This solution is loaded with chemical signatures acquired from rainfall, soil and bedrock impurities.

$$H_2CO_3(l) + CaCO_3(s) \longrightarrow Ca^{2+}(aq) + 2HCO_{3^-}(aq) \qquad (2.2)$$

Upon entering the cave environment carbon dioxide from this solution is lost by degassing, to the cave atmosphere. This process forces carbonate out of solution; forming a solid precipitate (speleothem) on the cave walls and floor (Equation 2.3).

$$Ca(aq) + 2HCO_3(aq) \longrightarrow CaCO_3(s) + CO_2(g) + H_2O(l) \qquad (2.3)$$

During the growth of speleothems, chemicals dissolved in the parent solution can be preferentially included or excluded from the crystal lattice. The speleothem chemical record therefore reflects a combination of chemical signals acquired from: rainfall, soil, bedrock, carbon dioxide outgassing and crystal filtering.

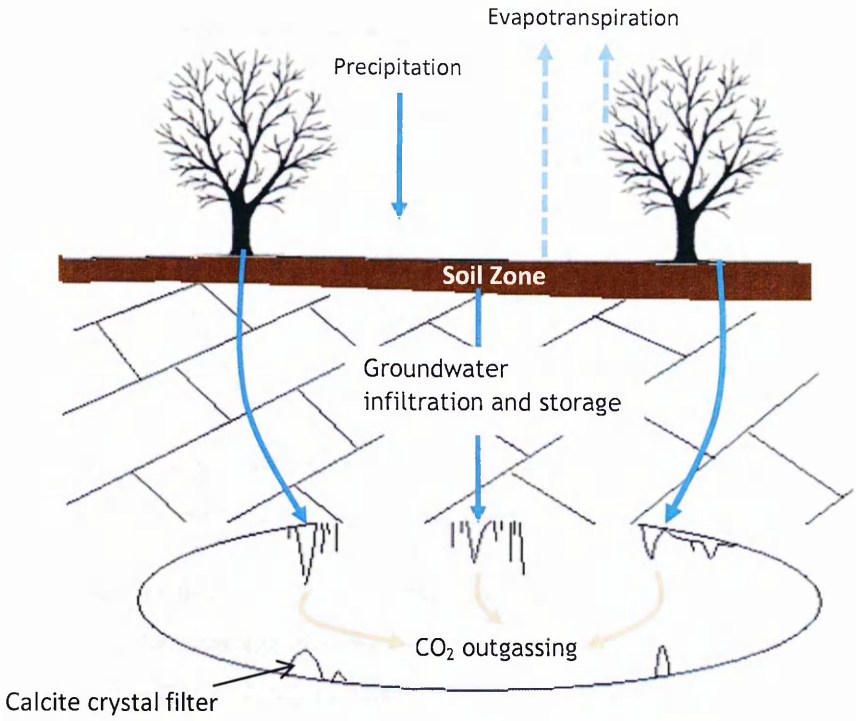

Figure 2.1: Mechanisms of climate signal transfer into speleothem calcite.

This composite signal can be deconvolved to produce records of atmospheric processes, soil and biogeochemical cycling, rock water contact, aquifer hydrology, in cave processes and crystal dominated patterns. Speleothems therefore offer high resolution palaeorecords of numerous processes, including karst and cave evolution, vegetation succession and climate change.

Due to uncertainty surrounding modern climate change and the role humans are playing in changing our environment, high resolution archives of natural climatic change are becoming increasingly important to facilitate the quantification of modern anthropogenic climate change. Records from our current interstadial, the Holocene are arguably of highest importance for understanding the impacts of human evolution and dissociating anthropogenic forcing from natural climatic perturbations. Speleothem records from climatically sensitive locations have an important role to play in the reconstruction of past climates, interpretation of modern change and steps toward successful climate change mitigation.

2.2 Cave Systems as Repositories of Climatic Change

Cave systems develop in karst environments, predominantly through the dissolution of limestone bedrock (Ford and Williams, 2007, White 1988, Frisia and Borsato, 2010, Li et al., 2008, Baldini et al., 2006a). Over long time scales many caves offer stable environments, ideal for the development and protection of palaeoclimate archives (Fairchild et al., 2007). Calcite deposits (speleothems) are the most commonly utilised climate archive from cave systems. Speleothems offer archives of atmospheric processes (Baker et al., 2010), soil and biogeochemical cycling (Rudzka et al., 2011), rock water contact (Dominguez-Villar et al., 2008), aquifer hydrology (Fairchild et al., 2006b), in cave processes (Fairchild et al., 2006a) and speleothem specific crystallographic effects (Frisia et al., 2000).

Chemical signatures from climatic parameters, predominately rainfall and temperature, are modified during their passage into the cave environment, eventually becoming archived in speleothem calcite (Figure 2.2) (Fairchild et al., 2006a, Carrasco et al., 2006).

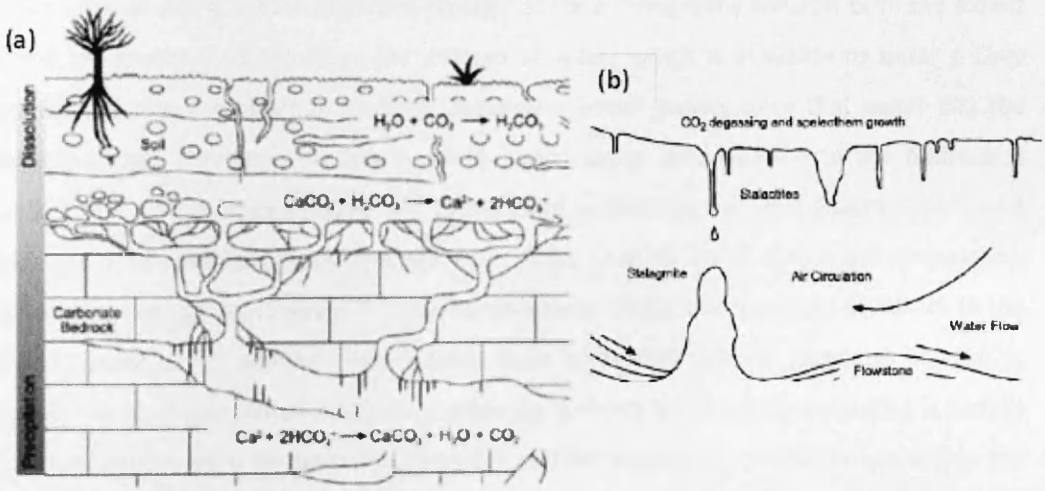

Figure 2.2: (a) the karst and cave system, highlighting zones of dissolution and precipitation of calcium carbonate bedrock. (b) expanded view of speleothem formation (Fairchild et al., 2006a).

The speleothem chemical signal can then be deconvolved to produce high resolution palaeorecords of numerous processes, including karst and cave evolution, vegetation succession and climate change (McDermott 2004).

2.2.1 Karst Weathering

The initial stage of karst (solution) weathering is the dissolution of carbon dioxide (CO_2) in water as it infiltrates through overlying soil (Equation 2.1) (Frisia et al., 2011, Fairchild et al., 2007, Frisia and Borsato, 2010). Vegetation and microbial respiration elevate soil air CO_2 concentrations above atmospheric values, producing a concentrated carbonic acid (Tooth and Fairchild, 2003, Proctor et al., 2002, Lange et al., 2010, Li et al., 2008). This acidic solution percolates through the soil and dissolves underlying calcium carbonate bedrock (Equation 2.2), the zone of most intense bedrock weathering is known as the epikarst (Bradley et al., 2010, Fairchild et al., 2006a). The barrier formed between the epikarst and the less porous bedrock often acts to retard water penetration forming extensive epikarst aquifers (Lange et al., 2010, Fairchild et al., 2006a, Bauer et al., 2005).

2.2.2 Hydrological Pathways

The rainwater catchment which actively recharges any given cave site is denoted by surface topography as well as underlying karst geology. Surface topography controls both the extent of the catchment (and therefore the amount of water which is available to enter a cave system) but also the direction of water movement under gravity once that water hits the ground surface (Fairchild and Baker, 2012). Initial water percolation into the bedrock is controlled by pre-existing conditions in the soil and epikarst as well as the permeability and structure of the bedrock (Baker and Brunsdon, 2003, Li et al., 2008). Soil water evaporation and aquifer storage act to delay, or occasionally totally inhibit the transport of rainfall to the bedrock surface, de-coupling rainfall inputs from infiltration outputs (Baker et al., 1997a, Carrasco et al., 2006). When water does enter the bedrock it flows its flow routing is initially controlled by the tilt of the underlying bedrock and the positioning of weaknesses within this rock. Water movement within karst is thought to progress under any of three hydrological regimes, depending upon the size of conduit in which it is flowing (White, 2002, Smart and Friedrich, 1987). Under normal conditions an arboreal drainage system develops due to the gradual dissolution of the bedrock, with many smaller passages draining into fewer larger ones (Bauer et al., 2005, Fairchild and Baker, 2012).

1. True matrix flow occurs along the intergranular permeability of bedrock, dictated by the primary porosity of that bedrock. Water flows slowly and under extremely high pressures. For the majority of Mesozoic limestone including the Aptian limestone (112-124 Ma) found in the Matienzo region (Quin 2010), primary porosity is low (1 -

5%) (Fairchild and Baker, 2012), meaning that only minimal amounts of water percolation occurs through this intergranular network.

Due to the relatively minimal hydrological contribution from intergranular matrix flow in limestone's the karst literature has often been used the term matrix flow to describe water movement in micro fractures (Smart and Friedrich 1987, Fairchild and Baker, 2012). To follow convention within karst literature this study will also use the term matrix flow to describe water flow through micro fractures, in what is normally through of as a continuously permeable membrane (Fairchild and Baker, 2012). Water flow through this membrane is often forced through a piston flow, where water entering the top of the matrix system displaces water from the base of the system, often in caves at speleothem drip sites. Matrix flow drip sites are classified by Smart and Friedrich (1987) as having a low coefficient of variation in speleothem drip rate, due to consistently low discharge.

2. Fracture flow is faster, occurring through two dimensional discontinuities (joints and faults) (Fairchild and Baker, 2012). Water exploits previously weathered sections of the matrix system (micro fractures), continuously enlarging vertical joints and horizontal bedding planes (Miorandi et al., 2010).
3. Conduit flow encompasses the largest underground passages usually referring to one dimensional channels (Fairchild and Baker, 2012); discharge varies dramatically in response to changing rainfall (Smart and Friedrich, 1987). Conduit drip sites have a high coefficient of variation in drip rates due to their intermittent and often high discharge (Smart and Friedrich, 1987). Large conduits act as overflow mechanisms when both matrix and fracture flow systems become fully saturated (Miorandi et al., 2010, Pronk et al., 2009, Williams 2008, Lange et al., 2010).

Theoretically, these hydrological systems interact to produce site specific hydrology. Piston driven flow of water in the matrix system often acts as a primary (continuous) mechanism for water movement; flow in fractures and conduits occurs only under wetter conditions (as a piston overflow system), when the matrix flow system is fully saturated. In reality, the complex nature of karst makes water flow pathways difficult to predict (Baker and Brunsdon, 2003). Cave drip sites may source water from several flow regimes or different regimes at different times, dependent upon hydrological conditions (Miorandi et al., 2010, Fairchild and Treble, 2009, Rudzka et al., 2011, Ayalon et al., 1998, Bradley et al., 2010).

During dry periods the karst often has open air spaces which enable carbonate to deposit before entering the cave system. These within karst processes can dramatically alter the chemical signatures of resultant cave speleothems and must be monitored before speleothem based palaeoclimate reconstructions.

2.2.3 Karst Calcite – Water Interactions

2.2.3.1 Prior Calcite Precipitation

Prior calcite precipitation (PCP) is the deposition of calcite within the karst zone above a cave site. This process removes Ca2+ ions leaving the remaining solution comparatively enriched in other elements (Palmer, 2010, Baker et al., 2000, Moreno et al., 2010, Fairchild and Treble, 2009). The PCP process can override other factors affecting chemical concentration in speleothem calcite, meaning periods of PCP can be easily identified by the co-variation of several "tracer" chemical components, predominantly trace elements and isotopes (Hellstrom and McCulloch, 2000). The positive co-variation of Mg and Sr for example is associated with PCP and indicative of dry phases in the overlying karst (McDonald et al., 2007, McMillan et al., 2005, Cruz et al., 2007).

2.2.3.2 Incongruent Calcite Dissolution

Incongruent calcite dissolution (ICD) is the release of minor trace element ions (Mg and Sr for example) into solution at different proportions (relative to Ca) than those found in the host bedrock (Sinclair 2011). This process is most common when dissolution occurs from fresh surfaces. Sinclair (2011) describes two theoretical models for ICD, where fresh surface dissolution occurs.

1) The incongruent release of Mg and Sr ions at freshly exposed crystal surfaces, e.g. after fresh bedrock exposure. Under this scenario Mg and Sr are seen to be preferentially incorporated only from the most mobile section of the crystal lattice (≈10 lattice units deep). Mg and Sr incorporation is enhanced in relation to Ca when the fresh surface is exposed to carbonic acid of a low pCO_2 and only minimal levels of $CaCO_3$ dissolution occur (McGillen and Fairchild 2005).

2) Congruent dissolution of $CaCO_3$ into solution, followed by incongruent re-precipitation of $CaCO_3$ from solution. The makeup of new calcite formed from this solution is controlled by the partition coefficients for Sr and Mg. Under this model simulation no net $CaCO_3$ deposition occurs, which is in contrast to processes such as PCP.

ICD can therefore act to complicate the chemical signature of subsequent in cave speleothem deposits so must be considered as part of cave monitoring studies.

2.2.4 Physio-Chemical Properties of Karst Hydrology

Understanding karst hydrology is fundamental before selecting speleothems to accurately represent climatic variations on an annual to sub-annual scale (Miorandi et al., 2010, Genty and Deflandre, 1998, Fairchild et al., 2006b, Baker and Brunsdon, 2003). A robust suite of natural physical and chemical tracers are therefore needed to assess water interactions within the karst (Kluge et al., 2010). Techniques most commonly asses flow physiology and water chemistry at cave drip sites (Ayalon et al., 1998, Lange et al., 2010). Physio-chemical variations act as proxies identifying soil characteristics, bedrock weathering rates and flow regime (Baker et al., 2000, Palmer, 2010).

2.2.4.1 Electrical Conductivity

Electrical conductivity (EC) is a measure of dissolved solids and salts within solution (Genty and Deflandre 1998). In karst regions the major dissolved solid is carbonate (CO_3). Dry periods leave karst waters isolated, increasing rock-water contact time and promoting the dissolution of calcium carbonate bedrock (Lange et al., 2010). High levels of dissolved calcium carbonate are recorded as higher EC in drip waters (Fairchild et al., 2006b). Conversely, reductions in rock contact time during rapid water infiltration traditionally lead to lower EC values (Pronk et al., 2009, Miorandi et al., 2010).

However, increased rainfall can create a piston effect, discharging matrix flow water with a high solute load at the drip site (Fairchild et al., 2006a, Genty and Deflandre, 1998). This scenario results in high EC during times of high rainfall input (Genty and Deflandre 1998, Miorandi et al., 2010). As EC acts as a tracer for CO_3 loading in drip waters, further studies need to focus upon high resolution monitoring of drip water EC, both to help characterise when and why EC changes within the cave environment and to act as a proxy for speleothem growth potential. Alongside EC monitoring, speleothem drip rate logging and the use of oxygen and hydrogen isotopic analysis can help to clarify the provenance water emerging at drip sites (Ayalon et al., 1998).

2.2.4.2 Stable Isotopes and Trace Elements

Individual rainfall events have unique Oxygen ($\delta^{18}O$) and Deuterium ($\delta^{2}H$) isotopic signatures imprinted by evaporation and condensation processes occurring at their source (Clark and Fritz 1997, Carrasco et al., 2006). Combined $\delta^{18}O$ - ^{2}H signatures for a specific location gives

the Local Meteoric Water Line (LMWL) (Craig 1961). Cave drip waters which correlate with the annual LMWL are presumed to have a karst storage component of less than 1 year (Carrasco et al., 2006, Pape et al., 2010, Schwarz et al., 2009). Speleothems formed from these waters would still be appropriate to analyse at a very high, annual resolution (Ayalon et al., 1998, Bradley et al., 2010). Evaporation in the soil and epikarst can however, leave water entering the cave depleted in the lighter ^{16}O isotope and seemingly offset from the LMWL (Jex et al., 2010, McDermott et al., 1999). Comparison of LMWL to cave drip $\delta^{18}O$ - ^{2}H signatures should therefore only be undertaken at suitable, well monitored cave locations.

Trace elements in cave drip waters are sourced mainly from soil leaching, carbonate dissolution and calcite – water interactions and have numerous modes of deposition once they are transported into karst and cave environments (Figure 2.3) (Fairchild et al., 2010, Treble et al., 2003). For high concentrations of bedrock sourced elements to be observed in cave drip waters requires long rock – water contact and significant bedrock dissolution.

In contrast to elements which are sourced from bedrock weathering, colloidal elements (those attached to other particulates) can be transported more readily during high infiltration events along larger conduit systems (Huang et al., 2001, Baker et al., 2008). These elements are sourced from soil leaching and washing of normally dry conduits, limiting their transport to extremely active hydrological conditions (Fairchild et al., 2007). Spikes in colloidal element concentration are often seen during the first flush of winter rain through dry karst (Baker et al., 1999, Borsato et al., 2007).

Isotope and trace element sources, sinks and mechanisms of incorporation into speleothem calcium carbonate are discussed in detail in Sections 2.8, 2.10 and 2.11.

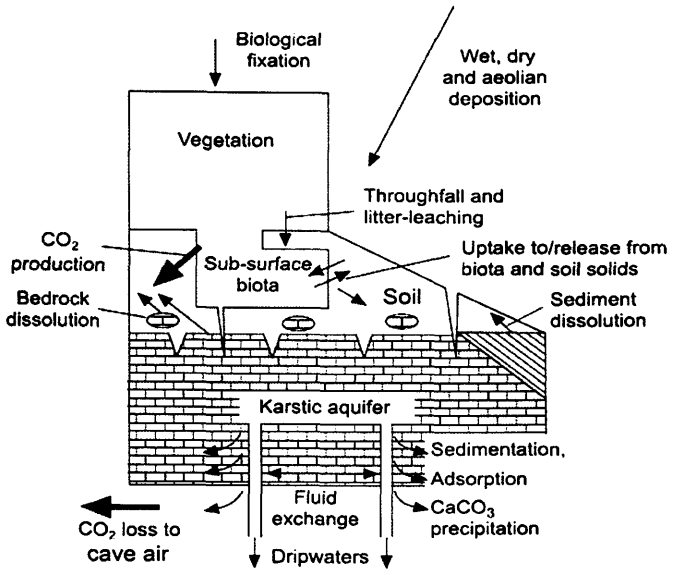

Figure 2.3: transport and deposition of trace elements within the cave and karst system (Fairchild and Treble 2009)

This section has shown that cave and karst environments can offer fantastic, stable locations for the acquisition of palaeoclimate archives, in the form of speleothems. However, the karst system can be a complex one acting to enhance, modify, delay or totally inhibit the transfer of chemical signatures from rainfall to calcite. For this reason detailed monitoring and quantification of the karst environment is essential before interpreting any speleothem record. Final modifications of the chemical signature in drip waters occur during speleothem deposition, making this just as important a process to understand and evaluate on a site specific basis.

However, whilst all cave sites have site specific controls over their hydrology and speleothem chemical uptake, some transfer of knowledge is possible if undertaken carefully. Not all cave sites can have a high level of monitoring, in these locations the interpretation of speleothem carbonate proxies must rely upon prior cave site studies. To ensure the most reliable interpretations similar sites must be considered in terms of geographical location, external rainfall patterns and amount, karst geology, bedrock depth, cave geometry and speleothem proxy being considered. If relatively close comparisons can be drawn between sites then tentative conclusions maybe made with regards to the interpretation of speleothem palaeoclimate proxies. The following cave monitoring study in Asiul only adds to the ever growing body of cave literature and may in the future be used to help interpret palaeoclimate records from similar cave locations.

2.3 Speleothem Formation

Speleothem formation occurs at locations where karst water emerges into air filled cave passages. High pCO_2 in the water degasses into the lower pCO_2 atmosphere of the cave void. The remaining solution becomes supersaturated in calcium carbonate, forcing the precipitation of solid $CaCO_3$ (Equation 2.3) (Frisia and Borsato, 2010). The speed of speleothem formation is therefore controlled by the rate of degassing, Ca^{2+} ion availability and water delivery to the drip site (Genty and Deflandre, 1998, Boch et al., 2011, Spötl et al., 2005, Dickinson et al., 2002).

2.3.1 Speleothem Growth Kinetics

In cave waters with a low supersaturation, the availability of Ca^{2+} ions limits the reaction rate, which progresses thermodynamically, close to equilibrium (Dickinson et al., 2002, Frisia et al., 2000). This is a slow, stable reaction which produces the majority of common speleothem crystal fabrics (Fairchild et al., 2006a). Under equilibrium conditions, chemical signatures from drip waters are directly imparted into speleothem deposits, any change in the chemical signature can be quantified under slow growth conditions (McDermott 2004, Hendy 1971, Kim and O'Neil 1997). Speleothems which develop in equilibrium are therefore ideal for the production of palaeoclimate records due to their preservation of chemical signatures directly linked to climate (Hendy 1971).

In high supersaturation waters, Ca^{2+} availability is not a limiting factor and the reaction is controlled by the rate of carbon dioxide degassing, and proceeds kinetically. Kinetic reactions describe those in which chemical exchange is incomplete before speleothem deposition occurs (Fairchild and Baker, 2012). Speleothems formed under kinetic conditions preserve a fractionated, or chemically manipulated archive of the original drip water chemistry (McDermott 2004). Analysis of these deposits for palaeoclimatic reconstruction is possible but should be viewed more cautiously due to the unpredictable chemical conditions in which the speleothem developed (McDermott 2004, Hendy 1971).

For solid $CaCO_3$ to "grow" a surface for crystal nucleation is required, the most common being cave walls, floors and existing speleothem deposits (Frisia and Borsato, 2010).

2.3.2 Crystal Fabrics

Although the formation of solid calcium carbonate is often portrayed as a relatively simple process (Equation 2.3), the morphology of growing $CaCO_3$ crystals is controlled by a variety

of factors (Onac 1997). Drip rate, temperature, saturation state and water film thickness all influence the rate and kinetics of CO_2 degassing which, in turn controls crystal formation, coalescence and ultimately speleothem morphology (Turgeon and Lundberg, 2001, Frisia et al., 2002, Frisia and Borsato, 2010, Ayalon et al., 1999, Gonzalez et al., 1993).

Under slow (equilibrium) conditions crystallite growth occurs in a number of steps from existing crystal faces, producing large, uniform columnar crystals (Frisia and Borsato, 2010, Kendall and Broughton, 1978, Gonzalez et al., 1993, Kendall, 1993). Under more rapid kinetic conditions crystallite formation becomes less regular, leading to the development of defect sites and variable growth orientations (Dickinson et al., 2002, Frisia et al., 2000). Crystal fabric identification is therefore critical to the interpretation of several chemical palaeoclimate proxies stored in speleothems, all of which rely upon an equilibrium growth mechanism (McDermott 2004, Frisia et al., 2000).

Speleothem formation is driven by the degassing of CO_2 from drip waters to the cave atmosphere. This reaction progresses either under equilibrium or kinetic conditions, each imparting different chemical signatures on the developing speleothem. Careful analysis of speleothem crystal structure can begin to unravel the often complex growth conditions of speleothem deposits. Trace elements incorporated into the crystal lattice offer a secondary, extremely high (sub-annual) resolution archive of changing hydrological and atmospheric conditions. The use of speleothems for palaeoclimatic reconstruction requires correct identification of growth kinetics to avoid incorrect interpretations of changing speleothem chemistry.

2.4 Speleothem Chemistry as an Archive of Climate Change

Accurate interpretation of speleothem deposits relies upon robust understanding of all the components which influence speleothem chemistry. This is often complex and occasionally impossible due to the extended timescales over which speleothems record climatic change and the complex nature of karst and cave systems. However, after careful analysis of modern climatic parameters, karst hydrology, cave atmospherics and speleothem crystal structure, ideal samples for palaeoclimatic analysis can be identified. If carefully selected, these speleothems can offer a diverse range of high resolution chemical palaeoclimatic proxies related to karst and cave evolution, vegetation succession and climate change.

As speleothems provide more long duration, high resolution records, it is important these can be supported by robust chronologies, over a wide range of time scales. Speleothem deposits incorporate trace amounts of uranium and can therefore be accurately dated using a U/Th decay technique, enabling the production of high resolution chronologies.

2.4.1 Dating Speleothems

Accurate dating of calcite is essential for comparison with other palaeoclimate records (Fairchild et al., 2006a, McDermott 2004, Boch et al., 2009, Drysdale et al., 2007, Spötl et al., 2010). The large range of ages associated with speleothem analysis and problems associated with "dead carbon", mean that ^{234}U isotope decay has become the conventional method for dating speleothem carbonate.

The decay of Uranium ^{234} into a stable element (Pb) has half lives ranging between 14 – 4.5 Gyr (van Calsteren and Thomas, 2006). This decay is made up from intermediate reactions, with half lives ranging between fractions of a second and hundreds of thousands of years (van Calsteren and Thomas, 2006, Zhao et al., 2009). It is the intermediate decay of ^{234}U to ^{230}Th which is used to date most speleothem studies, with a half life of 75.3ka (Fairchild et al., 2006a, St Pierre et al., 2009).

2.4.1.1 Uranium ^{234} - Thorium ^{230}

Speleothems normally have U concentrations between 0.05 and 0.5ppm, above the 0.01ppm required for analysis by mass spectrometry (Ford 1997). Depending upon the initial U content, this technique provides an absolute date, with minimal age uncertainties (0.5-2% of age). $^{234}U/^{230}Th$ dating requires an initial disequilibrium between parent (U) and daughter (Th) isotopes during carbonate deposition (Zhao et al., 2009, St Pierre et al., 2009).

Disequilibrium occurs due to differences in solubility of U and Th (Zhao et al., 2009). ^{234}U is soluble in water, leached from the soil zone and transported mainly as uranyl ions (UO^{22+}), while Th is insoluble and remains attached to soil particulates (Ford 1997, Fairchild et al., 2005, Ivanovich and Harmon, 1992).

Under closed system conditions ^{234}U, as UO^{22+} ions are incorporated during speleothem formation and decay into ^{230}Th, the decay ratio can then be used to establish the age of speleothem (Fairchild et al., 2007, Hellstrom, 2006). The technique is valid until calcite comes into secular equilibrium (activities of ^{234}U and ^{230}Th equalise), this takes about 7.5 half lives of ^{230}Th, extending the technique to just over 500ka (St Pierre et al., 2009). The decay of ^{234}U to ^{230}Th in modern samples is minimal, making the technique less accurate for "young" speleothems.

2.4.1.2 Non Radiogenic Thorium

The accuracy of U-Th dating is reduced if "non-radiogenic" or "initial" Th is deposited alongside Uranium, during speleothem formation (Zhao et al., 2009, Hellstrom, 2006). Initial Th is transported attached to clay particles, dust and other colloids (Fairchild et al., 2005, Ivanovich and Harmon 1992). If unaccounted for initial Th produces artificially old ages, when compared in ratio with ^{234}U (Ford 1997).

To overcome this inaccuracy ^{230}Th is compared with ^{232}Th which is transported and incorporated into speleothem calcite in the same mechanisms as ^{230}Th (Hellstrom 2006). ^{232}Th is therefore used as a proxy for initial levels of ^{230}Th in the speleothem. This value is subtracted from the total ^{230}Th to establish the amount of ^{230}Th produced solely from radiogenic decay. However, few calculations of the expected ratio of ^{230}Th to ^{232}Th within calcite have been undertaken (Figure 2.4) (Zhao et al., 2009).

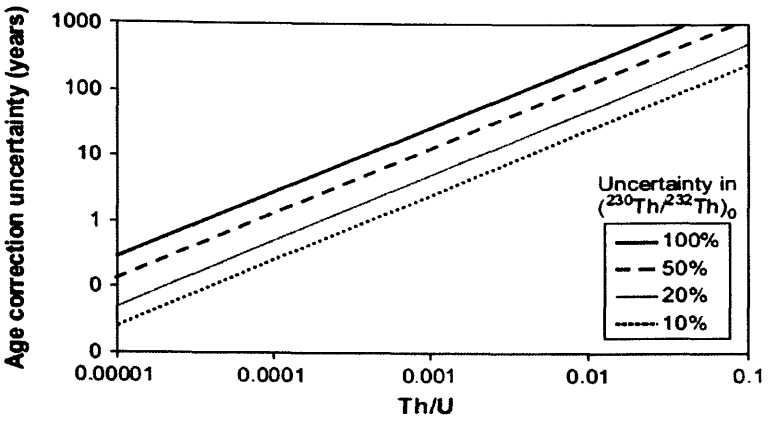

Figure 2.4: the relationship between the $^{232}Th/^{230}Th$ corrections and initial Th/U concentrations. As the initial Th/U concentration increases so does the error (in %) associated with correction (Zhao et al., 2009).

Often studies use the upper crust $^{230}Th/^{232}Th$ ratio (0.83 ± 50%) when analysing speleothem deposits, yielding corrected dates <30% younger than the original $^{234}U/^{230}Th$ dates. (St Pierre et al., 2009). For accurate dating, the purest calcite samples should be selected, comprising minimal levels of initial Thorium and high levels of Uranium (Zhao et al., 2009).

2.4.2 Speleothem Age Models

High resolution palaeoclimate analysis requires a high resolution chronology. ^{234}U / ^{230}Th analysis requires large volumes of sample (50-100mg) and is costly, making very high resolution dating impractical. A series of spaced ^{234}U / ^{230}Th dates can however, be interpolated to create an age model.

The simplest models are linear, inferring constant speleothem growth between fixed dates. More complex numerical models analyse fixed ^{234}U / ^{230}Th dates and their associated errors, to accurately account for hiatus's (breaks in growth) and changes to speleothem growth speed (Scholz and Hoffmann 2011). Speleothem layer counting can also be undertaken, counting visible layers between known dates reduces errors associated with varying growth rates on annual scales (Baker et al., 2008). A combination of techniques is often employed, resulting in extremely accurate speleothem chronologies, ideal for palaeoclimate reconstruction and comparison to instrumental data (Fairchild et al., 2007).

2.5 Trace Elements in Speleothems

As discussed in section 2.5, trace element concentration in speleothem carbonate is controlled by changing atmospheric inputs, soil physiology, karst hydrology, cave ventilation and uptake during crystal growth (Fairchild et al., 2006b, Fairchild et al., 2010, Roberts et al., 1999, Fairchild and Treble, 2009). The concentrations of different elements in a speleothem can therefore be used to interpret palaeo variations in each or all of these parameters (Fairchild and Treble, 2009). In this way, trace elements become a powerful palaeoclimate proxy when analysed alongside a robust speleothem chronology (Borsato et al., 2007).

2.5.1 Inputs into the Trace Element System

Rainfall acts as the initial source of trace elements within a cave site. However, over short time scales, trace elements concentrations in rainfall are relatively stable, and are often over shadowed by larger stores in the soil and karst (Fairchild and Treble, 2009). During dramatic environmental upheaval however, changes in prevailing wind directions and erosion zones can transport weathered trace elements such as Strontium (Sr) and Silica (Si) to cave sites (Goede et al., 1998, Hu et al., 2005, Fairchild and Treble, 2009, Bar-Matthews et al., 1999). Anthropogenic inputs of trace elements such as Sulphur (S) into the atmospheric system can also be stored in speleothem deposits, offering modern archives of anthropogenic pollution (Wynn et al., 2008, Wynn et al., 2010, Frisia et al., 2005).

2.5.1.1 Vegetation Controls

Alongside changes in rainfall trace element concentration, vegetation productivity and decay can control the concentration of elements such as Phosphorus (P) and in some locations Strontium (Sr) (Treble et al., 2003, van Beynen et al., 2008, Hellstrom and McCulloch, 2000). Increases in drip water and speleothem P concentration have been used to identify periods of enhanced rainfall and therefore vegetation productivity in Australia (Treble et al., 2003); P has also been seen to decrease during productive summer months, with a greater amount of soil P being incorporated into vegetation, leaving the soil zone depleted and reducing the amount P available for transport into the karst system. It is therefore clear that when considering the P system other proxies, for example those of rainfall amount may be valuable to ensure the correct interpretation of speleothem P archives. High vegetation productivity is known to increases soil CO_2 concentration, intensifying carbonic acid production, bedrock dissolution and through this process promoting the release of Sr for transport to speleothem growth sites (Hellstrom and McCulloch, 2000, van Beynen et al.,

2008). Concurrent changes to P and Sr may therefore indicate significant changes within the vegetation zone, especially linked to summer growth season productivity.

Vegetation decay is thought to release P into the soil zone, this process coupled with higher infiltration events can lead to an increase in P during autumn - winter season speleothem deposition (Borsato et al., 2007, Treble et al., 2003). Distinct peaks in the P record have been used in Ernesto Cave (Italy) to indicate the annual change between summer and winter hydrological regime (Borsato et al., 2007).

2.5.1.2 Soil Leaching and Karst Weathering

The soil and karst zones house the largest stores of trace elements available for transport to speleothem growth locations. Water infiltration rate influences the uptake, transport and deposition of these elements (Fairchild and Treble, 2009). Transport of trace elements occurs either in solution, or by colloids (Hartland et al., 2009, Hartland et al., 2011, Fairchild and Treble, 2009). During periods of water deficit, waters become stagnant, percolating slowly through the karst (McMillan et al., 2005). Slow percolation increases rock-water contact time, enhancing the dissolution of bedrock and the release of trace elements (Hellstrom and McCulloch, 2000).

Periods of water deficit and karst drying also act to enhance prior calcite precipitation (PCP) (Palmer 2010, Baker et al., 2000, Moreno et al., 2010, Fairchild and Treble, 2009). Speleothem records from arid periods are therefore relatively enriched in trace elements, both from enhanced weathering and intensification by PCP (McDonald et al., 2007, McMillan et al., 2005, Cruz et al., 2007). Covariation of elements such as Strontium, Silica, Magnesium and Barium in speleothem records is therefore used as an indicator of aridity.

Conversely, karst water excess reduces the above mentioned processes, limiting the transport of these elements to speleothem deposition sites. High water percolation rates often result in soil leaching and karst zone flushing, mobilising elements normally stored in these zones due to their low solubility (Hartland et al., 2012). Elements such as Yttrium (Y), Lead (Pb) and Copper (Cu) are transported by colloids, natural organic matter (NOM) or as salts. Many karst systems are dominated by an "autumnal flush", where high rainfall volumes rapidly infiltrate into the karst, flushing out minerals and organic matter stored during the drier summer season (Fairchild and Treble, 2009). Robust speleothem studies (Figure 2.5) have combined trace elements to produce a composite record of autumnal

flushing (Borsato et al., 2007). In some speleothems this hydrological record can be used as an annual marker, enabling accurate chronology development between known dates.

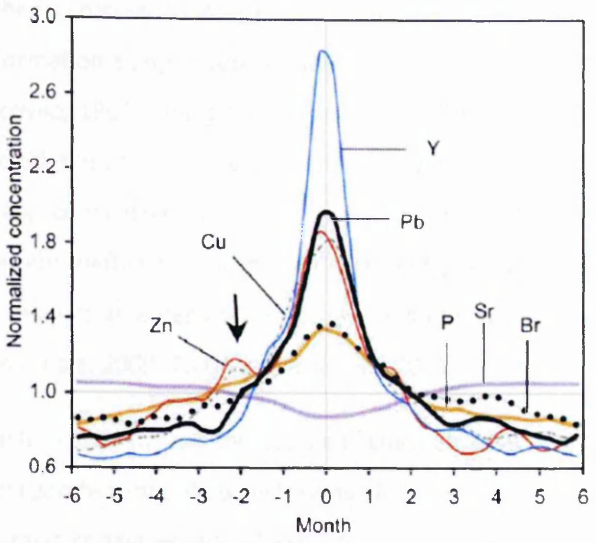

Figure 2.5: stack of average "annual" signal for 7 elements, showing a strong annual structure in Ernesto cave calcite (Borsato et al., 2007).

Trace elements can therefore offer both high resolution records of seasonal hydrology and longer term archives of vegetation and environmental change. However these records can become complicated during the incorporation of elements into the speleothem crystal lattice. The incorporation of any given element into a speleothem can be predicted using a known distribution coefficient (Fairchild and Treble, 2009, Fairchild et al., 2010).

2.5.2 The Distribution Coefficient

The majority of trace elements which are used for speleothem analysis are cations which substitute for Ca in the carbonate crystal structure (Fairchild and Treble, 2009, Fairchild et al., 2010). The concentration of trace elements within the crystal lattice therefore, depends upon a distribution coefficient (KTr) (Equation 2.4) (Fairchild and Treble, 2009).

$$(Tr/Ca_{CaCO3}) = K_{Tr} (Tr/Ca)_{solution} \quad (2.4)$$

Where Tr is the trace ion and K_{Tr} is the distribution coefficient.

K_{Tr} varies dependent upon the growth temperature, crystal morphology, growth mechanisms and speleothem precipitation rate (Fairchild and Treble, 2009, Fairchild et al., 2000).

2.5.2.1 *Factors Influencing the Distribution Coefficient*

The distribution coefficient and variations in drip water concentration make trace element storage in speleothems complex to interpret. The uptake of some elements, Mg for example, is influenced by formation temperature as well as elemental concentration (Fairchild and Treble, 2009, Gascoyne, 1983, Huang and Fairchild, 2001). Palaeothermometry using Mg/Ca concentration should therefore, be a possibility (Roberts et al., 1998). However, karst processes cause Mg concentrations to vary to a greater extent than the temperature dependent distribution coefficient. For this reason the Mg/Ca calcite ratio is more commonly representative of changes in water residence time and PCP within the karst (Roberts et al., 1999, Fairchild and Treble, 2009, Tooth and Fairchild, 2003).

Calcite crystal structure also controls the uptake of trace elements. Sodium (Na) and Chloride (Cl) are often incorporated into fluid inclusions (fluid filled voids) which develop during periods of interrupted crystal growth (Fairchild and Treble, 2009, Griffiths et al., 2010). Identified correlations between Na and Cl with other elements, transported by colloids, indicate that rapid infiltration events control the formation of fluid inclusions in the calcite lattice (Fairchild and Treble, 2009).

2.5.3 Trace Element Control on Speleothem Development

The incorporation of trace elements such as Sr and P can actively control the growth rate of speleothem crystals (Boch et al., 2011). However, in rapidly growing speleothems Sr incorporation is more likely controlled by crystal growth rates (Figure 2.6) (Fairchild and Treble 2009, Borsato et al., 2007, Huang et al., 2001). Huang et al., (2001) demonstrate that active sorption of P to calcite growth sites reduces speleothem growth rates. Sorption of P to calcite defect sites facilitates the incorporation of other ions, focusing trace element uptake at these sites (Fairchild and Treble 2009).

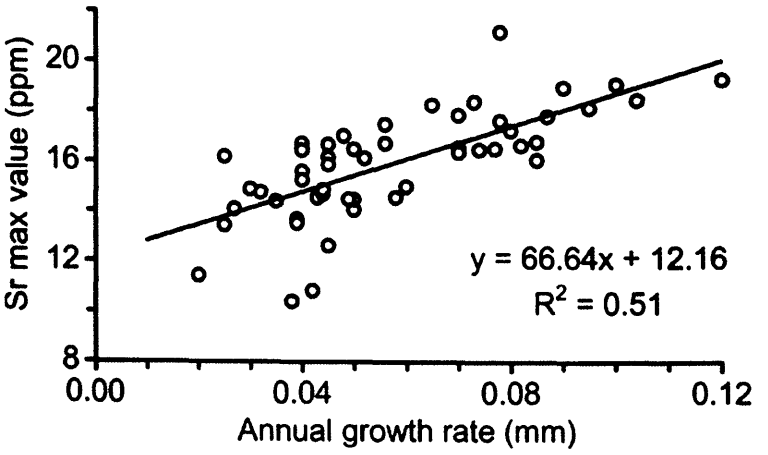

Figure 2.6: increasing Sr concentration with rapid speleothem growth rates (Borsato et al., 2007).

2.5.4 Atmospheric Particulates

The cave atmosphere can also act as a vector for trace element transport and deposition onto speleothem growth surfaces (Smith et al., 2013, Dredge et al., 2013). The mechanisms of incorporation and the concentrations of aerosol derived particulates in speleothems are not however, well understood. Aerosol particulates may well act in a similar manner to colloids, transporting trace elements to the site of speleothem deposition. Variations to cave ventilation regime and aerosol production within cave systems could partially dictate part of the trace element makeup of speleothems.

This section has demonstrated why the transport of trace elements from source to sink is one of the most complex chemical systems to interpret during speleothem analysis. Interactions and modification in speleothem trace element concentration result from soil processes, karst hydrology, bedrock weathering, the speleothem crystal filter and aerosol contributions. A combination of these processes occurs at different scales for each speleothem deposit. Robust speleothem studies therefore, aim to analyse a suite of trace elements alongside isotope records and extensive hydrological monitoring before drawing conclusions about changes in palaeoclimatic conditions. When accurately interpreted, trace elements from speleothems offer a vast array of palaeoclimate indicators, many of which are site specific and could not be reconstructed from other common palaeoclimate proxies.

2.6 Stable Isotopes: Principles and Applications

Elemental atoms are comprised of a nucleus, containing protons and neutrons and orbiting electrons. Isotopes have the same chemical properties as their parent element (same electron shell), but additional neutrons change the physical properties (atomic mass) (Hoefs, 1973, Allegre, 2008). Isotopic ratio analysis compares the two isotopes of highest abundance (for example: oxygen ^{16}O (99.8 %) and ^{18}O (0.205 %)) (Hoefs 1973, Allegre 2008).

2.6.1 Standardisation and Notification

Initial standardisation for O isotopes was developed by Craig (1961). This has been updated to the current V-SMOW standard which is derived from distilled sea water (Clark and Fritz 1997). Fractionation of oxygen isotopes can either be positive (comparatively more ^{18}O) or negative (comparatively more ^{16}O) in relation to the V-SMOW standard (Clark and Fritz 1997). Isotope ratios preserved in materials are an artefact of isotopic fractionation during their formation, giving insights into physical and chemical processes that acted upon them during formation (McDermott 2004).

Isotopic analysis measures the isotopic ratio of the sample against a known ratio within a reference material, rather than the true ratio within the sample (Fritz and Fontes 1980, Clark and Fritz 1997). Equation 2.5 is used to establish the ratio of the sample to the known reference. This relative difference is represented by a delta value (δ).

$$\delta^{18}O_{sample} = m(^{18}O/^{16}O)_{sample} - m(^{18}O/^{16}O)_{reference} / m(^{18}O/^{16}O)_{reference} \quad (2.5)$$

m = the mathematical error between the apparent and true ratios, this is cancelled out (Clark and Fritz 1997).

The more common expression of this equation is given below (Equation 2.6). The δ values are expressed in parts permil (‰), parts per thousand.

$$\delta^{18}O_{sample} = \left(\frac{(^{18}O/^{16}O)_{sample} - (^{18}O/^{16}O)_{reference}}{(^{18}O/^{16}O)_{reference}} \right) \times 1000 \quad (2.6)$$

The resultant δ value of any analysed isotope reflects the difference between ^{18}O and ^{16}O relative to a known reference. This value is then converted to a common standard (such as V-SMOW) allowing isotopic comparison between different host materials. This cross material

comparison is vital for palaeoclimate studies, which commonly utilise isotopic evidence from a range of proxies (McDermott 2004, Allegre 2008).

2.6.2 Isotopic Fractionation

Isotopic fractionation refers to the preferential incorporation of one isotope into a specific phase of a chemical reaction, fractionation is controlled by isotope vibration energy (Guo et al., 2008). Lighter isotopes have higher zero point vibration energies than heavier ones, so their bonds are broken more easily (Clark and Fritz 1997, Guo et al., 2008). This leads to an initial, disproportionate incorporation of light isotopes into the product of a reaction (Hoefs 1973, Dansgaard 1964). Isotopic reactions proceed along two reaction pathways controlled by the reaction rate.

1. Equilibrium reactions proceed for long enough for full isotopic exchange between the reactant and the product (Allegre 2008). Isotopic fractionation also occurs during equilibrium reactions. As the reaction proceeds, heavier bonds with lower zero point vibration energies survive longer, meaning heavier isotopes are preferentially partitioned into the most condensed phase (Clark and Fritz 1997). During equilibrium reactions these fractionations can be quantified (Clark and Fritz 1997, McDermott 2004)

2. Disequilibrium or kinetic reactions have a fast forward reaction and slow backward component, creating more products and using reactants (Clark and Fritz 1997). Kinetic reactions have isotopic fractionations that are difficult to quantify, creating a product enriched in lighter isotopes. For a reaction to stay in a kinetic mode, the effective separation of reactants and products must occur (Allegre 2008).

Isotopic equilibrium can exist during non-equilibrium chemical conditions, providing the net forward reaction does not greatly exceed the backward reaction (Frisia and Borsato, 2010). For example calcite can only be formed during a disequilibrium (supersaturation) chemical reaction, if the chemical reaction is slow, isotopic equilibrium can still be achieved (Clark and Fritz 1997, Frisia and Borsato 2010). The time required for an isotopic reaction to reach equilibrium is controlled by several factors (Allegre 2008).

1. Temperature, both kinetic and equilibrium reactions are driven by temperature with equilibrium reactions eventually dominating the kinetic at high temperatures.

2. The phase, isotopic exchange is faster in gasses than liquids or solids.

3. The position of the exchanging isotopes within the compound structure. Isotopes closer to the outside of the molecular structure exchange faster than those within the centre of the molecule (Allegre 2008).

2.6.3 Isotopic Fractionation Constant

An isotopic fractionation constant (K or α) is used to describe isotopic fractionation within any chemical reaction which proceeds in isotopic equilibrium (Fritz and Fontes, 1980). The calculation of this constant is shown in Equation 2.7 for water to vapour fractionation.

$$\alpha^{18}O_{water\text{-}vapour} = \frac{(^{18}O/^{16}O)_{water}}{(^{18}O/^{16}O)_{vapour}} \qquad (2.7)$$

This constant calculates the expected fractionation of isotopes under equilibrium conditions (Clark and Fritz 1997). For unidirectional, kinetic reactions there can be no quantitative interpretation of the isotopic fractionation (Fritz and Fontes 1980). The use of isotopic ratios for reconstructing chemical reactions therefore, relies upon isotopic equilibrium conditions and a known calculable fractionation constant (Fritz and Fontes 1980).

2.7 Oxygen Isotopes in Speleothems

Oxygen isotopic values recorded in speleothem calcite have similar controlling processes as other chemical parameters. The $\delta^{18}O$ value of speleothem calcite is dictated by the source of rainfall, atmospheric conditions, karst hydrology, in cave CO_2 degassing and speleothem uptake. Isotopic fractionation occurs during these processes and specific fractionations are then stored within the speleothem record. Common uses of isotopes from speleothems include: the identification of rainfall source, quantification of rainfall amount and the classification of karst conditions. High resolution oxygen isotopic analysis of speleothems can therefore, accurately depict changes in all of these systems, over extended time scales (McDermott et al., 1999).

2.7.1 Oxygen Isotope Values in Rainfall

Oxygen isotopes in moisture undergo a wide range of fractionations in the atmosphere due to a range of "effects" (Dansgaard 1964, Lachniet 2009). The final isotopic value of rainfall collected above a cave site is therefore a record of all chemical reactions (Figure 2.7) that have occurred within the water vapour as it travelled from source, to rainfall site and through the karst system (Lachniet 2009, Jex et al., 2010).

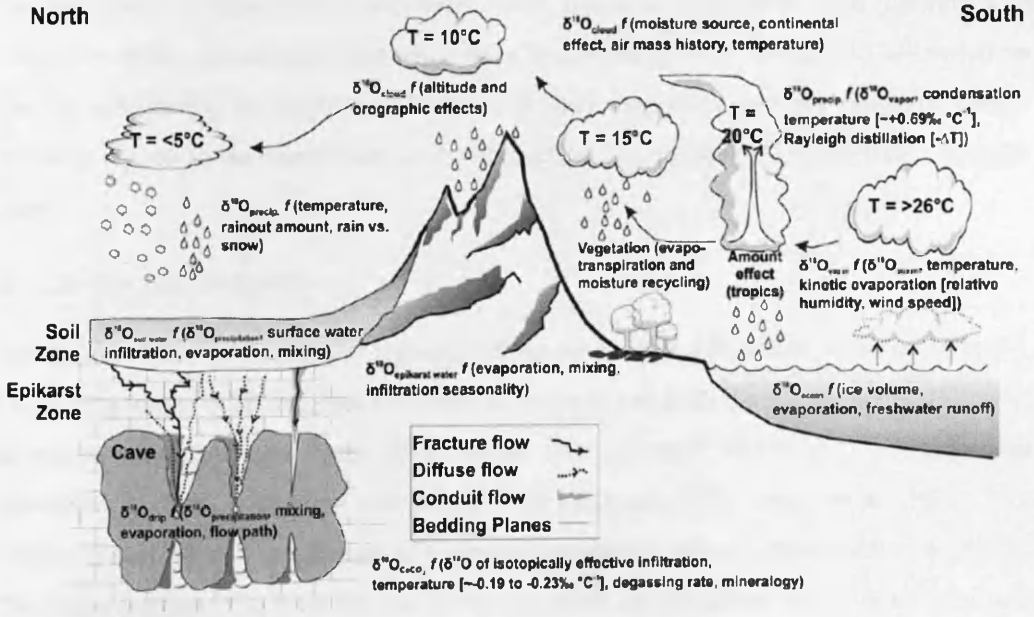

Figure 2.7: the primary processes related to the ^{18}O variations relevant to speleothem paleoclimatology (Lachniet 2009).

2.7.1.1 Moisture Uptake and Source Identification

The production of moisture by evaporation, is the first effect to influence the isotopic makeup of an air mass (Dansgaard, 1964). Evaporation is most efficient in warm dry air, over a large water body, conditions most prevalent within tropical regions (Lachniet 2009). If evaporation progresses in isotopic equilibrium the processes slightly enriches the vapour in lighter ^{16}O. Newly evaporated vapour is mixed with older air, complicating the isotopic signature. This first effect results in global average isotopic values of $\delta^{18}O$ = -4 ‰ (in relation to V-SMOW), derived from average rainfall values globally (Craig 1961, Clark and Fritz 1997).

Although an air mass is often influenced by numerous other effects during transport, its moisture source can be distinguished from rainfall chemistry (Lachniet 2009, Maher 2008). The global relationship between the hydrogen isotope Deuterium and $\delta^{18}O$ produces the global meteoric water line (Craig 1961). The intercept of this line is the global Deuterium excess value, calculated by Equation 2.8.

$$d = \delta^{2}H - 8\delta^{18}O \tag{2.8}$$

8 being the slope of the global meteoric water line as developed by (Craig 1961).

The Deuterium excess value of any evaporated vapour is dependent upon conditions of relative humidity, wind speed, and sea surface temperature (SST). This value is imprinted on the air mass during the initial evaporation and does not evolve with the air mass history, enabling rainfall to be traced back to its evaporative source (Andreo et al., 2004, Lachniet 2009).

2.7.1.2 Moisture Transport

Isotope fractionation during the transport of an air mass is influenced by other "effects". Firstly, the terrain (altitude) over which the air travels, and secondly the trajectory (latitude) of the air mass (Lachniet 2009). When an air mass is forced to rise over a topographic boundary, it cools, condenses and falls as rain (Lachniet 2009, Vogel et al., 1975). This rainout is controlled by the process of Rayleigh distillation (Lachniet 2009, Vogel et al., 1975). The heavy isotope (^{18}O) is rained out during the initial condensation phases due to isotopic fractionation, if air mass cooling persists rainfall contains increasingly negative isotopic values (Figure 2.8) (Vogel et al., 1975, Treble et al., 2005, Clark and Fritz 1997, Andreo et al., 2004).

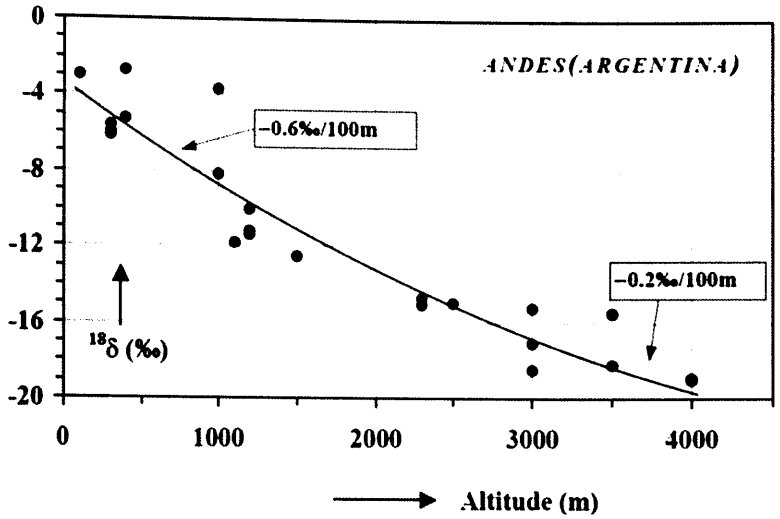

Figure 2.8: An example of the altitude effect from the Andes (Vogel et al., 1975).

The latitude and trajectory of an air mass is controlled by global atmospheric circulation systems (Lachniet 2009). Air masses formed in tropical ocean environments migrate polewards, often moving into continental interiors (Lachniet 2009). Polewards migration forces air mass cooling, condensation and Rayleigh style distillation. Palaeo-air mass trajectories have been inferred by variations in oxygen isotopes, highlighting periods of drastically different prevailing wind directions (Treble et al., 2005).

2.7.1.3 Rainfall Amount

The final effect influencing rainfall isotope chemistry is rainfall amount (Lachniet, 2009). Rainfall amount has a negative correlation with $\delta^{18}O$ rainfall in many regions (Fuller et al., 2008, Treble et al., 2005, Lachniet 2009). Intense rainfall events originate in the high atmosphere. Water vapour from this region undergoes numerous cycles of condensation and evaporation, enhancing isotopic fractionation (Dansgaard 1964, Treble et al., 2005). During intense rainout, water from this region falls as rain, characterised by extremely negative isotopic values (Dansgaard 1964). The negative correlation between rainfall amount and $\delta^{18}O$ is enhanced during light rainfall events. Light rains often fall through an unsaturated air column and evaporation causes rain droplets to fractionate ^{16}O to the surrounding air column (Treble et al., 2005, Dansgaard 1964). The remaining droplet is therefore enriched in ^{18}O, yielding higher $\delta^{18}O$ values for ground water sourced from light rains (Dansgaard 1964).

Local rainfall events are a combination of all these "effects", containing an isotopic signature which reflects air mass history. Variations in rainfall isotope chemistry are implanted in

palaeorecords, with carful interpretation these records can offer powerful archives for understanding a diverse range of atmospheric processes (Treble et al., 2005, Maher 2008).

2.7.2 Isotope Incorporation into Speleothem Calcite

Accurate reconstruction of rainfall characteristics using speleothems relies on drip waters, which correctly resemble incoming rainfall (Baldini et al., 2008, McDermott 2004), rather than within karst processes. Cave drip water isotope chemistry can therefore represent incoming rainfall, hydrological routing and drought conditions within the karst (McDermott 2004, Fairchild et al., 2005).

If cave drip water $\delta^{18}O$ accurately represents the $\delta^{18}O$ of incoming rainfall, speleothems developing from these waters should be ideal for palaeoclimate reconstruction (McDermott 2004). However, this relies upon regional rainfall which strongly exhibits isotopic change due to one single effect and minimal isotopic fractionation during speleothem calcite formation. These caveats highlight the importance of correct site selection both regionally and on a cave/speleothem specific scale before undertaking sampling for palaeoclimate analysis (Baldini et al., 2006a).

Calcite deposition includes two stages, both of which are influenced by isotopic fractionations, occurring either as equilibrium or kinetic reactions (Mickler et al., 2004). This two-stage reaction complicates the classification of calcite precipitation as occurring exclusively under equilibrium or kinetic conditions (Mickler et al., 2004). However, most speleothem studies still endeavour to determine under which reaction regime calcite was precipitated. Equilibrium fractionation is most common in cave sites with high relative humidity, with no evaporation (Jex et al., 2010, Mickler et al., 2004, McDermott et al., 1999). If this is the case, $\delta^{18}O_{calcite}$ represents $\delta^{18}O_{drip}$ plus a calculable temperature fractionation attributed to equilibrium conditions. (McDermott 2004, O'Neill et al., 1969).

Isotopic fractionation from drip to calcite has been calculated for equilibrium growth conditions by several studies (O'Neill et al., 1969, Scholz et al., 2009). This known fractionation (χ) enables the precise calculation of the incoming solute as shown in Equation 2.9.

$$\delta calcite = \delta drip - \chi‰ (/°C) \quad (2.9)$$

However, if the reaction progresses kinetically, the reaction product (calcite) incorporates proportionally more ^{18}O, resulting in a fractionation between $-\chi$ ‰ and 0 ‰ (Clark and Fritz

1997, Mickler et al., 2004). For accurate, easily interpreted palaeoarchives, speleothem deposition must be as close to equilibrium as possible (Fairchild et al., 2006a, McDermott 2004). If the reaction proceeds in equilibrium speleothem records importantly incorporate variations in the $\delta^{18}O$ of incoming rainfall, which over-shadows slight changes in $\delta^{18}O$ calcite related to fractionation temperature (McDermott 2004, Sundqvist et al., 2007, Moreno et al., 2010, Hammarlund and Edwards, 2008).

2.7.2.1 Short Term Controls on $\delta^{18}O$

Cave calcite is known to grow at different rates throughout the year, incorporating the isotopic value of the waters from which it has grown (McDermott 2004, Fairchild et al., 2006a, Spötl et al., 2005). In caves with a well-mixed annual aquifer there should be little seasonal variation in $\delta^{18}O$ calcite (Baldini et al., 2008). In caves with seasonal drip waters and/or enhanced growth during one season, the isotopic makeup of calcite is derived predominantly from a section of the annual rainfall (Spötl et al., 2005, Baker et al., 2007, Asrat et al., 2007). The two major controls on calcite deposition are supersaturation state of the drip waters and pCO_2 of the cave atmosphere, both vary seasonally (Spötl et al., 2005, Baker et al., 2007, Baldini et al., 2006a).

Supersaturation of cave waters is controlled by soil productivity, and carbonate dissolution rates (Fairchild et al., 2007). High soil productivity and high bedrock dissolution rates are often associated with summer months, meaning that the higher $\delta^{18}O$ values often found in summer rainfall percolate through the karst and are incorporated within speleothem deposits. Deposition of calcite from water derived solely from the summer season therefore reflects the greater incorporation of ^{18}O. If drip water supersaturation rates are the major control on speleothem deposition, this will predominantly be a summer process and incorporate summer isotopic values.

Cave air pCO_2 levels are controlled by cave ventilation, in most cave systems winter overturning occurs, where external air enters the cave system removing stagnant cave air, this creates atmospheric conditions in the cave similar to those of the external atmosphere (Spötl et al., 2005, Baldini et al., 2008). Low pCO_2 levels facilitate rapid drip water degassing and carbonate precipitation during the winter season (Fairchild et al., 2006a). Precipitating calcite incorporates more negative isotopic signatures from heavy winter rains and reduced karst dissolution (Baldini et al., 2008).

Which of these two processes eventually dominates carbonate precipitation is specific to the physiology of individual cave sites. Understanding the carbonate deposition regime is fundamental in caves with a seasonably variable δ^{18}Odrip (Baldini et al., 2008).

2.7.2.2 Unravelling Long Term Controls on $\delta^{18}O$

The most common interpretations of δ^{18}Ocalcite records assume that speleothem values reflect either temperature (derived from rainfall formation temperature), a rainfall amount effect or a rainfall source effect (McDermott 2004). Interpretations of speleothem records are open to scrutiny due to the large range of factors, both external and internal to cave environments that influence the incorporation of stable oxygen isotopes (Sundqvist et al., 2007, Sundqvist et al., 2008, Hammarlund and Edwards 2008). Robust studies should analyse the magnitude of isotopic fluctuations and quantify the climatic changes being inferred from speleothem records (Fairchild et al., 2006a, Maher 2008).

Modern monitoring data can help quantify natural fluctuations in isotopic incorporation and act as a guide for sensible palaeoclimatic reconstructions (Boch et al., 2009, Hardt et al., 2010). Temperature and rainfall amount correlations with δ^{18}O can be established and moisture source trajectories can be modelled (Baldini et al., 2010). In this way, modern controls on δ^{18}O entering the karst system are known, and can be tentatively used to analyse longer-term $\delta^{18}O_{calcite}$ records, if all other controls (including rainfall source, amount effect, karst storage times and speleothem growth equilibrium) are assumed to remain unchanged (Hardt et al., 2010). Whilst it is possible that controls over the isotopic makeup of calcite may have varied through the duration of the Holocene (Dominguez-Villar et al., 2009), the extent and modes of isotopic variation are extremely hard to quantify. To ensure as robust a climatic interpretation as possible stable isotope records will be assessed alongside other palaeoclimate and environmental proxies from two speleothem. These additional proxies have the potential to highlight periods of dramatic environmental change where the isotope records may have been dominated by different controls than those present today.

When combining the factors discussed in this section it becomes clear that the $\delta^{18}O_{calcite}$ value is influenced by a range of climatic, physiological and chemical processes. In most locations one of these parameters dominates, yielding a speleothem that preserves a long-term record of this parameter. Modern monitoring is important for the identification of this parameter. Studies must however, be aware of the dynamic nature of climatic and karst systems, understanding that processes which currently control speleothem isotopic values may not control speleothem chemistry over longer time scales. The major challenge for

speleothem science it to interpret isotopic records correctly and draw reasonable conclusions for the region of study. The use of comparative palaeoclimatic records can be invaluable for the interpretation and justification of records produced from speleothem calcite.

2.8 Carbon Isotopes in Speleothems

Speleothem carbon isotope records offer archives of vegetation change, karst hydrology and fractionation kinetics (McDermott 2004). Whilst carbon is sourced from CO_2, bedrock and plant organic matter, it is the relative proportion of carbon incorporated from each of these sources which determines the drip water $\delta^{13}C$ signature (Cosford et al., 2009, Hodge et al., 2008, Oster et al., 2010). Final speleothem $\delta^{13}C$ signature is also influenced by fractionations during calcite deposition (Hodge et al., 2008, McDermott, 2004).

2.8.1 CO_2 Isotopes in Vegetation, Soil and Karst

Atmospheric $\delta^{13}C$ of CO_2 values (≈-7 ‰) are incorporated into plants during photosynthesis (Clark and Fritz 1997). Fractionation occurs during carbon fixation by chloroplasts and diffusion into leaves, the extent of fractionation depends upon the photosynthetic pathway used by vegetation (Clark and Fritz 1997, Fritz and Fontes 1980). C3 plants (trees and shrubs) cause a large fractionation, producing CO_2 with a $\delta^{13}C$ value of -26 to -23 ‰, whereas C4 plants produce values of -10 to -16 ‰ (Dorale and Liu 2009, McDermott 2004, Clark and Fritz 1997, Allegre 2008). Vegetation isotopic value is incorporated into the soil zone during respiration and decay.

During productive seasons, vegetation and microbial respiration increases the concentration of CO_2 in the soil, decreasing the soil CO_2 isotopic value (Fritz and Fontes 1980, Genty et al., 2003). More negative $\delta^{13}C$ values preserved in speleothems have therefore been shown to reflect conditions favouring vegetation growth (Genty et al., 2003, Cosford et al., 2009, Jiménez de Cisneros et al., 2003). Speleothem $\delta^{13}C$ can also infer macro scale changes to vegetation density, vegetation type and soil respiration (Baker et al., 1997b, Baldini et al., 2005, Genty et al., 2003).

Soil $\delta^{13}C$ values are transferred through the karst in dissolved CO_2, HCO_3^- and CO_3^{2-} to speleothem deposition sites. In an open system there is full isotopic exchange between the soil CO_2 and percolating waters (McDermott 2004, Hendy 1971). The resultant $\delta^{13}C$calcite value represents the initial soil CO_2 value and known equilibrium fractionations (Figure 2.9) (Fairchild et al., 2006a).

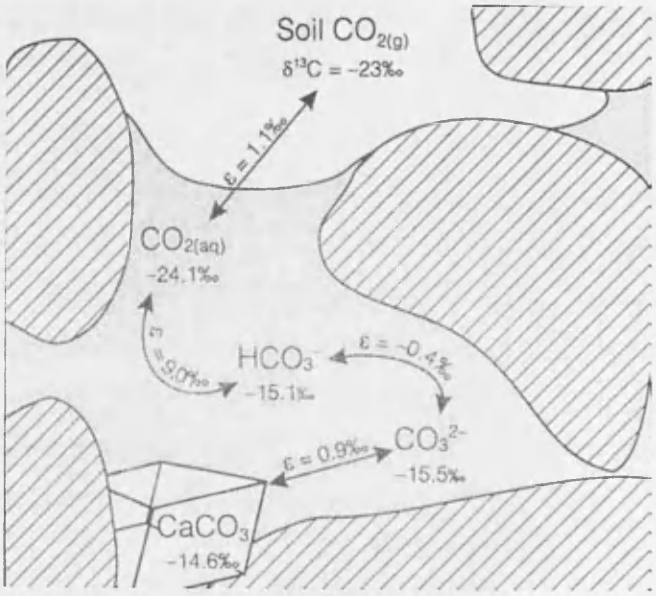

Figure 2.9: Equilibrium fractionation of CO_2 through to $CaCO_3$ formation showing $\delta^{13}C$ enrichment at 25°C. Initial $\delta^{13}C$ from the C3 plant pathway (Clark and Fritz 1997). White space represents soil air, black hashed space bedrock and solid grey shading soil water component. $CaCO_3$ is denoted as a solid white block.

Under open conditions with equilibrium isotopic exchange, C3 plants deposit calcite with a $\delta^{13}C$ value between -14 to -6 ‰ and C4 plants -6 to +2 ‰, enabling palaeo-vegetation type to be distinguished (Baker et al., 1997b, McDermott 2004, Luo and Wang, 2009).

In a closed system however, percolating water becomes isolated from the soil CO_2 reservoir (McDermott, 2004). Water incorporates a bedrock $\delta^{13}C$ value (≈1 ‰), resulting in higher $\delta^{13}C$ than under open system conditions. The carbon isotope signature of percolating waters can also be modified by PCP, leaving water with less negative $\delta^{13}C$ values than parent soil waters (Baker et al., 1997b).

2.8.2 Speleothem $\delta^{13}C$ values

Isotopic fractionation occurs during speleothem formation. Under isotopic equilibrium, known fractionation factors can be applied (as with oxygen isotopes). These fractionation factors incorporate known equilibrium fractionations, resulting from CO_2 degassing from drip water to cave atmosphere. Equilibrium degassing leads to an enrichment of ^{13}C in the remaining water as ^{12}C is preferentially lost to the cave atmosphere (Mickler et al., 2006). The longer water exchanges with the cave atmosphere the more enriched in ^{13}C it becomes. This Rayleigh style fractionation forms calcite with progressively high $\delta^{13}C$ values away from

the drip impact point. This process can be quantified under equilibrium conditions but not during kinetic reactions (Mickler et al., 2004).

Therefore, as with oxygen isotopes, it is important for carbon isotopes to be deposited under isotopic equilibrium (Frisia and Borsato, 2010, Dorale and Liu, 2009). If this occurs, direct interpretations about climate and vegetation change can be drawn (Fairchild et al., 2006a, Guo et al., 2008). To establish if isotopic equilibrium has been achieved, comparisons between oxygen and carbon isotopes are undertaken. Comparative analysis, first undertaken by Hendy (1971) is now common place, known as the Hendy Test. Isotopic comparison follows the sampling procedure in Figure 2.10, analysing horizontally across one growth layer and vertically through the speleothem (Hendy 1971, Mickler et al., 2006).

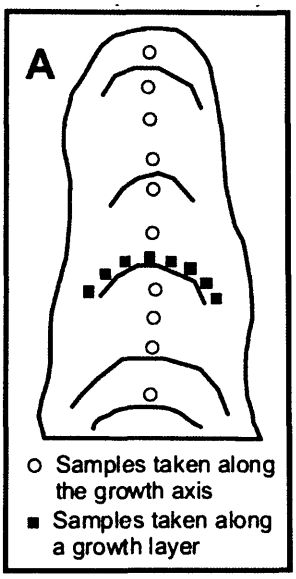

Figure 2.10: Sampling procedure for the Hendy test along the growth axis and growth layer (Mickler et al., 2006).

The Hendy Test relies upon different processes controlling carbon and oxygen isotopic values. When compared there should be no co-variation between them. If co-variation is found, kinetic fractionation due to in-cave processes can be the cause (Hendy 1971, Mattey et al., 2008). Speleothems exhibiting a strong isotopic co-variation may be unsuitable for extensive palaeo-climatic research (Hendy 1971).

However, legitimate co-variation in oxygen and carbon isotopes has been identified and attributed to overriding changes in climate, occasionally rendering the Hendy test inappropriate as a test of isotopic equilibrium deposition (McDermott 2004, Mickler et al.,

2006, Dorale and Liu, 2009, Lachniet 2009, Watanabe et al., 2010,). More appropriate tests compare isotopic variations in multiple speleothems from the same location, on the understanding that several speleothems could not record the same O and C isotopic trends unless cave conditions promoted equilibrium growth conditions for carbonates (Dorale and Liu, 2009).

Where speleothems are deposited in isotopic equilibrium, carbon isotopes become palaeoclimate proxies for vegetation change (Genty et al., 2003), soil productivity (Hodge et al., 2008, Cosford et al., 2009) and karst hydrology (Hodge et al., 2008). Therefore, by using oxygen and carbon isotope analysis, speleothems offer diverse archives of climatic and environmental change (McDermott, 2004). High resolution cave monitoring is still however, required to fully characterise both the O and C isotope systems operating in any given cave, before palaeoclimate reconstruction should be undertaken.

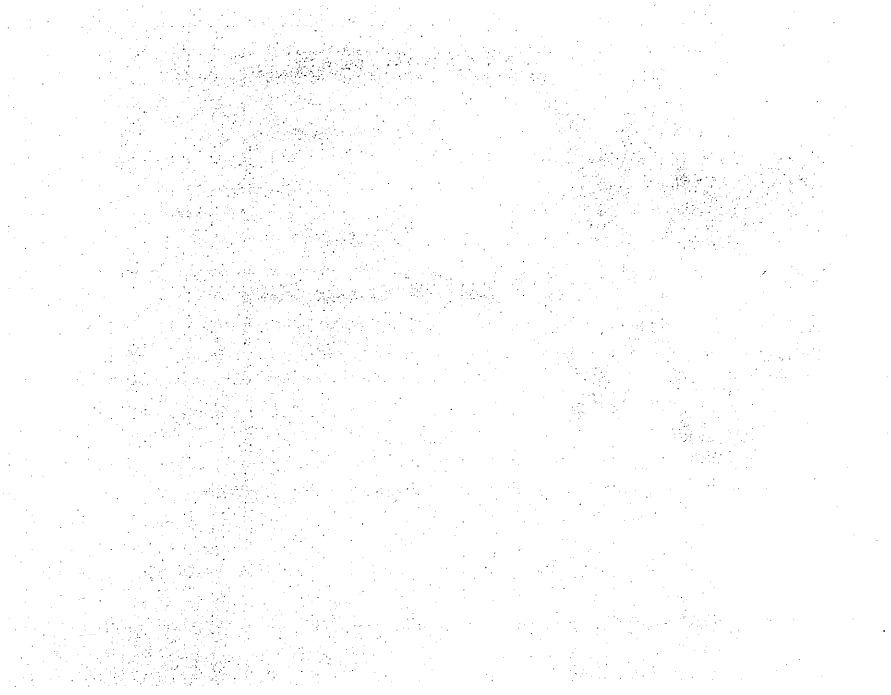

2.9 Late Glacial and Holocene Climate

The late glacial and Holocene encompass the last 13,000 years of Earth's history. The Holocene's interstadial climate enabled human civilisations to flourish, and is of great importance as a backdrop for understanding modern, anthropogenic climate change. Palaeorecords have pinpointed discrete periods of dramatic climate change throughout the Holocene (Mayewski et al., 2004) and longer duration climatic cycles (Bond et al., 1997). Large scale climatic shifts have strongly influenced regional weather systems (Griffiths et al., 2010), vegetation dynamics and human civilisations (Mayewski et al., 2004). When assessing the severity of modern climate change, these Holocene events offer the best recent examples of natural climatic extremes (Meyer et al., 2010, Alley 2000, Alley et al., 1997, Mayewski et al., 2004).

2.9.1 Holocene Climate Events

2.9.1.1 Early Holocene

The Younger Dryas (YD) event (12.9-11.5 ka) is a cold stadial event (GS-1) lasting for approximately 1400 years (Figure 2.11) (McManus et al., 2004, Bakke et al., 2009, Alley, 2000).

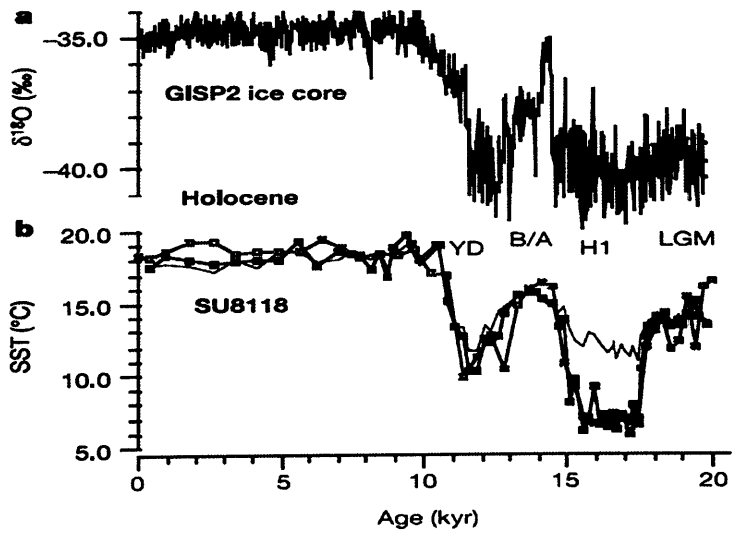

Figure 2.11: A comparison of sedimentary data from the subtropical Atlantic displaying variations in air and sea surface temperatures during the last 20,000 years. (a) $\delta^{18}O$ data from GRIP2 ice core, more negative isotopic values represent colder air temperature over Greenland. (b) Sea Surface Temperature (SST) estimates for the North Atlantic based on planktonic foraminiferal assemblage (open symbols) and alkenone unsaturation ratio (McManus et al., 2004).

Younger Dryas cooling marked the end of the warmer Allerød interstadial (B/A in Figure 2.11) and was one of two major reversions to cold dry conditions during de-glaciation (H1 and YD in Figure 2.11) (Anderson et al., 2007). Temperature decrease was synchronous across Europe at the onset of the YD, although the magnitude of change was spatially variable, with southern Europe exhibiting the largest temperature decreases (Anderson et al., 2007). Average temperature depression was 7-10 degrees centigrade in comparison to maximum temperatures in the late glacial (Figure 2.11) (McManus et al., 2004). The most probable cause of cooling during the YD is the massive inundation of melt water into the North Atlantic during the breakup of the Laurentide ice-sheet, causing a reduction in deep water convection and cooling in the North Atlantic (McManus et al., 2004, Meyer et al., 2010, Anderson et al., 2007, Alley, 2000).

The onset of the Holocene occurred at the termination of the YD, characterised by an extremely rapid rise in temperature (Figure 2.11), as much as 7-10 °C in only a few decades (Alley 2000, Taylor et al., 1997, Fawcett et al., 1997). This rapid shift in temperature in the North Atlantic region is thought to have been triggered by an abrupt reorganisation of thermohaline circulation, increasing the delivery of warm waters to northern oceans and drastically altering atmospheric circulation (Bakke et al., 2009, Taylor et al., 1997).

The early Holocene was a period of significant climatic improvement punctuated by a dramatic cooling event at 8.2 ka (Dansgaard et al., 1993, Anderson et al., 2007, Mayewski et al., 2004, Bond et al., 2001). The 8.2 ka event lasted for approximately 200 years with summer temperature decreases of ≈1 °C (Heiri et al., 2004, Anderson et al., 2007, Maslin et al., 2005, Alley et al., 1997) and winter temperature reductions which were approximately half as severe as the Younger Dryas (4-6 °C) (Maslin et al., 2005, Alley et al., 1997, Alley and Agustsdottir, 2005). The trigger for the 8.2 ka event is thought to be similar to that of the YD, an inundation of fresh water into the North Atlantic, which caused a change in oceanic circulation patterns (Alley et al., 1997, Anderson et al., 2007, Alley and Agustsdottir, 2005).

2.9.1.2 Mid Holocene

The Holocene climatic optimum occurred around 5.5 - 6 ka BP, this period was characterised by the warmest temperatures experienced during the Holocene (Anderson et al., 2007, Adkins et al., 2006). Temperature increases were more pronounced in northern Europe, with summer temperatures 3-4 °C higher than today (Anderson et al., 2007). Saharan African climate was possibly the most markedly different, with warm wet monsoon conditions dominating a savannah and lake environment (deMenocal et al., 2000b, Adkins et al., 2006,

deMenocal et al., 2000a). This period of warming was however, punctuated by several short lived cooling events (Bond et al., 1997, deMenocal et al., 2000a).

The end of the African Humid period (5.5 ka) and the onset of desertification in central Africa was followed by a cooling event at 4.2 ka, and the beginning of a longer lived Holocene cooling trend (Anderson et al., 2007, deMenocal et al., 2000b, Adkins et al., 2006, Staubwasser et al., 2003, Arz et al., 2006). The 4.2 ka event is the first Holocene cooling period to have well documented consequences on human populations (deMenocal et al., 2000a, Mayewski et al., 2004).

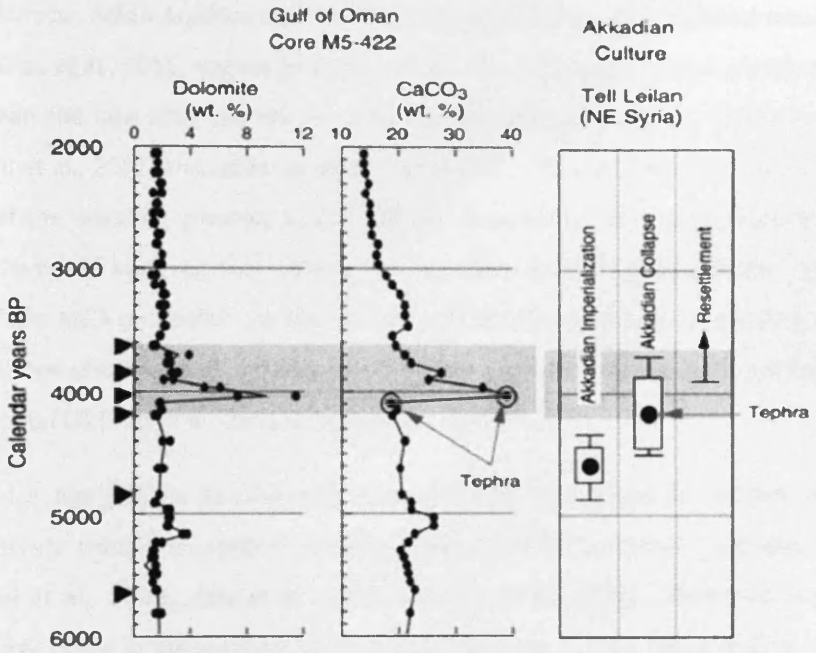

Figure 2.12: Adapted from (deMenocal 2001) showing palaeoclimate during the collapse of the Akkadian empire. Increases in wind-borne sediments deposited in the Gulf of Oman (left and central panels) represent a 300 year period of increased aridity in Iraq, Kuwait and Syria. This coincides with radiocarbon dating of archaeological remains in Tell Leilan (right hand panel) which document the abandonment and collapse of the Akkadian empire 4170 ± 150 BP.

Civilisation collapse during this period occurred in Egypt (Staubwasser et al., 2003), Mesopotamia (Figure 2.12) (deMenocal 2001), India and China (Huang et al., 2010), possibly due to much colder, more arid climates (Maslin et al., 2005, deMenocal 2001).

This general cooling and drying trend is punctuated in some regions by more extreme unstable climatic oscillations, demonstrated by large scale flooding and droughts in the

Jinghe River Gorge, China (Huang et al., 2010) and alternating wetting and drying in the western Mediterranean (Magny et al., 2009). The impact of climate change (on a scale with, or more dramatic than the 4.2 ka event) on modern populations is unknown; although these climatic shifts have been predicted by some climate models (Alley 2000).

2.9.1.3 Late Holocene

The Medieval Climate Anomaly (MCA) (750 - 1400 A.D.) was initially identified as a period of global warming, based on records from northern Europe and North America and marked by glacial retreat (Anderson et al., 2007). However, the lack of evidence for warming in southern Europe, South America and the Pacific possibly reflects the regional nature of this anomaly (Diaz et al., 2011, Hughes and Diaz, 1994). The MCA appears to have temperatures warmer than the late 20th century in some regions (Diaz et al., 2011, deMenocal et al., 2000b, Chu et al., 2002) and colder in others (Diaz et al., 2011, Hughes and Diaz, 1994). The duration of the warming anomaly is also difficult to quantify, with palaeorecords offering different timings of peak regional warmth (Cronin et al., 2010, Hughes and Diaz, 1994). The impacts of the MCA on rainfall are also varied; with wetter conditions dominating in north-western Europe (Proctor et al., 2000) while droughts were common in southern Europe and the continental US (Diaz et al., 2011, Cronin et al., 2010).

The Little Ice Age (LIA) is documented as a return to semi-glacial conditions, exhibiting several discrete winter dominated cooling events (3-4 °C) between 1300 and 1900 AD (deMenocal et al., 2000b, Chu et al., 2002, Sobrino et al., 2005). Cooling of Sea Surface Temperatures (SSTs) in the western North Atlantic appears to have begun before cooling in the eastern ocean. This regional disparity suggests the LIA may have been forced primarily by coupled ocean-atmosphere processes and subpolar deep water formation. The timing of the LIA fits with the 1500 year climate pattern of Bond et al. (2001) possibly indicating atmospheric – oceanic coupling during this period (Cronin et al., 2010, Bond et al., 2001).

2.9.1.4 Modern Climate Change

Modern climate warming (≈1800-2012 AD) is a controversial issue, not based around its existence, but the severity and cause (Rosenzweig et al., 2008, Anderson et al., 2007), as well as the routes towards effective mitigation (Hulme 2003). The best way to understand and contextualise modern climate change is by reviewing past fluctuations in climate indices (Hulme 2003, Chu et al., 2002). Abrupt climate changes such as those seen in the YD and 8.2 ka event are the most dangerous to human populations, due not only to their severity, but

their rapid and uncontrollable onset (Hulme 2003). Minor climate change events such as those seen at 4.2 ka have already destroyed relatively advanced civilisations; the potential impacts of major regional or global climate change on modern populations are difficult to predict and remain largely unknown (Hulme 2003).

Holocene palaeoclimate data sets have however, allowed for the identification of several major climate forcing mechanisms, both natural and anthropogenic. The continued production of high resolution data sets from throughout the Holocene is therefore, fundamental for understanding the severity of natural climate fluctuations and the impact human activity may have on the global climate system (Hulme et al., 1999).

2.9.2 Mechanisms of Climatic Forcing

Archives of major climatic events point to several major controls on the rate and severity of climate change. Much debate has focused upon the cause and effect relationships displayed by these major systems, and the inherent complexity of interactions between the extra-terrestrial and terrestrial systems (Anderson et al., 2007, Elkibbi and Rial, 2001). Climate response to external forcing is dependent upon internal feedback mechanisms (Elkibbi and Rial, 2001). These are dominated by interactions between the ocean, vegetation, and atmospheric systems (Elkibbi and Rial, 2001). Rapid onset climate changes are therefore thought to be triggered by solar activity and catastrophic events, which include the release of stored fresh water into the Northern oceans and volcanic eruptions (Anderson et al., 2007).

2.9.2.1 Solar Forcing and Climate Feedbacks

Solar forcing has been linked to climate changes throughout Earth's history (Moberg et al., 2005, Bond et al., 2001, Hu et al., 2003). This system is dominated by major (Croll-Milankovitch) orbital cycles, however, smaller scale fluctuations in solar irradiance can also influence global climate (Mayewski et al., 2004, Anderson et al., 2007, Bond et al., 2001). Solar insolation is known to have peaked between 10 and 11 ka at levels approximately 8 % higher than modern day (deMenocal et al., 2000a). The Earth's axial tilt and close orbit to the sun during mid-winter increased seasonality, creating warmer summers and relatively mild winters (deMenocal et al., 2000a, Anderson et al., 2007). Higher levels of northern hemisphere (NH) solar radiation increased the reach of the monsoons, enabling the spread of warmer wetter climates into central Africa. Solar insolation has slowly decreased in strength from peaks in the early Holocene to the modern day (Anderson et al., 2007).

Solar forcing is also thought to trigger non-linear responses within oceanic and atmospheric systems, which can drastically amplify or mediate climate change (deMenocal et al., 2000a, Anderson et al., 2007, Bond et al., 2001). Global system interconnectivity facilitates rapid changes in global temperature and rainfall, such as those recorded towards the end of most major Holocene events (Adkins et al., 2006, deMenocal et al., 2000a, deMenocal, 2011). Global feedback mechanisms are still relatively poorly understood due to their complexity (Anderson et al., 2007, Elkibbi and Rial, 2001). Major climate anomalies are often thought to be a combination of "top down" large scale changes in solar insulation and "bottom up" variations in regional to global climate forcers such as the North Atlantic Oscillation (NAO) and El Nina (Diaz et al., 2011).

2.9.2.2 Catastrophic Events

Large scale catastrophic events have also been prominent throughout the Holocene. These events cause major, discrete changes to the Earth's ocean and atmosphere systems. The inundation of the North Atlantic by melt water and the interruption of the thermohaline circulation (THC) is one such type of catastrophic event. Melt water inundation events can often be linked back to already changing climatic conditions forced by solar cycles. For example, the transition toward interstadial conditions (14-13 ka) induced rapid glacial melting in the NH, leading to the break-up of major ice masses, inundation of fresh water into the North Atlantic Ocean, a breakdown in thermohaline circulation and a reversion to semi-stadial conditions during the YD (Heiri et al., 2004, Bond et al., 2001). One area which requires further research is palaeoclimate reconstruction at the time of outburst events; to understand how changes in North Atlantic Ocean circulation may have influenced atmospheric circulation and therefore terrestrial climate.

2.10 Northern Iberian Climate and Vegetation Change

The position of the Northern Iberian Peninsula is such that regional climate is sensitive to changes in oceanic and atmopheric conditions (Allen et al., 1996, Pena et al., 2010, Anton et al., 2006, Sobrino et al., 2005). The strong interconnections between this region and the North Atlantic Ocean make it an ideal location to source palaeoclimate records of Holocene scale climate change (Eiriksson et al., 2006, Desprat et al., 2003, Martin-Chivelet et al., 2011). A range of palaeoclimate records are found from coastal regions of North Western Iberia (Pena et al., 2010, Allen et al., 1996, Sobrino et al., 2005, Desprat et al., 2003), but fewer archives are available from more central provinces such as Cantabria (Martin-Chivelet et al., 2011, Peña-Chocarro et al., 2005, Dominguez-Villar et al., 2009). This leaves a critical gap in palaeoclimatic interpretations, in a region which preserves some of Iberia's best documented evidence of human expansion and evolution (Peña-Chocarro et al., 2005).

2.10.1 Available Northern Iberian Palaeoclimate Archives

Pollen records from the late glacial period to YD transition in northern Iberia are characterised by an increase in Pine pollen, suggesting a shift from cold dry glacial conditions towards a slightly warmer but wetter climate (Allen et al., 1996, Moreno et al., 2010). Rainfall increases were driven by the warming of the North Atlantic, changes to atmospheric circulation and a subsequent increase in moisture delivery to Northern Iberia (Allen et al., 1996). The YD period intersects this warmer wetter period (Moreno et al., 2010), pollen records indicate the disappearance of late glacial tree cover and a return to herbaceous and dwarf shrub communities indicative of drier conditions (Allen et al., 1996, Sobrino et al., 2005). This return to dry conditions is possibly driven by a southward shift in the North Atlantic polar front, reducing evaporation over the North Atlantic Ocean (Ruddiman and McIntyre, 1981, Anderson et al., 2007, Pena et al., 2010).

The onset of the Holocene was marked by the re-emergence of deciduous tree species, peaking around 7 ka, with some pockets surviving to modern day (Allen et al., 1996, Anton et al., 2006, Kaal et al., 2011). However, evidence of lake sediment re-working during the early Holocene, suggests extreme reductions in winter rainfall, causing the drying of small water bodies (Allen et al., 1996). One such dry event may have occurred at 8.2 ka (Allen et al., 1996, Sobrino et al., 2005), linked to major changes in the North Atlantic Ocean which manifest as variations in rainfall isotopic values, archived within a speleothem deposit from Kaite Cave (Dominguez-Villar et al., 2009).

Pollen and speleothem archives encompassing the Roman warm period (2095-2060yr BP) and MCA (995-1050 AD) in Northern Iberia are characterised by dry conditions and temperatures up to 2 °C higher than today (Sobrino et al., 2005). Marine records from the west coast of Iberia demonstrate however, SST cooling and increased rainfall from 900AD, incorporating a 1.5 °C drop in SST temperature during the preceding 500 years (Eiriksson et al., 2006).

The LIA in Northern Iberia may have been limited to major climatic fluctuations during the 16th and 17th centuries. Climatic change during this period was characterised by rapid, large scale changes in regional temperature and rainfall, causing severe droughts and floods (Sobrino et al., 2005). Late Holocene cooling from 600 – 300 AD (Figure 2.13, A) reversed with a slight (~0.5 °C) rise in SST's since 250 AD recorded in planktonic and benthic foraminifera (Figure 2.13, A) (Eiriksson et al., 2006).

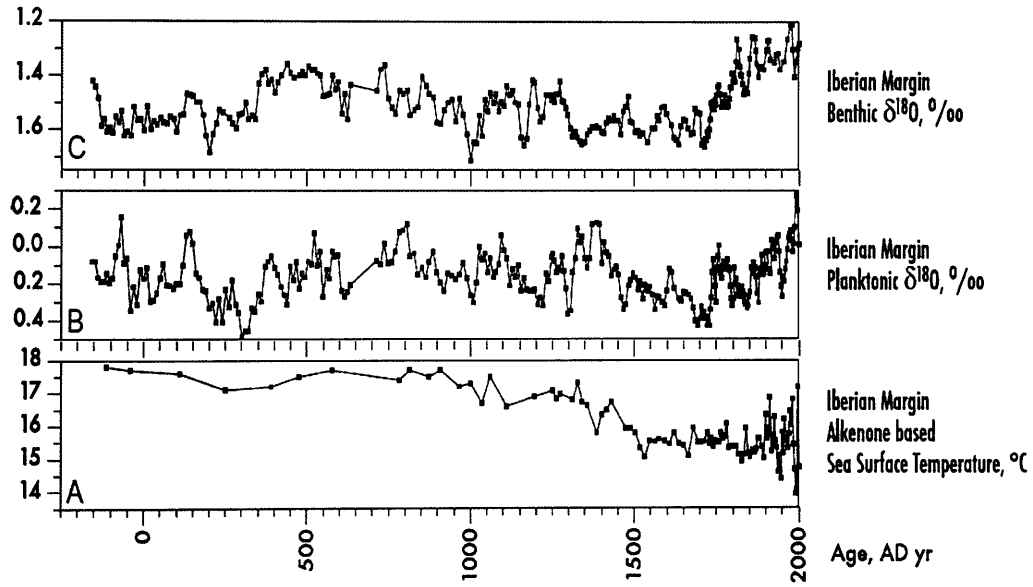

Figure 2.13: (a) SST's from the western Iberian margin from alkenones, (b) $\delta^{18}O$ record from planktonic foraminifera, (c) $\delta^{18}O$ record from benthic foraminifera (Eiriksson et al., 2006).

2.10.2 Human Populations in Northern Iberia

Early Holocene human populations experienced significant cultural upheaval with the transition from Magdalenian to Azilian cultural complexes (Straus and Morales 2012). As the Holocene progressed, Iberian populations became increasingly dependent upon agriculture, with the earliest agricultural practices identified by the emergence of cultivated cereal pollen around 6.5 ka, although this is likely to be primitive and localised (Lopez-Merino et al., 2010).

Larger scale, climatically derived forest regression occurred at the end of the Holocene climatic optimum (5.5 ka), coinciding with increased agricultural practices and forest burning for animal grazing (Kaal et al., 2011, Lopez-Merino et al., 2010). During the late Holocene, the northern coast of Iberia may have seen a transition toward a more maritime dominated climate, enhancing the spread of peatlands (Allen et al., 1996). This period of vegetation evolution ties in with increases in cereal pollen around 3ka BP, indicating human activity through forest clearance and the emergence of subsistence agriculture (Allen et al., 1996, Anton et al., 2006, Sobrino et al., 2005, Kaal et al., 2011). The human driven reduction of tree species culminates with a tree pollen minima 450yr BP (Sobrino et al., 2005).

2.10.3 Modern Climate

Current climate in Northern Iberia is influenced directly by North Atlantic storm tracks, which deliver rainfall to the region (Pena et al., 2010) and are controlled by the intensity of the North Atlantic Oscillation. The last 50 years have shown reductions in the intensity of these storms, creating regional drying (Goodess and Jones, 2002, Gallego et al., 2005). This interconnection means that oscillations in the North Atlantic directly influence moisture delivery to Northern Iberia. High resolution archives of moisture delivery to this region could therefore be critical for interpretation of the modern North Atlantic Oscillation (Hurrell et al., 2003) and how this atmospheric system may have changed throughout the Holocene.

2.11 Climatic Indices - NAO

The North Atlantic Oscillation (NAO) describes the interaction of sub-polar low pressure, centring over Iceland and anticyclonic high pressure in the Azores (Hurrell et al., 2003, Wanner et al., 2001). The relationship between these pressure systems creates a sea level pressure (SLP) dipole between the North and the South Atlantic (Hurrell et al., 2003, Barlow et al., 1993, Hurrell and Deser, 2009). This SLP dipole drives air mass movement, controlling prevailing wind directions and rainfall over the European continent (Hurrell et al., 2001, Pena et al., 2010, Trouet et al., 2009, Hurrell and VanLoon, 1997, Jones et al., 1997). The NAO's effect is dominant during the boreal winter (Dec-Feb), representing the major cause of seasonal to inter-decadal variability in Northern hemisphere atmospheric circulation and climate (Wanner et al., 2001, Hurrell, 1995, Hurrell et al., 2003, Hurrell et al., 2001).

2.11.1 Phases and Effects

The NAO Index is created by normalising the seasonal pressure difference between weather stations in The Azores and Iceland (Figure 2.14), and can be described as being in a positive or negative phase (Jones et al., 1997, Wanner et al., 2001, Hurrell and Deser, 2009)

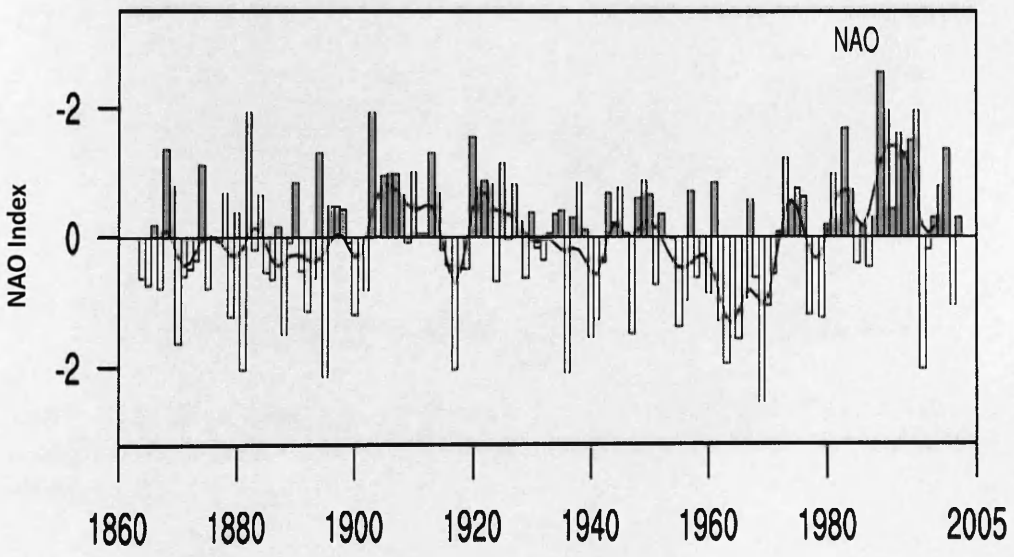

Figure 2.14: Index showing positive and negative fluctuations in the NAO (Hurrell et al., 2003).

Positive phases occur during periods of high pressure over the Azores and low pressure over Iceland (Hurrell et al., 2003, Hurrell et al., 2001, Wanner et al., 2001). Counter clockwise rotation of low pressure systems to the north and clockwise rotation of high pressure to the south create strong westerly winds over central and northern Europe (Hurrell and VanLoon,

1997, Barlow et al., 1993, Hurrell, 1995, Jones et al., 1997, Hurrell and Deser, 2009). Westerly winds lead to cool summers and warm wet winters in the north, and cool dry winters and dry summers in the south (Jones et al., 1997, Hurrell and Deser, 2009).

Negative NAO phases are associated with weak low pressure systems over Iceland and weak high pressure systems over the Azores (Hurrell et al., 2001), bringing colder winters and hot summers to the north of Europe and wetter conditions in central and Southern Iberia (Pauling et al., 2006). NAO phase changes manifest as variations in rainfall amount (Roig et al., 2009, Vicente-Serrano and Cuadrat, 2007) and therefore oxygen isotope ratio in areas of Northern Iberia which have exhibit a strong rainfall amount effect; making palaeorecords from this region ideally suited to recording long term NAO change, and quantifying its influence on regional climate (Moreno et al., 2010, Hurrell and Deser, 2009).

2.11.2 Instrumental records

Weather station records enable the NAO Index to be calculated until the 1860's (Figure 2.15) (Jones et al., 1997).

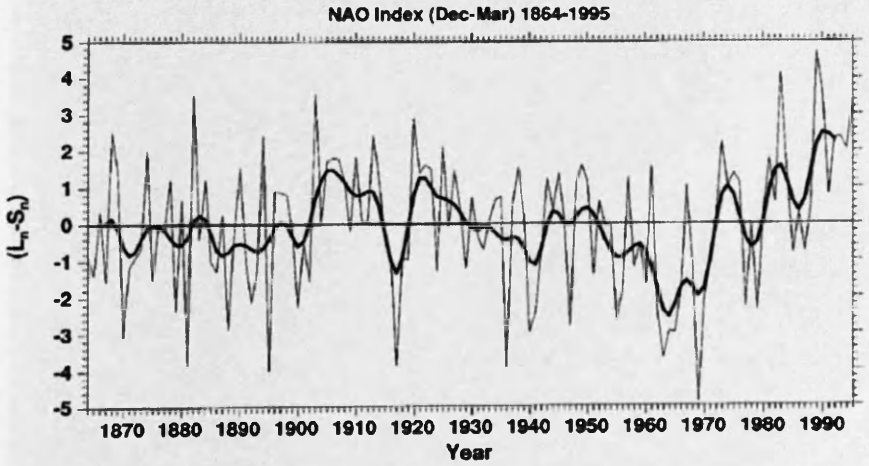

Figure 2.15: NAO index using normalised SLP for Lisbon and Stykkisholmur, a predominately positive trend is clearly evident from 1970 - 2000 AD (Hurrell and VanLoon 1997).

Positive and negative NAO phases during the 20th century correlate well with climatic variations, highlighting the NAO's role as a major controlling factor in European climate (Hurrell and VanLoon, 1997, Wanner et al., 2001, Semenov et al., 2008). Fluctuation between positive and negative NAO index occur with a 6-10 year periodicity during the latter half of the 20th century (Hurrell and VanLoon, 1997, Proctor et al., 2002, Appenzeller et al., 1998, Black et al., 1999, Proctor et al., 2000). These fluctuations however, occur during a time of

rapid anthropogenic change, with some studies suggesting modal fluctuations are controlled by factors external to the natural atmospheric system (Semenov et al., 2008, Hurrell and Deser, 2009).

However, using modern GNIP site data Baldini et al., (2008) show that central Europe and the northern Iberian cost line have a significant (p> 0.1) correlation (0.4; spearman's rank) between the winter NAO index (December, January, February, March) and rainfall $\delta^{18}O$ (Figure 2.16). This significant correlation indicates that northern Iberia is well suited for the production of NAO records which are reflected as changes in rainfall $\delta^{18}O$.

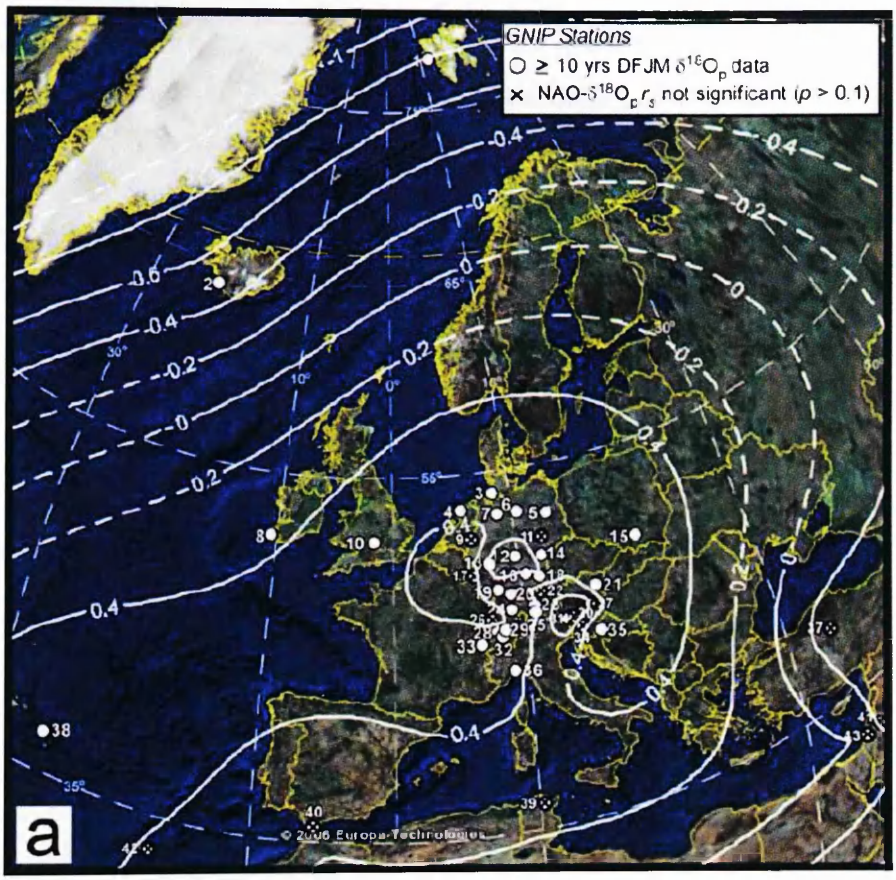

Figure 2.16: Contour map of Spearman's rank correlation coefficients (r_s) between winter (December, January, February, March; DJFM) NAO index and DJFM ($\delta^{18}O$) from 43 GNIP stations with ≥10 years of complete DJFM $\delta^{18}O$ data.

2.11.3 Palaeorecords of the NAO

Palaeoclimate and environmental records which record an NAO signature are primarily derived from lake (Trouet et al., 2009), ocean (Olsen et al., 2012), ice (O'Brien et al., 1995) and speleothems (Proctor et al., 2000) cores and can be used to extend currently available

instrumental data on NAO phase. These climate records can be analysed for a large range of proxies, often unique to the record being used. However, the accurate analysis of proxies can offer indirect evidence of the NAO e.g. evidence of enhanced sea storm conditions recorded as an increase in sea salt sodium flux ice cores, related to intense positive NAO conditions (O'Brein et al., 1995). A spatial range of palaeoclimate records (for example throughout Europe) related to the NAO can therefore be used to understand changes in NAO phase during major climatic events, and possibly aid our understanding of how the NAO may have contributed to climatic conditions (rainfall intensity or temperature) during those events (Appenzeller et al., 1998, Semenov et al., 2008, Trouet et al., 2009, Olsen et al., 2012).

Most high resolution records suggest the NAO played a role during middle to late Holocene climate change, throughout Europe (Trouet et al., 2009, Barlow et al., 1993). Mojtahid et al., (2013) have identified millennial scale fluctuations in the NAO from ocean cores extracted from the northern coast of Spain. These cycles in NAO style atmospheric positioning indicate the NAO has exacted a strong control over climate variability throughout Europe during the Holocene. However, the majority of Holocene scale NAO records breakdown during the early Holocene possibly due to the existence of major ice masses in the northern hemisphere (Giraudeau et al., 2010). This breakdown in NAO forcing during the YD and early Holocene either indicates that the NAO did not develop as a major climatic force until the mid Holocene or that current records of the NAO are poorly resolved / positioned to record a long duration NAO signal. The formation of longer duration, NAO sensitive palaeorecords may help to identify when the NAO began to control European climate.

2.11.4 Speleothems

Due to their sequential growth and long growth duration, speleothems offer an ideal archive type to record a long duration NAO signal. Production of high resolution speleothem records of the NAO relies however, upon having a suitable cave site. Baldini et al. (2006b) suggest the following criteria: 1) high amplitudes in the meteoric water $\delta^{18}O$, 2) strong comparison between meteoric $\delta^{18}O$ and NAO index (Baldini et al., 2008), 3) minimal retention of water in soil and karst zones, and finally 4) high speleothem growth rates. Several speleothem studies have reproduced a long term (< 3000yrs) records of NAO using speleothem growth layer thickness, which indicate changes in the hydrological system related to the intensity of precipitation driven by the NAO (Proctor et al., 2000, Proctor et al., 2002, Jackson et al., 2008. Accurately assessing annual growth layer width is however, complex and often inaccurate. Therefore, in cave sites such as those identified by Baldini et al. (2006b), high

resolution analysis of chemical proxies preserved within speleothems should be undertaken, many of which may be able to offer insight into changing hydrological conditions and therefore variations in the NAO.

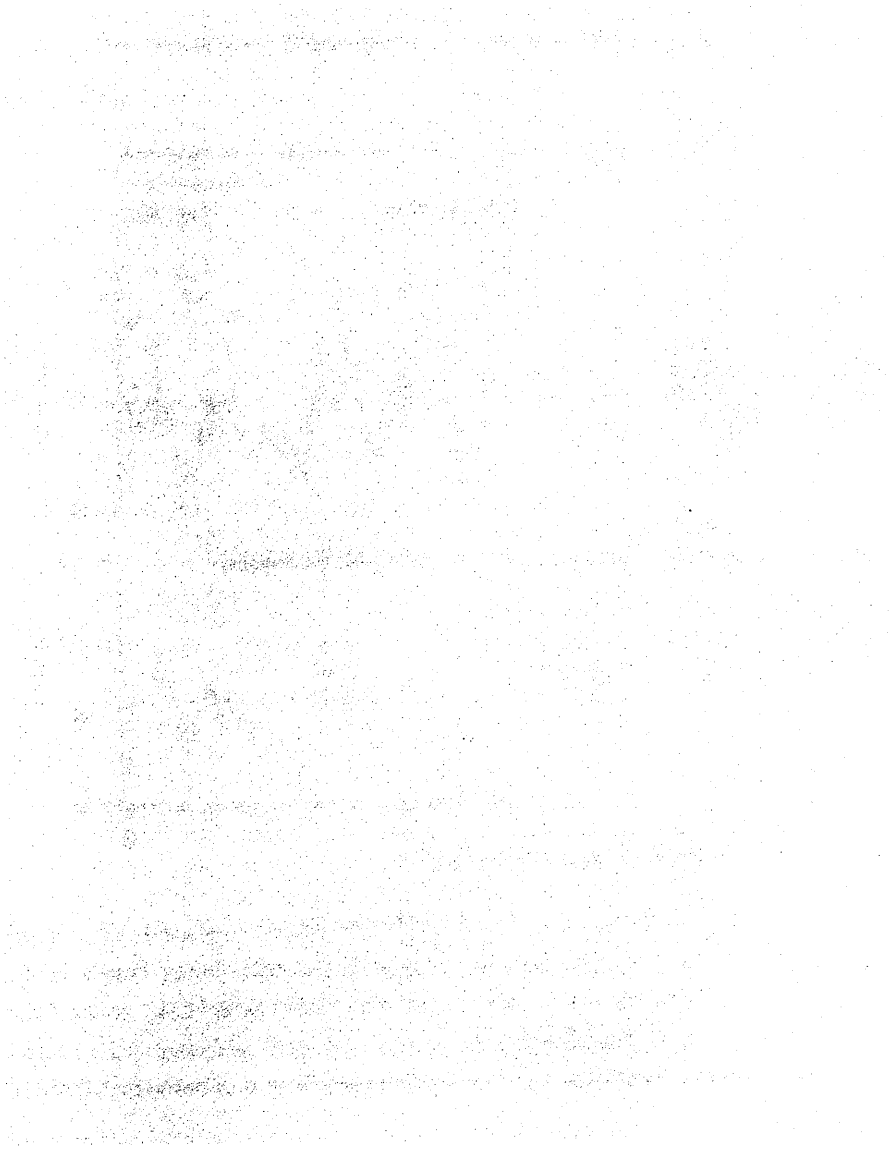

2.12 Climatic Indices – Oceanic Bond Cycles

Alongside major millennial scale Holocene cycles of the NAO, millennial cycles have been observed in North Atlantic Ocean sediment cores. These "Bond cycles" are cold periods observed throughout the Holocene in climate records; originally documented by Bond et al., (1997) and (2001). These papers used peaks in fresh volcanic glass (FVG) or hematite stained grains (HSG) to identify the southward and eastward advection of water from the Nordic and Labrador seas. Increases in FVG and HSG indicate the presence and melting of icebergs which originated in Iceland or Greenland and could only reach the southerly ocean coring sites during colder conditions. There are nine cooling events described during the Holocene (Figure 2.17).

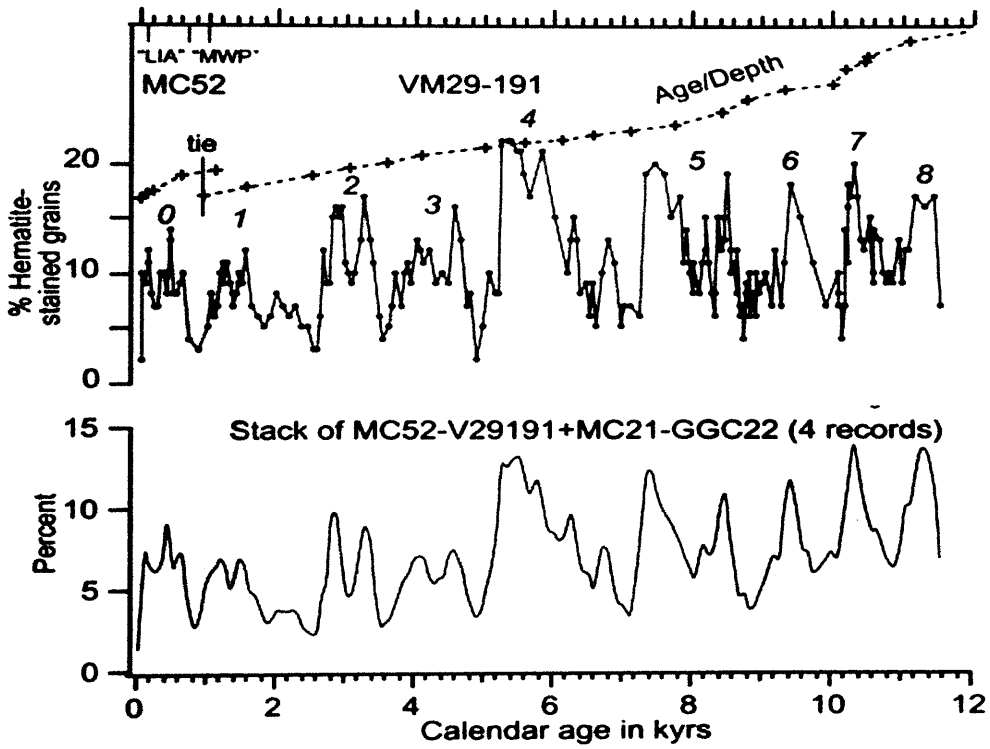

Figure 2.17: Holocene record of drift ice (as percent variation in lithic grains; Bond et al., 2001). Upper panel – the percentage of hematite stained grains in the 63-150μm range from cores MC52 and VM29-191. Lower panel – a combined stack of all petrologic tracers (HSG and FVG) from all 4 core sites in the North Atlantic (MC52, V29191, MC21, GGC22) presented as a percentage variation in the petrologic tracers.

Whilst attributing a single explanation as to the origin of these cooling events is complex (Wanner and Butikofer 2008), these events can be observed in ocean cores throughout the Holocene, with a frequency of 1500 ± 500 years (Bond et al., 2001). The regular pacing of

these large oceanic events suggests some climate modulation which promotes phase changes in the ocean system. Current explanations for these Bond events invoke external solar forcing and/ or atmospheric / ocean coupling to cause such large changes in ocean cores.

2.12.1 Solar Forcing

For the North Atlantic region, reductions in SST were originally linked to reductions in solar activity and a related reduction in NA deep water formation (Bond et al., 2001). Modern spectral analysis and modelling suggests however, that these 1500 year cycles are either forced by a combination of prominent 83, 280, 1000, 2500 and 6500 year solar cycles (Wanner et al., 2008, Dima and Lohmann 2009, Sejrup et al., 2012) or due to an internal ocean 1500 year cycle which became dominant in the past 8400 years (Debret et al., 2007, Debret et al., 2009, Thornalley et al., 2009, Sorrel et al., 2012).

2.12.2 Atmosphere - Ocean Coupling

Interactions between large atmospheric systems such as the NAO and the ocean surface have the power to regulate oceanic circulation and therefore the delivery of cold ice baring waters into the North Atlantic Ocean (Giraudeau et al., 2010). An intense positive NAO mode can act to strengthen the sub polar gyre forcing the southerly outflow of ice baring waters into the north Atlantic (Solignac et al., 2006, Staines-Urias et al., 2013, Sorrel et al., 2012). Such restructuring would result in a positive coupling of Ice rafted debris (IRD) events (Bond et al., 1997) and positive NAO phases (Fletcher et al., 2013). The production of strongly coupled ocean and atmospheric records is therefore fundamental to aid our understanding of cause and effect relationships which may exist between these global systems.

The previous sections have shown that Holocene climate was not, as first thought, intrinsically stable. Large scale climatic fluctuations marked this most recent transition from stadial to interstadial conditions. Solar cycles propagated a warming climate, whilst internal feedback mechanisms and catastrophic events regulated the range and scale of climate change. Regional response to climate variations is dictated by geographical location and atmospheric circulation, meaning no Holocene event had a single global outcome. Mechanisms of change operate on varying scales, both temporally and spatially and cycles of climate variability are still not fully understood. Holocene climate is however, known to be modulated by millennial scale climate fluctuations, including the NAO and 1500 year Bond cycles. More work is required to understand possible external (solar) modulation of the

atmosphere and oceans and to understand millennial scale coupling of these systems. To this end, high resolution regional archives are required from regions which are sensitive to variations in global atmospheric and ocean systems, both to help understand past climate changes and to help model natural climate fluctuations which may occur alongside modern anthropogenic climate change.

2.13 Summary

The accurate reconstruction of past climates is fundamental to our understanding of global systems and modern climatic change. Palaeorecords are essential for the accurate quantification of climatic processes, including modern global warming. Palaeoclimate reconstructions require high resolution, reliable proxies from a wide range of locations and on differing temporal scales. Traditional records mainly originate from Polar or maritime locations, but as climate changes are known to be globally uneven, more regional scale terrestrial records are fundamental to developing an interconnected understanding of Earth's oceanic and atmospheric systems and their forcing mechanisms.

Chemical analysis of speleothem carbonates offers one alternative long duration, high resolution archive with a robust technique for chronology production. Speleothems have been used to reconstruct many climatic and environmental parameters, including regional rainfall dynamics, temperature, prevailing wind direction and vegetation change. The chemical proxies stored in speleothems are artefacts of palaeoclimate and the karst and cave environments in which they are deposited. The speleothem record must therefore be interpreted carefully, alongside other available palaeoclimate information and modern monitoring. Future developments in chemical analysis will only act to increase the usefulness of speleothem deposits for climate reconstruction purposes. Speleothem studies should now target regions known to be critical during climatic changes, to help extend our knowledge regarding the impacts of climate change on terrestrial environments.

3. METHODS

3.1 Site Description and Monitoring Overview

3.1.1 Regional Setting and Geology

Asiul Cave (285 masl.) is located in the Matienzo depression (43°31'N, -3°58'W), 40 km inland from the Northern coast of Iberia, in the province of Cantabria (Figure 3.1 and Figure 3.2). The Matienzo valley is a ~28^2 km closed karstic depression (polje) situated in the Cantabrian Cordillera, the western most extension of the Pyrenees mountain range (Quin 2010).

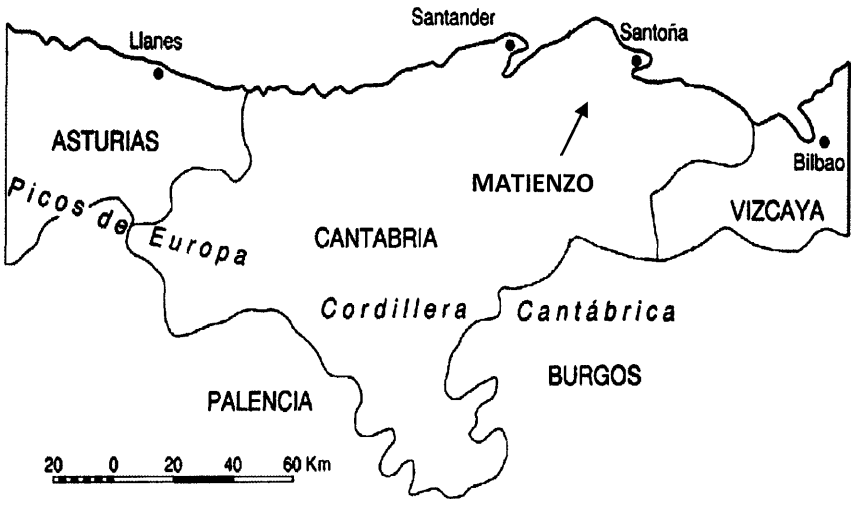

Figure 3.1: The approximate location of the Matienzo depression in relation to the northern Iberian coast and the closest GNIP site located in Santander.

The depression is formed in a Y shape with three distinct 'arms'; to the west is La Vega, to the north is La Sacada and to the south east is Ozana (Figure 3.2). This shape is derived predominately from the preferential dissolution of the east/west anticline which makes up the La Vega and Ozana arms of the depression. Anticline development occurred during a the formation of the Prynees in the early to mid Tertiary, as a result of Mesozic rocks thrusting southwards into the tertiary basins of the Duero and Ebro (Quin 2010). The slope of this anticline determines the general dip of the sediments that make up the northern and southern slopes of La Vega valley, although the geology can become more complex on a local level.

The hydrological catchment of the depression ranges in elevation from its lowest col at Cruz Usano (347 m) to the peaks of the Sierra de Mullir (839 m) (Quin 2010). The depression floor

covers approximately 4.5^2 km and has an average elevation of between 150 and 250 m.a.s.l. Whilst the vertical development of the depression has been primarily through karstic dissolution processes the current valley floor rests on an impervious layer of Barremian sandstones and marls, allowing rivers to flow overland through La Vega and out of La Secada (Figure 3.2).

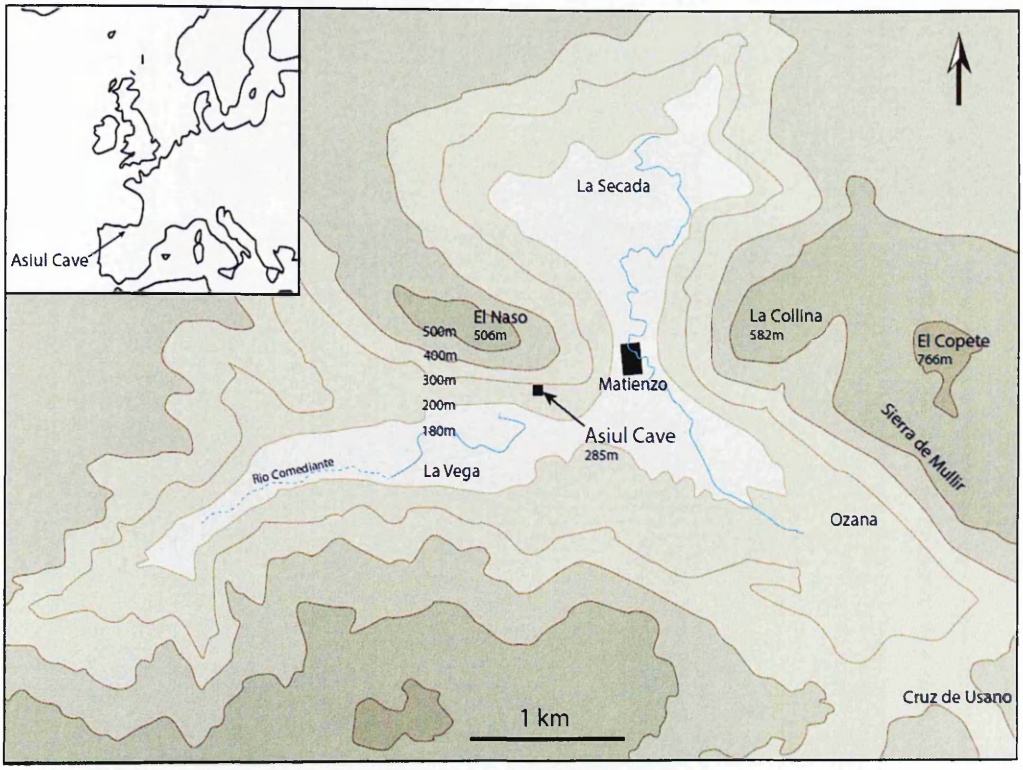

Figure 3.2: Map of the Matienzo depression showing the altitude of major features as well as the positioning of Asiul cave in La Vega and its proximity to the village of Matienzo where event based rainwater collection was undertaken. Inset map shows the approximate location of the valley in a European context.

Overlying the sandstones and marls are thinly bedded Aptian (112-124 Ma) limestone's which contain lenses of sandstone. Over which lay generally massively bedded Albian limestones (97 – 112 Ma) and the slightly younger more thinly bedded upper Albian limestones (Figure 3.3) (Quin 2010). These higher elevation sequences often outcrop as sheer cliff faces such as those above Asiul cave at the summit of El Naso.

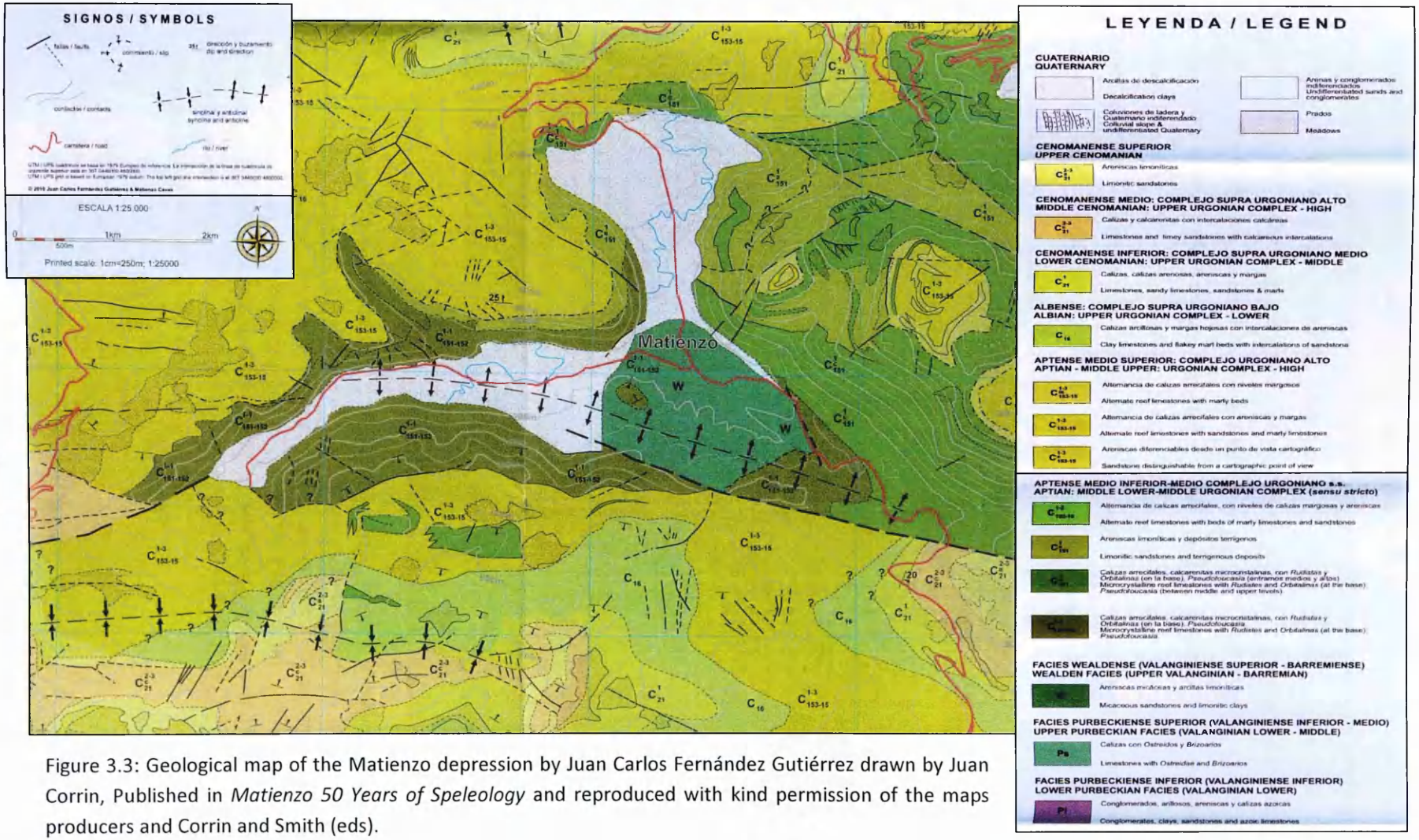

Figure 3.3: Geological map of the Matienzo depression by Juan Carlos Fernández Gutiérrez drawn by Juan Corrin, Published in *Matienzo 50 Years of Speleology* and reproduced with kind permission of the maps producers and Corrin and Smith (eds).

Modern land use in the valley consists of low intensity, mainly substance farming using traditional techniques. The more productive, flat valley floor is used for crop production predominately grass for use as animal fodder and cattle /donkey grazing (Figure 3.4a). The higher steep slopes of the depression are often covered with loose outcropping limestone and are therefore not suitable for crop production (Figure 3.4b+c). These slopes are occasionally used for very low intensity goat or donkey grazing. Vegetation in these upper slopes (including that around Asiul) remains largely unmodified by modern human habitation. These slopes have poor thin (~30-100 cm deep) soils which support primarily of shrub and grass communities (such as heather and bramble) common to the more mountainous regions of northern Spain.

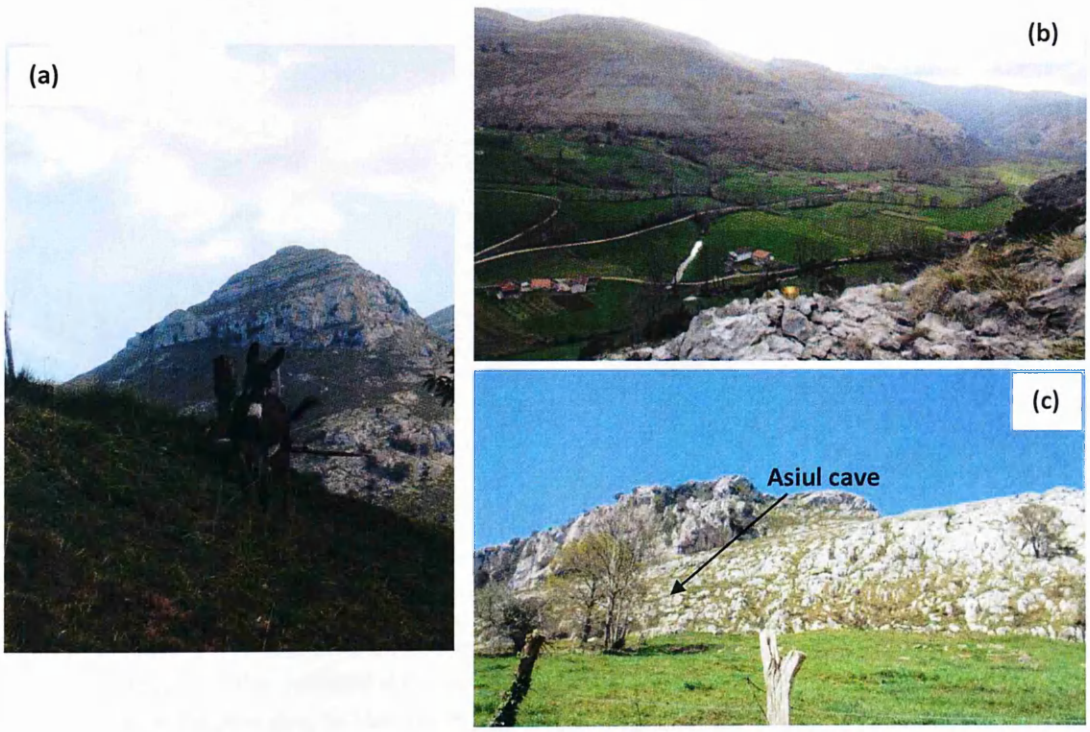

Figure 3.4: Images from Matienzo. a) one of the local farm animals, showing the more productive but still steep lower slopes of the depression, b) image across the La Vega arm of the depression, exposed limestone bedding can be observed on the southern slope of the valley, demonstrating how the valley incised through the pre-existing anticline, visible in the foreground is the Pluvimate rain gauge, c) a view up the slope of El Naso where Asiul is situated (approximate location shown) in the upper slope characterised by limestone outcropping.

3.1.2 Asiul Cave

Asiul is a small and uncomplicated cave system, with an approximate cave volume of 2.7 x 10^5 litres. The cave is horizontal, extending 75 m into the hillside below El Naso in a north westerly direction. Access is via a singular small entrance (<1.5m^2), followed by well sized passage, split by a series of larger chambers and ending in a boulder choke. No active streams exist within the cave but several large pools survive throughout the year, fed entirely by karst drip waters. Shallow rock overburden ranges from 10 to 40 m (Figure 3.5).

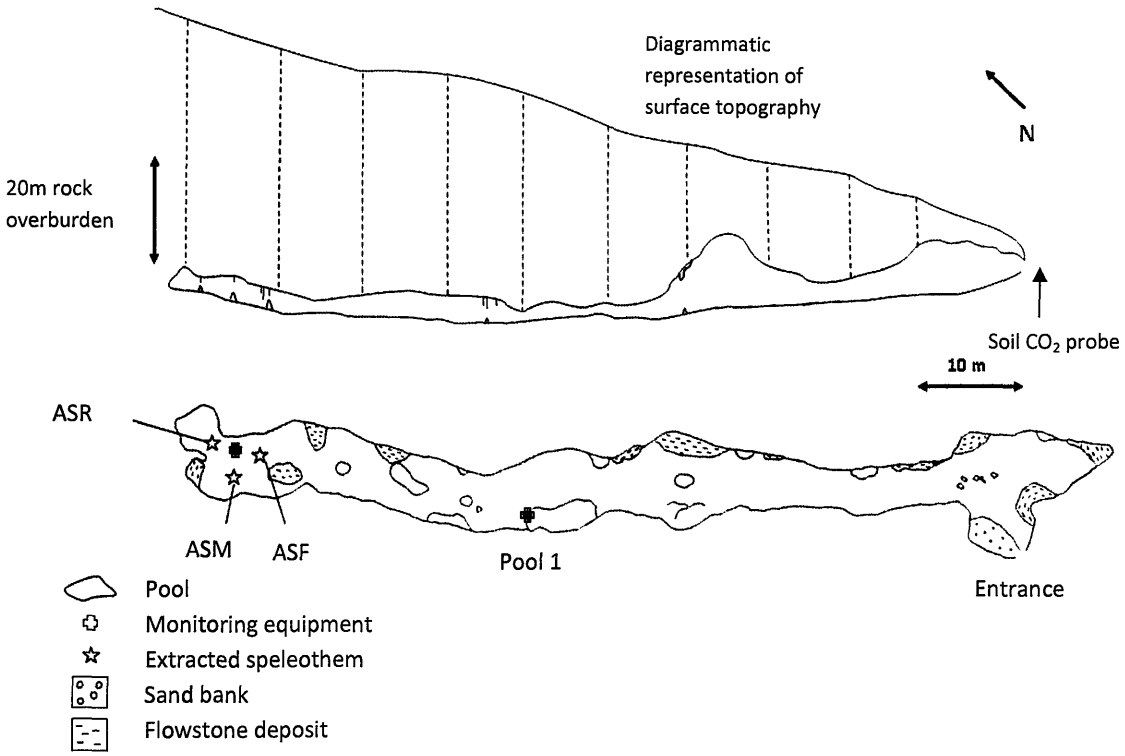

Figure 3.5: Cave survey for Asiul, including both a cross section to display passage morphology and the external position of the soil sampling device relative to the cave entrance and a plan view to identify monitoring locations. Monitoring equipment at pool 1 consists of 1 TinyTag Plus2 temperature and humidity logger. The 'main monitoring' location at the rear of the cave housed 2 TinyTag Plus2 temperature and humidity loggers (next to speleothem ASF), the CTD Diver (EC probe on speleothem ASF), a Vaisala CARBOCAP GM70 (CO_2 probe, suspended above speleothem ASF) and three Driptych acoustic drip rate loggers (one each on ASF, ASM and ASR). This was also the location for the majority of monthly monitoring, including monthly drip water collection and cave air $\delta_{13}C$ of CO_2 sampling.

Like many caves in the Matienzo region, Asiul was formed by limestone dissolution, under the ancient local water table. The cave entrance was subsequently exposed and the cave left dry by the continued dissolution of the depression floor and reduction in the local water

table. The cave appears to have undergone at least two distinct phases of development before final drying, with large calcite shelves being apparent mid way up the cave walls (Figure 3.6a+c); suggesting that the cave possibly formed during a period of water table fluctuation. The exact mechanism driving a change in local water table is unknown in this region, although it may be related to variations in past sea level and the effect this has on local water tables in mountainous regions.

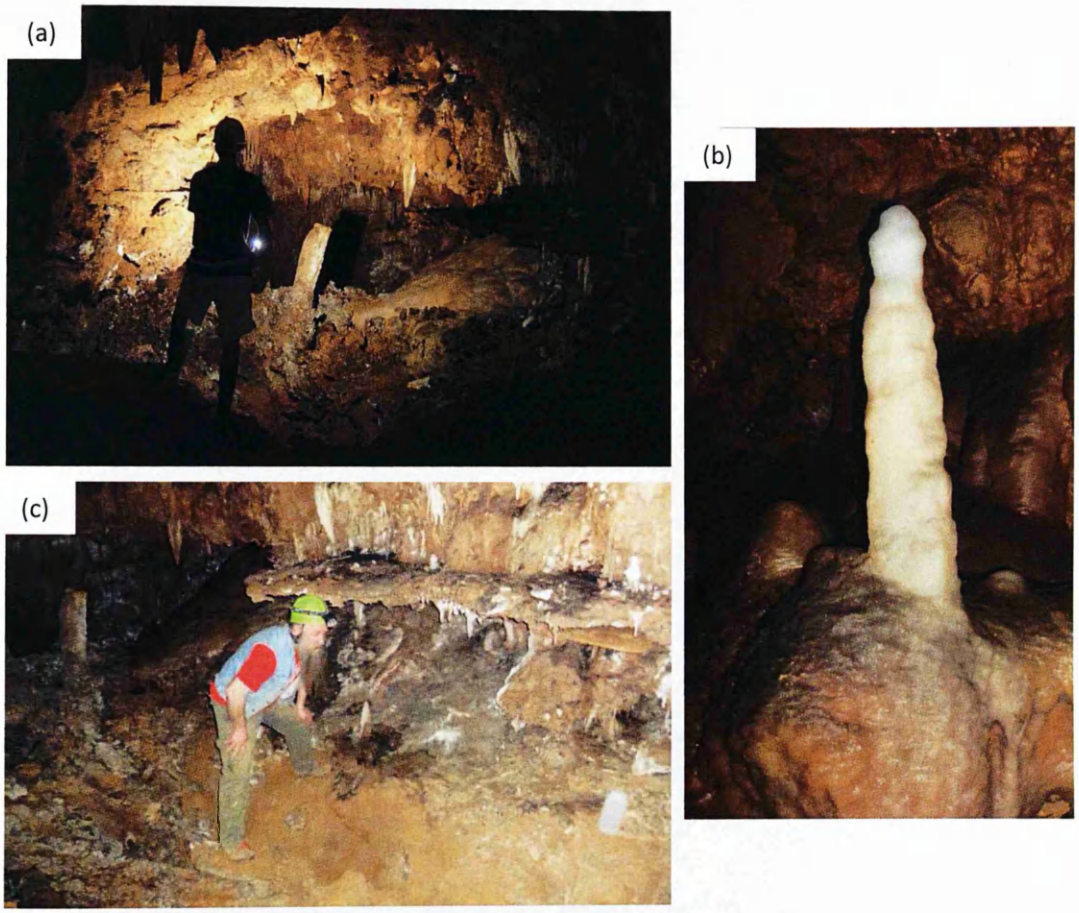

Figure 3.6: Images of Asiul cave. a) Cross section showing the phreatic shape of the cave passage and on the RHS an example of false floor development, b) speleothem ASM before sampling, c) more evidence of false floor development and varying stages of speleothem growth.

3.1.2.1 Speleothem Morphology and Structure

Asiul is well decorated, mainly with relatively small, ancient stalagmites and stalactites as well as few larger active flowstone deposits (Figure 3.6a+c). The rear chamber (main monitoring chamber) of the cave importantly housed three, actively growing, translucent, candle shaped stalagmites thought to be ideal for palaeoclimate reconstruction (ASF, ASM

and ASR), ASM is shown in its growth location in Figure 3.6b. These speleothems ranged between 20 and 35 cm in height and grew within a few meters of each other, fed by small straw stalactites. Two speleothems (ASR and ASF) were sampled using a coring device with diamond encrusted drill bit to minimise visual damage within the cave site, the third (ASM) was completely removed due to its awkward growth position. Only two samples (ASR and ASM) could be analysed for palaeoclimatic proxies due to analysis time / cost. Speleothem ASF was discounted after the sample was cut in half due to the existence and complexity of a drip channel which ran through the entire length of the core. Samples ASR and ASM did not display evidence of a similar channel and were therefore thought more suitable for initial analysis (Figure 3.7a and b).

Speleothem ASM (Figure 3.7a) totalled a length of 35 cm and is comprised of compact, initially translucent and then white columnar crystal fabric which elongate along the vertical growth axis (Kendall and Broughton, 1978, Frisia et al., 2000), this sample exhibits minimal evidence of growth banding throughout the sample length. Where relatively faint growth bands can be identified (Figure 3.7a) as an area of darker carbonate deposition, columnar crystal fabrics are seen to grow, without interruption through these bands (Frisia et al., 2000).

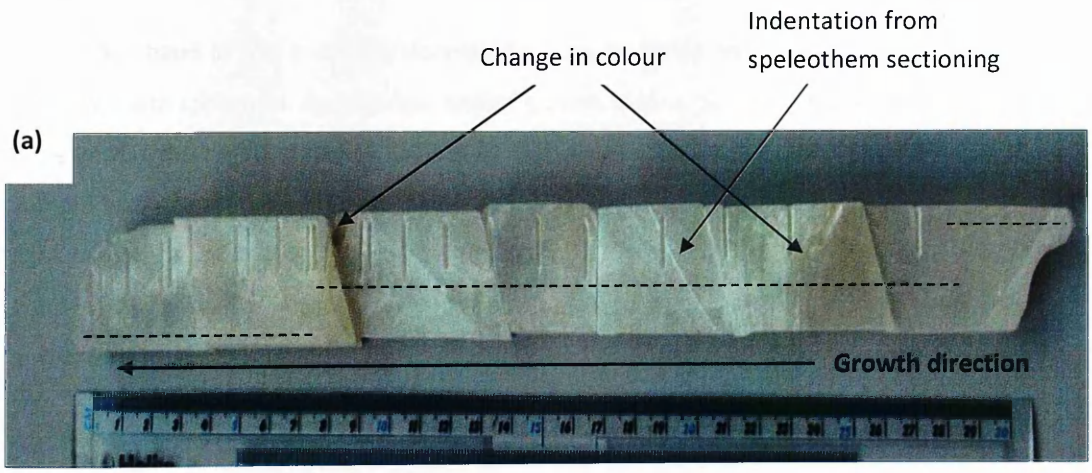

Figure 3.7a: The Central portion of speleothem ASM, divided into 7 sections to enable trace element analysis; rectangular pits denote the position of U/Th samples and dashed black lines the location of stable isotope analysis. The presence of two distinct colour changes is not marked by any change in columnar crystal growth, with crystals growing through these sections. These colour variations allow for the identification of the centre of the ancient speleothem, giving a guide for later stable isotope and U/Th analysis. Left to right lines which are visible in some sections of the picture are artefacts of speleothem sectioning not growth dynamics.

Speleothem ASR totalled 18 cm in length and is initially composed of compact translucent columnar calcite with crystals which elongate along the vertical growth axis (Figure 3.7b and Figure 3.8a; Kendall and Broughton, 1978, Frisia et al., 2000). This fabric structure breaks down in 2.5 cm from the speleothem top, broken by a band of darker microcrystalline fabric. The youngest section of the sample is characterised by white columnar crystal development with a greater number of inclusions than are seen in any other section of the sample.

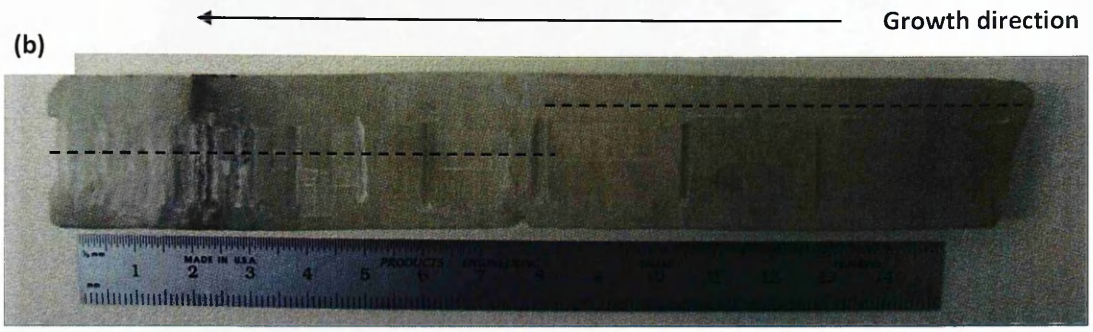

Figure 3.7b: Speleothem ASR is 18 cm in length, the position of U/Th drilling pits can be identified as can a clear dark band which formed during the mid Holocene 8-5 ka. The dashed black lines indicate the location of the stable isotope analysis track. A thin break can be seen in the centre of the image, this was caused during sampling but the speleothem can be re-joined using the remaining crystals, leaving a flat surface for analysis.

The darker band in ASR is initially denoted by a single darker line through which columnar crystal growth continues. As columnar crystal growth ceases, marked growth banding can be observed in the microcrystalline section of the sample (Figure 3.8). As this section of the sample was of particular interest it was analysed more closely using polarised and normal light magnification at NIGL, Keyworth, UK. Figure 3.8 clearly identifies the microcrystalline band in ASR, as well as crystal growth before and after this feature using a 10x magnification and polarising light filter.

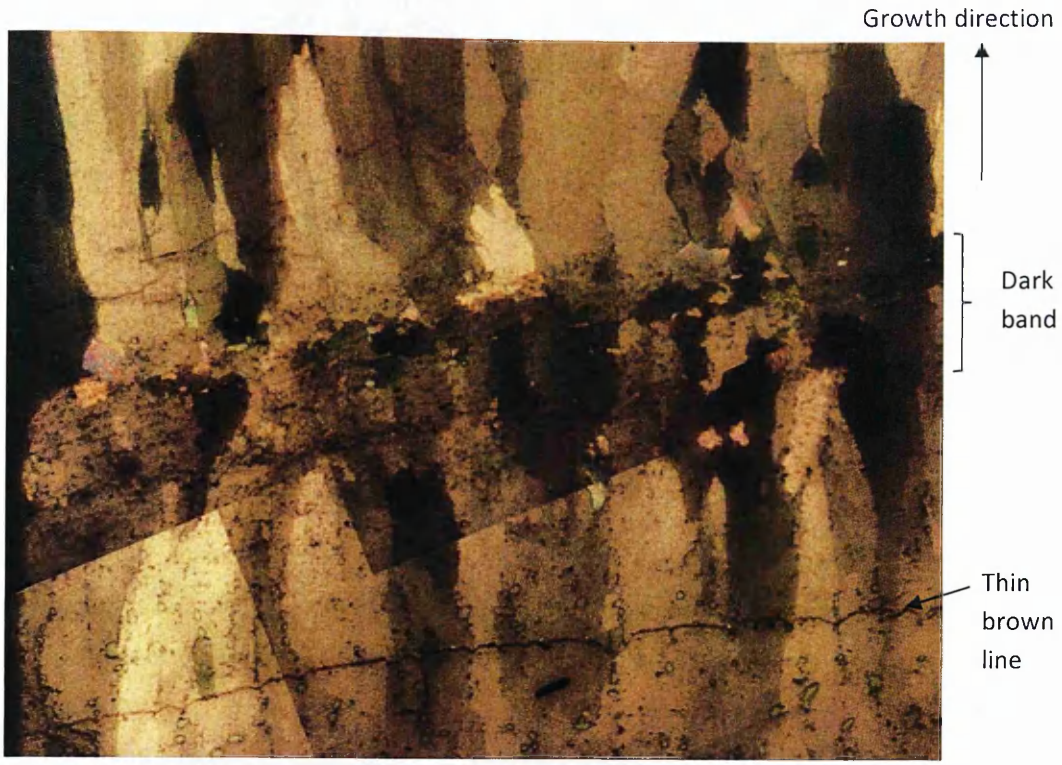

Figure 3.8) Stitched 10x magnification polarised light image of the dark band in ASR, this is initially characterised by a very thin brown band and then by a thicker microcrystalline section which appears to have a number of growth bands within it. Columnar crystal growth continues after this band.

In subsequent sections of the thesis (Chapter 6) this banding is identified as having occurred during the mid-Holocene (8-4 ka). Very slow carbonate deposition rates and the change in crystal structure during this period may identify this as a major growth hiatus, which is not uncommon in speleothems of this age from northern Spain (Stoll et al., 2013). However, comparison of trace element profiles from this period in ASR and ASM indicate some coherence between the records (displayed in Chapter 6), indicating that speleothem ASR grew enough during this period to accurately portray changes in hydrologically sourced trace elements. What appears clear form the analysis of the more rapidly growing ASM sample is that Asiul cave was hydrologically active during the mid Holocene but that speleothem growth rates in some sections of the cave were significantly reduced or ceased under dryer hydrological conditions (demonstrated by ASR). The mid Holocene is therefore highlighted as a period where careful climatic reconstruction must be undertaken, relying on the more rapidly growing ASM sample. This period must also be considered carefully when using stable isotope records as it is clear that speleothem growth conditions were considerably different than those which prevail in the cave today, possibly altering isotopic growth conditions.

3.1.3 Groundwater Catchment and Karst Hydrology

Ground water tracing was not undertaken as part of this study both due to time and equipment constrains but also to remove the possibility of foreign chemicals entering the cave system and complicating the drip water analysis program. However, a tentative reconstruction of the Asiul water catchment can be undertaken to assess the range of possible source water to this cave system.

Initial cave formation occurred under an ancient water table before valley incision exposed the cave entrance, meaning that Asiul has never been a major vadoes sink or resurgence cave. The lack of evidence for active stream ways at this site indicates relatively low levels of water throughput under modern conditions, driven only by water percolation through the bedrock above and below the cave profile. At this site, the underlying geology and the hill slope direction control where cave drip water is sourced. As the cave is situated on the south facing slope of El Naso it has developed in bedrocks which make up La Vega anticline, although the exact slope angle of the underlying geology is unknown it is relatively shallow 10-30° approximately dipping south – north (Figure 3.9). This dip on the underlying bedding plans should therefore promote the flow of water from its point of contact with the ground surface in a northerly direction until it intersects with the cave system.

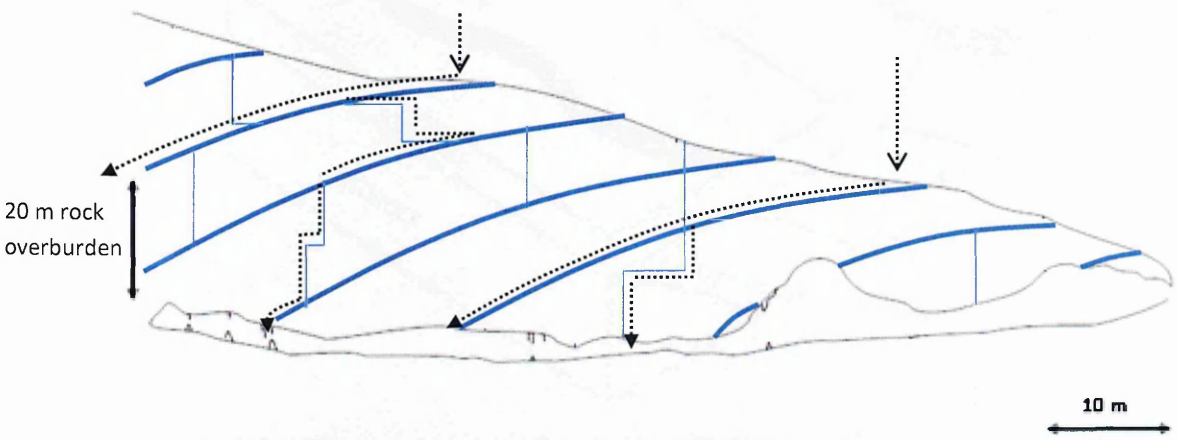

Figure 3.9: Diagrammatic representation of Asiul cave, the hill slope above the cave and the underlying geology with a slope between 10 and 30 ° (blue lines). Possible flow routing (black dashed lines) is identified from the point of rainfall impact on the surface to possible point of interaction with the cave profile. In most cases water percolation follows the slope of underlying geology and gravitational action.

However, the gravitational component of this system would work in the opposite direction allowing preferential movement downslope under gravity in a southward direction (Figure 3.9). The relative interaction of these two systems and the exact flow routing of water through the karst is unknown, however it is likely that the extent to which either karst geology or gravitational energy dominates water percolation depends upon the positioning and size of bedrock fractures, both micro (matrix flow) and macro (conduit flow). Possible mechanisms for water movement around Asiul are diagrammatically depicted in Figure 3.10.

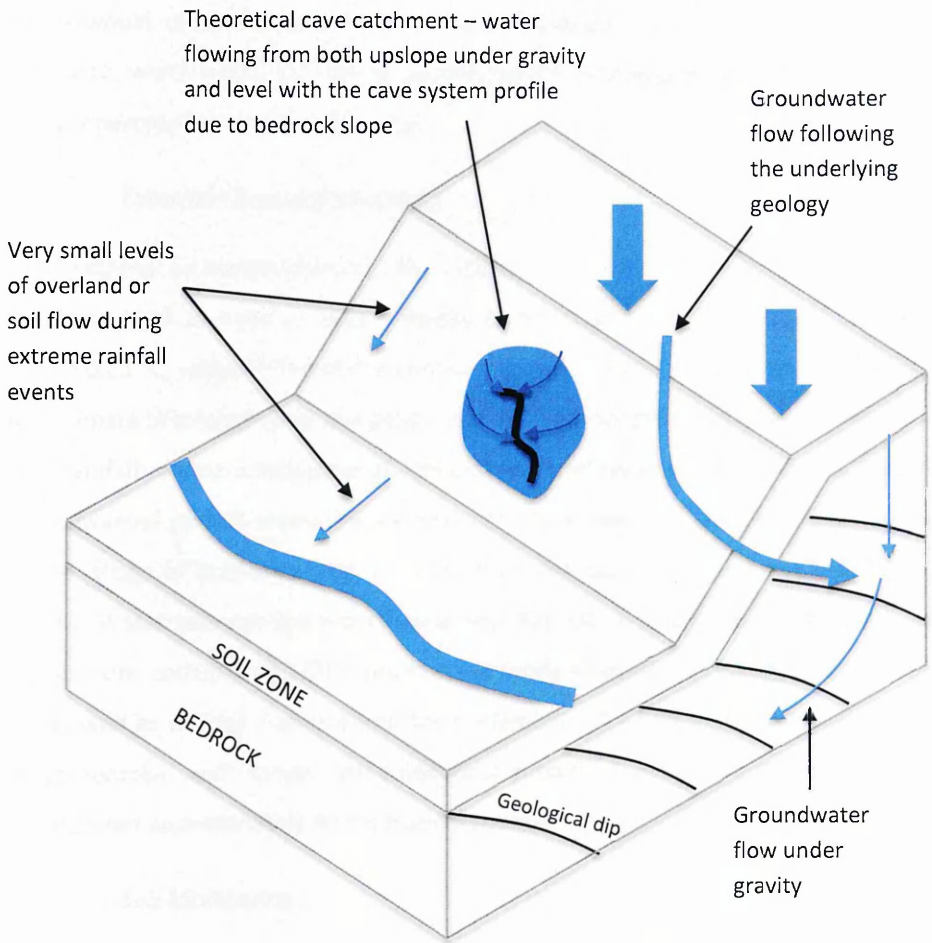

Figure 3.10: Possible routes of water flow on the southern slope of El Naso which acts as the groundwater catchment for Asiul cave. Water percolation is dominated by gravitational energy and the dip of underlying bedrock. The Asiul source area is limited to areas vertically above, horizontally adjacent to and possibly slightly below (due to the angle of underlying bedrock) the cave profile. On the scale of the hill slope the feeding area for cave drip waters is relatively small, reflected in the fact that Asiul has comparatively minimal levels of water movement and is obviously not a major source or sink of water.

Given to the relatively low levels of water which percolate into Asiul and the south – north dip on bedding plane geology the water catchment for this site would be limited to the hill slope directly adjacent to the cave location. Water percolation would be horizontal as well as vertical, suggesting a catchment area of a few 100 m^2, existing mainly upslope and directly above the profile of the cave and extending horizontally from the cave profile. The small source area means that all of the rainfall entering this cave site lands locally and there should therefore be no problem with mixed or complicated climatic signals which may occur if water karst sources come from very spatially different locations. However, to prove these conclusions would require an extensive tracer experiment. This is one possible area for future research, which would aid both in quantifying the hydrological catchment but also the rate of water percolation to major drip sites.

3.1.4 External Climate Monitoring

Since 2010 external air temperature has been logged using a TinyTag Plus2 logger, operating at a time interval of 10 minutes, with a measurement uncertainty of ±0.02 °C and limit of detection of 0.01 °C, within 250m of the entrance to Asiul Cave. Rainfall amount is measured using a Pluvimate drip logger and rain gauge at a different location within 100 m of the cave entrance. Rainfall volume is subsequently calculated based upon a rain gauge drip volume of 0.012 mm. Manual rainfall measurement and collection was also undertaken on an event basis in the village of Matienzo (approx. 2 km from the cave site), between Feb 2011 and March 2013. Water volumes were converted into mm using traditional equations. Rainfall subsamples were collected in HDPE bottles and were analysed for oxygen and hydrogen isotopes as well as cations / anions and trace elements. Rainfall monitoring data sets are used in conjunction with longer meteorological records from Santander meteorological station, which lies approximately 40 km from Matienzo.

3.1.5 Soil Monitoring

Soil monitoring includes temperature logging at a depth of 15 cm using a TinyTag TGP 4500 logger (April – Oct 2011) and instillation of a soil air sampling device (Figure 3.11), positioned at the transition between the base of the soil zone (50cm depth) and the epikarst enabled analysis for soil air pCO_2 and $\delta^{13}C$ (Jan 2012 onwards). Only one soil air extraction site could be set up (within 2 m of the cave entrance) due to restrictions in equipment availability and personnel time. This restriction may under sample spatial variations in soil zone productivity, but the relatively homogenous vegetation and soil cover surrounding the cave site means that any spatial variability is thought to be minimal. The extraction of soil gas for isotopic

analysis was undertaken using a small diameter silicon tube which extended to the far end of the CO_2 sampling device (Figure 3.11c). This small diameter tube allowed for gas extraction using a 30 ml capacity syringe, minimising any disturbance within the soil zone and reducing the risk of contamination with external air.

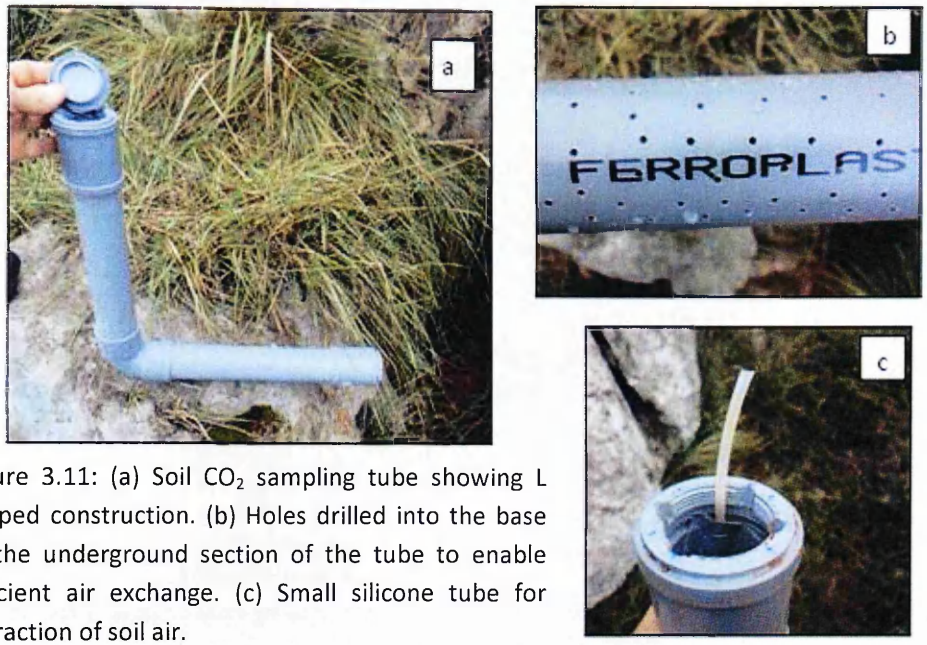

Figure 3.11: (a) Soil CO_2 sampling tube showing L shaped construction. (b) Holes drilled into the base of the underground section of the tube to enable efficient air exchange. (c) Small silicone tube for extraction of soil air.

Soil CO_2 concentrations were measured at the same time as gas extraction, using a Vaisala GM70 monitor and GMP221 probe with measurement uncertainty of ±2 % and operational range of 0 – 10,000 ppm. Readings were calibrated using a secondary probe at atmospheric levels. All readings were corrected to standard atmospheric pressure (1013 hPa) following Spötl et al., (2005) using Equation 3.1:

$$CO_2 \text{ (ppm volume)} = CO_2 \text{ (measured)} \times 1013/\text{pressure (measured)} \quad (3.1)$$

3.1.6 Cave Monitoring

Cave monitoring has been undertaken in Asiul since April 2010, with periodic enhancements being made to the suite of monitoring equipment within the cave. Monitoring consists of automated logging of cave atmospheric and hydrological components, field based water sampling and automated logging of external climate parameters. Monitoring parameters and equipment are summarised in Table 3.1.

Monitoring Parameter	Equipment	Logging Interval	Sensitivity / Accuracy	Start Date
Cave and external air temperature and RH. Soil temperature	Tiny Tag Plus2 TinyTag TGP 4500	30 mins	Temp – 0.01 °C RH – 3 %	19.04.2010 soil 04.04.2011
Speleothem drip rate	Stalagmate Mk 2+3	10 mins	0.15 ml drip at max 5/second	19.04.2010
Electrical conductivity	CTD Diver	10 mins	±1 % of reading	12.02.2011
H_2O temperature, EC and pH	WTW 350i probe	One off field measurements	Temp – 0.5 °C EC – 0.1 µm/cm pH – 0.01	19.04.2010
H_2O temperature, EC and pH	Hannah probe	One off field measurements	Temp – 0.5 °C EC – 1 µm/cm pH – 0.01	12.02.2011
Alkalinity	Hatch alkalinity test kit – AL-DT	One off field measurements	0.1 mg/l	3.11.2011
Cave and soil Air CO_2 concentration	Vaisala CARBOCAP GM70 and GMP221 probe	30 mins Soil – once/month	±2 % of reading 0-10,000 ppm range	12.02.2011 soil 10.11.2011
Cave air $\delta^{13}C$	Syringe and evacuated 12 ml exetainer	Once/month	0.15 per mille	10.11.2011
Drip water $\delta^{13}C$	Syringe and pre-acidified evacuated 10 ml glass vial	Once/month	0.15 per mille	08.12.12
External precipitation	Pluvimate Mk 1+2	10 mins	0.006 mm/hour	19.04.2010
Modern carbonate growth	Glass growth slide	-	-	19.04.2010

Table 3.1: Summary of monitoring procedures and equipment used for data collection in Asiul Cave.

The majority of monitoring in Cueva de Asiul focuses on 3 actively growing candle shape speleothems in a chamber toward the back of the cave, Asiul Front (ASF), Asiul Middle (ASM) and Asiul Rear (ASR) (Figure 3.5). These speleothems were chosen for detailed monitoring due to their internal location, active growth, constant water availability and suitable morphology for palaeoclimate analysis. Speleothem drip rates are logged using Stalagmate acoustic drip loggers (Collister and Mattey 2008) at each of these sites.

Cave air temperature, relative humidity and CO_2 concentrations were automatically logged at sub hourly intervals near these speleothem deposits (65 m depth into cave) whilst temperature and RH were also measured approximately half way through the cave system (45 m depth into cave). Cave air relative humidity was measured with minimal success due to moisture build up on the probe; suggesting relative humidity remains close to 100 % year round. Cave air CO_2 concentration was measured between Feb 2011 and November 2013 but probe malfunctions (possibly due to condensation) mean records from winter 2011 have been eliminated from the study. Monthly collections of cave air were undertaken for $\delta^{13}C$

analysis by injecting cave air into a pre-evacuated 12 ml glass vial following the same protocol as for soil air samples. All samples were analysed on delivery back to Lancaster University.

Hydrological monitoring included the sub hourly logging of Electrical Conductivity (EC) as well as bulk water collections; where 125 ml of cave drip water was sub-sampled for isotopic and trace element analysis from a well-mixed bulk vessel, which contained approximately one month's drip water. EC measurements were obtained using a "drip in, drip out" style housing for the CTD diver probe, ensuring constant submergence of the probe in drip water. The EC logging device was positioned on speleothem ASF in line with a Stalagmate drip counter and bulk collection device (Figure 3.12).

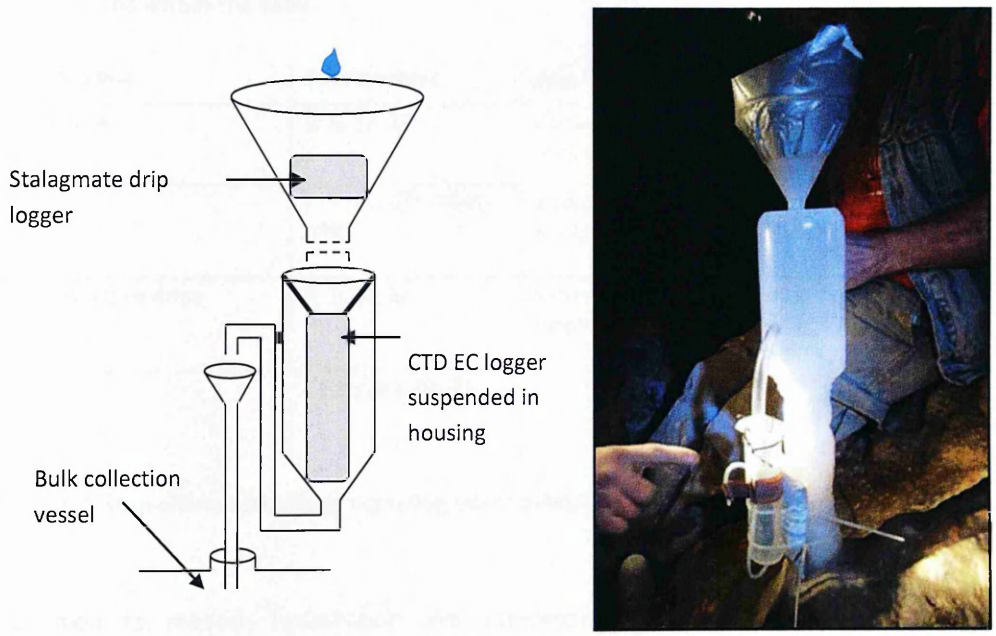

Figure 3.12: Diagrammatic representation of the monitoring equipment placed on speleothem ASF and photo of this equipment in situ.

Instant water collections of 10 ml (mean residence time approx. 1-4 hours) from the straw stalactites feeding speleothems ASF and ASR was also undertaken on a monthly basis, enabling isotopic comparison with bulk waters. The composition of instant samples showed little variation for most measured parameters from the longer residence time bulk samples.

Additionally, aliquots of bulk (and when available instant) drip water were collected for $\delta^{13}C$ of DIC analysis on a monthly basis, following the protocol of Spötl et al., (2005) and Frisia et al., (2011). Three drops of phosphoric acid were injected into a 12 ml evacuated exetainer. Approximately 3 ml of cave drip water was then added in the cave environment and samples

were immediately sent to Lancaster University for the analysis of carbon isotopes in CO_2 by isotope ratio mass spectrometry.

Secondary to monitoring at the major speleothem drip sites, drip water from fourteen other sites spaced throughout the cave was also collected during five different field trips from 2010 – 2012. These samples were analysed for isotopic values (^{18}O and ^{2}H) and trace element concentrations for comparison with the major speleothem monitoring sites. Drip rates and visual characteristics of associated carbonate precipitates suggest these sites reflect a range of discharge regimes (Table 3.2): 1) fracture flow feeding flowstone deposits, 2) constant slow drips with some rainfall response, 3) seasonally active drips with only minimal calcite saturation and no obvious speleothem development. Five pool sites were also monitored at varying depths within the cave.

Discharge Regime	Site Numbers	Drip Rate	Carbonate precipitation
1) Fracture flow	4, 5, 12, 13	Continuous – 5 seconds	Flow stone covering flow pathway
2) Slow drips	8, 9, 10, ASF, ASM, ASR	5 seconds – 5 minutes	Small flow stone deposits - candle shaped speleothems
3) seasonally active drips	6, 7, 11, 14	5 minutes to intermittent	Small candle shaped speleothems – no carbonate deposition
Pool site	P1, P2, P3, P4, P5	-	Seasonal calcite build up was identified upon the water surface

Table 3.2: Drip characteristics of sampling sites in Asiul Cave.

In addition to modern hydrological and atmospheric monitoring, carbonate growth experiments were undertaken within Asiul.

3.1.7 Calcite Growth Plates

Calcite growth plates (upturned 10 cm diameter watch glasses) were introduced into the cave system at several locations in 2010 and allowed to develop calcite until they were removed in 2011. Plates were located centrally atop actively growing stalagmite deposits using small sand bags. The crescent shape of the watch glasses was thought to best represent the growth surface of natural stalagmite deposits, and remove the possibility of un-natural water pooling, which may be associated with a flat glass plate. No attempt was made to undertake crystal seeding so it is possible that calcite growth was delayed (Tremaine et al., 2011). Once calcite growth had been visually identified, the calcite plates

were dried over a period of several hours within the cave environment, before removal. Plates were then sampled (calcite removed with a scalpel) at regular spacing across the width of calcite growth. Removed carbonate was analysed for O and C isotope co-variation. Small subsamples of plate carbonate and bedrock samples were also dissolved using 7 ml of 0.1M HNO_3 for 24 hours and subsequently analysed for trace elements using the same methodology as defined in section 3.2.1.1.

3.2 Laboratory Analysis

An overview of all laboratory work and associated results is presented in this section. Unless otherwise stated, the errors and machine limits of detection (LOD's) presented within this section encompass all subsequently presented geochemical results. Limits of detection, calibration ranges and Standard Deviation of repeats on standards (StD) are displayed for elements and isotopes where appropriate in (Table 3.3). LOD's are calculated either as mean blank value + 3 * StD of the blanks; or where the mean blank is negative, as three times the StD of all blank samples. In some cases repeat sample analysis has been undertaken following several different methodologies and using different instrumentation, in these cases all analytical techniques and LOD's are presented. Lab work has been undertaken at the NERC Isotope Geosciences Laboratory (NIGL) Keyworth, UK, Lancaster University, UK, The Centre for Ecology and Hydrology, Lancaster node, UK and Royal Holloway University London, UK.

Analyte	Substance	Instrument Model	Analysis	Calibration / Standard	LOD	StD
Ca	Water	Thermo Scientific iCAP 6000	ICP-OES	0-100000 ppb	36 ppb	12 ppb
	Carbonate	Agilent 7500ce/cs quadropole ICPMS	LA-ICPMS	NIST612	120 ppb	40 ppb
Mg	Water	Thermo Scientific iCAP 6000	ICP-OES	0-50000 ppb	6 ppb	2 ppb
	Carbonate	Agilent 7500ce/cs quadropole ICPMS	LA-ICPMS	NIST612	780 ppb	260 ppb
Na	Water	Thermo Scientific iCAP 6000	ICP-OES	0-10000 ppb	45 ppb	15 ppb
K	Water	Thermo Scientific iCAP 6000	ICP-OES	0-10000 ppb	63 ppb	21 ppb
Si	Water	Thermo Scientific iCAP 6000	ICP-OES	0-1000 ppb	8.2 ppb	2.7 ppb
Sr	Water	Thermo Scientific iCAP 6000	ICP-OES	0-1000 ppb	0.39 ppb	0.13 ppb
	Water	Thermo Scientific X-7	ICP-MS	0-100 ppb	0.75 ppb	0.25 ppb
	Carbonate	Agilent 7500ce/cs quadropole ICPMS	LA-ICPMS	NIST612	29 ppb	10 ppb
SO_4	Water	Thermo Scientific ICS 4000	Dionex	Spex Certiprep	159 ppb	53 ppb
NO_3	Water	Thermo Scientific ICS 4000	Dionex	Spex Certiprep	80 ppb	27 ppb
Cl	Water	Thermo Scientific ICS 4000	Dionex	Spex Certiprep	525 ppb	175 ppb
Mn	Water	Thermo Scientific X-7	ICP-MS	0-100 ppb	0.45 ppb	0.15 ppb
	Carbonate	Agilent 7500ce/cs quadropole ICPMS	LA-ICPMS	NIST612	36 ppb	12 ppb
Co	Water	Thermo Scientific X-7	ICP-MS	0-100 ppb	0.06 ppb	0.02 ppb

	Carbonate	Agilent 7500ce/cs quadropole ICPMS	LA-ICPMS	NIST612	50 ppb	17 ppb
Cu	Water	Thermo Scientific X-7	ICP-MS	0-100 ppb	1.1 ppb	0.37 ppb
	Carbonate	Agilent 7500ce/cs quadropole ICPMS	LA-ICPMS	NIST612	16 ppb	5 ppb
Y	Water	Thermo Scientific X-7	ICP-MS	0-100 ppb	0.009 ppb	0.003 ppb
	Carbonate	Agilent 7500ce/cs quadropole ICPMS	LA-ICPMS	NIST612	11 ppb	4 ppb
Ba	Water	Thermo Scientific X-7	ICP-MS	0-100 ppb	0.36 ppb	0.12 ppb
	Carbonate	Agilent 7500ce/cs quadropole ICPMS	LA-ICPMS	NIST612	8 ppb	3 ppb
Al	Carbonate	Agilent 7500ce/cs quadropole ICPMS	LA-ICPMS	NIST612	326 ppb	109 ppb
P	Carbonate	Agilent 7500ce/cs quadropole ICPMS	LA-ICPMS	NIST612	2039 ppb	679 ppb
Fe	Carbonate	Agilent 7500ce/cs quadropole ICPMS	LA-ICPMS	NIST612	50 ppb	17 ppb
V	Carbonate	Agilent 7500ce/cs quadropole ICPMS	LA-ICPMS	NIST612	78 ppb	26 ppb
Zn	Carbonate	Agilent 7500ce/cs quadropole ICPMS	LA-ICPMS	NIST612	54 ppb	18 ppb
Ce	Carbonate	Agilent 7500ce/cs quadropole ICPMS	LA-ICPMS	NIST612	7 ppb	2 ppb
Pb	Carbonate	Agilent 7500ce/cs quadropole ICPMS	LA-ICPMS	NIST612	11 ppb	4 ppb
$\delta^{18}O$	Water	VG Isoprime 100	IRMS	VSOW2		0.6 ‰
	Carbonate	VG Optima IRMS	IRMS	VPDB		0.08 ‰
δD	Water	VG Isoprime 100	IRMS	VSOW2		0.6 ‰
$\delta^{13}C$	Water DIC	Isoprime coupled to a Trace gas Pre-concentrator	IRMS	VPDB		0.15 ‰
	Air	Isoprime coupled to a Trace gas Pre-concentrator	IRMS	VDPB		0.15 ‰
	Carbonate	VG Optima IRMS	IRMS	VPDB		0.05 ‰
U	Carbonate	Agilent 7500ce/cs quadropole ICPMS	LA-ICPMS	NIST612	6 ppb	2 ppb
	Carbonate	Thermo Scientific Neptune Plus multicollector MS	MC-ICP-MS		600V of 238U per 1 ppm U solution	
Th	Carbonate	Thermo Scientific Neptune Plus multicollector MS	MC-ICP-MS		1200V of Th per 1 ppm Th soultion	

Table 3.3: Analysed elements and isotopes. Table includes analytical procedure, machine model, standard used / calibration range, StD and LOD's. Standard deviation (StD) refers to the StD of known standard materials (at least 2 duplicates run for all elements) and limits of detection (LOD) are calculated either as mean blank value + 3 * StD of the blanks; or where the mean blank is negative, as three times the StD of all blank samples.

3.2.1 Cave Drip and Rain Waters

All waters from the cave site, both rain and cave drip waters were collected and immediately sealed in new Nalgene plastic bottles (15, 50 and 125 mL). These bottles were completely filled, to eradicate problems with isotopic exchange between water and air within the bottle. In the case of waters which were analysed only for stable O and H isotopes, 2 mL clear glass vials with plastic septa screw caps were used for storage. These vials were also completely filled to remove the possibility of fractionation through evaporation.

3.2.1.1 Trace Cations, Anions and Metals

Cations, Calcium (Ca), Magnesium (Mg), Potassium (K), Sodium (Na), Silica (Si) and Strontium (Sr) were analysed in cave drip and rain waters at Lancaster University using inductively coupled plasma optical emission spectrometry (ICP-OES). Before analysis, all water samples were acidified in their collection bottles using ultra-pure (Primar grade) HNO_3 to create a 0.1 mole nitric acid solution. 7 mL subsamples were removed from the bottle for analysis on the ICP-OES. Samples were analysed alongside standard solutions made using 1000 ppm elemental standards, diluted into the expected concentration range for cave and rain waters. Elemental concentrations in the unknown samples were later calculated using calibration equations derived from these standard solutions. A secondary, independent multi-element standard was also diluted and run at discrete points throughout the analysis to verify the calibration curve, ensure machine stability and determine continuity between analysis sequences.

Anions, Sulphate (SO_4^{2-}), Chloride (Cl^-) and Nitrate (NO_3^-) were analysed at Lancaster University by Dionex Ion Chromatography on a 10 ml aliquot of unacidified sample. Samples were run alongside a custom produced Spex Certiprep water standard (WR1). A secondary standard WR2 was also used and is a 2x dilution of the original Spex Certiprep standard. Data processing was undertaken using Chromeleon software. Long term machine standard deviation is 0.3 mg/L of S for SO_4^{2-}, 0.75 mg/L for Cl^- and 0.025 mg/L of N for NO_3^-.

Trace metals, including Manganese (Mn), Cobalt (Co), Copper (Cu), Yttrium (Y) and Barium (Ba) were all analysed at Lancaster University using inductively coupled plasma mass spectrometry (ICP-MS). Before analysis all samples were acidified to a 0.1M HNO_3 solution using the same methodology as for ICP-OES analysis. Standards were calibrated to 100 ppb due to the low expected trace metal concentrations. Alongside standard solutions, an internal standard of Rhodium (Rh) was added into the unknown solution to enable an

assessment of machine stability throughout the run. Unknown sample concentrations (ppb) are calculated on-line based upon 7 (0-100 ppb) standard solutions and machine variance from Rh concentrations.

3.2.1.2 Stable Isotopes

During rainfall and cave water collection, 2 mL glass vials were filled without headspace for isotope analysis. Oxygen and Deuterium isotopes in waters were subsequently analysed at NIGL via Isotope Ratio Mass Spectrometry (IRMS) using an Isoprime 100 coupled to a Multiprep and EuroPyrOH. Duplicate unknown samples were run periodically throughout the analysis to ensure accurate sample replication. Both O and ^{2}H isotopes are reported against the also run VSMOW2 standard, with an average StD of 0.7 ‰ for ^{2}H and 0.05 ‰ for O during all analysis runs.

3.2.2 Soil and Cave Air

Soil and cave air samples were collected in pre-evacuated 12 ml exetainers with un-waxed caps and presented for $\delta^{13}C$ air analysis alongside cave drip waters processed to a headspace gas (see section 3.1.3). $\delta^{13}C$ in all samples was analysed at the NERC Life Sciences Mass Spectrometry Facility, Lancaster node, CEH Lancaster within 20 days of collection. Delta ^{13}C values of the CO_2 were then measured using a GV Instruments Tracegas Pre-concentrator coupled to an Isoprime IRMS. 4-8 µls of headspace was introduced into the injection port of the Pre-concentrator, where water was removed and CO_2 was cryogenically focused before entering the IRMS. Unknown CO_2 samples were compared to pulses of a known reference gas and reported as a delta value relative to the V-PDB standard. Within run StD based on the daily analysis of blank samples is better than or equal to ± 0.16 ‰. Tests to verify the stability of $\delta^{13}C$ in CO_2 over longer storage times have been completed by the NERC Life Sciences Mass Spectrometry Facility, Lancaster node, CEH Lancaster and are presented in Table 3.4 (A. Stott unpublished data). Tests used 2 x CO_2 standards (500 and 1000ppm) and analysed them following the procedure laid out above at weekly intervals for 35 days. Isotopic integrity remained intact for the duration of the experiment with sample StD's remaining within that (±0.16 ‰) quoted for the analysis of daily blanks.

500ppm CO_2 (days)	NO WAX	WAX
0	-30.62	-30.61
7	-30.55	-30.54
14	-30.35	-30.48
21	-30.38	-30.54
28	-30.35	-30.25
35	-30.29	-30.33
Average	**-30.42**	**-30.46**
Stdev	**0.13**	**0.14**

1000ppm CO_2 (days)	NO WAX	WAX
0	-28.31	-28.3
7	-27.91	-28.1
14	-27.92	-28.07
21	-28.01	-28.13
28	-28.16	-27.98
35	-27.99	-27.98
Average	**-28.05**	**-28.09**
Stdev	**0.16**	**0.12**

Table 3.4: 35 day exetainer degradation experiments, using 500 and 1000 ppm CO_2 standards and showing the isotopic ($\delta^{13}C$) composition of the analysed gas on a weekly basis.

3.2.3 Cave Carbonates

Cave speleothems were extracted from Asiul cave either as a core from the central growth axis, using a hollow centred drill bit; or as a complete specimen removed at the base. Coring was used on easily accessible speleothems with the aim of reducing visual damage to the cave environment. Where speleothems were less accessible complete removal was undertaken. Speleothem sections were then cut vertically down the central growth axis at the NIGL rock cutting facility. Pure H_2O was used as a lubricant during cutting to remove any chance of sample contamination with oil. One half of each speleothem core was used for destructive analysis. Where possible, the other half was kept as an archive.

3.2.3.1 Sampling Method and Stable Isotopes

Cave carbonate powders were milled from the flat central side of speleothem samples using an automated micro-mil drill at NIGL. Samples were drilled using a 0.3 mm diameter diamond encrusted dentist drill piece at a sampling resolution of 0.1 mm and depth of 0.2 mm. This sampling protocol created between 50 and 100 μg of powder for each sample, enough for stable O and C isotope analysis. Oxygen and Carbon isotopes were analysed at NIGL from the micro-milled carbonate powders, using a VG Optima Isotope Ratio Mass Spectrometer (IRMS) with manifold. Unknown samples were run alongside an in house carbonate (KCM) standard material with a standard deviation of better than 0.1 ‰ for both stable C and O isotopes. Isotopic values are reported as a delta value relative to the international VPDB standard.

3.2.3.2 *Trace Elements*

Trace element concentrations in speleothem carbonate were analysed using Laser Ablation Inductively Coupled Plasma mass Spectrometry (LA-ICPMS) at Royal Holloway University of London, UK. Speleothem sections were cut into smaller (max 50 x 50 mm) sections to fit into the sample holder and then polished using a fine grained diamond polishing substrate before mounting and analysis. The laser ablation system consists of a 193 nm ArF excimer laser (RESOlution M-50 prototype, Resonetics LLC, USA), coupled to a two – volume laser ablation cell (Laurin Technic, Australia). Following laser-based surface cleaning (pre-ablation; 50Hz, 5mm/min) laser data acquisition used a rectangular slit of 10 μm width by 140 μm length; at 1.5 mm/min and a laser repetition rate of 15 hz in continuous profiling mode. An approximate sample resolution of 37 μm is achieved, ideal for extremely high resolution analysis. Ablation is undertaken in a pure He atmosphere with continuous He flow to which H_2 (5 ml/min) was added as a diatomic gas and Ar (600 ml/min) is added as a carrier gas downstream of the LA cell (Stoll et al., 2012). Further specifications for the LA-ICPMS system are discussed by Muller et al., (2009). Speleothem slices were analysed for Mg25, Aluminium (Al27), Phosphorus (P31), Ca43, Vanadium (V51), Mn55, Iron (Fe57), Co59, Zinc (Zn66), Sr88, Y89, Ba138, Cerium (Ce140), Lead (Pb208) and Uranium (U238).

Samples were analysed alongside external standards National Institute of Standard Technology NIST SRM612, NIST10 and an internal glass standard KL2G. Ca was used as the internal standard and all sample concentrations are reported based upon a stoichiometric Ca concentration in $CaCO_3$ of 40 % m/m (Jochum et al., 2011) Trace element concentrations in the unknown samples were calculated using Equation 3.2.

$$C^x_{sample} = C^r_{sample} * C^x_{std}/C^r_{std} * i^x_{sample}/i^r_{sample} * i^r_{std}/i^x_{std} \quad (3.2)$$

Where C^x_{sample} is the unknown concentration of any given element in the sample, C^r_{sample} is the concentration of the reference element (Ca) in the sample (400000 ppm), C^x_{std} is the isotopic correction required due to isotopic abundance within the sample, C^r_{std} is the concentration of the reference element (Ca) in the standard, i^x_{sample} is the intensity (raw counts) of the unknown element in the sample, i^r_{sample} is the intensity of the reference element (Ca) in the sample, i^r_{std} is the intensity of the reference element (Ca) in the external standard and i^x_{std} is the intensity of the unknown element in the external standard.

3.2.4 U / Th Dating

Speleothem carbonate was also sampled for U/Th dating. An approximately 1 mm width, 10 mm length and 6 mm depth track was hand milled using a Como dentist drill for each U/Th date to produce enough powder (80 -120 mg) for analysis. Milling was undertaken using the same 0.3 mm diameter diamond encrusted drill bit as for O and C isotope sampling.

3.2.4.1 Sample Preparation

The samples are weighed and then dissolved using 15.5M purified and distilled laboratory grade nitric acid (HNO_3) from Romil Ltd and distilled water in Savillex PFA Teflon vials. After dissolution, samples were spiked with a high purity $^{229}Th/^{236}U$ tracer solution. Tracer solutions are made in house and calibrated gravimetrically against accurately weighed high purity U (CRM 112a) and Th (Ames National Laboratory crystal bar) metals dissolved in high purity HNO_3, Hydrochloric acid (HCl) and trace Hydrofluoric acid (HF). Samples were then allowed to equilibrate before they were oxidised using concentrated HNO_3 and Hydrogen Peroxide (H_2O_2). A high purity Iron Chloride (FeCl) solution in 1M HCl (prepared from high purity Johnson Matthey Puratronic Fe Nitrate) was then added. U and Th could then be co-precipitated out of solution with Fe oxides through the addition of ammonia. This precipitate is then isolated by centrifugation and washed in Milli-Q water to eliminate any unwanted sample matrix. This washing / centrifuge procedure is repeated 3 times to ensure sample purity.

Samples are then re-dissolved in 7M HNO_3 and loaded into 0.6 ml ion exchange columns containing Eichrom anion exchange resin (AG1 x 8). Any residual unwanted matrix elements including Fe were washed from the column using 8M HCl. Sample U is subsequently washed from the column. Th is finally re-processed through a second ion exchange column to enhance Th purity. Both U and Th fractions are dried and strongly oxidised with concentrated HNO_3 and H_2O_2, removing any residual organic impurities. Prior to mass spectrometry all samples were filtered through 0.22 micron Millipore PTFE syringe filters to eliminate particulate matter that could potentially plug the nebulizer tip.

Due to the extremely low concentrations of U and Th discovered within the first set of carbonate samples, subsequent sample preparations were undertaken using an Evapoclean system rather than the traditionally used HEPA filleted work station. The Evapoclean system consists of a large heating block housing small sub-boiling distillation units comprised of two Savillex PFA vials connected via a 90° PTFE elbow. Samples were placed in one vial connected

to the elbow and a second vial on the Evapoclean block. The acid matrix of U and Th fractions were distilled over the cold side of the system until only dry residue remained in the sample vial and all the acid had condensed into the secondary vial. This system ensured a much lower chance of sample contamination both from fall in contaminates and cross contamination during the final drying down stages.

3.2.4.2 Mass Spectrometry

Analysis by mass spectrometry was undertaken using a Thermo Scientific Neptune Plus multicollector ICP mass spectrometer (MC-ICP-MS). The mass spectrometer is equipped with 9 Faraday cups, two full size discrete dynode secondary electron multipliers (SEM's), 4 additional compact SEM's located on the low mass side of the Faraday cup array, and a retarding potential quadrupole (RPQ) energy filter. Samples were introduced using a Cetac Aridus II desolvating nebulizer which enables the indirection of samples dissolved in acid as dry aerosol particulates suspended in a stream of high purity Argon (Ar) and (Nitrogen) N_2 gas. Sample uptake was c. 50-70 microliters / minute controlled by an ESI low-uptake PFA Teflon nebulizer attached to the Aridus II.

U measurements were made with normal Ni-sample and X-skimmer cones mounted on the Neptune Plus. Resulting in U sensitivities in the order of 500-600 V of ^{238}U measured per ppm U in solution at an uptake rate of between 50-70 microliters / minute. Th measurements were undertaken separately using the JET-sample and X-skimmer cone combination, which gave higher sensitivities of c. 1000-1200 V/ppm at an uptake rate of between 50-70 microliters / minute.

Prior to unknown sample analysis, an in house standard (CRM 112a) was used to characterise the hydride production and down mass tailing on the Neptune Plus. Hydride production was measured by monitoring $^{238}U+H$ ions (mass ~ 239) on the axial SEM with ^{238}U in the L1 Faraday cup. The down-mass tailing was monitored at mass 237 in the axial SEM with ^{238}U in the H1 Faraday cup. During the course of this study, the hydride production was $\leq$ 3.5 ppm and down-mass tailing $\leq$ 2.5 ppm. The hydride and tailing corrections were applied to all measured data. Two types of on-peak zeros were also determined for the U and Th measurements. The first order correction was made using ^{234}U-^{235}U-^{236}U-^{238}U or ^{229}Th-^{230}Th-^{232}Th measured in the axial SEM (dynamic peak jumping) on clean acid identical to that added to the samples (0.2M HCl + 0.05M HF). This measurement yielded the contributions of U and Th from the sample introduction system. Finally, unknown sample U and Th isotope ratios where measured alongside standards on the Neptune Plus, using static

multicollector standard/sample bracketing protocols, with electronic baselines being measured before each sample and standard acquisition.

Sample ^{234}U was measured in the axial SEM with ^{235}U, ^{236}U and ^{238}U measured in the adjacent H1, H2 and H3 Faraday cups. Prior to sample analysis, several CRM 112a solutions spiked with a high purity ^{233}U-^{236}U tracer (IRMM 3636) were analysed to check instrument performance and to determine correction factors for instrumental mass fractionation. Following analysis of the spiked CRM 112a's, several unspiked CRM 112a analyses were obtained so that the SEM/Faraday calibration factor could be determined. Unknown samples were run in batches of 5 bracketed by spiked and unspiked CRM 112a solutions. Sample Th measurements were obtained in a similar manner to the U, with ^{230}Th measured in the axial SEM and ^{229}Th in the L1 Faraday cup, and ^{232}Th in the H2 cup. SEM/Faraday gain and instrumental mass fractionation correction factors were determined by analysis of an in-house reference Th solution calibrated against CRM 112a. The Th reference solution was made by adding high purity ^{229}Th to high purity ^{230}Th and high purity natural Th (mainly ^{232}Th) in the approximate proportions of 0.9:1:2000.

3.4.4.3 Data Reduction

An in-house Excel workbook is used to process raw mass spectrometer data and generate raw isotope ratios. Sample raw ion beam intensities on individual data integrations were corrected for hydride and down-mass tailing and on peak zeros. Isotope ratios based on these ion beam intensities were then calculated and corrected for mass fractionation and SEM/Faraday gain. The final corrected ratios were used to calculate mean and standard error for critical isotope ratios ($^{236}U/^{235}U$, $^{234}U/^{235}U$, $^{229}Th/^{230}Th$, $^{230}Th/^{232}Th$). These isotope ratios were then processed in an Excel spreadsheet using the Isoplot 3 add-in to yield the following: U and Th concentrations; measured U and Th activity ratios; activity ratios corrected for "detrital Th" contributions; $^{230}Th/^{234}U$ ages and uncertainties propagated from measurement uncertainties, spike calibration uncertainties and sample reproducibility.

Cave monitoring and lab based methodologies for research in Asiul Cave have followed comparatively standardised techniques to ensure a robust characterisation of the cave environment and speleothems extracted from this site. The following four chapters present the results and discussion from this work. The first two chapters focus on cave monitoring and how the Asiul system is best characterised under modern conditions; the second two chapters use our understanding of modern cave conditions to interpret speleothem archives.

4. CAVE HYDROLOGICAL DYNAMICS AND THE SPELEOTHEM RECORD

4.1 Introduction

Before the accurate interpretation of speleothem carbonate can be undertaken, with the aim of understanding past climate and environmental change, we must strive to fully understand the conditions within which speleothems have formed. One major component of interest is the hydrological system which operates above speleothem drip sites, this system controls water delivery to the cave, influencing speleothem growth rate and the delivery of elements which may be used for palaeoclimatic reconstruction.

Initial inputs of water to the hydrological system occur through regional precipitation; including both rainfall and occasionally snowfall at this site (the term rainfall is used rather than precipitation for the remainder of the thesis to remove confusion with calcite precipitation). Incoming rainfall caries a unique isotopic and elemental makeup, which can provide information about moisture source, trajectory and rainfall amount. This signature may subsequently be modified during rainout through the process of evaporation, dependent upon evaporative conditions within the air column.

Once rainfall contacts the ground surface it may undergo further evaporative effects or be removed from the hydrological system through transpiration. Rainfall that percolates into the soil and underlying karst constitutes the groundwater which is available to feed Asiul cave. This water is sourced locally to the cave system; its transport is dictated initially by the soil zone but very quickly by gravitational flow through the bedrock and the underlying geology of that bedrock. During this percolation, rainwater mixes with older stored karst waters and incorporates $CaCO_3$ and trace elements through bedrock dissolution. The final isotopic and trace element makeup of water entering the cave site is therefore a function of all its component parts and processes, including importantly: the initial makeup of rainfall, karst water mixing, bedrock dissolution and karst water routing.

Due to the complex nature of this system the following section aims to characterise the hydrological system above Asiul and identify the major controls over the isotopic and trace element composition of both incoming rainwater and cave drip waters, allowing the characterisation of karst influence over drip water elemental and isotopic composition and ultimately speleothem carbonate chemistry which may be used for climate reconstruction.

4.2 Regional Rainfall Dynamics

Event based rainfall collection undertaken in Matienzo for two years gives a temporal snapshot of rainfall dynamics in this location. This data set is used alongside longer time series from Santander meteorological station to help develop our wider understanding of regional rainfall and hydrology. The timing and delivery of rainfall is not only critical for above ground environmental development but, as rainfall is the main source of karst aquifer water it plays an important role in the development of cave systems and speleothems. Monitoring highlights how karst recharge in the region is seasonally sensitive, and indicates controls on speleothem chemistry.

Matienzo's close proximity to the Northern Iberian coastline and its mountainous location means that the climate is generally wet and mild. Total annual surface rainfall between April 2011 and March 2013 was approximately 1500 mm/year, with the majority falling in the winter months (October to March). This is higher than long term average data sets from the closest meteorological station to Matienzo, Santander (43°28'N, -3°48'W; 52 masl.) which receives ≈ 1050 mm/year (10 year average) (Figure 4.1).

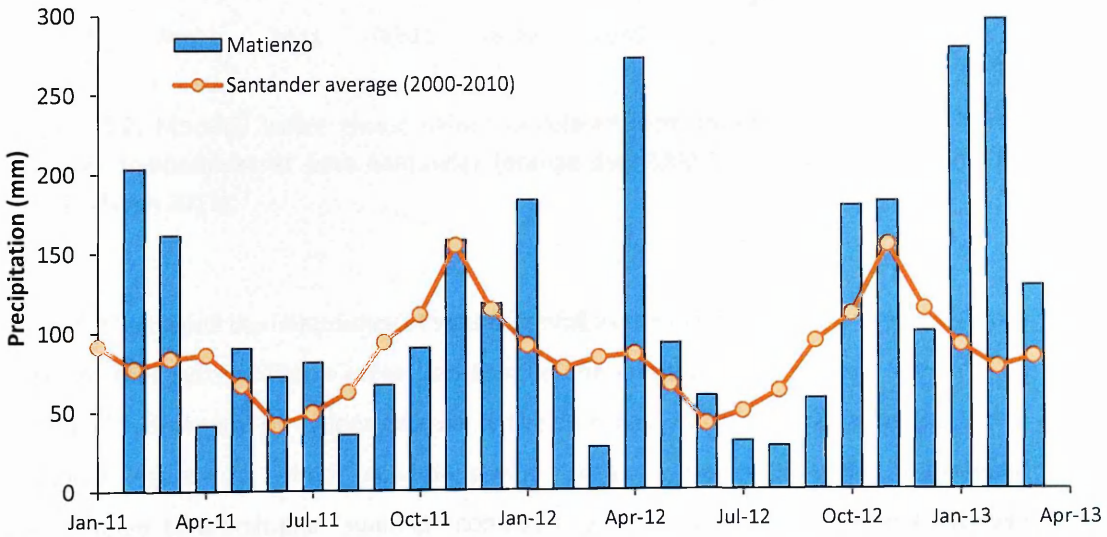

Figure 4.1: Monthly rainfall amount for Matienzo (Feb 2011- March 2013) shown by blue bars and average monthly rainfall amount for Santander (2000-2010) (orange line).

Although total rainfall amount is important for understanding above ground environmental development, only water which actively infiltrates into the karst can affect the cave environment. Therefore water excess calculations were undertaken following Thornthwaite

(1948). Major periods of water deficit occur between June and September, in both Matienzo and Santander (Figure 4.2).

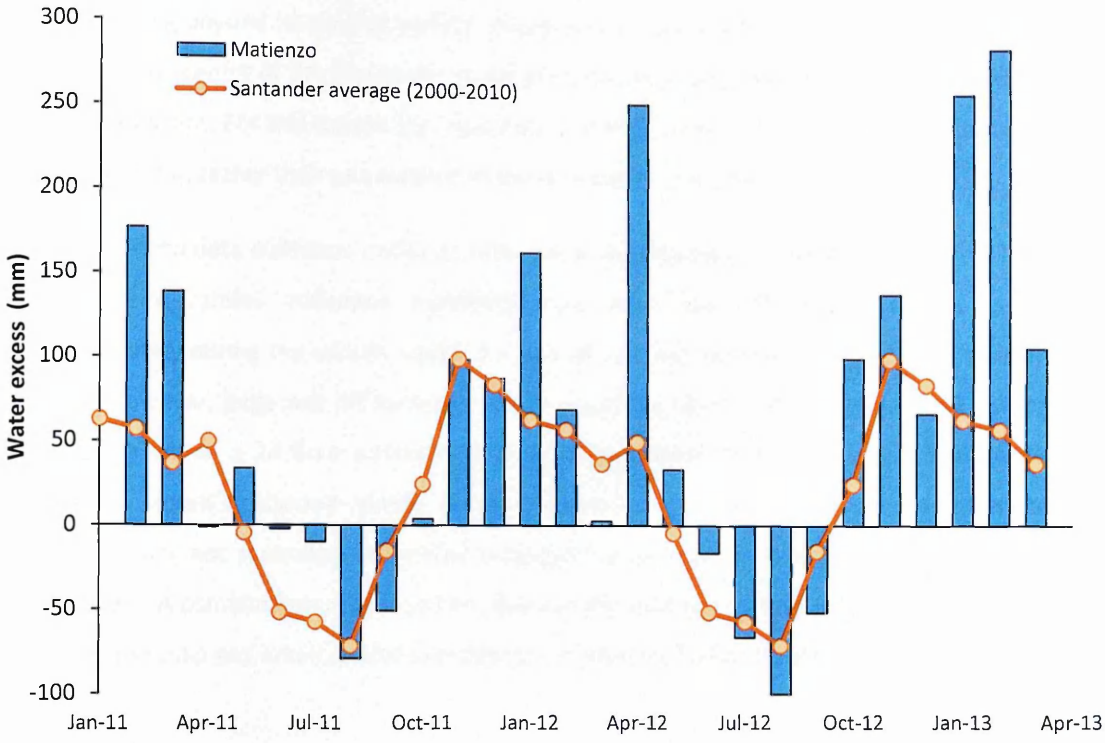

Figure 4.2: Monthly water excess values calculated from monthly total rainfall and average temperature at both Santander (orange line 2000-2010) and Matienzo (Feb 2011- March 2012).

Figure 4.2 highlights the importance of winter rainfall as the major input of water into Asiul's karst and cave system. Water excess can provide one method of segregating "winter" and "summer" hydrological conditions external to the cave. Based upon long term data sets from Santander (Figure 4.2), "winter" conditions with a positive water excess would be expected from October to March and "summer" conditions with a negative water excess between April and September.

Analysis on such a coarse (monthly) scale may however, fail to identify hydrologically important one off rainfall events, which contribute water into the soil and karst systems. From February 2011 to March 2013 event based water volumes were recorded in Matienzo to establish when major rainfall events occurred. A Pluvimate rain gauge was also in operation throughout this period. Problems with the Pluvimate installation have however, limited this automated rainfall record. Figure 4.3 shows rain gauge data alongside collected

monthly rainfall values (both event and monthly totals) to highlight periods of rainfall maxima and minima. Discrepancies in the collected and logged records occur during summer 2011 and spring 2012 (red bars in Figure 4.3). These differences are possibly due to the rain gauge shifting beyond its original vertical emplacement meaning that water drops no longer contacted the centre of the Pluvimate, causing the pressure sensitive surface to fail to detect falling rain drops. For this reason the Pluvimate system is used to confirm the occurrence of a rainfall event, rather than as a method of event volume quantification.

However, both data collection methods show general agreement in seasonal rainfall trends. Event based rainfall collection highlights that large one off rainfall events occur predominately during the winter, whilst the bulk of summer rainfall is derived from smaller events. However, large one off summer rainfall events do occur with as much as 50 mm of rain falling within a 24 hour period (e.g. 19-09-2011). These single events can contribute >50% of a month's collected rainfall, meaning water excess calculations (based on monthly averages) may not accurately determine if rainfall has percolated into the karst zone on an event scale. A combination of speleothem drip records and water chemistry can help to fully characterise how and when rainfall significantly contributes to karst water.

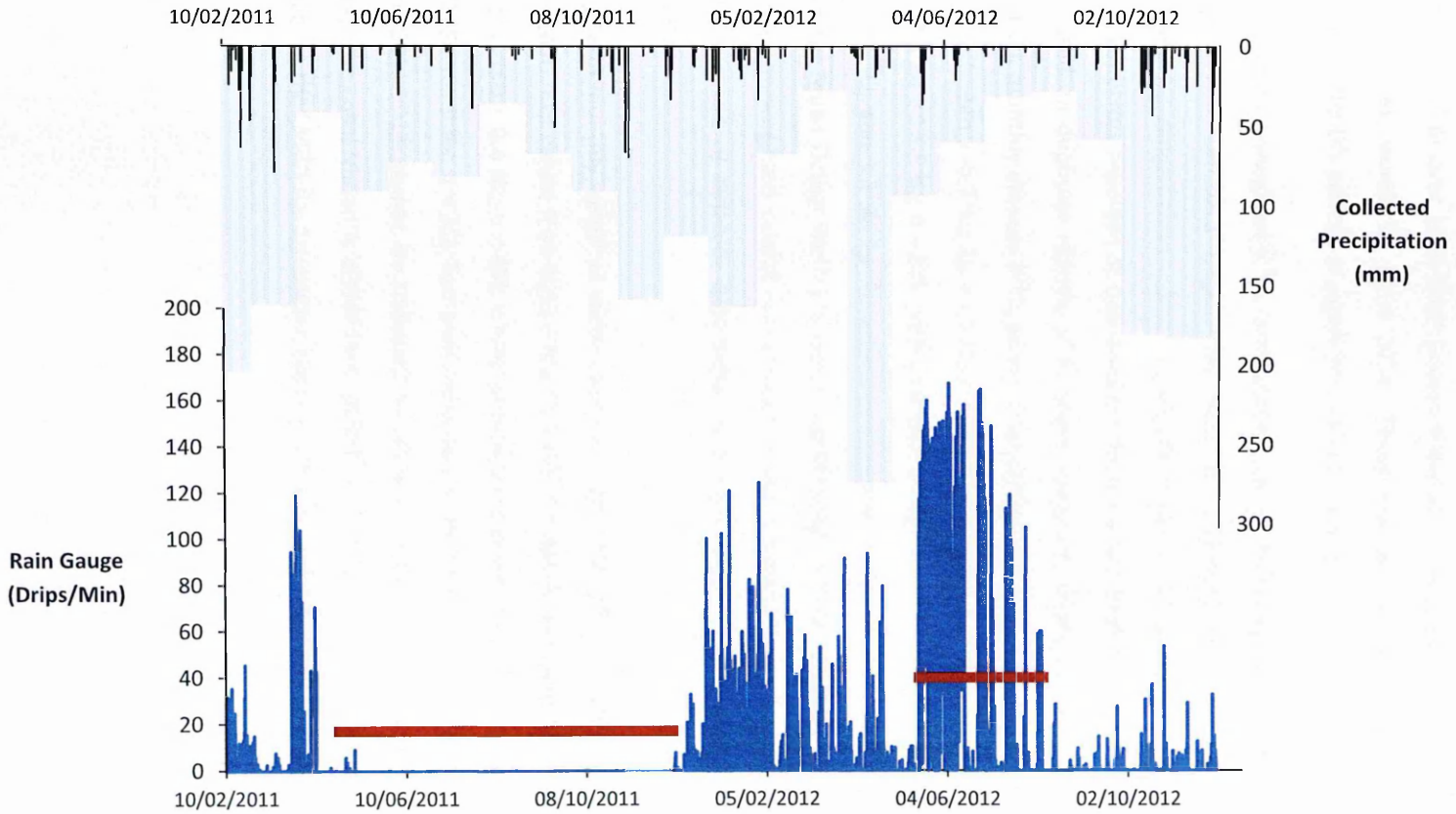

Figure 4.3: Total monthly collected precipitation (light blue bars) and event based collection totals (black bars compared to Pluvimate rain gauge data (dark blue lines) between Feb 2011 and Nov 2012. Red bars indicate periods of significant discrepancies between the data sets and possible logger malfunction.

4.2.1 Rainfall Isotope Chemistry

Oxygen and Deuterium (^2H) isotopes have been routinely measured for over 50 years in global rainfall at over 1000 GNIP (Global Network of Isotopes in Precipitation) sites across 125 countries, worldwide (IAEA 2014). These isotopes can be used as chemical tracers, helping to identify periods of significant water infiltration.

Event based un-weighted $\delta^{18}O_p$ (precipitation) values for rainfall events in Matienzo between Feb 2011 and April 2013 ranged from -16.51 to +4.45 ‰ (mean = -4.89 ‰; 2σ = 6.1 ‰; n = 198) and δD ranged from -130.65 to +12.78 (mean = -27.44 ‰; 2σ = 43.8 ‰; n = 195); analytical errors reported at one standard deviation are 0.06 ‰ for $\delta^{18}O_p$ and for δD are 1 ‰, based on duplicate repeats of in house standards. Matienzo rainfall compares to un-weighted monthly average $\delta^{18}O_p$ taken at Santander (2000-2006) which ranged from -9.61 to -1.73 ‰ (mean = -5.2 ‰; 2σ = 1.7 ‰; n = 82) and δD ranging from -63.2 to -8.7 ‰ (mean = -29.8 ‰; 2σ = 13.1 ‰; n = 82); with analytical errors reported at 1 standard deviation as 0.4 ‰ for $\delta^{18}O_p$ and 3.5 ‰ for δD based on repeated measurements of the VSMOW (Vienna Standard Mean Ocean Water) standard, conforming to GINP regulations. Santander has an average un-weighted rainfall composition which is slightly more negative than Matienzo, either a result of different data sampling periods or the slight difference in geographic location.

Long term monthly weighted mean values for Santander 2000 - 2006 are also slightly offset from Matienzo values (Feb 2011 – March 2013). Santander averages are reported as -5.7 ‰ for $\delta^{18}O$ (SD = 0.4 ‰, n = 83); whilst weighted mean averages for Matienzo are -4.6 ‰ for $\delta^{18}O$ (SD = 1.9 ‰, n = 26). Santander was only a GNIP site between 2000 and 2006 so data from 2011-2013 cannot be obtained to compare with data collected in Matienzo (IAEA 2014). The Local Meteoric Water Line (LMWL) for Matienzo is presented in Figure 4.4 and is similar to the LMWL for Santander; slightly offset from Global MWL (Dansgaard 1964).

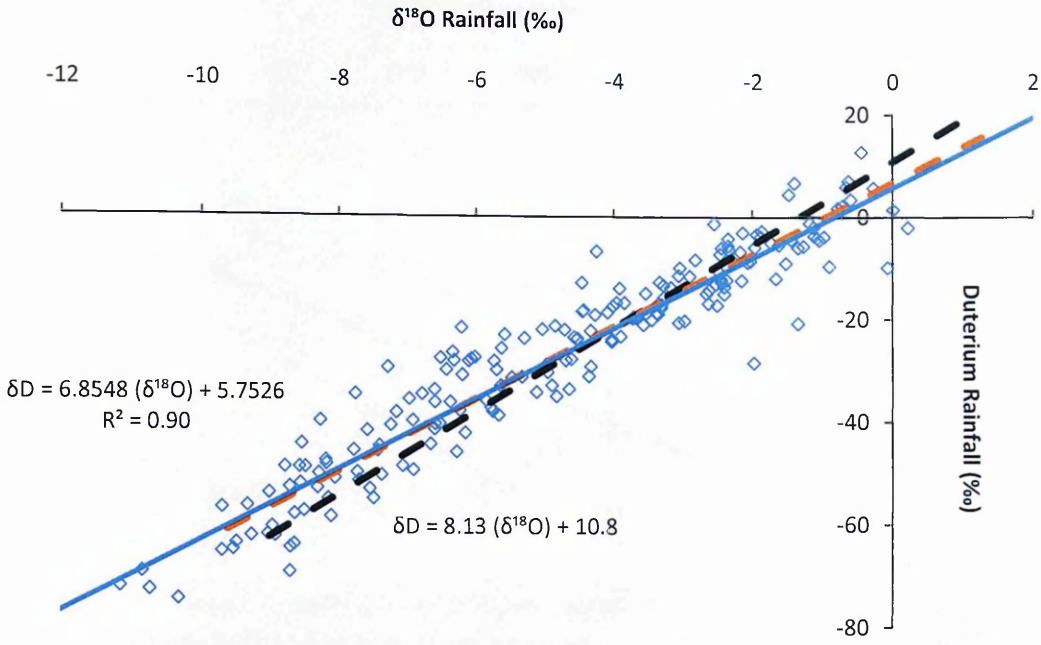

Figure 4.4: Local meteoric water line for Matienzo (blue) from 195 rainfall events (Feb 2011-March 2013). Black dashed line represents the Global MWL as denoted by Dansgaard (1964) and the orange dashed line the LMWL for Santander (IAEA 2014).

Close agreement between the slope and intersect of the Matienzo and Santander LMWL's reflect their close geographical proximity. The slight offset from the global line is to be expected due to the regionally sensitive nature of the sampling.

Event based Matienzo rainfall shows no correlation between $\delta^{18}O$ and event rainfall amount, for those events where accurate amounts can be calculated (Pearson correlation; r = 0.12; p>0.01; n-2 = 91). However, the monthly weighted mean isotopic value of rainfall is positively correlated (Pearson correlation; r = 0.72; p<0.01; n-2 = 23) to rainfall amount (Figure 4.5) as are weighted mean rainfall values from Santander (Pearson correlation; r = 0.71; p<0.01; n-2 = 10). Months with higher rainfall totals are associated with more negative $\delta^{18}O_p$ values, producing a classic "amount effect" relationship (Figure 4.5). The correlation of $\delta^{18}O$ and rainfall amount at the courser monthly resolution indicates that some within karst water mixing and storage (> 1 month) is required for the Matienzo rainfall amount effect to be reflected in cave drip waters.

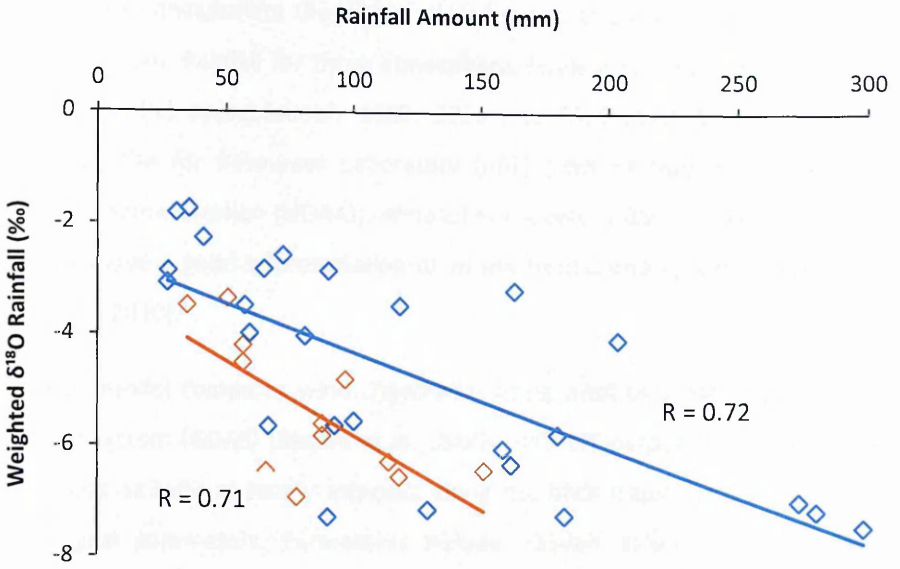

Figure 4.5: Monthly weighted mean $\delta^{18}O_p$ vs. rainfall amount for Matienzo between Feb 2011 and March 2013 (Blue line) and mean Santander (IAEA 2014) values between 2000-2006 (Orange line).

The Matienzo weighted mean rainfall amount relationship is derived from 26 months of rainfall collection between Feb 2011 and March 2013. Each month's data set is made up from between 3 and 16 individual rainfall collections.

Rainfall amount is however, not the only possible cause of oxygen isotope variation. If the source of rainfall varies dramatically over the year, this can control water chemistry and overshadow the amount effect described above. Event based analysis of moisture source was undertaken for rainfall events to determine the range of moisture sources which contribute rainfall to the annual budget in Matienzo and to establish if the source of rainfall may control the isotopic composition of cave drip waters and therefore speleothem carbonate.

4.2.2 Rainfall Source Effects

Rainfall source for one year of Matienzo rainfall (82 individual rainfall events, between Feb 2011 and Feb 2012) was estimated using the Hybrid Single-Particle Lagrangian Integrated Trajectory (HYSPLIT) Model (Version 4.8). This model was provided online by the National Oceanographic and Atmospheric Administration Air Resources Laboratory (NOAA ARL) (Draxler and Rolph, 2014). The air mass history of each rainfall event was calculated using five-day (120-h) kinematic back trajectories originating from Matienzo (43°31'N, -3°58'W), in a similar manner to (Baldini et al., 2010). These models originate at the end of each rainfall

collection day to encapsulate the whole rainfall event, this is essential as the peak rainfall period is unknown. Rainfall for three atmospheric levels was computed (850, 700 and 500 hecto-pascals, hPa) approximately 1500, 3015 and 5575 masl (Baldini et al., 2010). As suggested by the Air Resources Laboratory (ARL) (part of National Oceanographic and Atmospheric Administration (NOAA)), atmospheric levels of 850 and 700 hPa were used for modelling to give a good approximation of where frontal and synoptic rainfall is delivered (Baldini et al., 2010).

The HYSPLIT model computes wind trajectories using wind field data from the global data assimilation system (GDAS) (Baldini et al., 2010). HYSPLIT outputs reveal air mass latitude, longitude and altitude at hourly intervals along the back trajectory and generate data on meteorological parameters. Parameters include: rainfall, relative humidity, atmospheric pressure and ambient temperature. To ensure the numerical accuracy of the HYSPLIT modelling, forward modelling from the endpoint of the original back trajectory model was undertaken. All return trajectories ended after 120 hours, close to Matienzo (43°31'N, -3°58'W). Rainfall source trajectory was calculated by averaging the angle of modelled back trajectories (850 and 700 hPa) over the 120 h period. This technique was carried out for 82 rainfall events for comparison to isotopic signature of rainfall (Figure 4.6).

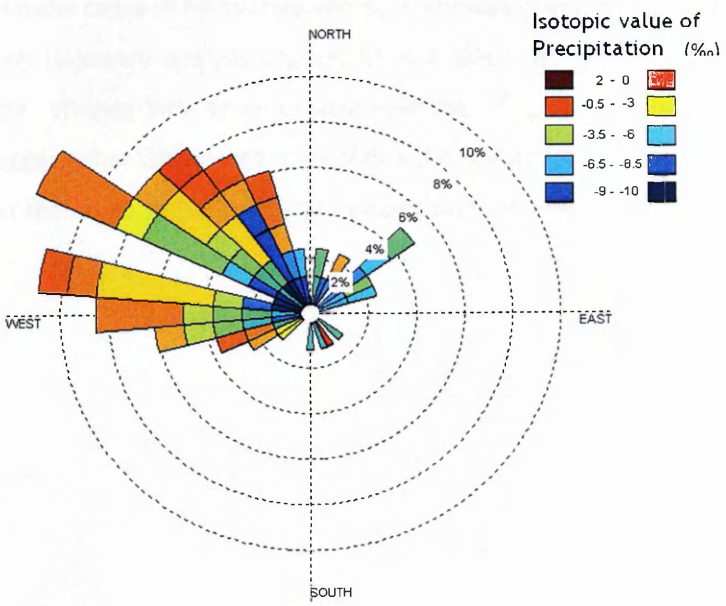

Figure 4.6: Wind rose displaying the percentage (dashed contours) and isotopic ($\delta^{18}O$) makeup of Matienzo rainfall originating from any source throughout the period Feb 2011- Feb 2012. Isotopic values of the rainfall are displayed as coloured blocks with more negative values in blue and more positive values in red. Rainfall trajectories were grouped into 10° blocks for rose production.

Matienzo rainfall source can clearly be seen to originate from a predominantly NW-W direction (79 % of rainfall events). This moisture source trajectory is associated with the whole range of isotopic values recorded in rainfall, with no obvious bias toward more positive or negative isotopic values at any given source location. Correlation analysis (Spearman rank) indicates no strong relationship between the direction of rainfall source and the isotopic value of that rainfall for all recorded rainfall events in 2011 (r_s = 0.05; p>0.01; n=83).

Figures 4.7a and b further assesses if any isotopic source effect relationship exists within the data set. The most positive (+0.01 to -4.09) (Figure 4.7a) and most negative (-4.1 to -9.56) (Figure 4.7b) isotopic rainfall events are mapped. Isotopically negative events exhibit a slightly more northerly source location in comparison to isotopically positive events. However, for the large range of isotopic values recorded in Matienzo rainfall, such slight source region modifications are through unlikely to reproduce such a large isotopic response (Dominguez-Villar et al., 2009).

Secondly, the potential influence of seasonality is tested in Figures 4.8a and b. Seasonal plots show that summer (April to September) (Figure 4.8a) and winter (November to March) (Figure 4.8b) events both predominantly originate in the North Atlantic, although winter events show a wider range of NA sources and a predominance of extremely negative isotopic values. All back trajectory analysis suggest for the Matienzo cave site, rainfall source is relatively stable, offering little or no control over the $\delta^{18}O_p$ on either annual or seasonal scales. This suggests that the amount of rainfall is the key control over rainfall $\delta^{18}O$ value at this site, rather than large spatial variations in moisture source location.

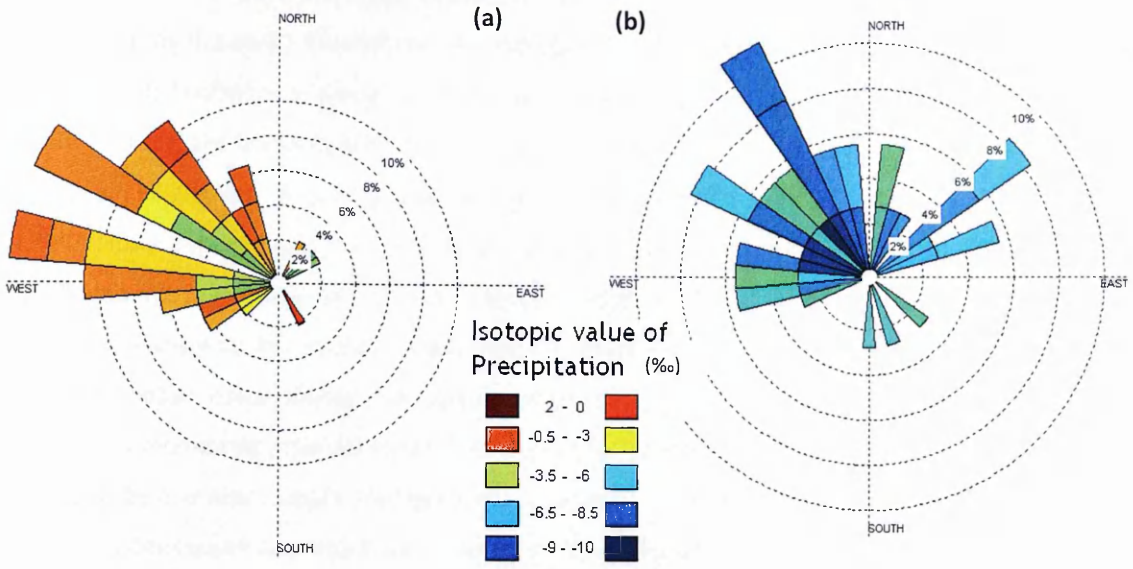

Figure 4.7: (a) Wind rose's displaying the source location of rainfall (% of that years rainfall from any given source is identified by dashed contours) with more positive isotopic ($\delta^{18}O$) values (+0.01 to -4.09) and (b) more negative isotopic ($\delta^{18}O$) values (-4.1 to -9.56).

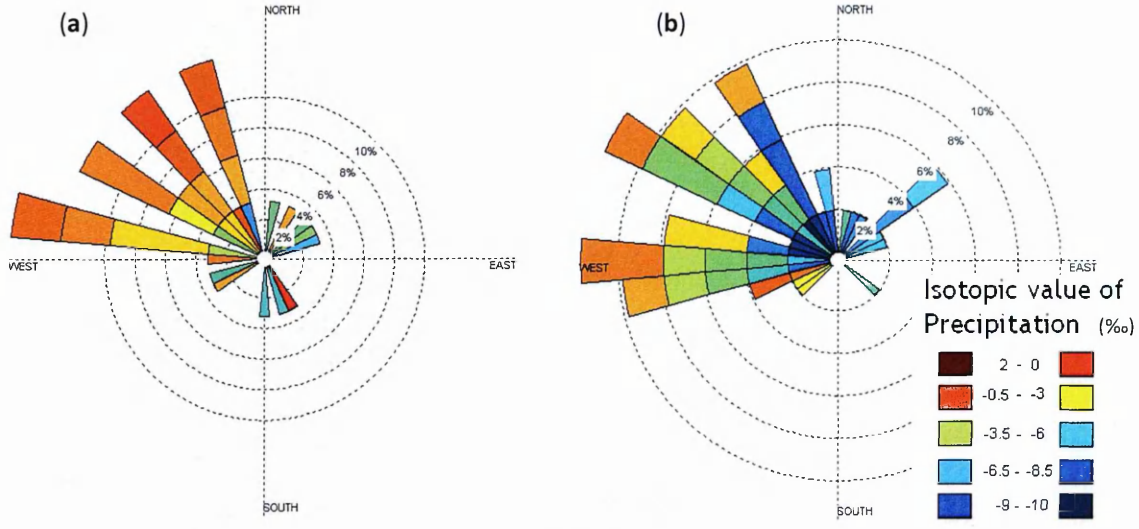

Figure 4.8: Wind roses showing seasonal differences in rainfall source (% of that years rainfall from any given source is identified by dashed contours) and associated isotopic ($\delta^{18}O$) value. (a) Summer values show more positive isotopic values but a similar rainfall source to winter values (b).

Long term data sets from Santander exhibit similar trends in rainfall to those collected in Matienzo during this study. Rainfall trajectory modelling shows a significant range of isotopic values in rainfall collected in Matienzo which are mostly related to a single, seasonally stable moisture source, the North Atlantic Ocean. Rainfall amount however, varies seasonally with highest rainfall amounts occurring in the winter and lowest in the summer. The amount of rainfall holds a strong control on the isotopic value recorded in this rainfall; higher monthly rainfall amounts are associated with more negative weighted mean isotopic values and vice versa for months with less rainfall. Water excess calculations indicate periods of maximum water infiltration occur during the winter months, dominating karst water recharge. Hydrological monitoring external to the cave site therefore shows karst aquifer water to be dominated by a winter isotopic and chemical signature. This relationship between external climatic conditions and cave processes is the focus of subsequent sections.

4.3 Drip Site Hydrology

Cave hydrology is primarily influenced by external rainfall. However, the soil and karst zones can act to modify the timing and amount of water delivered to the cave environment. Intensive cave monitoring is used to assess the responsiveness of the cave hydrological system and the magnitude of any changes induced by the soil and karst zones. Monitoring is therefore essential to understanding the conditions under which speleothems develop, lending detailed insight into how these records should be interpreted during palaeoclimate analysis.

4.3.1 Speleothem Drip Response

Although water chemistry has been collected from a number of drip sites throughout Asiul, high resolution drip rate monitoring using stalagmate loggers (Collister and Mattey 2008) could only be undertaken at three sites. Drips which feed the main speleothems of interest (ASF, ASM and ASR) show distinct hydrological regimes which vary on a range of different scales. The longest record is related to speleothem ASF, which has been monitored from April 2010 to November 2013, allowing for a detailed assessment of drip hydrology. This speleothem demonstrates a seasonal cyclicity of increasing (winter) and decreasing (summer) drip flow, which is closely coupled with annual cycles of water excess (Figure 4.9).

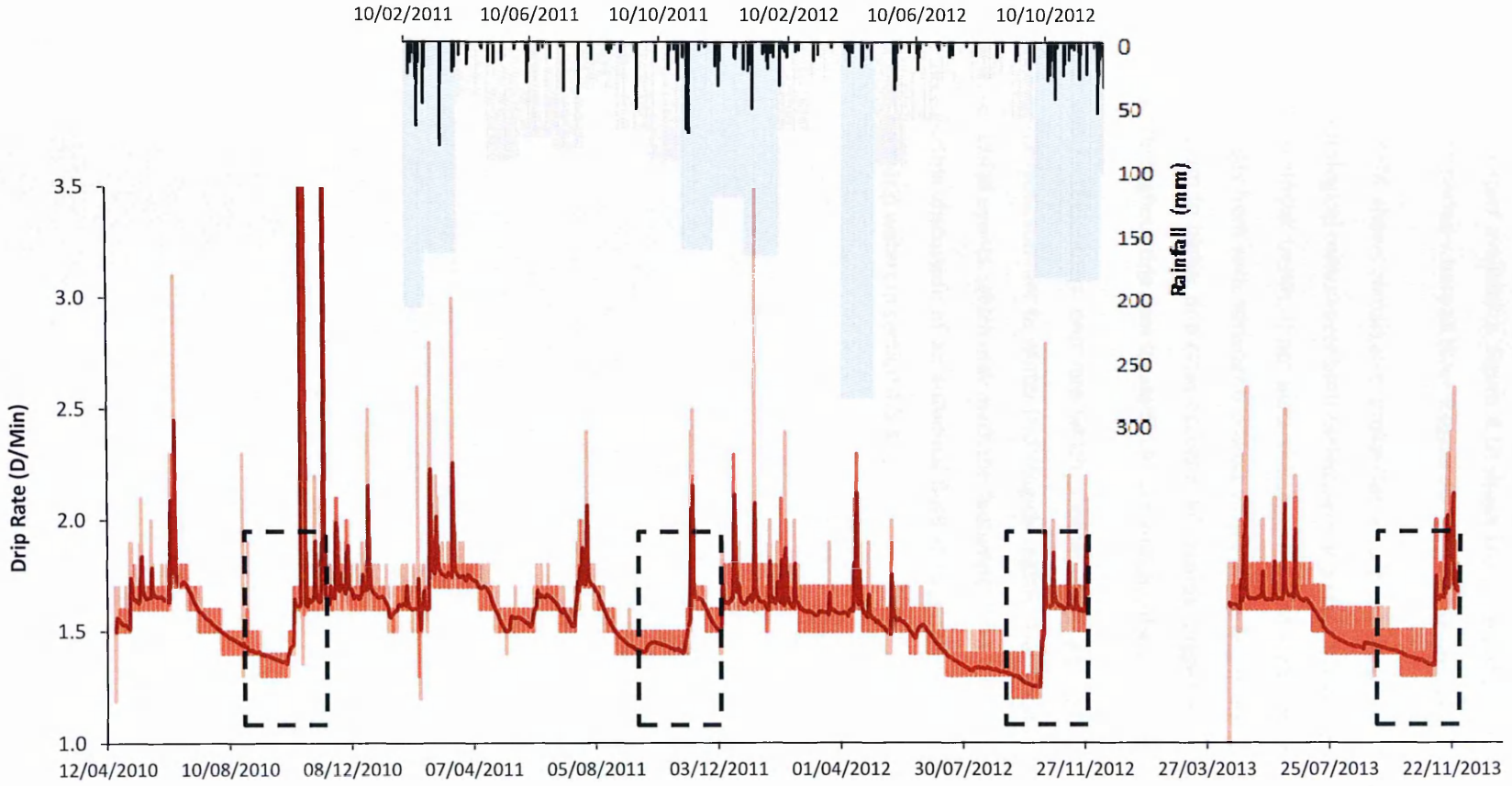

Figure 4.9: ASF speleothem drip record April 2010 to Nov 2013 (red line), with collected event (black line) and monthly (blue bars) rainfall volumes from Feb 2011 to Jan 2013. Black dashed boxes indicate transition periods from summer to winter drip regimes.

The two other major speleothem drip sites ASM and ASF have shorter records due to restrictions in logger availability. Figure 4.10 shows the relationship between the three drip sites during the period where all three loggers were operating simultaneously.

Speleothem ASM shows remarkable similarities in drip architecture to ASF, suggesting a common hydrological control over both speleothem drip sites. The longer records of ASR and ASF also show similar trends, if not quite the same detailed architecture. Higher drip rates decrease steadily from early summer to lowest values at the beginning of the autumn, when a dramatic return to higher drip rates occurs in all records; suggesting a significant input of karst water throughout drip sites located in Asiul's end chamber.

The increase in speleothem drip rate which is observed in all speleothems (Figure 4.10) marks a switch from summer to winter hydrological regime. This occurs rapidly, triggered by a few large rainfall events, which may mark the "autumnal flush" (Borsato et al., 2007) at this cave site. Further discussion of an autumnal flush is considered using trace element data within the cave drip waters in section 4.5.3.

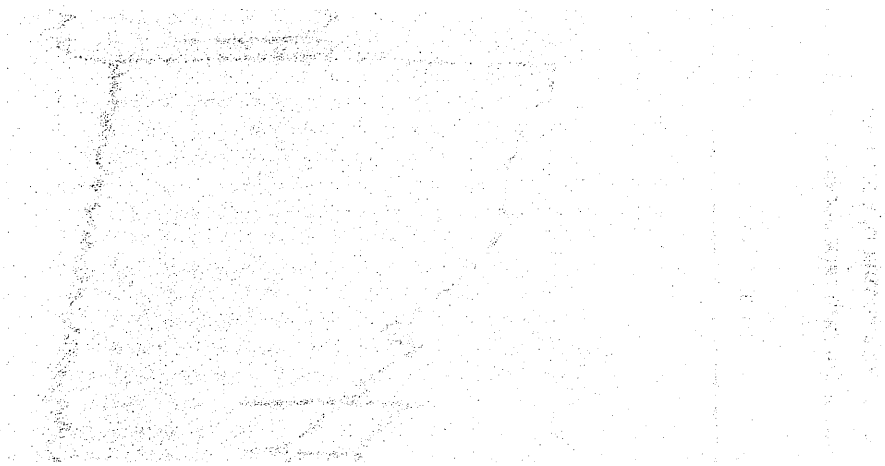

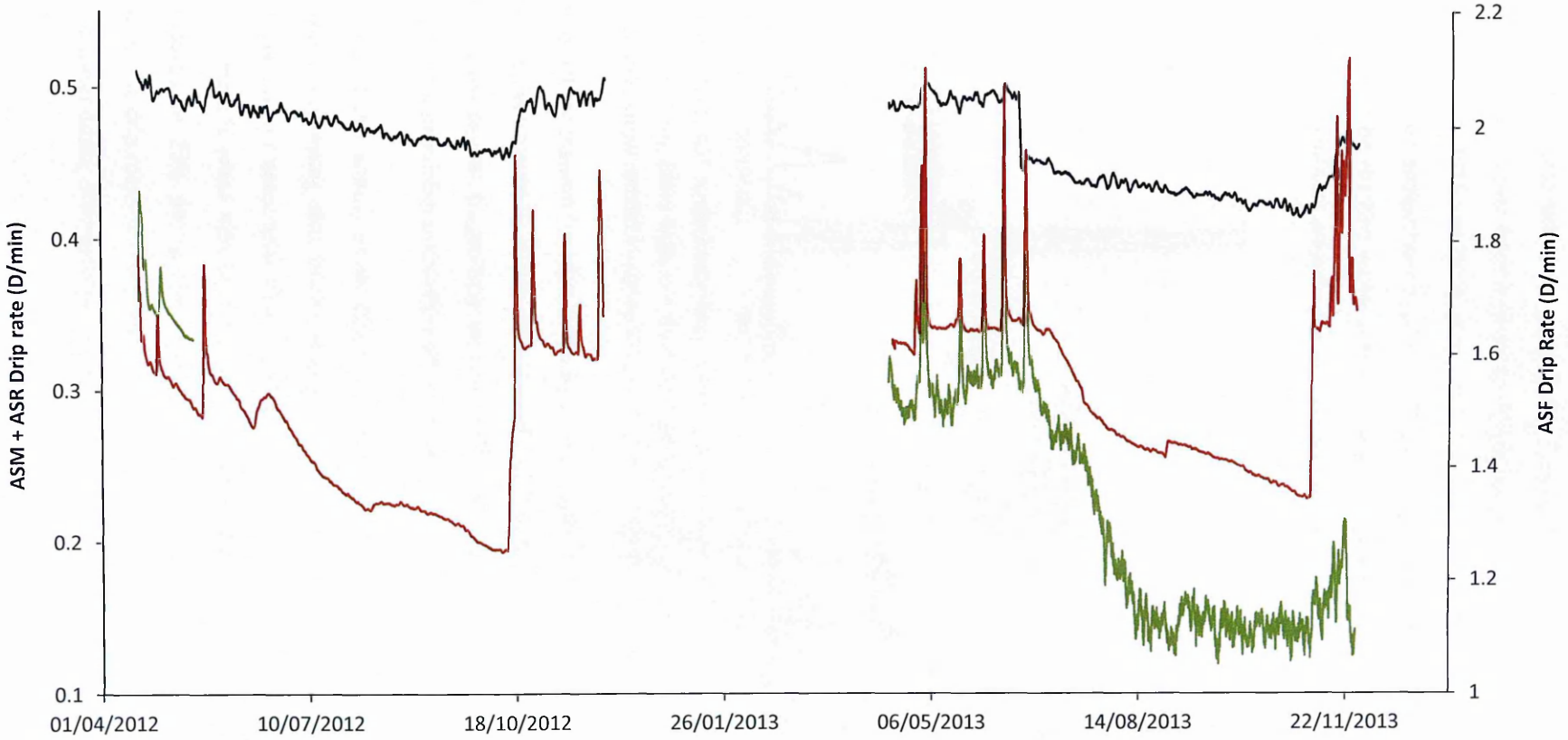

Figure 4.10: Speleothem drip rate between April and November 2013. All three speleothems ASF (red line), ASM (green line) and ASR (black line) are situated in the small end chamber of Asiul Cave.

Monitoring at speleothem ASF identifies how rapidly the karst reacts to the input of rainfall during the switch over from summer to winter drip regime (Figure 4.11). On both occasions in Figure 4.11 (2011 and 2012), large rainfall events precede the main rise in drip rate, with little impact on speleothem hydrology. The next major rainfall event however, prompts a threshold to be reached within the karst aquifer; triggering the winter flow regime and a release of a significant amount of water to cave drip sites.

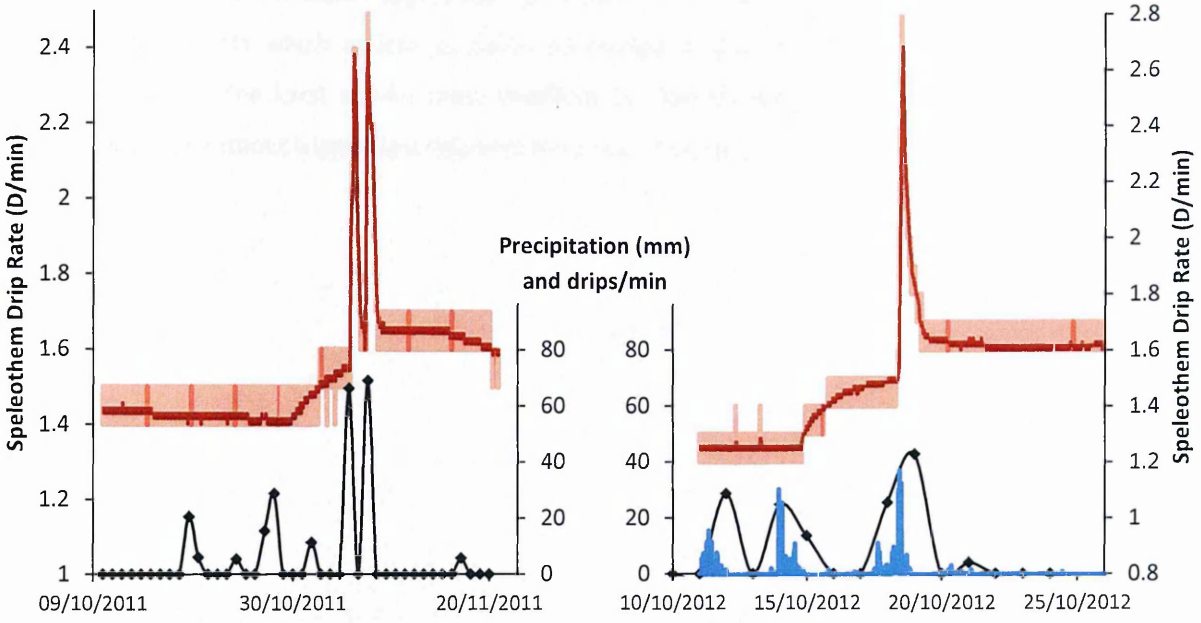

Figure 4.11: ASF speleothem drip record during two years of hydrological regime switch over (red line). Black lines and diamonds denote collected rainfall amount (mm/day) and blue bars show rainfall in (drips/min) from the Pluvimate rain gauge, when operational.

The exact mechanism for karst recharge at these specific times is unclear. Soil and epikarst water replenishment by several rainfall events may be enough to cause significant saturation of the karst aquifer, triggering a rise in base drip rates. After karst recharge, the transmission of high volume rainfall events through the karst occurs more efficiently.

On top of this annual trend, spikes in speleothem drip rate correlate with precipitation maxima; suggesting that hydrologically significant, event based increases in karst water percolation can occur year round. Spikes in drip rate occur more commonly during the winter months when 66% of rainfall events correspond to a rise in speleothem discharge, compared to 25% during the summer. The fact that not all rainfall events trigger a concurrent drip response suggests the existence of a karst reservoir which can incorporate more water during drier summer conditions.

Winter months have the highest associated base speleothem drip rate (1.6 – 1.8 D/min), whilst summer months exhibit a gradually decreasing base drip level, from 1.7 to 1.25 D/min. Drip rate maximums occur in November 2010 and minimums in October 2012.

Figure 4.12 shows how speleothem ASF responds within hours of major rainfall events. After cessation of the rainfall event, drip rates peak within a few hours, eventually falling back to background levels within approximately 24 hours. Also observed in the record are smaller rainfall events which appear to cause no change in drip discharge, even under winter conditions. The karst aquifer must therefore be able to incorporate a certain volume of rainwater without triggering a response from cave drip sites.

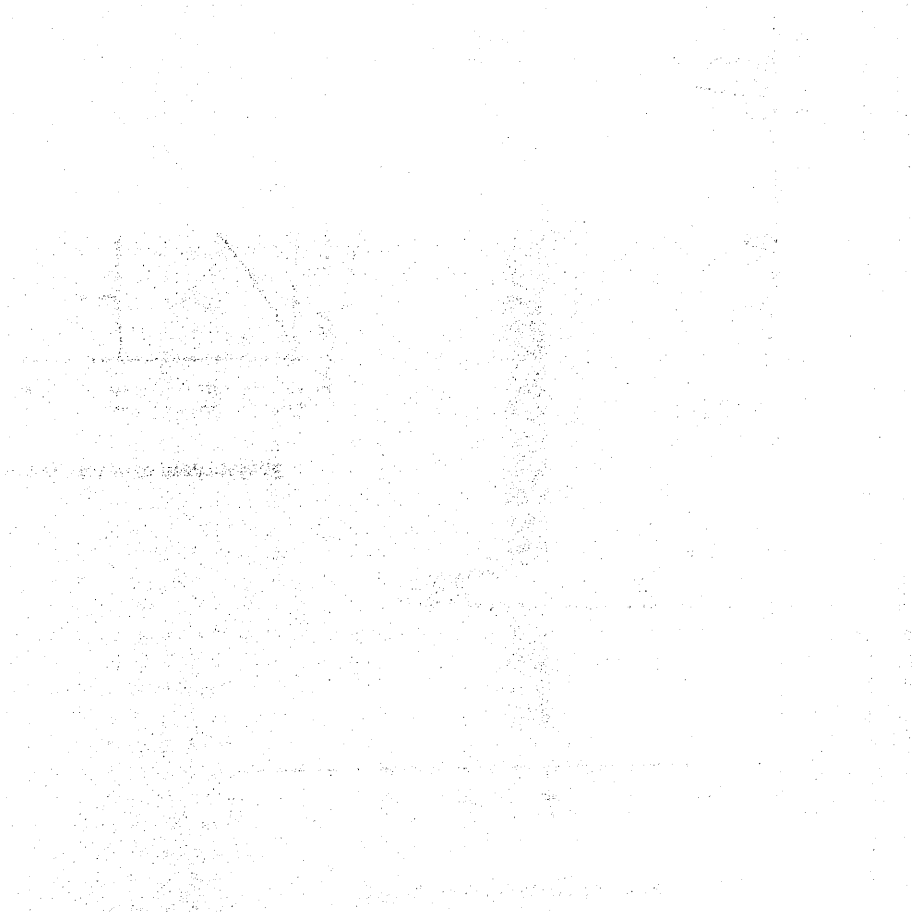

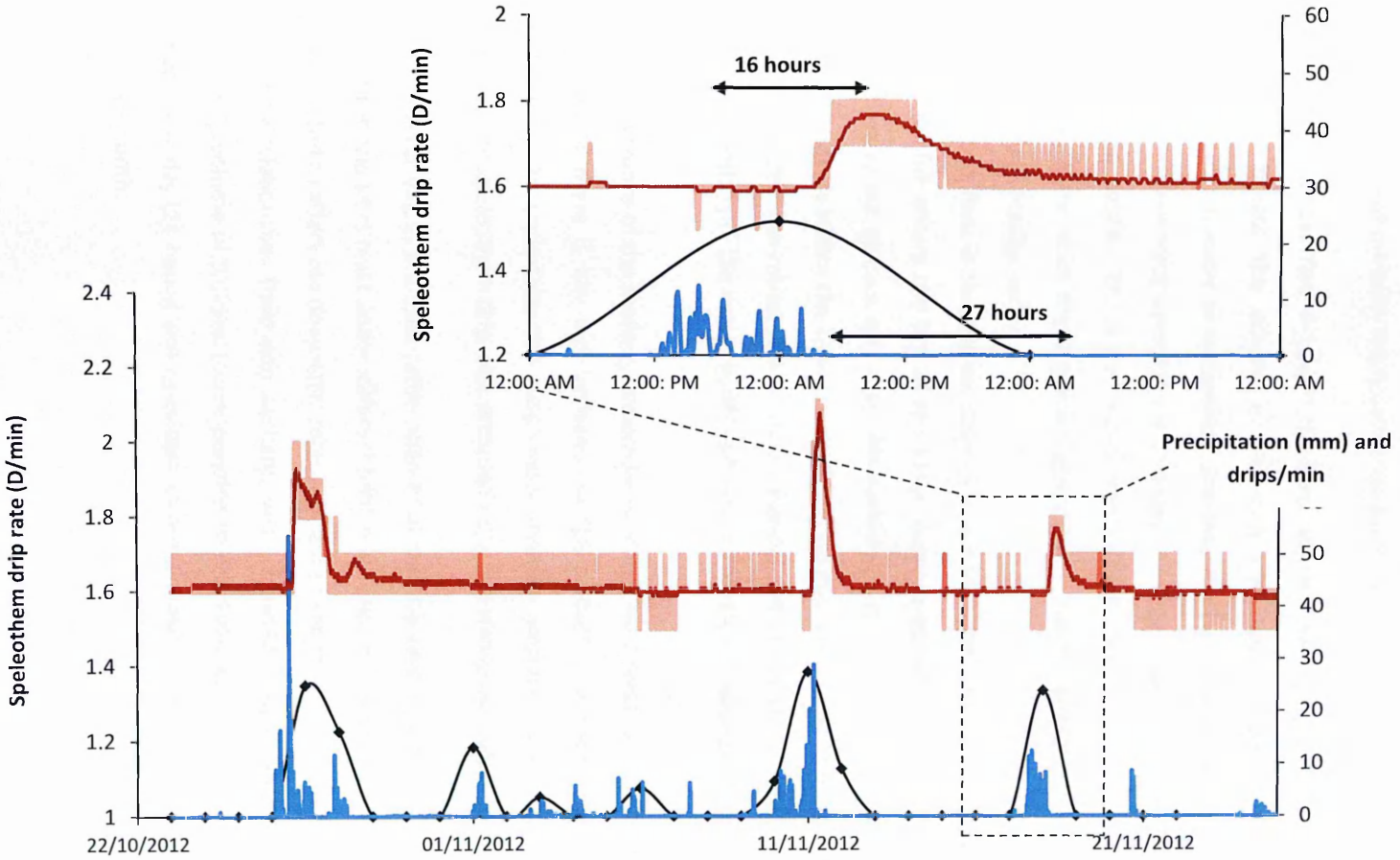

Figure 4.12: ASF speleothem drip record (red line) during three major winter rainfall events. Daily rainfall (mm) is denoted by a black line and diamonds, Pluvimate rainfall data is shown by blue bars (D/min). Inset graph shows detail of the rainfall event on the 17-11-12, black arrows indicate speleothem response times from maximum rainfall to maximum drip discharge and from the termination of rainfall to cave drip discharge recovery.

The inability of the karst to incorporate large rainfall events indicates that it is relatively shallow, with a limited storage capacity. Under such conditions, one of two mechanisms for water transit most probably exists within the karst zone.

1) Conduit overflow occurs if the karst aquifer reaches capacity and can no longer incorporate the volume of incoming rain water. Overflow would contribute additional water to speleothem drip sites but only when inputs of water remained high. Depending upon karst physiology, overflow water may completely bypass the main aquifer. This water would not mix with older stored karst water and may therefore retain the chemical signature of a specific rainfall event, rather than that of bulk aquifer water.
2) Piston flow is the transmission of a water "pulse" through the karst aquifer. As rainfall enters the top of the karst, water pressure builds forcing stored aquifer water out at cave drip sites. Speleothem discharge would remain high until water pressure within the karst returned to a normal level. Under piston flow conditions it is older well-mixed water which emerges within the cave. This should reflect the chemistry of the karst aquifer and not an individual precipitation event.

Further evidence of the shallow, responsive karst overlying Asiul cave can be observed when assessing if there is any link between rainfall amount and speleothem drip discharge (litres/day). To undertake this assessment monthly average water excess values were compared to speleothem drip rate, recorded using the stalagmite logger system.

Water excess values are used rather than total monthly rainfall, with the aim of identifying how cave drip sites react under different infiltration regimes, as only effective rainfall would be expected to affect the deep karst zone. Figure 4.13 shows the monthly water excess / drip discharge relationship. Daily drip discharge was calculated using average monthly drip rate and a drip volume of 0.075ml (corresponding to drip volumes collected at ASF). An average volume per day (24 hours) was calculated to remove discrepancies associated with variable days per month.

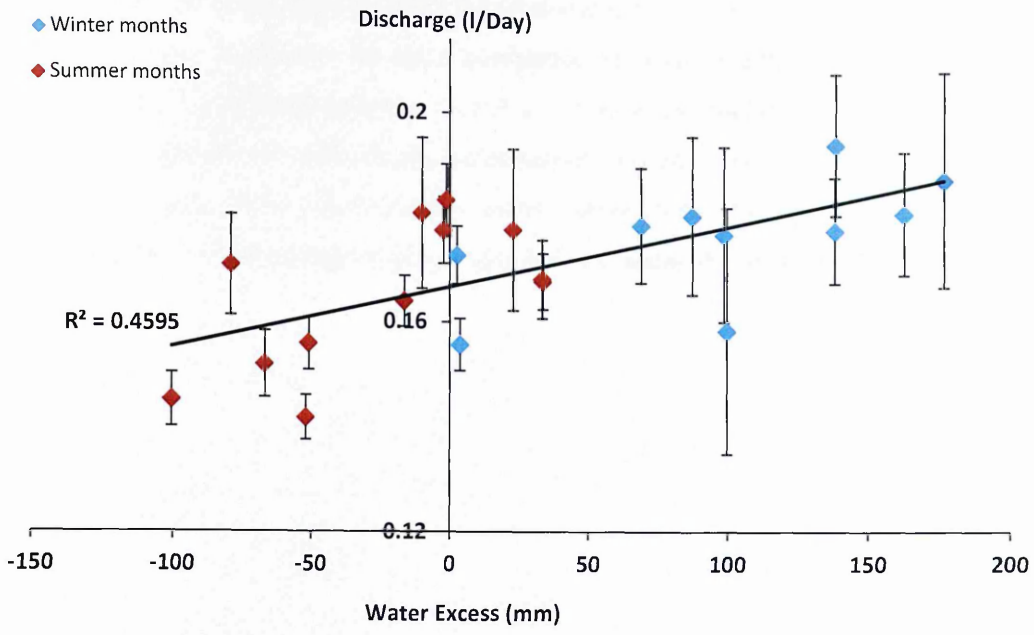

Figure 4.13: Relationship between water excess (mm) and discharge (l/day). Blue diamonds represent winter months (October - March) and red diamonds summer months (April - September). Error bars equate to the coefficient of variation (% standard deviation about the mean) at ASF during any given month.

Drip discharge shows a positive linier relationship to the amount of effective rainfall (linier regression; r^2 = 0.45) throughout the year. This relationship shows no obvious lag time (within a month) from water input to water output suggesting a highly responsive and semi-predictable karst system over both event and monthly scales. Months with a high drip discharge (occurring mainly during winter months) are also characterised by a high coefficient of variation, calculated as the percentage standard deviation about the mean (Smart and Friederich 1987; Tooth and Fairchild 2003).

This section has dealt with physical changes to cave and karst hydrology. Drip monitoring in Asiul shows that the main speleothems assessed in this study show similar seasonal trends in discharge. Speleothem ASF has the longest uninterrupted monitoring record which includes three annual cycles of summer discharge minima and winter maxima. At the onset of winter rainfall, the cave drip sites show a rapid transition into a winter discharge regime, characterised by higher base drip rates and more isolated peaks in discharge. This hydrological transition occurs around October – November each year. Whilst drip sites exhibit strong seasonality, heavy rainfall events can trigger a hydrological response from cave drip sites year round, within hours of peak rainfall. Drip site recovery occurs more

gradually, but maximum discharge levels fall relatively rapidly back to base flow conditions. Defining the exact mechanism for water percolation however, is difficult using infiltration volumes alone. Comparison between rainfall and drip water chemistry is undertaken in section 4.4.4 with the aim of identifying the dominant mechanism of karst water flow at this site. However, prior to drip water isotopic analysis other phyiso-chemical characteristics of cave drip waters will be considered, to establish baseline water chemistry for this site.

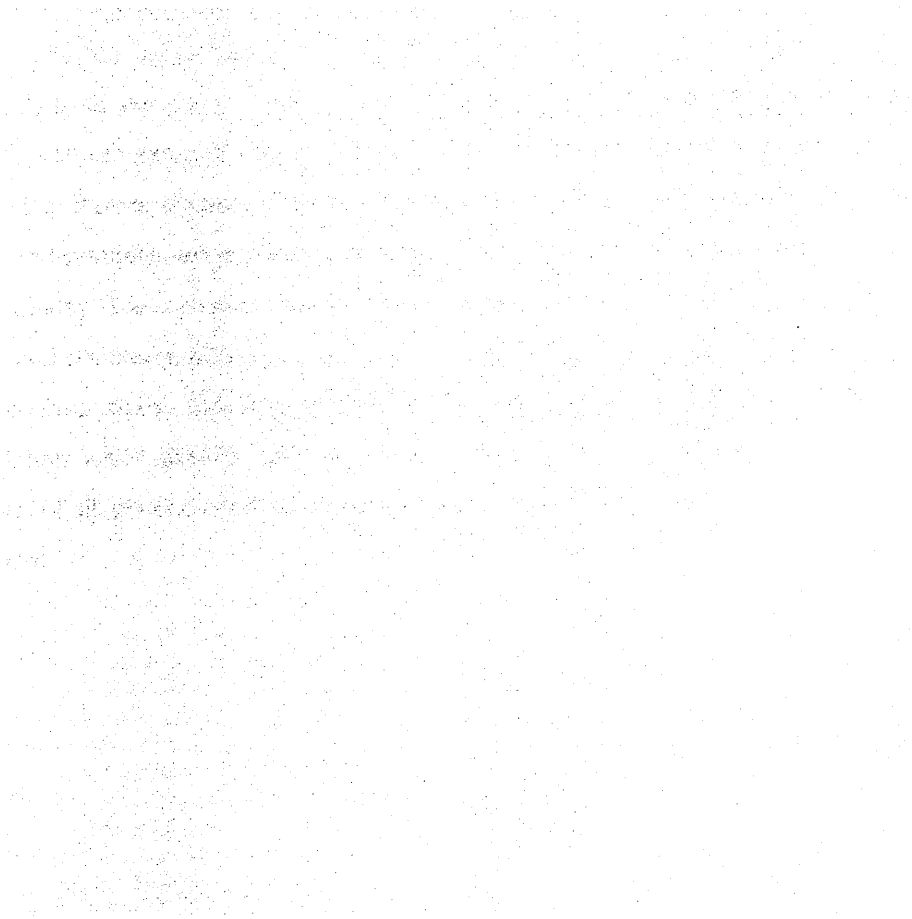

4.4 Chemical Characteristics of Cave Drip Waters

The chemical characteristics of cave drip waters reflect the chemistry of the parent solution (rainfall) and secondary physical and chemical interactions which occur during water infiltration. The relatively stable nature of rainfall chemistry means drip waters are routinely used to identify variations in karst water mixing, as well as assessing the intensity and duration of chemical reactions which occur during karst storage. As well as being an important tool for the assessment of karst hydrology, the chemical characteristics of drip waters can profoundly influence the precipitation of speleothem carbonate within the cave. Assessment of drip water chemistry is therefore fundamental; to establish changes within the karst and to identify modes of speleothem deposition.

4.4.1 Baseline Water Chemistry

All drip water from speleothems ASF, ASM and ASR between Feb 2011 and April 2013 has been collected using "bulk" water collection vessels. These vessels were sampled on a monthly basis and emptied after sampling, to collect water the following month. Bulk water pH, EC and temperature were measured within the cave before a subsample was sent for isotope and trace element analysis. All EC values are calibrated to a specific conductivity at 25°C and synthetic values were calculated using the Rossum (1975) equation to cross check data quality. Trace element concentrations were measured via ICP-OES for major cations, silica and strontium, ICP-MS for trace metal concentrations, and Dionex chromatography for anion composition. Alkalinity and saturation index were calculated using MIX4 chemical speciation, whilst alkalinity was compared to within cave titrations. Table 4.1 shows available monthly bulk physico-chemical values for drip waters collected from speleothems ASF, ASM and ASR.

	Speleothem ASF						Speleothem ASR						Speleothem ASM			
	EC (µS/cm)		pH	Temp (°C)	Alkalinity (mg/l)	SI calcite	EC (µS/cm)		pH	Temp (°C)	Alkalinity (mg/l)	SI calcite	EC (µS/cm)		pH	Temp (°C)
	Measured	Calculated					Measured	Calculated					Measured	Calculated		
Dec-11		334	8.65		177	0.91	425	347	8.59		180	0.86				
Jan-12		328	8.15	13.5	169	0.4		340	8.32	13.4	174	0.58				
Feb-12		325	7.64	13.5	165	-0.11		348	7.63	13.7	177	-0.08				
Mar-12	325	333	8.29	13.6	172	0.54	325	339	8.25	13.9	174	0.52				
Apr-12	314	345	8.10	13.7	176	0.4	326	380	8.05	13.9	195	0.44				
May-12	307	422	8.00	13.9	221	0.55	330	378	7.94	14.0	193	0.34				
Jun-12	302	340	7.97	13.9	175	0.25	319	347	7.92	14.0	162	0.18				
Jul-12	299	318	7.94	14.0	161	0.17	321	341	7.94	14.2	172	0.23				
Aug-12	291	305	7.96	14.0	155	0.15	322	341	7.90	14.1	172	0.18				
Sep-12	276	292	8.02	14.2	147	0.16	314	333	7.95	14.2	167	0.2				
Oct-12	298	315	7.99	14.0	160	0.21	319	342	7.94	14.2	172	0.23				
Nov-12	304	318	7.99	13.9	160	0.21	319	347	7.90	14.1	175	-0.39				
Dec-12	299	317	7.96	13.8	159	0.17	304	319	7.89	14.0	160	0.1				
Jan-13	308	324	7.98	13.6	162	0.22	303	319	7.98	13.9	160	0.19				
Feb-13	303	316	8.04	13.4	155	0.24	319	337	8.06	13.8	168	0.32				
Mar-13	314	328	7.95	13.4	160	0.18	299	341	7.92	13.8	170	0.19	342		8.07	13.5
Apr-13	310		8.01	13.5			306		7.94	13.8			356		8.17	13.6
May-13	343		8.17	13.5			335		7.87	13.9			365		7.88	13.7
Jun-13	334		7.94	13.6			351		8.05	13.9			353		8.23	13.7
Jul-13	308		8.14	13.6			327		8.18	13.9			328		8.24	13.7
Aug-13	301		8.22	13.7			315		8.19	13.9						
Sep-13	301		8.18	13.8			315		8.14	13.9						
Oct-13	303		8.19	13.8			323		8.22	13.8						

Table 4.1: Physical and chemical data from bulk monthly water sampling at drip sites ASF, ASM and ASR.

Water temperatures are similar between sites, driven by a combination of incoming rainfall, rock and cave atmospheric temperatures. Maximum water temperature is recorded during summer months (14.2 °C) and minimum values during the winter (13.4 °C), showing a clear seasonality similar to cave atmospheric temperature. Drip water SI remains positive for most drip collections, indicating that drip waters are saturated with $CaCO_3$ year round. This means that cave speleothems have the potential to be deposited independent of seasonality.

Unexpectedly, pH does not show any strong relationship with other hydrological or atmospheric components of the cave system. However, the long residence time of bulk waters before sampling (≈1 month in the cave) will likely facilitate CO_2 degassing to the cave atmosphere. Bulk water pH may therefore reflect a combination of hydrological and atmospheric end members, potentially masking any original relationship with other chemical components of the hydrological system.

To further explore the role of the cave atmosphere in controlling drip water chemistry, an assessment of cave drip water and cave air interactions is undertaken. One method of tracing air – water interactions is to assess the extent of CO_2 equilibrium between phases.

4.4.2 Cave Water Saturation State and CO_2 Equilibrium with Cave Air

Under equilibrium conditions, cave air pCO_2 controls CO_2 degassing from drip waters and $CaCO_3$ precipitation rate. Tremaine et al., (2011) show if drip water pCO_2 is in chemical equilibrium with cave air pCO_2 then drip water saturation state (after interaction with a speleothem surface and equilibrium $CaCO_3$ deposition) should be a function of cave air pCO_2.

Water pCO_2 vs. cave air pCO_2 (Figure 4.14) from Asiul, shows pool waters to be (one exception) in equilibrium with the surrounding cave air, using the expected 1:1 CO_2 partitioning ratio of Tremaine et al., (2011). Speleothem ASR bulk drip waters do not however, reflect equilibrium drip water vs. cave air pCO_2 conditions, despite being open to the cave atmosphere for up to 1 month. All ASR and ASF bulk drip waters lie above the 1:1 CO_2 partitioning ratio expected under equilibrium conditions (black dashed line in Figure 4.14). The fact that ASR bulk drip waters lie above the expected equilibrium line suggests they are either still degassing at the time of collection, or they have equilibrated with an atmospheric pCO_2 higher than that of the cave air.

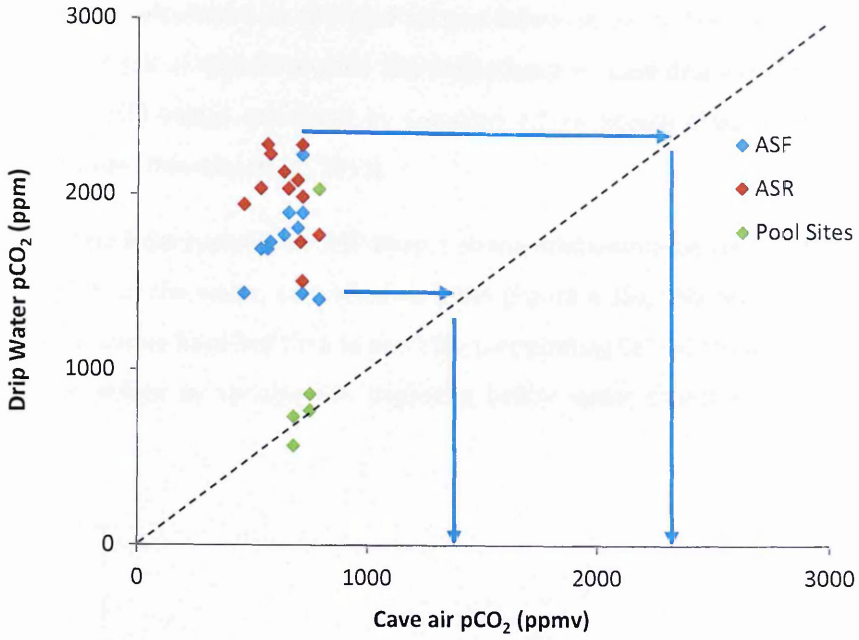

Figure 4.14: Cave water pCO_2 (calculated) vs. cave air pCO_2 (measured). Black dotted line represents the 1:1 partitioning ratio expected when CO_2 in drip waters is in chemical equilibrium with the cave air CO_2 (most pool samples sit on this line). Samples lying above this line should either still be degassing at the time of sampling or are in equilibrium with an atmospheric pCO_2 higher than that of the cave air. Blue arrows indicate the range of air pCO_2 that bulk cave drip waters appear to be in equilibrium with, possibly a function of jerry can micro atmospherics.

Due to apparent incomplete degassing the hyperbolic relationship between cave air pCO_2 and drip water saturation state expressed by Tremaine et al., (2011) would not be expected in Asiul bulk drip waters.

When calculated using MIX4 (as LOG IAP/K_s) drip waters are typically supersaturated with respect to calcite, except Feb 2011 for ASF which is slightly under saturated (saturation index range calculated by MIX 4 = -0.11 to 0.91). However, calcite saturation state (Ω) calculations undertaken independently from the MIX4 speciation program using Equation 4.1 (Tremaine et al., 2011), indicate that all drip waters are all just supersaturated with respect to calcite (saturation range = 1.8 to 20.2; where oversaturation is $\Omega > 1$).

$$\Omega = (Ca^{2+}) * (CO_3^{2-}) / K'_{SP} \quad (4.1)$$

Where Ca^{2+} ions are in mMols, CO_3^{2-} ions are in µMols and K'_{SP} is calculated as $3.75*10^{-9}$ based upon an average Asiul cave water temperature of 13.8 °C.

Saturation state calculations in the next section follow those of Tremaine et al., (2011). Subsequent analysis of saturation state (SS) dependence on cave drip water pCO_2 and cave air pCO_2 uses (SS) values calculated by Equation 4.1 to enable direct comparison with preceding studies (Tremaine et al., 2011).

Bulk drip waters from speleothem ASF show a strong relationship between saturation state (Ω) and $1/pCO_2$ of the water, calculated by MIX4 (Figure 4.15). This relationship indicates that cave drip waters have had time to react (by precipitating $CaCO_3$) to changes in the pCO_2 of the water, driven by variable CO_2 degassing before water collection (Tremaine et al., 2011).

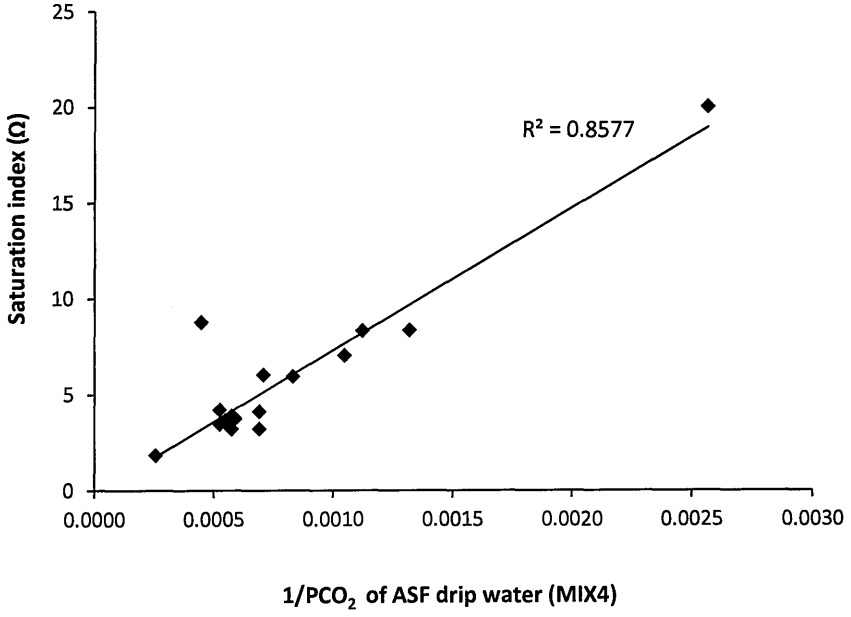

Figure 4.15: $1/pCO_2$ of ASF drip rates vs. saturation state (Ω) calculated using Equation 4.1.

There is however, no obvious evidence that bulk water SS is influenced by monthly average cave air pCO_2, as shown by Tremaine et al., (2011). Asiul bulk drip waters therefore, appear to be in partial equilibrium, where drip water saturation state is strongly related to the drip water pCO_2 value (near equilibrium $CaCO_3$ deposition has occurred); but the pCO_2 of the drip water is not in equilibrium with the surrounding cave air. This is unexpected over such a long sampling time period ($\approx$ 1 month).

One possible explanation of this unexpected disequilibrium between measured cave air and collected bulk drip water samples is the method of within cave water collection. Bulk water samples are collected in large plastic jerry cans with a small entrance hole. Drip water

collected within the cans will equilibrate CO_2 with the surrounding air. Due to the constricted entrance, poor air flow and the high density of CO_2, it is possible jerry can collected waters are equilibrating with a layer of higher pCO_2 air, sourced directly from water CO_2 degassing within the cans, and not cave air pCO_2 values. It is possible this problem will be ubiquitous within cave sites which use bulk water collection vessels. If this hypothesis is correct, drip waters within the jerry cans are in equilibrium with the jerry can's micro atmosphere. Using Figure 4.14, jerry can air can be calculated as reaching values between 1500 and 2500 ppmv. This problem with sampling procedure explains why cave pool waters (fully exposed to the cave air pCO_2 and cave ventilation) and bulk drip waters reflect different water pCO_2 equilibrium conditions; when apparently exposed to the same atmospheric conditions.

4.4.3 Drip Water Electrical Conductivity

Electrical conductivity (EC) measurements taken from bulk drip water collection vessels (primarily ASR and ASF) and the CTD diver housing demonstrate decreasing values throughout the summer and a return to higher levels at the onset of winter (Table 4.1). Monthly average data shows a strong positive correlation between EC and average drip rate (Pearson correlation; $r= 0.61$; $p<0.01$; $n-2 = 20$). Contrary to these observations previous studies have associated high EC values in cave drip waters with long rock water contact times and low drip rates (Borsato et al., 1997, Fairchild et al., 2006, Miorandi et al., 2010). These relationships are however, not observed in Asiul (Figure 4.16). Both bulk water collections and high resolution EC logging suggest in Asiul the opposite occurs; maximum EC values correspond to high drip rates and a less arid karst. Factors controlling EC cannot therefore be linked to karst water residence time and bedrock dissolution at this site.

High resolution data logging uses stalagmate drip counters and a CTD EC probe which is housed, constantly submerged in 100 ml of water and open to cave atmospherics. Water exchange time for this housing is calculated using an average drip rate of 1.6 D/min and drip volume of 0.076 as approximately 14 hours. This time reflects the required interval for full water exchange; it is expected that rapid changes in EC would be smoothed due to the exchange and mixing of water.

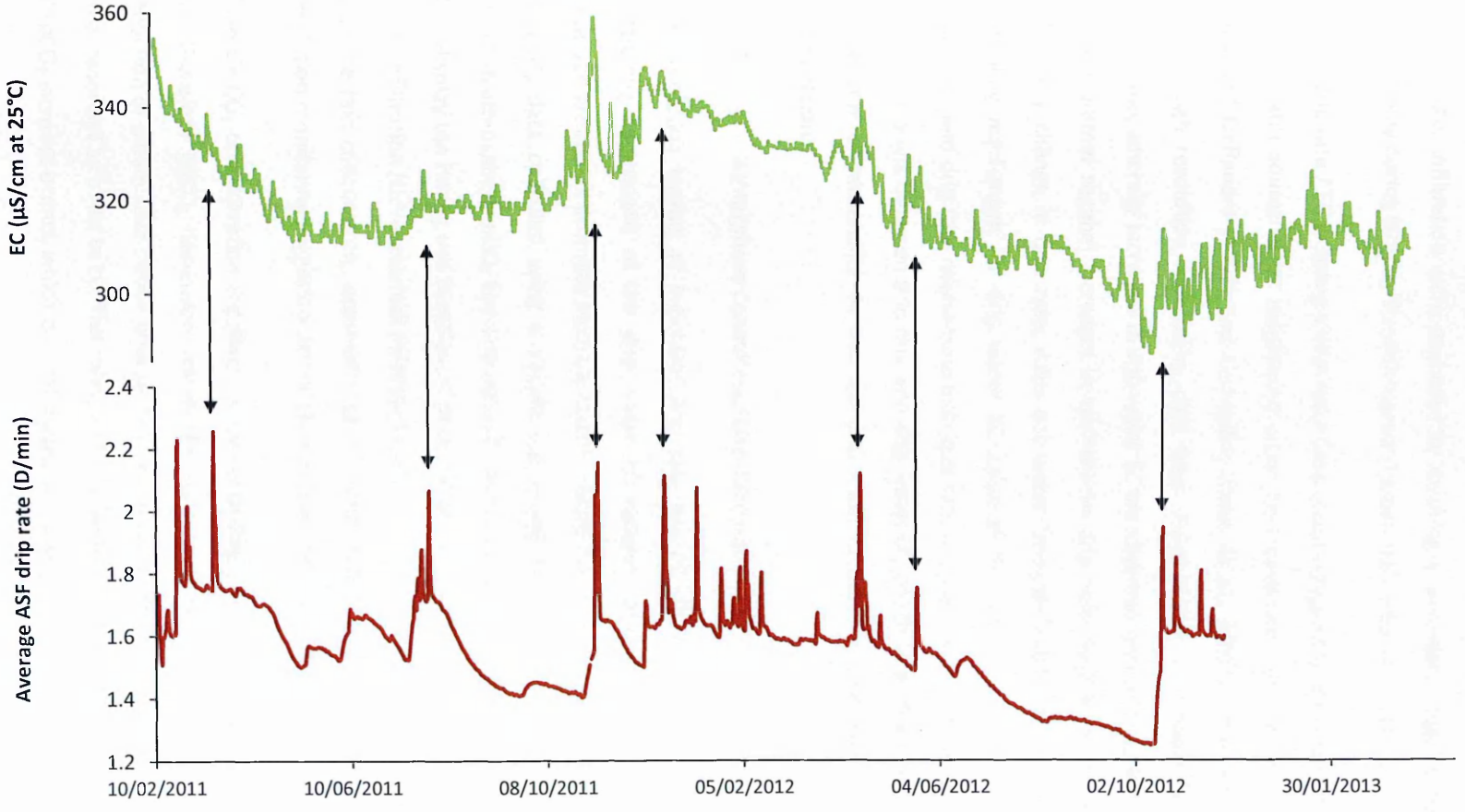

Figure 4.16: Speleothem ASF average drip rate (red line) and CTD diver logged EC (green line) between Feb 2011 and April 2013.

Continuous CTD Diver logging highlights the positive EC vs. drip rate co-variation during peak flows, indicated in Figure 4.16 by black arrows. This relationship has been observed before in cave drip waters by Genty and Deflandre (1998). In that study, increases in EC during periods of high water infiltration were explained by invoking a secondary (high EC) water source, activated only during large infiltration events (Fernandez-Cortes et al., 2007).

Positive drip rate / EC coupling within Asiul Cave could indicate the activation of a secondary, high EC water source under heightened water flow conditions, as previously observed by Genty and Deflandre (1998) and Fernandez-Cortes et al., (2007). However, unlike these studies, high resolution monitoring data from Asiul depicts a variable EC / drip rate relationship; whereby increases in drip water EC are observed both after (winter regime) and before (summer regime) increases in speleothem drip rate. Such a rise in drip water EC before any change in drip rate, rules out water from secondary high EC source as the controlling mechanism for drip water EC value at this site. This temporally decoupled positive EC and drip rate relationship indicates that another component of the cave system must act as a link between drip rate and drip water EC, controlling measured drip water EC independent of seasonality. At this site drip water EC value is controlled by cave air CO_2 concentration.

4.4.3.1 Atmospheric Control over Drip Water EC

High resolution logging of individual drip rate and EC increase events indicates a third controlling component of the drip water EC system. Atmospheric pCO_2 increases are observed around all drip rate increase events. Figure 4.17 incorporates high resolution cave air pCO_2 data collected using a Vaisala CO_2 probe which shows a positive co-variation between atmospheric pCO_2 and drip water EC at the ASF drip site. The dashed lines in Figure 4.17 display the timing and duration of pCO_2, EC and drip rate events, surrounding one high water infiltration (storm related) increase in July 2011. EC and cave air pCO_2 rise and cave air pressure falls concurrently, approximately 12 hours before any rise in drip rate. This high resolution monitoring suggests a de-coupling of drip water EC from drip rate.

Cave air CO_2 concentration regulates EC by controlling drip water CO_2 degassing potential and therefore $CaCO_3$ deposition within the cave chamber (Tremaine et al., 2011). The reduction of within cave calcite precipitation leaves drip waters with a higher dissolved solid load, recorded as a rise in EC. This relationship is observed most clearly during discrete cave air pCO_2 increase events, which occur throughout the year in Asiul.

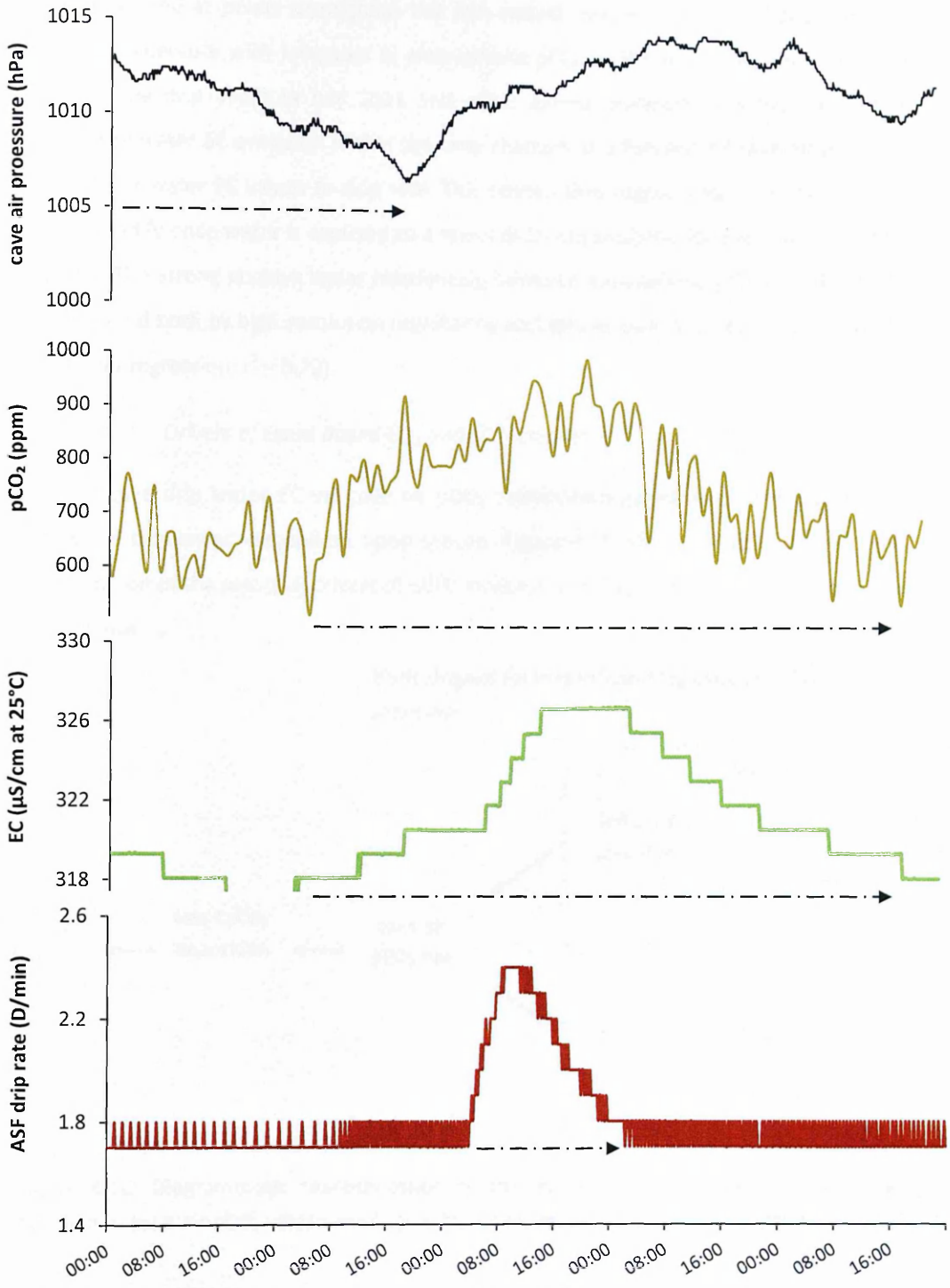

Figure 4.17: Cave air pressure (black line), EC (green line), drip rate (red line) and atmospheric CO_2 (gold line) from 24th to 29th of July 2011. CO_2 measured every hour and pressure, drip rate and EC every 10 minutes. Dashed black arrows indicate the timing and duration of an event which affected all measured parameters.

This is confirmed at points throughout the ASR record, where increases in drip water EC occur simultaneously with increases in atmospheric pCO_2 whilst no change to drip rate is observed. The drip event in July 2011 and other events analysed at a high resolution, indicate drip water EC evolution within the cave chamber is a function of cave air pCO_2, not variable karst water EC values or drip rate. This relationship suggests karst water EC values begin to modify once water is exposed to a lower pCO_2 atmosphere, for example that of the cave void. This strong positive linear relationship between atmospheric pCO_2 and drip water EC is observed both by high resolution monitoring and also in waters collected on a monthly scale (linear regression; $r^2 = 0.72$).

4.4.3.2 Drivers of Event Based CO_2 and EC Increases

The Asiul cave drip water EC vs. cave air pCO_2 relationship appears to have two distinct behavioural sequences, dependent upon season. Figure 4.18 offers a simple diagrammatic representation of the seasonal drivers of pCO_2 increase and therefore increases in drip water EC at this site.

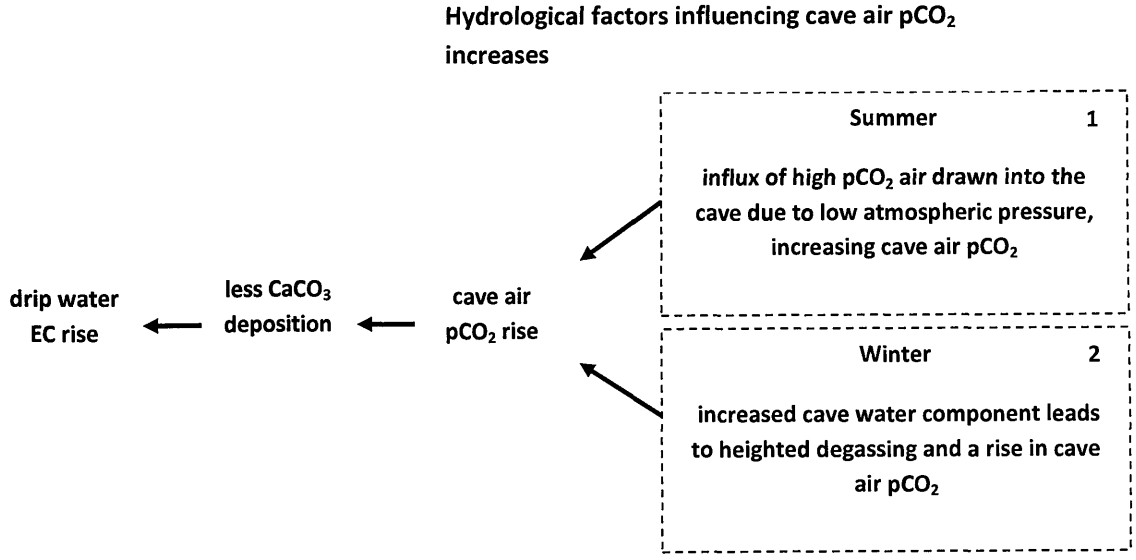

Figure 4.18: Diagrammatic representation of the driving forces behind EC rise as a function of cave air pCO_2 within Asiul cave. Numbers relate to textual description.

Seasonally variant CO_2 increases, associated with periods of heightened drip discharge can be a result of two different processes (Figure 4.18), dictated by karst hydrological conditions.

1) Under summer conditions cave air pCO_2 and EC are shown to increase and air pressure decrease hours prior to the onset of high infiltration drip events (Figure 4.17), marked as an increase in drip rate. During the dry summer months, seasonal

density driven ventilation acts to slowly draw high pCO_2 soil air down through the karst, into the cave system (Spotl et al., 2005). However, this seasonal process cannot explain the rapid increases in cave air pCO_2 experienced prior to hydrological events. Observed pCO_2 increases are still the result of karst air draw down, but are derived from a secondary ventilation process. Secondary ventilation is driven by external air pressure, which decreases under enhanced storm activity (Genty and Deflandre, 1998). Low external pressure draws air out of the cave system, in turn lowering the atmospheric pressure of the cave void (Figure 4.19). Reductions in cave air pressure results in the rapid drawdown of karst air. The addition of soil or karst air into the cave causes cave air pCO_2 and consequently drip water EC to increase, hours before any rise in drip rate is observed (a result of enhanced water infiltration under storm conditions). Once drip rates begin to increase, a further rise in cave air CO_2 concentration would be expected associated with enhanced drip water degassing, similar to winter conditions (below). This process of pressure induced air drawdown has been seen before by Genty and Deflandre, (1998) coupled to an increase in drip rate, although this control over drip rate is thought to be less prevalent under low discharge summer conditions.

2) During winter drip events however (shown in Figure 4.20), atmospheric pCO_2 increases slightly after drip rate. During the winter, large areas of the karst operate under phreatic conditions, inhibiting the drawdown of high pCO_2 (soil) air. It is therefore, the increased volume of water entering the cave which causes a rise in CO_2 degassing and therefore cave air pCO_2 (Figure 4.18 + 4.19). This rise in cave atmospheric pCO_2 subsequently drives EC increase, explaining why pCO_2 and EC values only rise after drip rate during the winter.

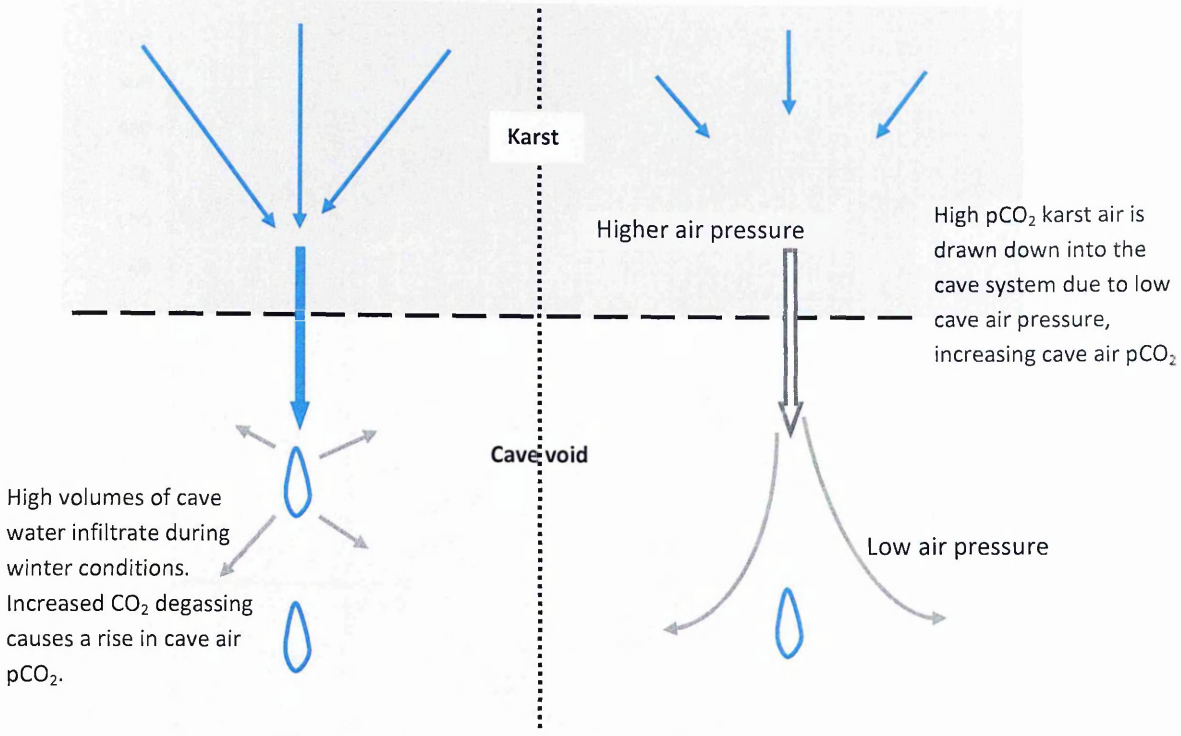

Figure 4.19: Diagrammatic representation of karst and cave processes which result in a cave air pCO_2 increase during water infiltration during both winter (left) and summer (right) conditions.

Figure 4.20 displays the winter system; an almost concurrent increase in pCO_2 and drip rate is observed at the beginning of the winter infiltration event. Large volumes of water enter the cave system during the event and begin to degas CO_2 immediately, triggering a rise in atmospheric CO_2 values. It is not for 5.5 hours after the initial rise in drip rate and pCO_2 that EC values begin to increase. This delay in EC rise may be influenced by the flushing time of the CDT Diver housing, which impedes the immediate transition to higher EC values.

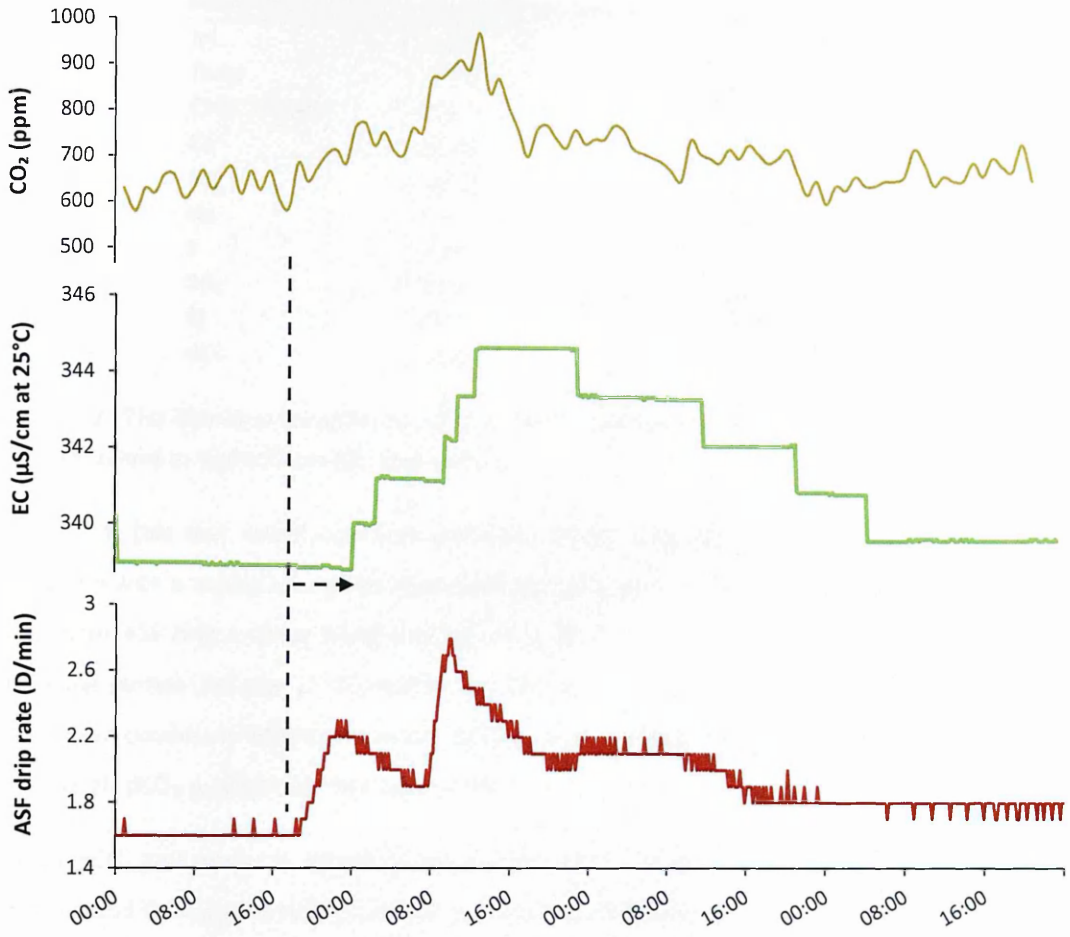

Figure 4.20: EC (green line), drip rate (red line) and atmospheric CO_2 (gold line) from 21st to 24th of Feb 2011. Dashed black arrows show the delay associated with EC increases after the onset of the event.

EC, pCO_2 and drip rate logging at high resolution has demonstrated the complex physical and chemical relationships which occur within the Asiul Cave system. Using MIX4 speciation modelling the interconnections between drip water EC and cave air CO_2 can be simulated under experimental conditions to estimate a change in EC for any given increase in atmospheric pCO_2.

4.4.3.3 Modelling EC Change as a Function of Atmospheric pCO_2

To ensure that the ranges of EC change monitored in Asiul can be fully attributed to a change in cave air pCO_2; EC was modelled using a combination of MIX4 speciation and the Rossum (1975) equation for a series of different monitored cave air pCO_2 variations. A "test" cave water, with average bulk drip water values (from speleothem ASF) was created; the makeup of this simulated water is shown in Table 4.2.

Model component	Average drip water value	Units
pH	8.06	
Temp	13.75	°C
CTOT (Or DIC)	205	ppm
Ca	38.11	ppm
Mg	16.05	ppm
Na	4.39	ppm
K	0.24	ppm
SO_4	1.02	ppm
Cl	6.92	ppm
NO_3	0.33	ppm

Table 4.2: The chemical constituents of the "test" solution run in MIX4 derived from average values in speleothem ASF drip waters.

Using MIX4, this test water was then degassed whilst allowing $CaCO_3$ to precipitate in equilibrium with a calcite saturation index held at 0.32 (equal to the average value found in speleothem ASF drip waters) using a LOGk value of -8.05. The model simulates a slowly decreasing partial pressure of CO_2 within the test water. This is used as an analogue for natural cave conditions where cave water $pCO_{2\ (aq)}$ is expected to be in chemical equilibrium with cave air $pCO_{2\ (g)}$, shown by cave pool waters.

As high pCO_2 test water is forced to equilibrate with a lower pCO_2 cave air, both CO_2 degassing and $CaCO_3$ precipitation would be expected. The MIX4 model shows under lower cave air pCO_2 conditions the test water Ca ion concentration, CTOT and alkalinity all decrease after $CaCO_3$ precipitation has been simulated (Table 4.3).

MIX4 step coefficient	Ca TOT (ppm)	CTOT (ppm)	PPCO2	Ca SI	Alkalinity (ppm)	pH	EC from Rossum (µS)
0	38.11	205	2.83	0.3	166.3	8.06	302.41
0.0001	34.82	193.93	2.93	0.32	158.0	8.14	288.68
0.0002	31.35	182.55	3.02	0.32	149.4	8.21	274.23
0.0003	27.85	171.12	3.13	0.32	140.6	8.28	259.53
0.0004	24.34	159.67	3.24	0.32	131.8	8.37	244.75
0.0005	20.83	1448.23	3.37	0.32	123.1	8.46	229.99
0.0006	17.37	136.85	3.51	0.32	114.4	8.51	215.32

Table 4.3: Model outputs from MIX4 and Rossum (1975) as degassing and $CaCO_3$ precipitation are modelled from test water.

Calcite precipitation and the attributed reduction in dissolved solids are present as a reduction in alkalinity and therefore synthetic EC. For the Asiul test solution the relationship between $ppCO_{2\,(aq)}$ and EC follows a linear model (linear regression; $r^2 = 0.995$), presented in Equation 4.2.

$$\text{Drip water EC} = (-129.31 * ppCO_2) + 666.25 \quad (4.2)$$

Therefore if cave air $pCO_{2\,(g)}$ and cave water $pCO_{2\,(aq)}$ are in chemical equilibrium, we would expect drip water EC to be a function of cave atmospheric pCO_2 following the linear model of Equation 4.2. The validity of this model was then tested using cave analogue conditions.

Equation 4.2 shows for a 0.05 $ppCO_2$ (100 ± 9.15 ppmv) change in atmospheric pCO_2 an expected change of 6.5 ± 0.8 µS in drip water EC would occur if simulated equilibrium conditions hold true. Table 4.4 displays the modelled output for theoretical EC change during real covariant increases in $pCO_{2\,(cave\ air)}$ and $EC_{(drip\ water)}$ monitored between 2011 and 2013 in Asiul Cave.

Date	Background pCO_2 (ppm)	Monitored pCO_2 rise (ppm)	Monitored EC rise (µS)	Modelled EC rise (µS ± 1.3)	Difference (µS ± 1.3)
21-02-2011	590	260	5.9	16.8	10.9
16-03-2011	730	200	8	14.2	6.2
24-07-2011	510	480	10	31	21
24-05-2012	780	470	8.5	26.5	18
29-05-2012	570	370	7.3	28.1	20.8
01-06-2012	630	220	4.9	16.8	11.9
12-06-2012	680	80	2.4	6.2	3.8
21-06-2012	580	120	2.5	10.3	7.8
27-06-2012	530	510	11	44.6	33.6
13-07-2012	450	190	3.7	19.8	16.1
18-07-2012	510	300	7.3	25.9	18.6
24-07-2012	480	320	6.2	28.7	22.5
15-01-2013	620	180	12.2	14.3	2.1
17-01-2013	630	240	10.7	18.1	7.4
02-02-2013	540	260	7.7	22.1	14.4
06-02-2013	620	190	8.8	15.0	6.2
21-03-2013	540	400	7.5	31.1	23.6

Table 4.4: Measured and modelled changes in EC driven by event based changes in $pCO_{2\,(cave\ air)}$ during two events in 2011.

However, equilibrium (modelled) increases in EC are always higher than those observed naturally within the cave environment. The offset between measured and modelled EC change as a function of pCO_2 rise is due to either 1) water mixing within the EC probe

housing or 2) incomplete equilibrium degassing of individual drips. In the second case, the offset between modelled and observed EC values shows that either drip water CO_2 degassing or secondary $CaCO_3$ precipitation remains temporarily enhanced under increasing cave air pCO_2 conditions; suggesting some disequilibrium in the cave carbon system during rapid increases in cave air pCO_2. In reality, combinations of these processes are probably responsible for the lower than expected increases in drip water EC. Regardless of the observed offset, data from Asiul Cave shows that in all cases natural changes to drip water EC and therefore $CaCO_3$ deposition can be explained by a changes in cave air pCO_2; without the need to invoke changes in karst hydrology, as suggested by previous studies.

This finding is important for high resolution cave speleothem analysis. Until recently, the resolution of speleothem trace element analysis for palaeoclimate reconstruction was at best seasonal (Treble et al., 2003, Johnson et al., 2006), so there was little requirement to understand sub-seasonal or event based variations in speleothem growth rate and trace element incorporation. However, recent work using synchrotron micro-X-ray fluorescence (μXRF) has improved the resolution of speleothem trace element analysis to such an extent that individual hydrological events can be identified within the speleothem record (Wynn et al., 2014). Therefore, the need to understand the mechanisms which control such high resolution changes in speleothem deposition and elemental uptake is become ever more important.

Work to understand the observed high resolution changes in cave air pCO_2 in Asiul, ties in well with the recent high resolution speleothem analysis undertaken in Obir Cave (Wynn et al., 2014). Wynn et al., (2014) identify significant positive co-variations between Zn and SO_4^{2-} during three years of speleothem growth. Whilst Zn increases are attributed to high water flux events which actively mobilise natural organic matter (NOM) and colloidal material to which Zn is bound (Hartland et al., 2012), increases in speleothem SO_4^{2-}/CO_3^{2-} ratio are related to enhanced cave air CO_2 concentrations and a relative reduction in CO_3^{2-} uptake into speleothem deposits (Frisia et al., 2005, Wynn et al., 2014). The short lived co-variations in speleothem Zn and SO_4^{2-} concentrations observed in Obir require a concurrent change in both hydrological and atmospheric systems, similar to that described from cave monitoring in Asiul. Further high resolution analysis is therefore required especially from cave sites from which speleothems are extracted for very high "event" resolution climate analysis.

4.4.4 Drip Water Isotope Chemistry: Oxygen

Drip waters were collected throughout Asiul at discrete time intervals between April 2010 and April 2013 for isotopic and trace element analysis. Oxygen isotope values of cave drips and pools ranged between -8.34 and -3.68 ‰ with an average value of -6.00 ‰ (n= 155). Only a small (1 ‰) seasonal variation is observed in drip water oxygen isotopic value throughout the cave, with little obvious relationship between drip rate and isotopic value throughout the cave site. Cave drip sites (including very high throughput sites) do not exhibit the range of isotopic values which are observed in rainfall. Infiltrating water must therefore undergo some mixing within the bedrock above the entirety of the cave.

Bulk (monthly) water isotopic values from speleothems ASF, ASM and ASR show similar seasonal homogeneity (Table 4.5).

	Summer average		Winter average		Total average	
	$\delta^{18}O$	δD	$\delta^{18}O$	δD	$\delta^{18}O$	δD
Speleothem ASF	-6.12 (n=12)	-34.62	-6.06 (n=14)	-33.98	-6.09 (n=26)	-34.26
Speleothem ASM	-5.99 (n=6)	-37.09	-6.38 (n=5)	-36.59	-6.03 (n=11)	-34.87
Speleothem ASR	-6.12 (n=6)	-34.23	-6.06 (n=10)	-34.17	-6.08 (n=16)	-34.19

Table 4.5: Oxygen and Deuterium isotope values of bulk waters collected at the three main speleothem sampling sites. The numbers of samples which make up these average values are shown alongside the $\delta^{18}O$ values.

The homogeneity of values across sites and throughout the year suggests the karst aquifer above Asiul is predominantly replenished by one, isotopically similar source of water, and not subject to fractionation in different parts of the aquifer. Previous water excess calculations (section 4.2) suggest the aquifer at this site should primarily be replenished by winter rainfall. Oxygen and deuterium isotope measurements from seasonal rainfall in Matienzo and cave drip waters are presented together in Figure 4.21a and 4.21b.

Bulk cave drip waters (collected throughout the year) cluster over both the average isotopic value of winter (October-March) rainfall (n= 111) and also the LMWL of winter rainfall (δD = 7.1646 ($\delta^{18}O$) + 8.847) (Figure 4.21a). This suggests karst waters are, as expected from external monitoring, primarily composed of winter rainfall. Drip waters exhibit a smaller isotopic range (range: $\delta^{18}O$ = 1.6 ‰; δD = 14.7 ‰) than their parent winter rainfall (range: $\delta^{18}O$ = 15.9 ‰; δD = 134.2 ‰), indicating significant mixing within the karst zone. Speleothems from Asiul are therefore expected to reflect long term variations in bulk

(average) winter rainfall chemistry, rather than a representative composite of the whole year's rainfall.

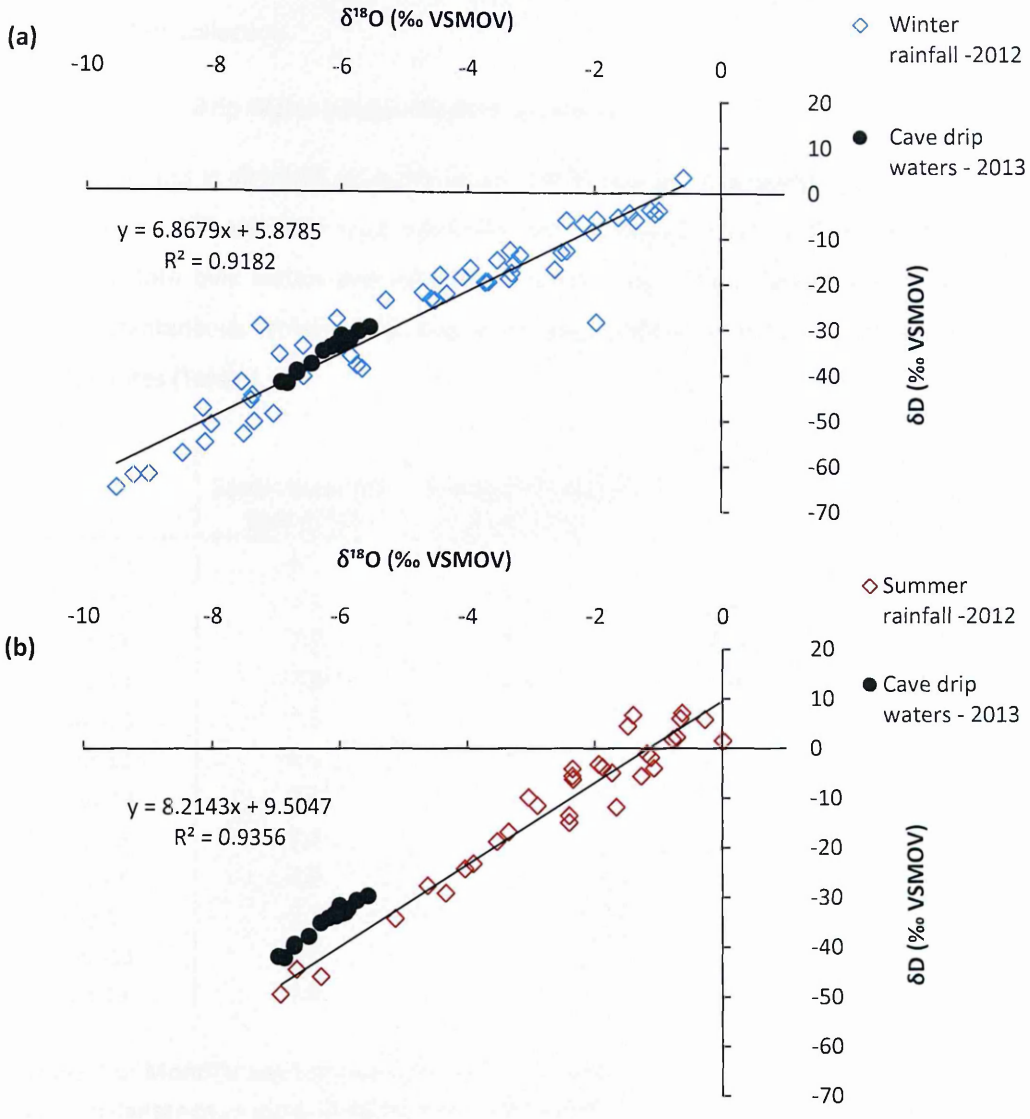

Figure 4.21: (a) Winter precipitation (Oct – March 2012) values (blue diamonds) and LMWL (equation) alongside cave drip waters (2013, black circles). (b) Summer precipitation (April – September 2012, red diamonds) and LMWL (equation) with cave drip waters (2013).

The dominance of a winter rainfall isotopic signature in cave drip waters (including those collected in the summer months) indicates that one single source of cave water exists at this site. Under such conditions, piston flow is the most likely mechanism responsible for causing increases in speleothem drip rates. However, it is possible that periods of water overflow or direct through flow are under or misrepresented within the data set. The sampling regime

employed (both bulk monthly sampling and one off instantaneous drip water collection) means heavy rainfall events which may travel through the karst as overflow events, may not be captured due to the timing of instantaneous sampling trips or may be diluted in the case of bulk waters collection.

4.4.5 Drip Water Isotope Chemistry: Carbon

Carbon isotopes in dissolved inorganic carbon (DIC) have been measured in Asiul drip waters (speleothems ASF and ASR) since November 2012, meaning annual cyclicity cannot yet be assessed. Both bulk waters and instantly collected waters have been analysed, although fewer instantaneous samples exist due to the long duration collection times, especially at low drip rates (Table 4.6).

	Speleothem ASF Bulk ($\delta^{13}C$)	Speleothem ASF Instant ($\delta^{13}C$)	Speleothem ASR Bulk ($\delta^{13}C$)	Speleothem ASR Instant ($\delta^{13}C$)
Nov-12	-6.6		-6.5	
Dec-12	-7.3	-7.9	-6.8	-9.3
Jan-13	-7.0	-8.8	-6.6	-7.5
Feb-13	-7.8	-8.4	-7.1	-7.2
Mar-13	-5.3		-5.3	
Apr-13	-8.1	-10.4	-8.3	-5.8
May-13	-9.4		-9.8	
Jun-13	-7.3		-7.2	
Jul-13	-7.8		-7.0	
Aug-13	-7.1		-6.6	
Sept-13	-6.9		-7.2	
Oct-13	-7.3		-8.0	

Table 4.6: Monthly average cave drip water $\delta^{13}C$ values from two speleothem drip sites, both instantaneous and bulk water collections are shown. Only ASR sample Apr-13 shows the bulk sample $\delta^{13}C$ value to be less negative than the instantaneous value.

For the majority of cases (excluding ASR Apr-13) bulk water sample carbon isotope values are less negative than their corresponding instantaneous water sample (by 1.3 ± 1.2 ‰); as would be expected under a Rayleigh style fractionation process associated with CO_2 degassing and the preferential loss of lighter ^{12}C to the cave atmosphere as time progresses. This explains why bulk (fully degassed) samples show a strong positive linear relationship between drip sites (linear regression; $r^2 = 0.9$) as both sets of water are equilibrating with a

similar parcel of cave air (although this may have been a jerry can induced micro-atmosphere, similar at both collection sites).

Instantaneously measured cave waters should not have had a chance to evolve within the cave chamber; however these waters already display signs of modification prior to their collection at the stalactite tip (Figure 4.22). Equilibrium fractionations for $\delta^{13}C$ from soil gas to drip water CO_3^{2-} are well established, with an approximate enrichment in ^{13}C by 8.6 ‰ between phases at 15 °C (Clarke and Fritz 1997). For C3 plant communities present above Asiul, the pCO_2 of overlying soils (Asiul average = -18.7 ‰) equilibrates with percolating waters and should form an equilibrium dissolved carbonate value of ≈ -10.1 ‰ (Clarke and Fritz 1997). This value is however, slightly more negative than any water collected in the Asiul cave site (Figure 4.22).

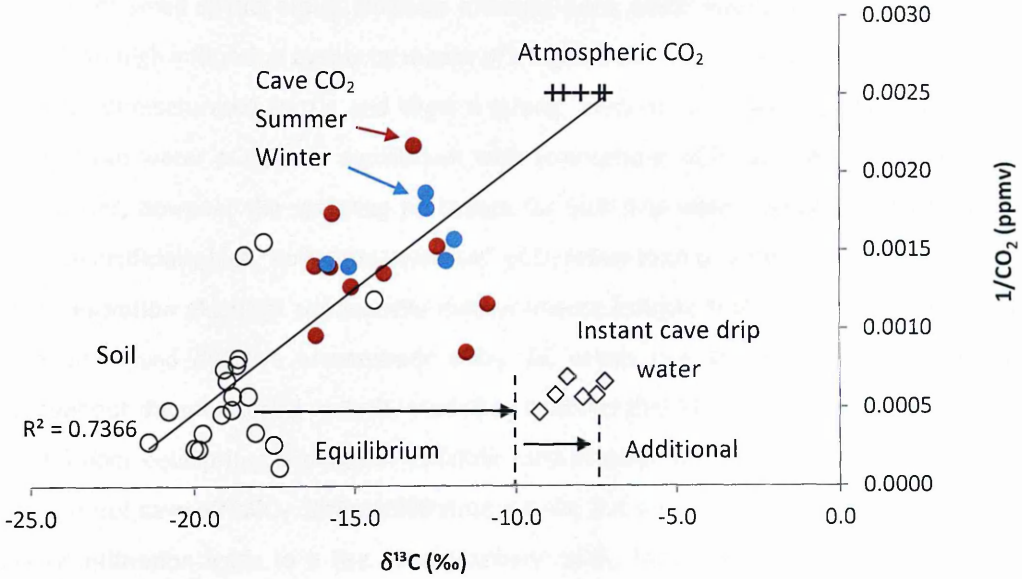

Figure 4.22: pCO_2 concentration vs. $\delta^{13}C$ of air samples from the external atmosphere (black crosses), cave atmosphere (coloured circles) and soil atmosphere (hollow circles) as well as values from cave drip waters (hollow diamonds). Black arrows and hashed lines denote firstly the expected equilibrium fractionation between soil air and cave drip water $\delta^{13}C$ at 15 °C (Clarke and Fritz 1997) and secondly the additional fractionation experienced in Asiul cave waters.

Modification of Asiul drip water $\delta^{13}C$ toward less negative isotopic values, which lie away from a theoretical $\delta^{13}C$ value of -10.1 ‰ can occur through several processes; but should not be effected by within cave degassing due to the instantaneous collection technique. Firstly, if water percolates under closed system conditions it becomes isolated from the overlying soil air $\delta^{13}C$ value (McDermott 2004), subsequent dissolution of bedrock drives the $\delta^{13}C$ value of

waters toward a bedrock value (≈ 1 ‰). The second process which could have caused the increase the $\delta^{13}C$ value of drip waters is PCP. During PCP CO_2 degassing occurs in the karst, leaving drip waters relatively enriched in ^{13}C increasing the $\delta^{13}C$ values measured within the cave environment. Without further analysis of within karst processes such as PCP it is not possible to identify whether closed system dissolution or PCP causes the observed offset in $\delta^{13}C$ between expected and measured values. Drip water sampling in Asiul shows that the $\delta^{13}C$ value of cave drip waters does not directly reflect a soil or plant productivity value. Karst processes act to modify this signal over short time periods, possibly reducing the capability of $\delta^{13}C$ to be used as a palaeo-vegetation indicator from speleothems deposited at this site.

Section 4.4 has demonstrated through the use physical and chemical parameters in cave drip water that winter rainfall as the primary source of karst recharge. The homogeneity of the karst over small spatial scales indicates effective karst water mixing. Cave drip sites react rapidly to high infiltration events by means of a highly sensitive piston effect. Drip waters are usually supersaturated for Ca and show a strong relationship between SS and drip water pCO_2. Cave water pCO_2 is in equilibrium with atmospheric pCO_2 as shown by pool water collections, however the sampling procedure for bulk drip waters means they equilibrate with an artificially high "collection vessel air" pCO_2 rather than true cave atmospheric values. High resolution electrical conductivity measurements indicate that drip water chemistry is also influenced by cave atmospheric pCO_2. EC values rise as cave air pCO_2 increases throughout the monitoring records. Modelling confirms that EC is a function of atmospheric pCO_2 under equilibrium conditions. Differing karst atmospheric and hydrological conditions can control cave air pCO_2 during infiltration events, but under all conditions an increase in water infiltration leads to a rise in atmospheric pCO_2. Increases in pCO_2 during drip rate increase events (by whichever mechanism) retards the deposition of $CaCO_3$ at the site if all other conditions remain stable. Speleothem development would therefore be expected to reduce under higher water input, high cave air pCO_2 conditions.

Instantaneous drip water carbon isotope analysis, indicates that a within karst process either, closed system conditions or calcite-water interactions control drip water and therefore speleothem $\delta^{13}C$. For this reason, speleothem $\delta^{13}C$ is not thought to present a robust archive of vegetation and soil processes at this site, but may be used in conjunction with other proxies to establish within karst conditions, over longer time periods.

4.5 Trace Element Chemistry

Trace element chemistry is regularly analysed in precipitation and cave drip waters. Trace elements can be used to help identify the trajectories of rain bearing air masses and the extent to which infiltrating water may have experienced evaporation throughout the karst. Cave drip waters are analysed to identify changes in karst dissolution, periods of karst water deficit, or excess and the occurrence of prior calcite precipitation (PCP) or incongruent calcite dissolution (ICD) (McGillen and Fairchild 2005, Sinclair et al., 2012). Trace elements can be used in conjunction with drip water pH and temperature data to assess the evolution of karst waters using MIX4 chemical speciation (Plummer et al., 1975, Fairchild et al., 1994, Fairchild et al., 2000). MIX4 is used to model karst system end members (for example soil pCO_2) and within cave reactions (CO_2 degassing and calcite precipitation). Modelled outcomes help assess the extent to which drip waters have evolved during their transit from soil to cave.

4.5.1 Rainfall Trace Element Chemistry

Water collected during rainfall events and from cave drip sites was analysed for a suite of trace elements (Mg, Si, Sr, Ca, K, Na, Cl, SO_4, and NO_3). Table 4.7 shows the average weighted mean concentration of trace elements within seasonal rainfall events collected in Matienzo between Feb 2011 and Feb 2012 (no of analysed events = 28). All trace elements exist in very low concentrations in rainfall; Ca and Mg concentrations lie below the LOD and are therefore not included in Table 4.7. The low rainfall trace element concentrations measured at this site indicates that as with many cave locations the karst is the predominant source of cave drip water trace elements.

4.5.2 Soil, Vegetation and Karst Contribution to Trace Element Concentration

The soil, vegetation and karst zones are the major sources for trace elements incorporated into cave drip waters. Elemental uptake into infiltrating water occurs through the processes of colloidal and particulate flushing (Hartland et al., 2012), bedrock dissolution (McDermott 2004) and soil biogeochemical processes (Treble et al., 2003, Borsato et al., 2007). These processes entrain different trace elements at different rates or times, dependent mainly upon supply processes (trace element weathering, soil and vegetative processes, atmospheric fluxes) and removal processes (mineral precipitation, solid deposition and adsorption) (Fairchild and Baker 2012). The key process which controls the uptake of elements is water residence time within the soil and upper karst zones. Long residence times

allow slower weathering processes to occur, releasing elements derived from less soluble sections of the karst; whilst short residence times can only release highly soluble elements or those transported attached to solid particulates. Trace element concentrations can therefore be used as a proxy to describe hydrological conditions within the karst. Average trace element values in Asiul cave waters are shown in Table 4.7. Using precipitation data the percentage of trace element derived from the soil and karst is calculated.

	Ca (ppm)	Mg (ppm)	Na (ppm)	K (ppm)	Si (ppb)	Sr (ppb)	Cl (ppm)	SO_4 (ppm)	NO_3 (ppm)
Weighted Average Rain Waters	-	-	1.35	0.07	12.70	4.16	2.96	0.52	0.18
Weighted Average Cave Waters	38.01	16.36	4.42	0.33	501.27	11.27	6.91	1.08	0.32
% Trace Element derived from soil, vegetation cycling or karst	**100**	**100**	**69.4**	**78.7**	**97.4**	**63.1**	**57.2**	**51.7**	**43.3**
LOD	0.036	0.006	0.045	0.063	8.227	0.394	0.525	0.159	0.021
Blank standard deviation	0.012	0.002	0.015	0.021	2.742	0.131	0.175	0.053	0.007

Table 4.7: Average weighted mean trace element concentrations in rainfall and average cave water values. The percentage of each element sourced within the soil and karst is also displayed.

Table 4.7 shows greater than 50% of trace elements (excluding NO_3) are sourced after rainfall reaches the surface, either within the soil and karst or due to concentrating effects during evaporation. In subsequent sections the seasonality of trace element uptake from soil, vegetation and karst zones is addressed at Asiul Cave. Elements such as NO_3 and SO_4 which exhibit a significant contribution from rainfall have been corrected for a marine aerosol contribution using Equation 4.3, this allows for the analysis of soil, vegetation cycling and karst contributions to elemental concentration so we can assess how these processes may vary over seasonal scales.

Karst TrE total = Drip water TrE – Rainfall TrE (4.3)

Karst TrE total refers to the amount of any element which is sourced from the karst zone; drip water TrE refers to the concentration of any given element in Asiul cave drip waters and Rainfall TrE refers to the initial concentration of the element measured in rainfall collected in Matienzo.

4.5.4 Trace Element Reaction to Soil and Karst Water Evaporation

Some trace elements become enriched in solution during evaporation from the soil and upper karst. Cl can be used in conjunction with SO_4 to assess such evaporative effects throughout the karst system. Both elements are derived from a marine aerosol source, producing a distinct SO_4/ Cl ratio in rainfall. During evaporation SO_4 and Cl concentrations intensify, but the ratio of elements remains constant. If cave drip waters exhibit the same SO_4/ Cl ratio but higher concentrations than original rainfall, evaporation in the soil or karst must have occurred.

In Asiul, a slight enrichment of both Cl (3.2 ppm enrichment between rainfall and drip water) and SO_4 in cave drip waters (0.63 ppm enrichment between rainfall and drip water) occurs during the winter. During winter a stable SO_4/ Cl ratio is recorded between rainfall (ratio = 0.14) and cave drip water (ratio = 0.16), suggesting evaporation is the main source of the observed trace element enrichments. Summer enrichments of Cl (5.3 ppm between rainfall and drip water) and SO_4 (1.0 ppm between rainfall and drip water) are greater than those observed during the winter. The SO_4/ Cl ratio of summer rainfall (ratio = 0.42) is not however, the same as cave drip waters (ratio = 0.22), suggesting evaporation is not the source of this trace element enrichment. The observed change between summer rainfall and cave water ratio is either due to 1) sulphate loss within the karst zone or 2) the mixing of small amounts of summer rainfall (SO_4/Cl ratio = 0.42) into karst waters predominantly derived from winter rainfall (SO_4/Cl ratio = 0.14).

Due to the minimal amount of summer rainfall infiltration into the karst, this second process effectively eradicates the signal of summer rainfall (SO_4/Cl ratio = 0.42), creating a bulk, mainly winter derived karst water SO_4/Cl ratio. SO_4/Cl ratio analysis therefore concurs with calculations of effective precipitation and oxygen isotope analysis in suggesting summer rainfall may offer only a minimal amount of water input to the karst aquifer. The chemical (SO_4/Cl) signature of any summer infiltration is overprinted by the larger reservoir of winter derived karst water. The following section assesses seasonality in other trace elements, with

the aim of understanding driving forces behind the trace element concentration of cave drip water.

4.5.3 Drip Water Trace Element Seasonality

Temporal evolution of drip site trace element chemistry can be observed in bulk monthly samples collected from speleothem drip sites. Drip sites ASF and ASR have multi annual trace element records (Figure 4.23) in which, the behaviour of major elements can be observed on seasonal scales.

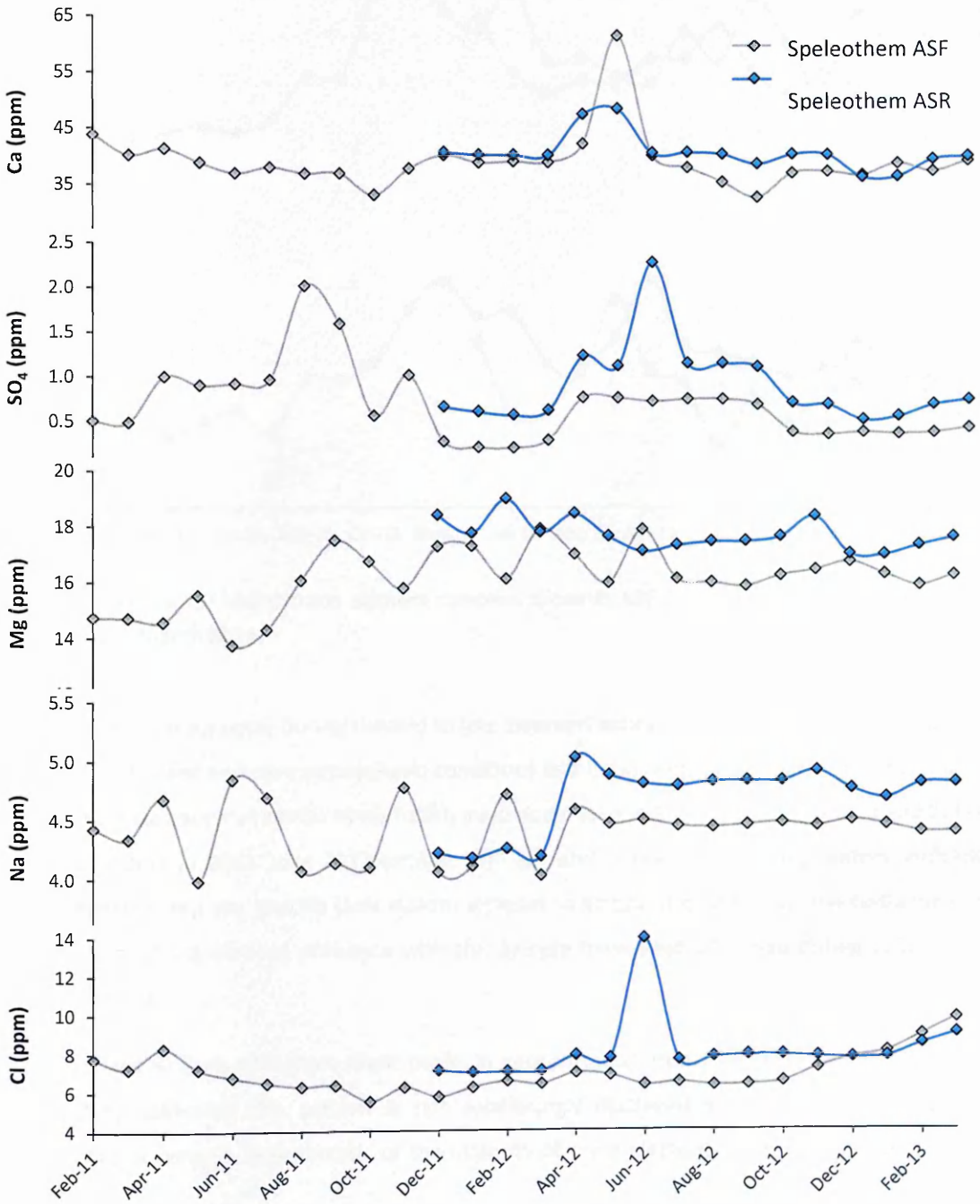

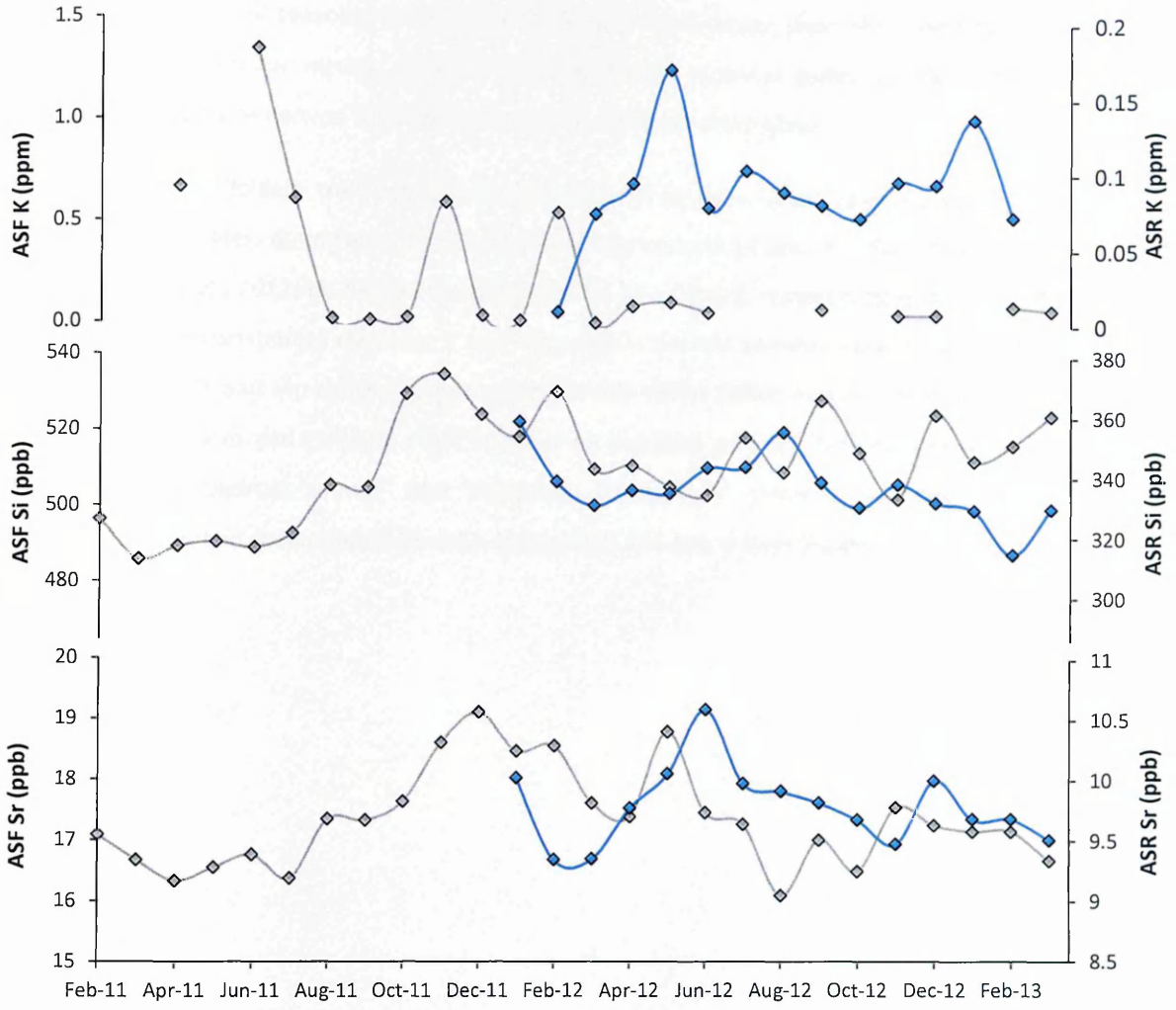

Figure 4.23: Major trace element concentrations in ASF drip waters between Feb 2011 and March 2013.

Ca minimums occur during the mid to late summer, indicating that both sites are exposed to similar karst and cave atmospheric conditions and $CaCO_3$ deposition rates. Early summer Ca increases occur at similar times to SO_4 maximums seen in 2011 in the ASF record and at both drip sites in 2012. June 2012 exhibits high SO_4 and Cl values in ASR drip waters, indicating either a drip site specific (one month) increase in anions or possible sample contamination, although no obvious problems with this sample have been observed during collection or analysis.

Sr and Si from ASF show slight peaks in concentration from late summer through winter 2011, although this pattern is not convincingly displayed in samples from 2012. This inconsistency is symptomatic of the majority of trace elements in Asiul drip waters, which

exhibit a lack of seasonal cyclicity. This homogeneity in water chemistry suggests there is significant aquifer mixing, often eradicating strong seasonal cycles in trace elements, especially those derived from rainfall or calcite / bedrock dissolution.

However, colloidally transported trace elements which have been shown to appear within cave drip waters during an annual flush (either late summer or autumn) (Borsato et al., 2007, Baldini et al., 2012) do display seasonal cyclicity in Asiul drip waters (Figure 4.24). Peaks in colloidally transported elements Y and Mn occur in the late summer season (July – August). Maximum Y and Mn concentrations co-inside with water deficit maxima, peak soil air pCO_2 concentrations and exhibit a slight negative co-variation with Sr. This negative relationship between "bedrock soured" and "colloidally transported" elements has been identified before, both in speleothems (Borsato et al., 2007) and drip waters (Baldini et al., 2012).

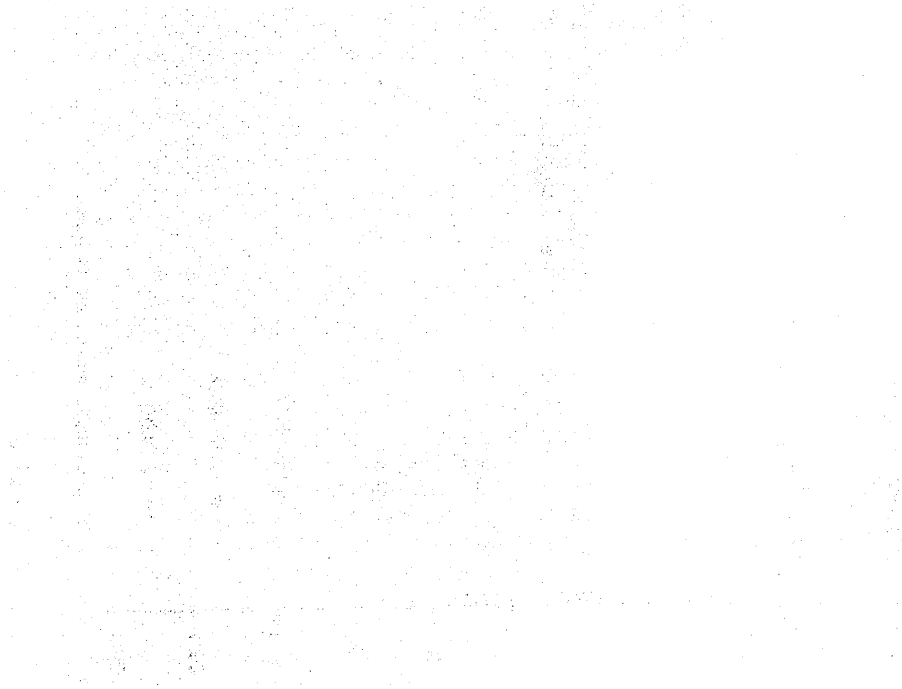

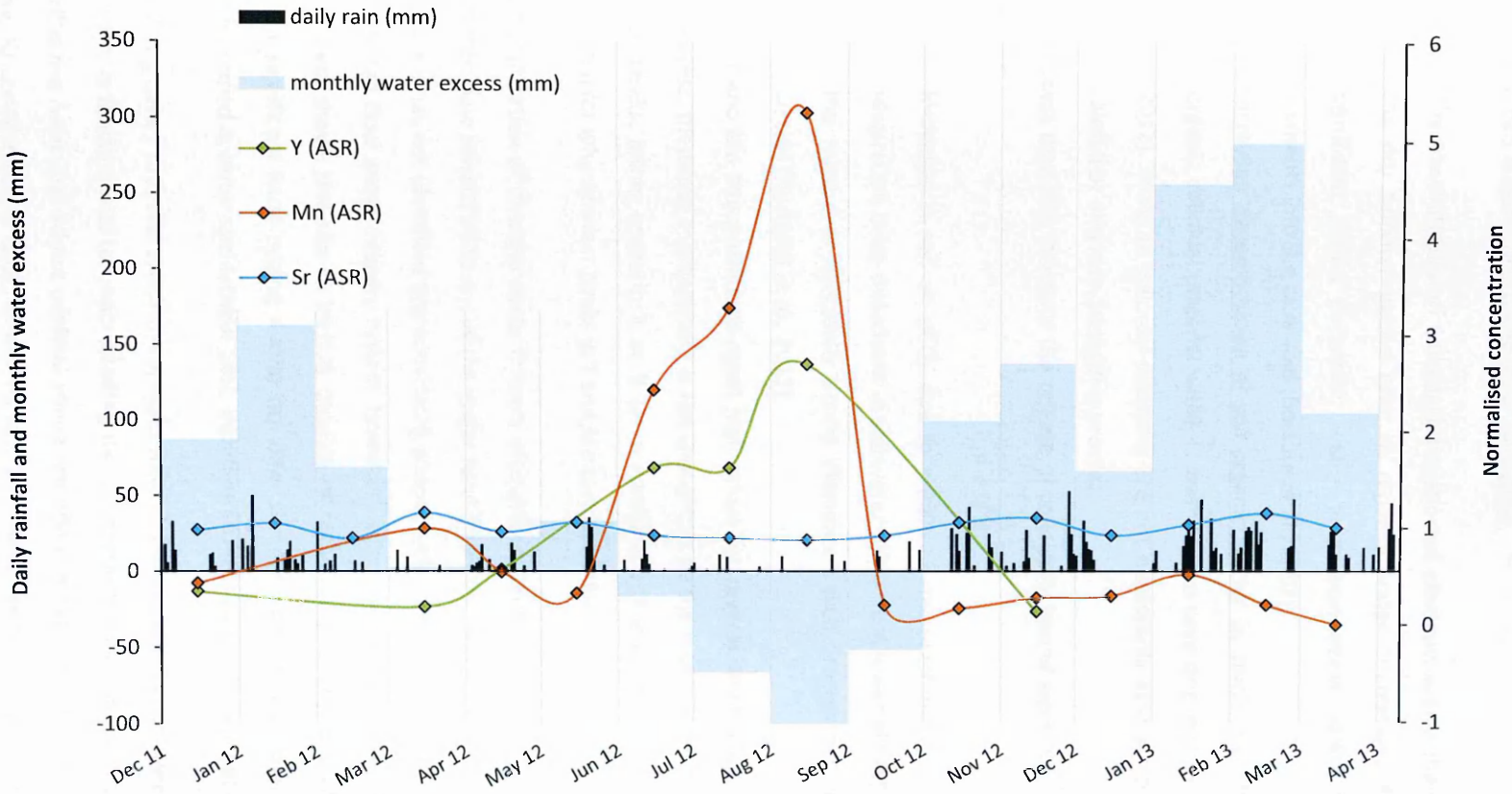

Figure 4.24: Monthly water excess and daily rainfall amount (mm) from Dec 2011 – April 2013. Trace element data is normalised by dividing each bulk monthly value by the data set average value through the presented period, see Borsato et al., (2007) for details.

Peak concentrations in drip water Y and Mn towards the end of the dry season have been attributed to two major processes at other cave sites:

1) The concentration of colloidally transported elements within the soil zone over the dry summer period (due to reduced water infiltration), followed by a significant (often autumnal) water infiltration event which flushes these elements into the cave void (Borsato et al., 2007).
2) Increased decomposition of soil organic matter by micro-organisms, releasing organic colloidal material which is washed into cave drip waters (Baldini et al., 2012). Peaks in colloidal elements are not necessarily associated with peaks in rainfall or drip rate during this process.

A third process may also influence the release of colloidally bound elements under summer conditions.

3) Increases in soil air pCO_2 due to enhanced microbial activity and vegetation respiration drive reductions in soil water pH, in turn lower pH values may cause the release of colloidally bound elements which are washed into cave drip waters (Hartland et al., 2012).

At Asiul, Y and Mn concentrations reach high values for several months without a positive water excess, therefore explanation 1 is not thought to be the major control over summer Y and Mn peaks. Either scenario 2 or 3 (or a combination) may offer the most plausible explanation for why summer peaks in Y and Mn concentration are observed at drip site ASF.

The identification of discrete peaks in trace element concentration is the first indication of non-piston flow conditions at any of the major Asiul drip sites. Monitoring of speleothem ASF drip waters has not identified any convincing annual cycles, suggesting aquifer homogeneity and a piston flow water delivery system. However, summer Y and Mn peaks in speleothem drip waters shows this site at least is capable of responding rapidly to infiltrating water, without significant karst mixing during the drier summer season. This duel response has been identified at other speleothem sites, including Ernesto Cave (Miorandi et al., 2010).

Identifying cave / drip site specific processes which influence the composition of drip water chemistry is fundamental to understanding the elemental makeup of speleothem deposits. For sites like Asiul Cave where minimal annual variations in major trace element (Ca, Mg, Sr, Si, Na, K) concentrations exist, elemental concentrations are driven mainly by evaporative processes, vegetation cycling, karst dissolution and calcite – water interactions within the karst. The existence of annual peaks in Y and Mn during periods of water deficit indicates

that under dry conditions some speleothem drip sites may be fed directly by percolating waters, which do not interact with a larger karst aquifer and therefore record more directly changes in atmospheric and soil sourced trace elements. However, drip water oxygen isotope, trace element and drip rate monitoring indicates that the majority of water entering karst is incorporated into karst aquifers and delivered to cave drip sites through a piston flow effect. The incorporation of water into the karst for longer periods of time may mean that certain trace elements are affected by calcite-water interactions within the karst zone and could therefore when preserved in speleothems could be used as long duration proxies of karst conditions. The impact of calcite-water interaction in the karst is discussed below.

4.5.5 Calcite - Water Interactions

Rather than assessing single element concentrations, many studies look at the relationship between trace elements to derive an understanding about karst processes. Trace element relationships can be used as tracers to define important calcite – water interactions such as dilution, prior calcite precipitation (PCP) and incongruent calcite dissolution (ICD). The simplest relationships described however, are those between trace elements and karst hydrological components, such as drip rate or water excess.

At the Asiul cave site one of the most fundamental relationships exists between Ca and drip rate. Calcium concentration positively co-varies with speleothem drip rate over monthly to annual time scales (linear regression; $r^2 = 0.53$) (Figure 4.25). This relationship may be derived in the same manner as the EC - drip rate relationships. Increased speleothem drip rates enhance the degassing of CO_2 within the cave void; this reduces the potential for $CaCO_3$ deposition leaving Ca values apparently enriched in the remaining solution.

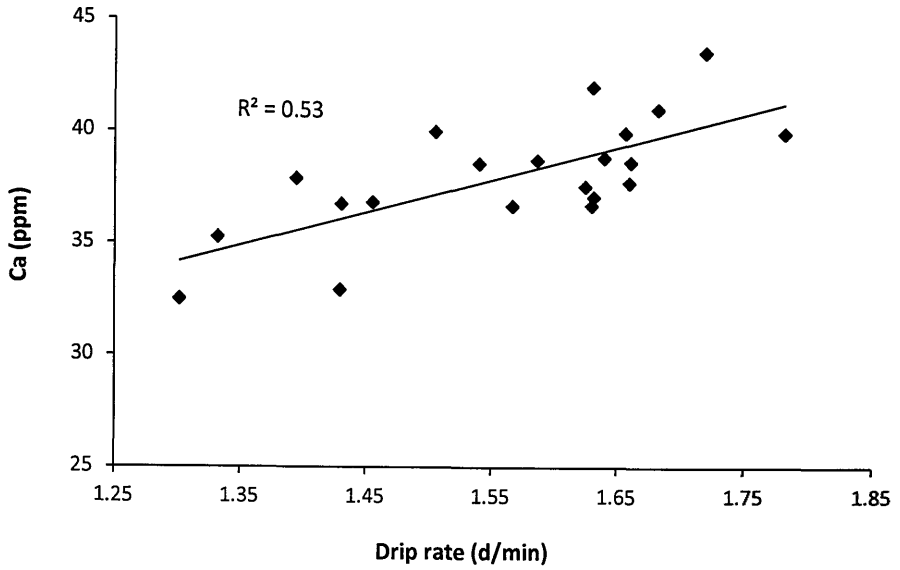

Figure 4.25: Positive co-variation between Ca concentration (ppm) and speleothem drip rate over 22 months of monitoring.

Other elements including Mg and Sr are also affected by drip rate and periods of water excess (or deficit) within the karst through the interaction of water and calcite and the processes of ICD and PCP.

4.5.5.1 Incongruent Calcite Dissolution

Sinclair (2011) identifies ICD as two possible, separate processes. Firstly, the preferential leaching of Sr or Mg during fresh karst bedrock dissolution, this process can only occur within the thin outside layer of the dissolving bedrock. Secondly is the re-dissolution of previously deposited $CaCO_3$ within the karst. This reaction is controlled by the solution Sr/Ca and Mg/Ca ratios as well as the partition coefficients for each element. Under both mechanisms Sr or Mg become enriched in solution in comparison to Ca.

4.5.5.2 Prior Calcite Precipitation

The process of PCP acts to preferentially incorporate Ca into $CaCO_3$ deposited within the karst, leaving minor ions with partition coefficients below unity, relatively enriched in solution (Huang and Fairchild 2001; Sinclair et al., 2012) (Equations 4.4 and 4.5). PCP is often enhanced during periods of water deficit due to an increase in karst air space, heightened CO_2 degassing and a rise in $CaCO_3$ deposition within the karst zone (Fairchild et al., 2000; Huang and Fairchild 2001).

Slight peaks in Mg and Sr in ratio to Ca can be observed during dry periods and lower speleothem drip rates at Asiul (Figure 4.26). Calcite – water interaction produce such

characteristic and often diagnostic relationships between elements such as Mg / Ca and Sr / Ca. These relationships are derived from differential partitioning of elements during both bedrock (or calcite) dissolution and $CaCO_3$ deposition (Sinclair 2011, Sinclair et al., 2012).

Equations 4.4 and 4.5 describe how Ca is preferentially incorporated into the $CaCO_3$ crystal lattice during $CaCO_3$ deposition, leaving the remaining solution relatively enriched in minor trace ions. The extent of partitioning between Ca and Sr or Mg ions at the point of $CaCO_3$ deposition is dependent upon the partition coefficient for each minor ion.

$(Tr/Ca)_{CaCO_3} = K * (Tr/Ca)_{solution}$ (Fairchild et al., 2006b) (4.4)

The partition coefficient of Mg (K_{Mg} = 0.02) and Sr (K_{Sr} = 0.15) have been experimentally determined (Equation 5).

$K_{Mg} = (Mg/Ca)_{water}/(Mg/Ca)_{calcite} = 0.02$ (Fairchild et al., 2000; et al., 2010). (4.5)

$K_{Sr} = (Sr/Ca)_{water}/(Sr/Ca)_{calcite} = 0.15$ (Tooth and Fairchild 2003) or 0.3 (Mattey et al., 2010).

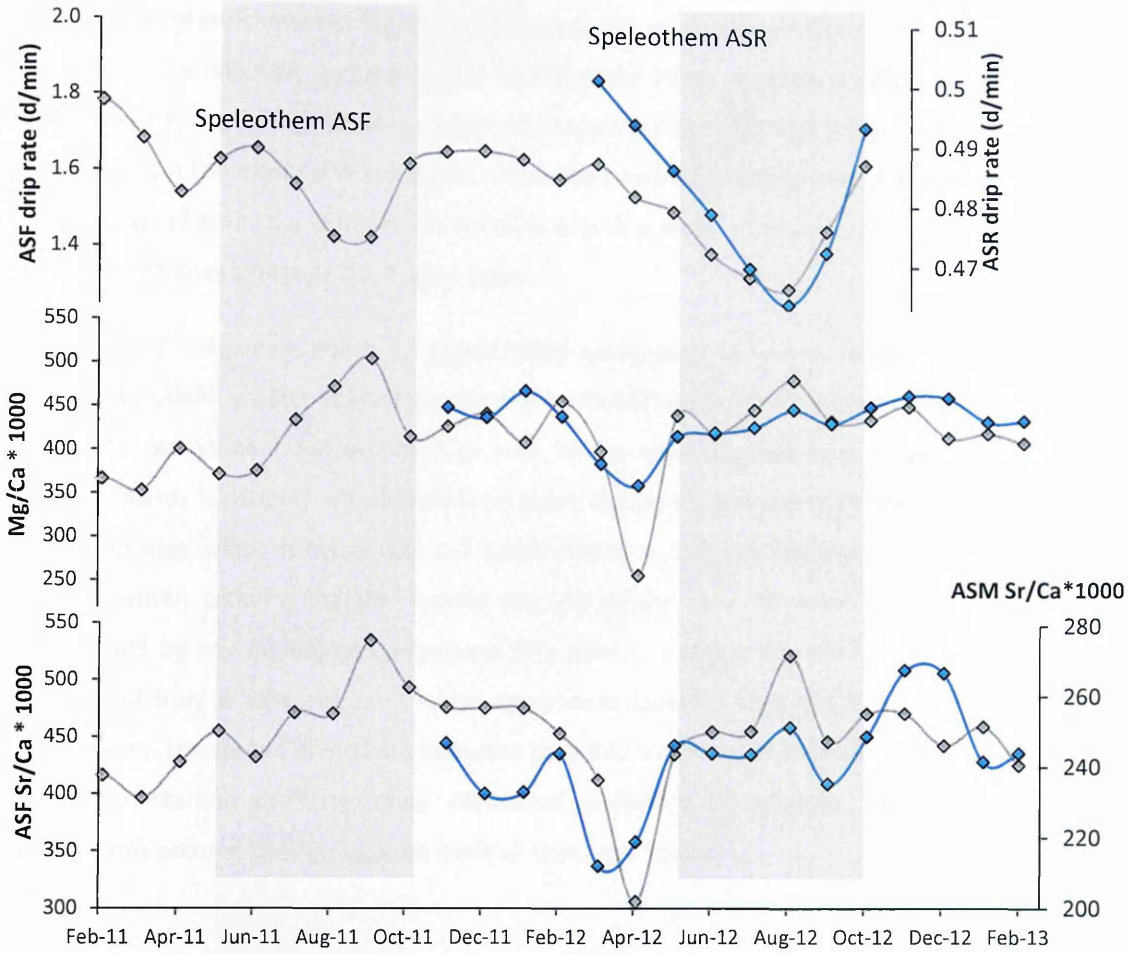

Figure 4.26: Drip rate, Mg/ Ca*1000 and Sr/ Ca*1000 ratios from ASF (grey) and ASR (blue) drip waters between Feb 2011 and March 2012. Grey boxes indicate periods of negative water excess calculated using Thornthwaite (1948).

The partitioning of these elements within the crystal lattice means elemental ratios in drip waters can characterise periods of within karst $CaCO_3$ deposition or incongruent dissolution. Drip waters from sites within Asiul have been analysed for elemental ratios to assess the extent of calcite – water interactions. It should be noted that processes of PCP and ICD are difficult to distinguish from one another using this methodology and although these processes are described separately, data from Asiul drip waters can only identify if calcite – water interactions have occurred. The following sections describe the process by which drip water trace element concentrations may be enriched within the karst and then aim to characterise if calcite – water interactions occur at this site.

4.5.5.3 Modelling Calcite – Water Interactions

The theoretical enrichment of Mg/Ca during prior $CaCO_3$ deposition or ICD can be calculated using the experimentally derived (Huang and Fairchild 2001) partition coefficient for Mg (K_{Mg}) and MIX4 modelling. MIX4 produced theoretical PCP (or ICD) lines (Figure 4.27) which originate from the most Ca rich drip and pool waters collected in Asiul and incorporate the whole range of both Ca and Mg values found in cave drip water. Figures 4.27 and 4.28 show the modelled lines alongside Asiul cave waters.

In Figure 4.27 minimum values of Mg/Ca*1000 correspond to waters which were least affected by calcite – water interactions and two modelled trajectories are used to best fit the data. The requirement for two lines to best fit the data suggests cave pools 1 and 2 (predominantly associated with line A) have lower Mg source bedrock than the majority of other drip sites, which fit better with line B (Fairchild et al., 2006b). These pools are situated close together, within a chamber toward the rear of the cave. However, neither pool is directly fed by any monitored speleothem drip waters meaning that these two locations maybe fed from a different karst water component (aquifer) than the main monitoring speleothem. The spread of instantly collected cave drip waters from collections sites 1-14 (a spatial distribution of 75m) along theoretical trajectory B indicates calcite - water interactions occur at sites throughout most of Asiul, year round.

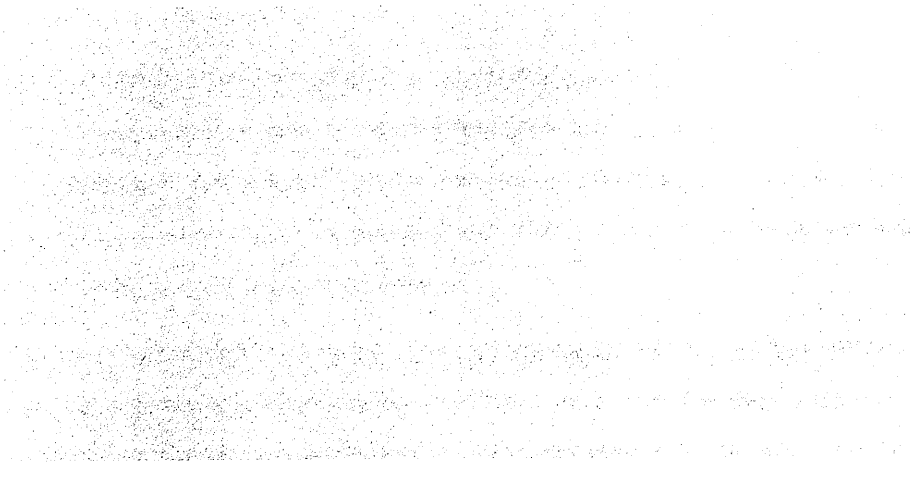

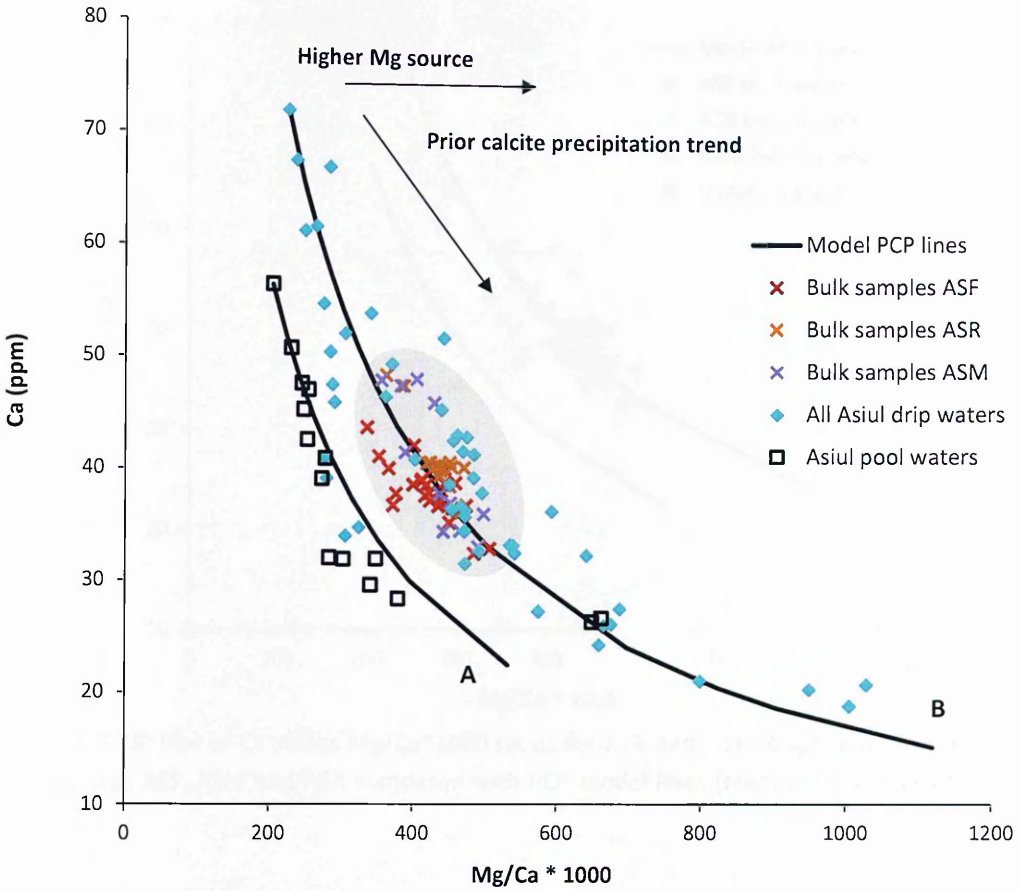

Figure 4.27: Plot of Ca verses Mg/Ca*1000 ratios for Asiul Cave waters compared with PCP model lines (black lines) derived from MIX4. Grey box highlights the clustering of bulk speleothem collections. The distribution coefficient for Mg used for modelling is 0.02, but the lines are not sensitive to this exact value (Fairchild et al., 2001, Mattey et al., 2010).

Bulk waters collected from the three main monitoring speleothems show relatively stable Ca and Mg/Ca values, clustering around but exhibiting minimal spread along trajectory B. These three speleothems are spatially distinct from other sampling sites, isolated within the furthest cave chamber. The lack of evident karst - water interaction at these sites is possibly a function of bulk water collection techniques.

To thoroughly test if bulk water residence times are responsible for the lack of any obvious relationship at these drip sites instantly collected waters from the three sites (n = 8 from ASF; n = 2 from ASM) are included alongside PCP model lines and bulk drip waters, in Figure 4.28.

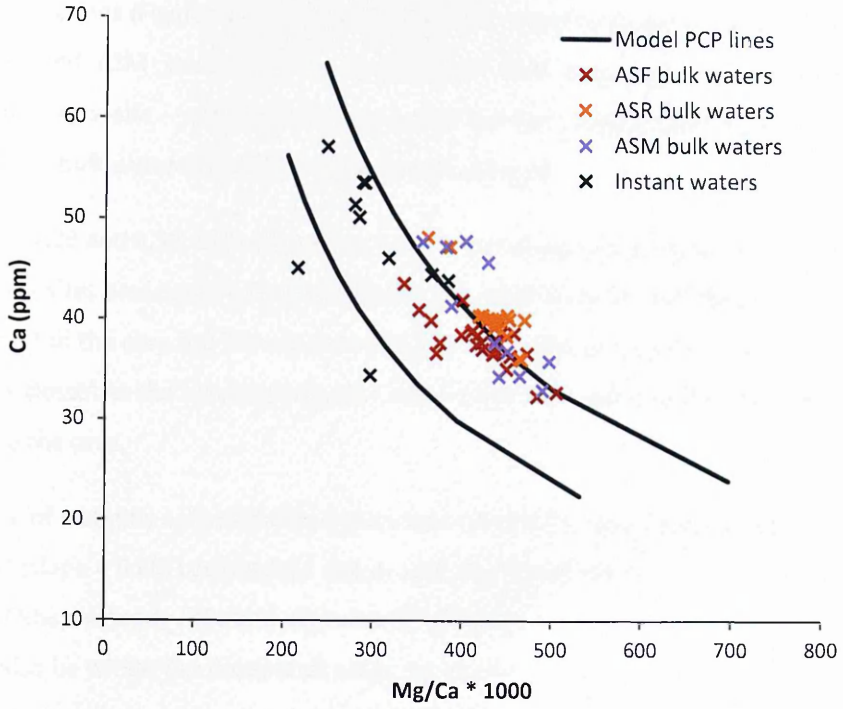

Figure 4.28: Plot of Ca verses Mg/Ca*1000 ratios for bulk and instant speleothem waters from sites ASF, ASM and ASR compared with PCP model lines (black lines) derived from MIX4.

Instantaneously collected waters from the drip sites display extension away from the clustered, bulk waters lying close to modelled trajectories. This spread in instantly collected samples suggests that bulk water sampling techniques overprint the natural trace element make up of these waters. However, the small number of instantaneous samples means further assessment of PCP or ICD processes at major monitoring sites should be undertaken. To further test if calcite – water interactions have occurred an additional trace element ratio technique is applied to Asiul drip waters and speleothem trace element values.

Fairchild et al., (2000) and then McMillan et al., (2005) observed a constant relationship between Sr/Ca and Mg/Ca when plotted logarithmically during conditions of PCP. The constant slope (0.88 ± 0.13) identified from ln(Sr/Ca) vs. ln(Mg/Ca) was used as a tracer for PCP, which works for drip waters or speleothem deposits (McMillan et al., 2005; Sinclair et al., 2012). Sinclair (2011) identify this slope as more correctly, a tracer of calcite - water interactions as PCP and ICD processes produce the same log / log slope. Waters which have interacted with calcite within the karst should have a theoretical log / log slope of 0.88 and a possible range of 0.709 and 1.003 (Sinclair 2011). Asiul drip waters are compared to this slope to identify which sections of the karst aquifer may experience significant calcite –

water interactions (Figures 4.29, 4.30 and Table 4.8). Instantly collected water samples from sites ASF and ASM show how the evolution of bulk drip waters may possibly mask occurrence of calcite - water interactions within the karst zone (Figure 4.29), possibly also observed by bulk water clustering in Figures 4.27 and 4.28.

In Figures 4.29 and 4.30, bulk drip waters have been segregated to show the three main drip monitoring sites associated with speleothems ASF, ASM and ASR. For Figure 4.30 and Table 4.8 the rest of the cave has been broken into 2 sections. The first section (DW1) incorporates drip sites closest to the cave entrance (0 – 40m) whilst the second (DW2) includes sites 45 – 75 m into the cave.

The slope of instantly collected drip waters from the major speleothem collection sites ASF and ASM (slope = 0.89) corresponds closely with the "ideal" calcite - water interaction slope of 0.88. Other instantly collected drip waters from sites throughout Asiul (DW1 = 0.74; DW2 = 0.72) also lie within the theoretical range for calcite – water interaction; these sites have already displayed a strong relationship with modelled PCP / ICD trajectories in Figure 4.27. The only bulk drip waters to display a slope within the theoretical range for karst calcite water interaction is ASF (Slope = 0.72). Bulk waters from ASM (slope = 1.14) and ASR (slope = 0.67) sit above and below the range respectively (Figure 4.30).

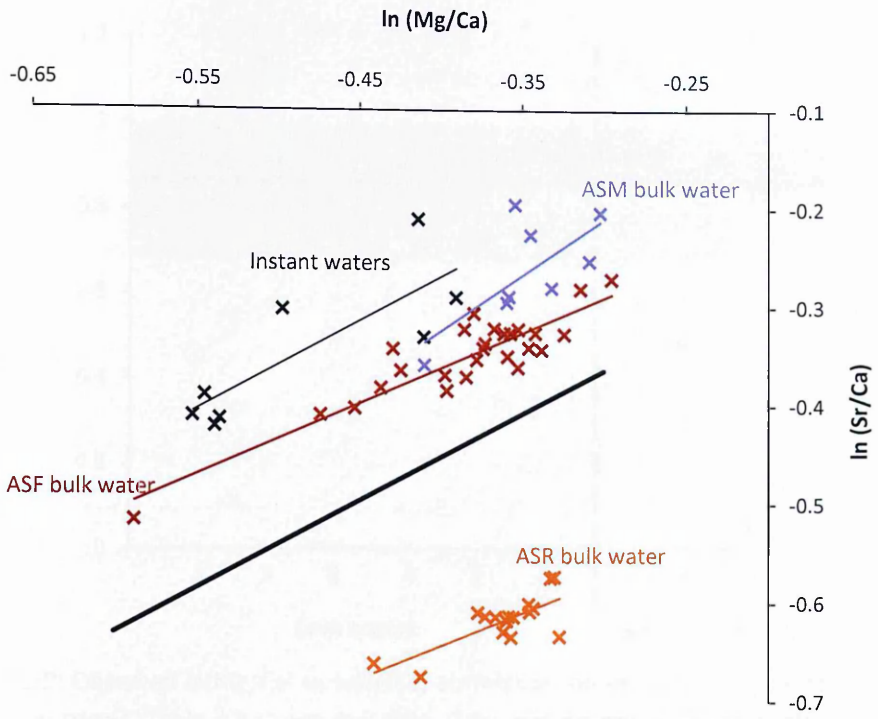

Figure 4.29: ln(Sr/Ca) vs. ln(Mg/Ca) for bulk speleothem drip waters collected in Asiul cave. Thick black line denotes the theoretical slope of 0.88 (Sinclair 2011; Sinclair et al., 2012). Speleothem ASF (red; slope 0.72) and instantly collected drip waters from the three sites (black; slope = 0.89) both lie within the theoretical boundary (0.709 and 1.003) for calcite water interaction. Speleothem ASM (purple; slope = 1.14) and ASR (orange; slope = 0.67) both lie outside this theoretical range.

The difference between instantly collected and bulk drip waters suggests although calcite – water interactions occur within the karst above Asiul (captured in instant samples) these processes can be masked by bulk water collection techniques. For a rigorous assessment of calcite - water interactions from cave drip water; instant sampling should therefore be used in preference to bulk water collection.

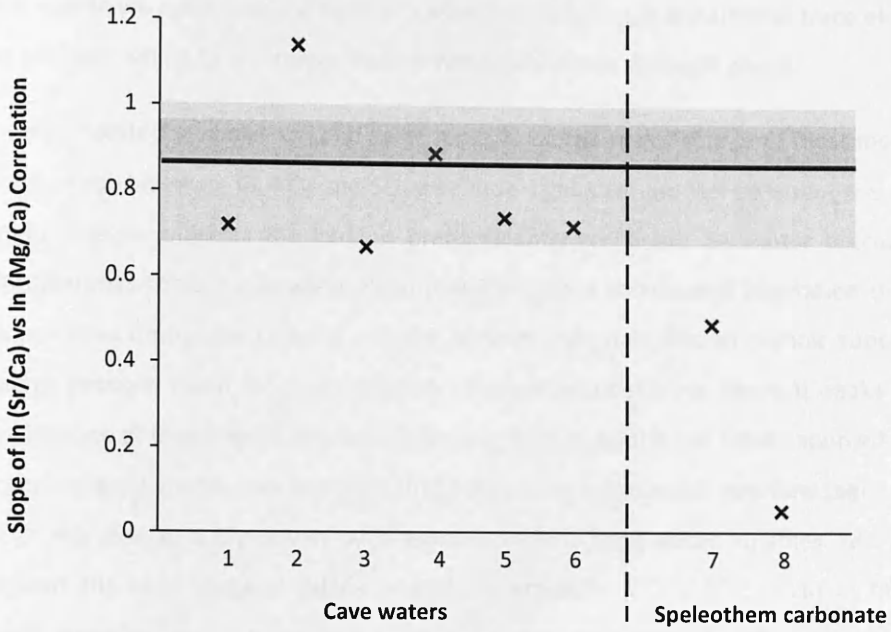

Figure 4.30: Observed ln(Mg/Ca) vs ln(Sr/Ca) correlation slopes in Asiul drip waters and cave speleothems. Table 4.9 shows raw data. Grey bars display confidence intervals for calcite – water interactions (Sinclair et al., 2012).

Observation	Slope of linear regression	Figure Reference
PCP / ICD theory "most likely"	0.877 – 0.973	Dark grey
PCP / ICD theory max and min	0.709 – 1.003	Light grey
ASF bulk drip water	0.72	1
ASM bulk drip water	1.14	2
ASR bulk drip water	0.67	3
Instant waters from ASF & ASM	0.89	4
DW1 (instant collection)	0.74	5
DW2 (instant collection)	0.72	6
Speleothem ASR (top)	0.49	7
Speleothem ASM (top)	0.05	8

Table 4.8: Observed ln(Mg/Ca) vs ln(Sr/Ca) linear regression slopes in Asiul drip waters and cave speleothems.

Using both drip water degassing trajectories (which simulate $CaCO_3$ deposition) and using the lnSr/Ca vs. lnMg/Ca slope analysis, we establish significant calcite - water interactions within the karst above Asiul drip sites. However, it is difficult to differentiate between PCP and ICD as the source of the observed enrichments of Mg or Sr in ratio to Ca (Sinclair 2011).

For this reason we would suggest both processes may play a role in enriching trace elements within solution, whilst Ca is incorporated preferentially within the solid phase.

Drip water monitoring shows soil and karst zones to be the major source of most measured trace elements; however, Cl, NO_3 and SO_4 also have significant aerosol contributions. Cl and SO_4 ratio analysis suggests the karst is predominantly recharged by winter precipitation which undergoes some evaporation. Heightened microbial activity and vegetation turnover in the soil zone during the summer months releases colloidally bound organic substances, leading to peaks in Y and Mn concentration. Discrete summer trace element peaks in drip waters indicate at least one of the main drip sites (ASR) in Asiul is not totally sourced from a homogenous karst supply. This indicates that both piston and conduit overflow regimes may occur at this site, possibly driven by seasonally variant karst water volumes. Monitoring throughout the cave suggests calcite – water interactions (PCP / ICD) occur at instantly collected drip sites. Bulk drip waters however, display little conclusive evidence of either process, possibly suggesting long water standing times associated with bulk water collection methodologies act to mask the signs of calcite water interactions. It is therefore recommended that water sampling is undertaken instantaneously, when trying to assess the extent of calcite – water interactions in cave environments. The monitoring of hydrological conditions and drip water chemistry at this site has been undertaken to explain speleothem growth conditions and chemistry. The implications for speleothem development are discussed below (section 4.6).

4.6 Implications for the Speleothem Record

To facilitate accurate palaeoclimate reconstruction, modern cave hydrological conditions have been reviewed. At the Asiul Cave site modern rainfall is dominated by a unidirectional source of moisture, originating in the North Atlantic Ocean, whilst isotopic values are related to rainfall amount. Moisture delivery to the karst overlying Asiul is dictated by water excess, which occurs predominantly during winter months. Karst water accurately reflects the oxygen isotopic signature of winter rainfall, indicating that low rainfall levels and high evapotranspiration rates effectively limit the ingress of infiltration during summer months. Speleothems developing from this relatively homogenous karst water would therefore be expected to isotopically reflect changes in winter precipitation amount, sourced from the North Atlantic Ocean.

Speleothem drip rates reflect the volume of rainfall over both seasonal and event scales. For the most part, a highly effective piston flow system forces well mixed (homogenous) karst aquifer water to drain into the cave system from aquifer storage. Seasonal drip hydrology at Asiul is dominated by winter infiltration maxima and summer minima, replicated in several multi-annual drip records. Constant water delivery, which is super saturated in respect to $CaCO_3$ to cave drip sites means speleothem growth is possible throughout the year.

Atmospheric CO_2 concentration has been observed to control drip water electrical conductivity values on seasonal to event scales; by dictating the volume of $CaCO_3$ deposition before drip water sampling. Cave air pCO_2 increases are closely linked to high water infiltration events, although the mechanism varies seasonally. Speleothem deposition within the cave may therefore be limited at times of maximum water infiltration. High resolution drip water EC monitoring offers one possible mechanism of identifying periods of speleothem growth minima and maxima, with higher EC values representing lower speleothem deposition rates.

During periods of active speleothem growth, trace elements are incorporated into the speleothem crystal lattice. Speleothem feeding drip waters lack any obvious trace element seasonality (for most elements) but instantly collected waters from throughout the cave suggest significant karst calcite – water interactions, either PCP or ICD. These "above" speleothem interactions leave drip waters relatively enriched in trace ions (in relation to Ca); these enrichments may be used in speleothem deposits to indicate periods of maximum and minimum calcite – water interaction. Colloidally bound elements are preferentially released

under summer conditions within the soil zone, due to enhanced microbial activity and vegetative decay. Peak summer Mn and Y values at one monitored drip site (ASF) indicate that water is directly sourced from the soil, via conduit overflow mechanisms. Colloidally bound elements may be used as a marker within this speleothem deposit to identify summer conditions, if the sample can be annually resolved. Finally, cave monitoring has highlighted the importance of collecting drip water samples instantaneously, as bulk water chemistry is prone to modification during the long standing time of water within collection vessels.

The subsequent chapter aims to characterise cave atmospherics, looking closely at seasonal cycles in cave temperature and atmospheric flushing, which are fundamental to the growth of speleothem deposits. The final part of Chapter 5 aims to assess how accurately modern "grown" calcite deposits reflect ancient speleothem growth and therefore how best to interpret speleothems in terms of palaeoclimate reconstruction.

5. CAVE AIR CHARACTERISTICS AND THE GROWTH OF SPELEOTHEM DEPOSITS

5.1 Introduction

Recent studies (Spötl et al., 2005, Mattey et al., 2010 and others) have highlighted the importance of monitoring and understanding the composition of cave air as well as characterising cave ventilation on a site specific basis. Changes in cave ventilation dynamics, cave air carbon dioxide composition and cave air temperatures hold important controls over the growth of speleothems and therefore the incorporation of chemical proxies at a range of time scales.

Variations in cave ventilation and composition are primarily driven by conditions external to the cave site. A range of factors have been identified as driving forces behind air ventilation patterns in cave sites, including temperature (density) driven air flow, pressure driven air flow, air flow past cave entrances (the Venturi effect) and wind blowing directly into cave systems. At most sites, one or a combination of these factors interact with the morphology of cave passages to control air flow within the cave at a range of different temporal resolutions (diurnal – multiannual).

At many cave sites major upheavals in the cave ventilation process are observed twice a year, in response to external seasonality in air temperature as part of a density driven ventilation regime. At sites such as Obir Cave (Austria) and Ernesto Cave (Italy) cold external air temperatures during the winter cause an inflow of cold air with a low CO_2 content into the cave system, reducing cave air temperatures and the CO_2 content of air in the cave void (Spötl et al., 2005, Miorandi et al., 2010). Under summer conditions colder cave air flows out of these systems, drawing warm, CO_2 rich air down through the karst from the soil zone; increasing cave air temperatures and CO_2 content. However, not all cave systems act in this manner. St. Michaels Cave (Gibraltar) is also influenced by external air temperatures but at this site the morphology of the cave systems leads to lower summer time CO_2 concentrations and higher wintertime levels (Mattey et al., 2010). These examples highlight the importance of site specific cave monitoring to accurately characterise cave ventilation and cave air CO_2 content.

Monitoring has therefore been undertaken within Asiul Cave 2010, with the aim of understanding conditions under which speleothems grow, specifically concerning cave air temperature and CO_2 dynamics.

5.2 Temperature and Ventilation Dynamics

Long term (1986-2010) regional air temperature data from Santander demonstrates a gradual warming during the last 20 years (IAEA 2014), consistent with warming throughout the Iberian peninsula (Rodriguez-Puebla et al., 2001, Brunet et al., 2005). Temperature minima occurred in 1986 (13.2 °C) and maxima in 2006 (15.6 °C), since which decreasing temperatures have been recorded. Santander mean annual temperature is 14.4 °C, slightly higher than Matienzo during 2011 (13.9 °C, taken with 250 m of Asiul cave entrance).

Monthly average temperatures from Santander (2000-2010) and Matienzo (2011) exhibit a strong seasonal trend (Figure 5.1). Temperature minima occur in February for both Santander (10.3 °C) and Matienzo (Feb 2012 = 5.1 °C), whilst temperature maxima occur during August in both records (Santander =20.4 °C; Matienzo =21.2 °C).

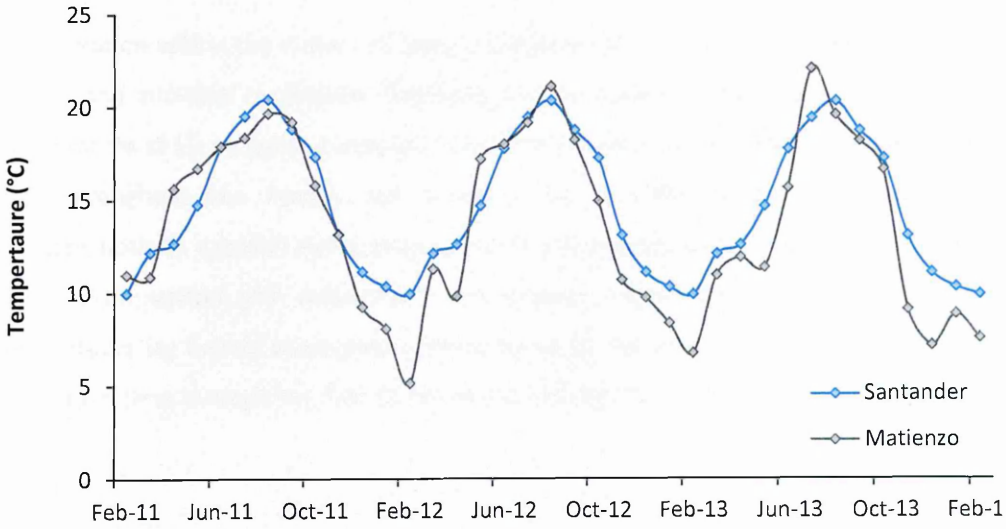

Figure 5.1: Average monthly temperatures for Santander (2000-2006, IAEA 2014) and monthly averages (2011-14) for the Matienzo valley (taken with 250 m of Asiul cave entrance).

Monthly average temperatures for Matienzo during 2011 are displayed in Table 5.1, demonstrating monthly temperature ranges. During 2011 temperature maxima in Matienzo reached 40.9 °C (June) and minima were as low as -1.1°C (March).

	Average (°C)	Max (°C)	Min (°C)	Range (°C)
Jan-11	11.3	23.0	6.9	16.1
Feb-11	10.9	23.7	3.4	20.3
Mar-11	10.9	25.2	-1.1	26.3
Apr-11	15.6	33.7	3.5	30.1
May-11	16.7	36.4	8.1	28.3
Jun-11	17.9	40.9	6.7	34.2
Jul-11	18.4	36.2	9.4	26.9
Aug-11	19.7	35.2	9.9	25.4
Sep-11	19.2	37.4	9.0	28.4
Oct-11	15.8	33.8	4.2	29.6
Nov-11	13.3	23.2	1.1	22.0
Dec-11	9.3	20.4	-0.9	21.3

Table 5.1: Matienzo monthly temperatures in 2011. Data averaged form half hourly monitoring external to the cave entrance. Range is the difference between max and min temperatures.

5.2.1 Soil Temperature

Heat retention within the upper soil zone is fundamental for regulating vegetation growth patterns and microbial respiration. Therefore, soil temperature logging was undertaken for seven months at 15 cm depth during 2011 (April –November), in the thin soils overlying Asiul cave. Throughout the record, soil temperatures replicate atmospheric temperature variations both on monthly and diurnal scales. Soil temperatures have a slightly dampened range in comparison with atmospheric temperature (Figure 5.2). At 15 cm depth, soil temperatures lag behind atmospheric values by up to five hours; this lag time represents heat transit time through the first 15 cm of the soil and the heat retention capacity of the soil.

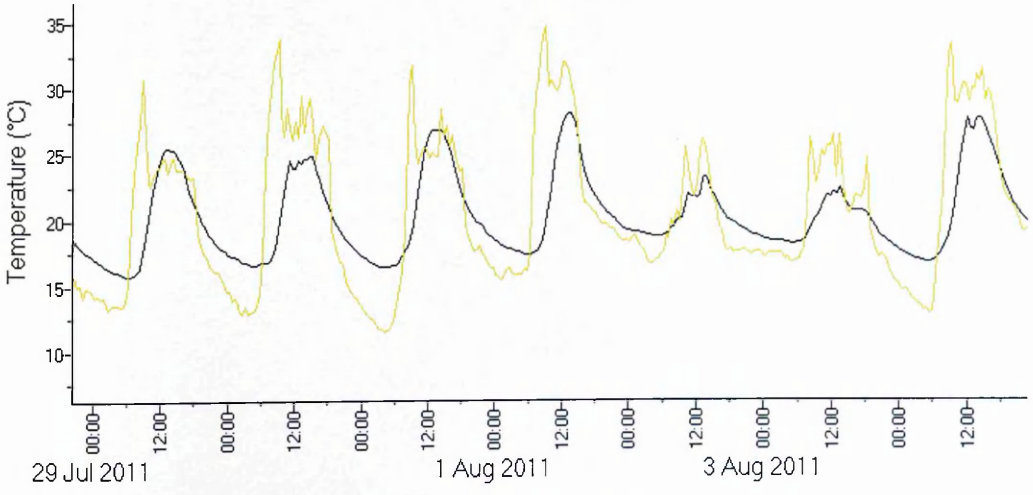

Figure 5.2: External temperature (gold line) and soil temperature (black line) from seven daily cycles in 2011.

5.2.2 Cave Temperature

Average cave air temperature has been monitored by continuous logging at two sites in Asiul, one at 45 m distance from the cave entrance (Figure 3.5, Pool 1) and the other at the main monitoring location at the rear of the cave (Figure 3.5). Yearly average cave temperature in the main monitoring chamber reflects accurately average yearly external temperature (13.8 °C).

Cave temperature seasonality is similar at both cave logging sites. Temperatures increase slightly with depth into the cave system from 45 (Pool 1) – 65 m (main monitoring chamber) suggesting the Asiul system is possibly not long enough to reveal the gradually attenuated temperatures with depth described by Spötl et al., (2005). At Pool 1, the average temperature is 13.2 ± 0.5 °C whilst at the rear of the cave, air temperatures are slightly higher (13.7 ± 0.4 °C) but exhibit a similar temperature range.

Seasonal similarities between the two cave loggers suggest changes in cave temperature occur relatively synchronously (within one month) throughout the cave system (Figure 5.3). Cave temperature minima are observed in March (13.3 °C at 65 m) and maxima in November (14.0 °C at 65 m), three months after external temperature maxima (Figure 5.3). This lag indicates a significant (3 month) delay in temperature maxima between the external and deep cave environments.

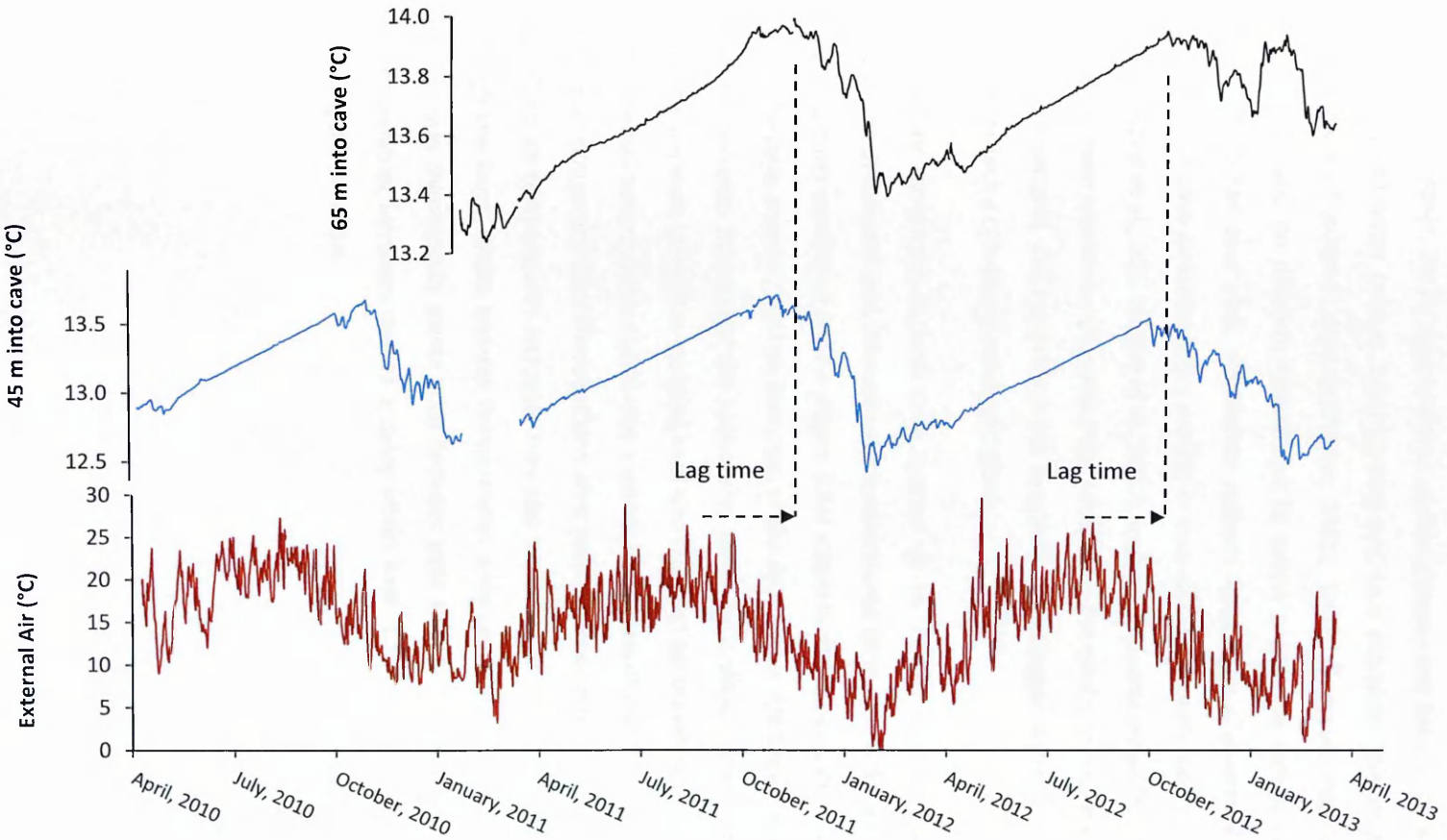

Figure 5.3: A three month offset (Aug – Nov) in maximum temperatures is observed between external atmosphere (red line) and cave temperature at 45 m underground (blue line) and 65 m underground (black line).

5.2.3 Cave Ventilation

Cave ventilation can be driven by a range of processes, including pressure induced air flow (Fairchild and Baker, 2012), density driven air flow (Wigley and Brown, 1976), the presence of underground water courses, wind blowing past cave entrances (the Venturi effect) and direct inflow of external wind (Smithson, 1991). These processes can act alone or in combination and on different time scales to create a complex annual cave ventilation regime. At other cave sites, ventilation regimes have been characterised through the assessment of cave air temperature profiles or cave air CO_2 concentrations, or a combination of both (Spötl et al., 205, Mattey et al., 2010). In Asiul, temperature profiles taken at Pool 1 and in the main monitoring chamber (Figure 3.5) offer the most convincing evidence of cave ventilation patterns. CO_2 records are less complete due to logger malfunction and therefore fail to offer such a convincing seasonal pattern.

Seasonal air movement in Asiul cave appears to be density driven, related directly to differences in external and internal cave temperatures (Wigley and Brown, 1976). During Asiul's summer ventilation regime (Figure 5.4a) external air temperature is higher than that within the cave, meaning cool air flows out of the cave's main entrance. Cave temperatures gradually increase throughout the summer as warm air is drawn down through the karst from the soil zone to replace escaping cool air. This karst air drawdown is seen to continue after external temperatures switch into a winter regime, resulting in the continued increase in cave air temperature for three months after peak summer external temperatures (Figure 5.3). Cave air temperatures increases may also be driven by the conduction of heat down through the karst. Whilst bedrock temperatures were not measured directly in Asiul, this process may theoretically create a lag between peak solar heating (mid-summer) and cave air temperature increases due to a delay whilst heat is transferred through the bedrock overlying the cave site.

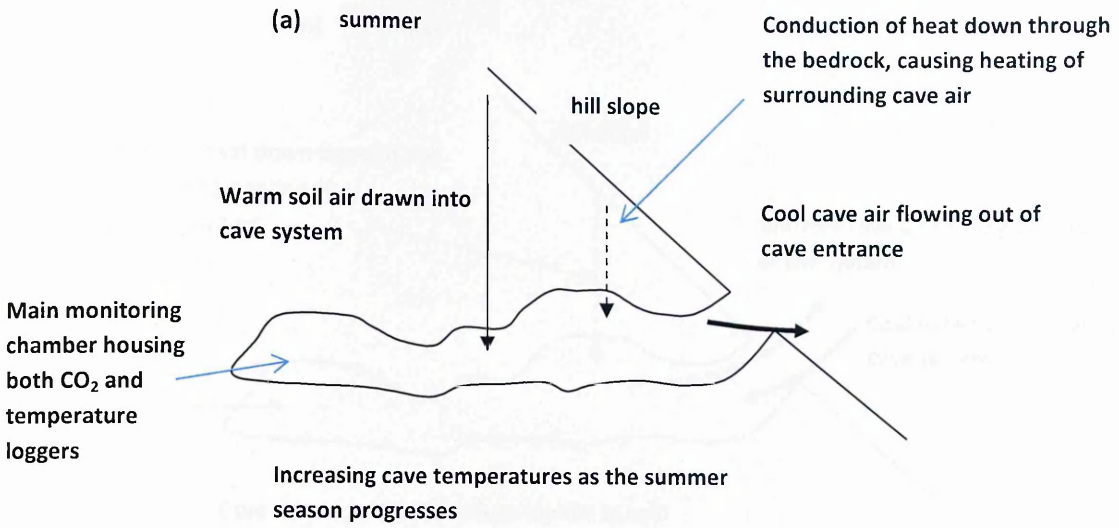

Figure 5.4(a): Diagrammatic representation of summer ventilation conditions in Asiul cave, soil air is drawn down into the cave as colder cave air is expelled through the main cave entrance. Additional cave air heating maybe a result of conductive heat transport down through the karst.

Winter ventilation regime in Asiul is initially characterised by reductions in cave air temperature, occurring once the external air temperature drops below the mean annual temperature (MAT) of the cave air. This causes cave ventilation to reverse and cold external air to flow into the cave system (Figure 5.4b). This reversal results in a sudden reduction of cave temperature and the transition into a winter ventilation regime.

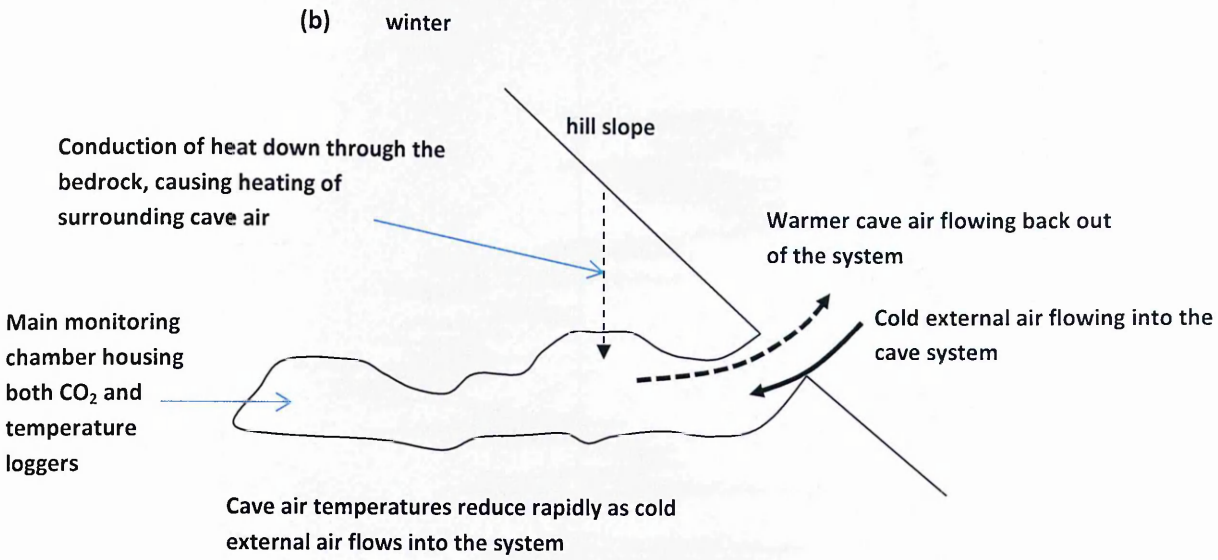

Figure 5.4(b): Diagrammatic representation of the winter ventilation regime, external air temperature falls below the MAT of the cave causing cold air to flow into the cave void, reducing cave air temperatures throughout the system. Cave air heating may still occur due to the warmer surrounding bedrock during the winter, but this process is likely masked in the records due to the large variations in cave temperature related to in the ingress of external air.

The timing of temperature variations in the cave air can be observed in Figure 5.5 which helps to characterise seasonal ventilation regimes based upon external – internal cave air temperatures. Only when cave air temperatures exceed those externally does cold air flow into the cave system, leading to a turnover in ventilation regime which marks the beginning of winter ventilation.

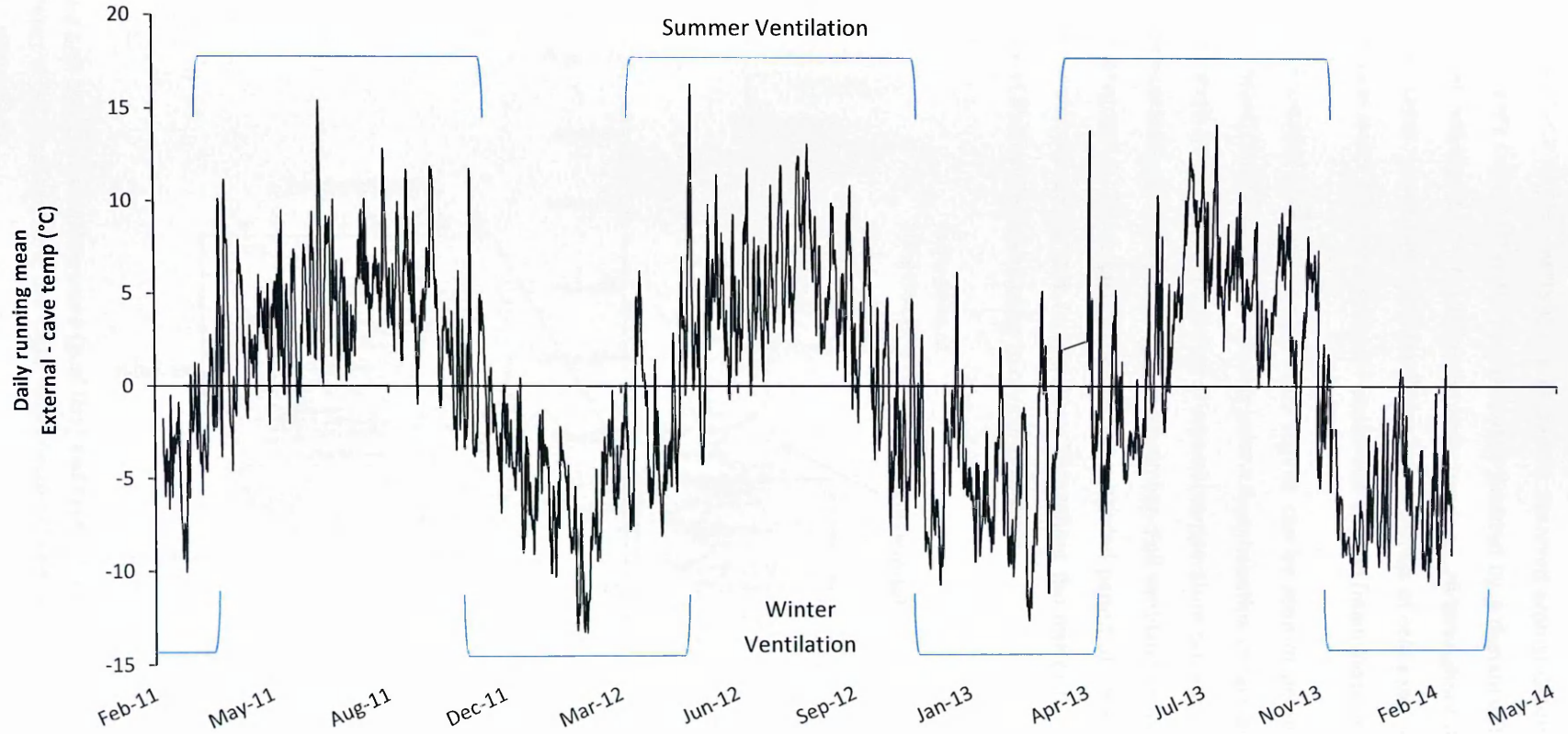

Figure 5.5: External temperature minus internal cave temperature at 65 m underground (main monitoring chamber). Positive values drive summer ventilation and negative values winter ventilation.

The transition to a winter ventilation mode can be observed around October / November each year (Figure 5.5). Ventilation switch over is denoted by a destabilisation of cave air temperatures followed by a rapid reduction in air temperature throughout the cave system (Figure 5.6). Temperature reductions are driven by the ingress of cold external air and occur initially at 45 m depth (Pool 1) and several weeks later at 65 m (main monitoring chamber).

The initial transition to a winter ventilation regime can be seen in detail in Figure 5.6a occurring around the 15th of October. At this point a destabilisation of cave air temperatures can be observed. In 2010 a brief increase in external temperature causes an initial recovery in cave temperature, lasting until the 6th of November. Full ventilation regime switch over (summer to winter) is then triggered by the first extended period of time, where external temperature remains below cave temperature. Throughout the rest of the winter external temperatures fluctuate below or close to cave temperature.

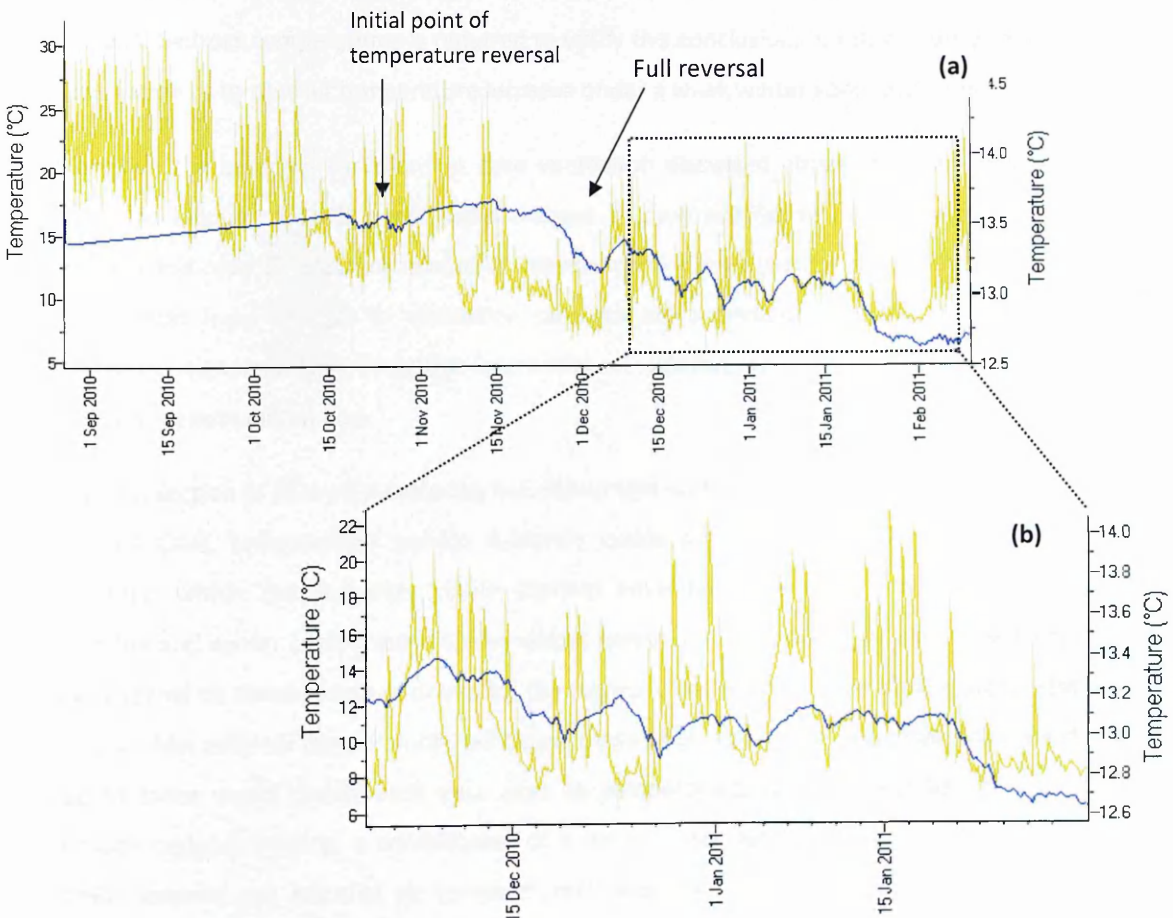

Figure 5.6: (a) External temperature (gold line) and cave temperature at 45 m (blue line). (b) Inset of (a) demonstrating the close relationship between external temperature and cave temperature.

Under winter ventilation conditions reversals in cave breathing can be observed as fluctuations in cave temperature (Figure 5.6b). Ventilation reversals indicate a relatively unstable thermal environment within the cave, driven directly by changes in external atmospheric temperature.

However, a combination of summer and winter density driven ventilation fails to explain the entirety of the temperature profile found in Asiul (Figure 5.3). At the end of the winter season (February –March each year) cave air temperatures begin to increase (for up to three weeks) before average daily external temperature exceeds the cave air temperature and summer ventilation regime becomes established. This gradual rise in air temperature un-related to dominant ventilation regime maybe a result of conductive heat transport into the cave, via the bedrock. It may only be at the very end of the winter season when transport of air into the cave under winter ventilation is at a minimum that bedrock heating becomes a dominant factor in the regulation of cave air temperatures. Further work to establish seasonal bedrock temperatures is required to verify this conclusion, but this offers a rational explanation as to cave air temperature increase under a weak winter ventilation regime.

Alongside the seasonal variations in cave ventilation discussed above, are the previously discussed (Section 4.4.3.2) event scale changes in cave ventilation driven by changes in external and cave air pressure related to intense storm events (Genty and Deflandre 1998). These short lived changes in ventilation strength are superimposed upon the seasonal ventilation signal derived from the interaction of external and internal cave air and a resultant density driven flow.

This first section of cave air monitoring has shown that within the main monitoring chamber of Asiul Cave, temperatures remain relatively stable on an annual scale (within 1 °C). However, within this relatively stable thermal environment annual cycles of summer warming and winter cooling exist. Under winter conditions, the strong coupling of external and internal air temperature is driven by the ingress of cold air into the cave system. This occurs when external temperatures fall below those of the cave void. However, for a short (up to three week) period each year cave air temperatures maybe controlled primarily through bedrock heating, a combination of a weak winter ventilation process (related to similar internal and external air temperatures), and the conduction of solar heat down through the overlying karst. Under summer ventilation, warm air is gradually drawn through the soil and karst to replace colder cave air which is expelled from the main entrance.

Cave air temperature evolution demonstrates how effective ventilation reaches the whole cave system and the importance of bedrock warming especially during the transition between winter and summer regimes. Cave ventilation at this site importantly reaches regions of speleothem deposition (the main monitoring chamber). Cave ventilation dynamics have often been shown to play an important role in influencing the timing, extent and chemical composition of speleothem growth (Spötl et al., 2005, Scholz et al., 2009, Wynn et al., 2014). Under natural cave ventilation conditions the extent, timing and atmospheric composition of exchanging air masses offer vital controls over the preservation of chemical signatures between water and calcite phases, especially carbon isotopic values (Dulinski and Rozanski 1990, Frisia et al., 2011). For this reason, a review of cave ventilation and atmospheric composition is undertaken. The aim of this review is to identify which components of the system influence the makeup of cave air, and how and when cave atmospherics may influence speleothem growth.

5.3 Soil and Cave CO_2 Concentration and $\delta^{13}C$

5.3.1 The Soil CO_2 System

Monthly atmospheric carbon dioxide concentration in the soil overlying Asiul cave was recorded at 50 cm depth and samples taken from this depth for $\delta^{13}C$ analysis. Only one soil depth (as close to the top of the epikarst as possible) was measured due to the thin and often patchy nature of the soil zone. pCO_2 values within the soil zone are consistently higher than values measured within the cave system. All measurements were undertaken using the Vaisala GM70 monitor and GMP221 probe with a measurement uncertainty of 2%. Readings were calibrated using a secondary probe at atmospheric levels. All readings were corrected to standard atmospheric pressure (1013 hPa) following Spötl et al., (2005) and Equation 5.1.

$$CO_2 \text{ (ppmv)} = CO_2 \text{ (raw)} * 1013 / p \quad (5.1)$$

Corrected values are presented as ppmv following the rationale of Spötl et al., (2005). Maximum soil pCO_2 concentrations were measured in the warm season (July 2012 = 4283 ppmv) and minimum values were measured in the cold season (Feb 2012 = 647 ppmv). The most dramatic transition in soil air pCO_2 occurs between July 2012 and Feb 2013 where a drop of approximately 3600 ppmv in soil pCO_2 values can be observed (Figure 5.7).

Soil pCO_2 shows a weak linier relationship with external atmospheric temperature (linear regression; $r^2 = 0.30$). It would be expected that soil pCO_2 values would show a similar or stronger relationship to soil temperatures (Frisia et al., 2011), although no overlap between monitoring exists at this site due to the loss of the soil temperature logger.

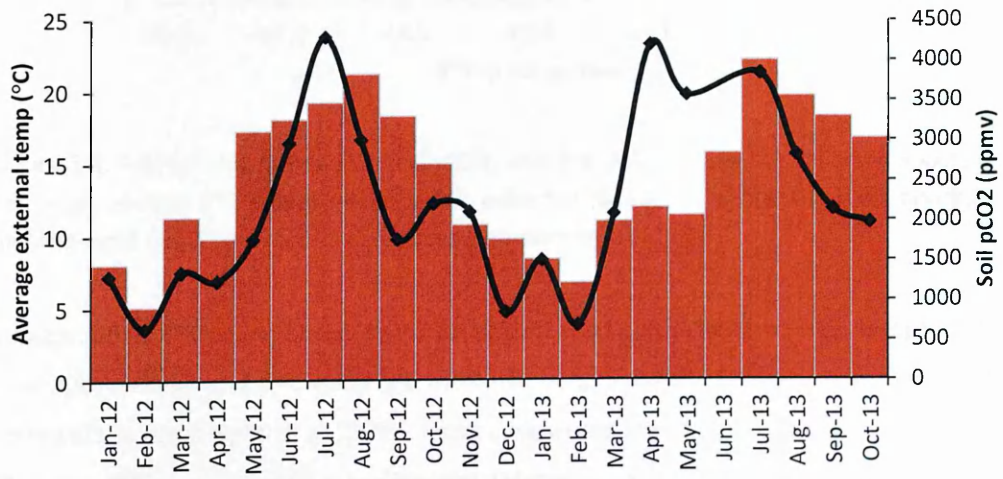

Figure 5.7: Soil pCO_2 (black diamonds, ppmv) and average monthly external air temperature (red bars). Peak soil pCO_2 values occur in the spring and summer seasons and lows during the winter months.

Monitoring indicates peak soil pCO_2 values occur between April and August with increases in soil CO_2 as early as March each year, whilst peak external air temperatures occur between May and October and begin to increase in March. Soil CO_2 monitoring has therefore highlighted a period of peak vegetation and microbial respiration within the summer season. Biogenic CO_2 production appears to respond rapidly to increasing air temperatures (within 1 month) similar to that at Ernesto Cave (Italy, Frisia et al., 2011). However, peak soil CO_2 concentrations do not last as long as peak summer temperatures, indicating a short (spring to early summer) growth season. The reduction in biogenic CO_2 production possibly reflects the reduced availability of soil water as the summer progresses.

Soil air $\delta^{13}C$ was measured monthly from the soil sampling site at Asiul. Average winter values (-18.7 ‰) corresponded to the lowest CO_2 concentrations, whilst during the summer when soil air pCO_2 is high, more negative $\delta^{13}C$ values are recorded (May 2013 = -21.4 ‰) (Figure 5.8).

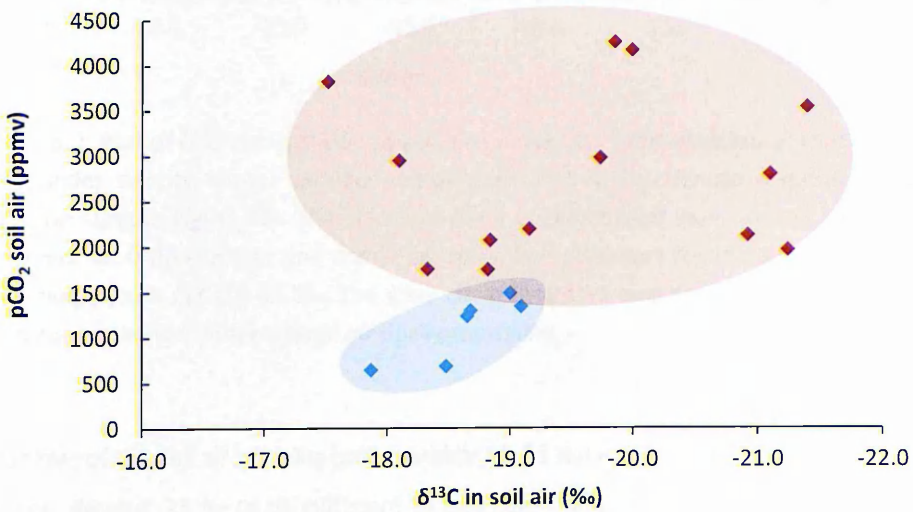

Figure 5.8: Relationship between soil air pCO_2 and $\delta^{13}C$ values (note the reversed x axis). The most positive $\delta^{13}C$ values relate to CO_2 collected during the winter (blue diamonds) and the most negative to summer samples (red diamonds).

Although soil air $\delta^{13}C$ values appear to reflect seasonal soil productivity and CO_2 composition, soil air CO_2 makeup and $\delta^{13}C$ value are known to be composed of mixed atmospheric and respired CO_2 sources (Spötl et al., 2005). Using a measured atmospheric end member (pCO_2 = 400 ppmv, $\delta^{13}C$ = -8 ‰) and a keeling plot (Mattey et al., 2010), light soil air $\delta^{13}C$ end members above Asiul can be calculated.

Figure 5.9 indicates Asiul soil air mixing lines are seasonally invariant, with both summer and winter values requiring the same range of respired CO_2 end members, calculated as -18 ‰ to -25 ‰ for the majority of samples and -35 ‰ for two samples.

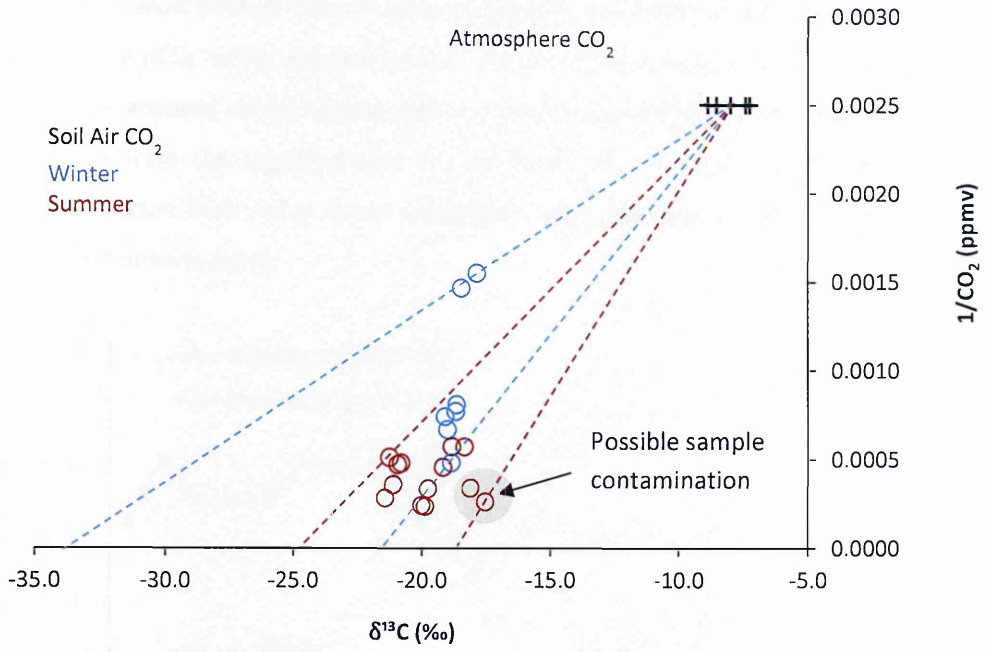

Figure 5.9: Plot of $\delta^{13}C$ composition of soil air vs. the CO_2 concentration of that air. Open blue circles denote winter samples whilst open red circles denote summer samples, corresponding to Figure 5.8. The intercept point of the dashed lines defines soil CO_2 end members for both summer and winter samples. End members for the soil system above Asiul range from -18 to -34 ‰. The grey circle indicates two samples which may have been contaminated with external air during sampling.

All but two of the soil air samples (end member of -35 ‰) indicate that a CO_2 end member of between -18 and -25 ‰ to be sufficient to give the % CO_2 and $\delta^{13}C$ values measured at this site. The lighter of these values concur with expected respiration values for the overlying C3 type vegetation (Clarke and Fritz 1997). However, the heavier soil air $\delta^{13}C$ of CO_2 values suggest either a different plant respiration pathway or that contamination by air with a heavier isotopic value may have occurred. There is no evidence for vegetation species which use a C4 respiration pathway at the cave site, suggesting that contamination is a possible factor for at least two of the heaviest samples. This contamination is most probably a result of human error during sampling.

Soil water DIC $\delta^{13}C$ could not be measured due to the rapidly draining shallow nature of the soils above Asiul cave; making it difficult to quantify soil water pCO_2 or $\delta^{13}C$ values at this site

and impossible to identify if soil air and water DIC systems are in isotopic equilibrium. However, MIX4 modelling (using measured drip water chemistry) has been used to simulate the minimum soil /karst air pCO_2 conditions to which drip waters would have been exposed during their transit through the soil zone. Only during the height of the summer season do measured soil pCO_2 values reach or exceed the predicted minimum pCO_2 values to which waters were exposed during their transit to the cave site (Figure 5.10). Measured soil air pCO_2 values from the sampling tube (50 cm depth into the soil) are therefore almost consistently lower than values which would have been recorded in deeper sections of the soil, epikarst or karst zones.

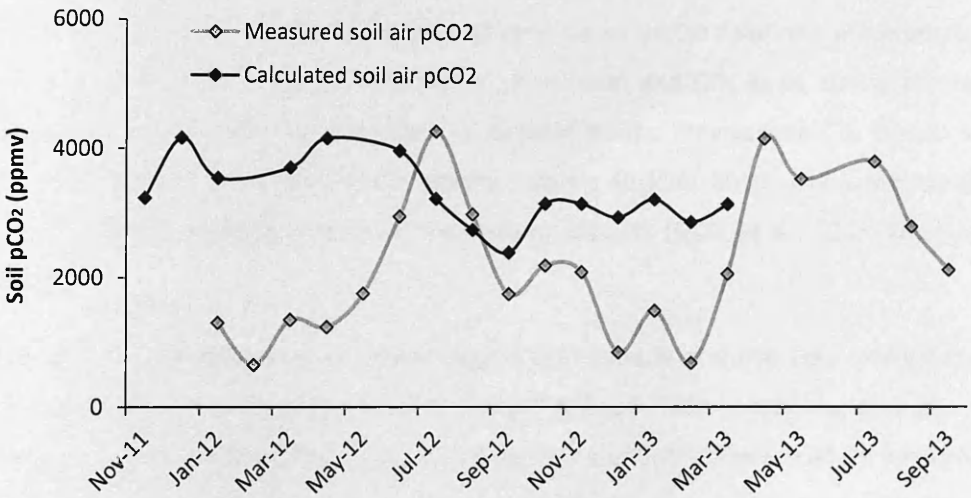

Figure 5.10: Seasonal minimum soil CO_2 concentrations both measured (grey diamonds) and modelled (may include karst air CO2; black diamonds) using MIX4.

As monitoring equipment was located as close to the base of the soil zone as possible, MIX 4 modelling suggests drip waters must come into contact with pCO_2 values which are higher than any measured within the soil zone (throughout most of the year). Mattey et al., (2010) suggest secondary sources of CO_2 rich ground air may include: 1) CO_2 degassed from drip waters, 2) CO_2 from the soil zone which has penetrated the epikarst as a gas phase, 3) CO_2 respired from plant roots which penetrate deep into the epikarst, and finally 4) CO_2 produced by the decomposition of colloidal or dissolved organic matter transported by percolating water.

If as thought, the soil air collection tube has been located close to the top of the epikarst, gaseous CO_2 from the soil zone would already be fully sampled. Due to the shrub like vegetation above Asiul it is also unlikely that deeply penetrating root systems could produce

a zone of elevated pCO_2 below the soil measuring tube. Therefore, it is most probable either CO_2 degassing from drip water or organic matter decomposition within the epikarst creates a zone of heighted CO_2 concentration, which equilibrates with percolating water. As Mattey et al., (2010) suggest it may be this zone of heightened CO_2 concentration which truly constitutes "ground air". Infiltrating waters equilibrate with this zone of CO_2 rich air before percolating deeper into the karst and finally into the cave.

5.3.2 The Cave CO_2 System

Cave air CO_2 is derived from a number of sources and is balanced by input fluxes, such as drip water degassing, soil air penetration and cave ventilation and the out flux of air through cave entrances. To understand the importance of these fluxes on the Asiul cave atmospheric CO_2 system, modelling of CO_2 end members is undertaken and CO_2 input during drip water degassing is quantified. It is important to characterise the atmospheric CO_2 system when establishing periods of speleothem growth maxima (Baldini 2010) and when trying to understand the chemical makeup of speleothem deposits (Spötl et al., 2005, Frisia et al., 2011).

Cave air CO_2 concentrations have been logged continuously at a one hour interval (logger removed for a few days each month to charge) in Asiul's main monitoring chamber since February 2011 using the same Vaisala GM70 monitor and GMP221 probe which was used for spot measurements of soil pCO_2. For a period between August 2011 and April 2012 the original Vaisala monitor malfunctioned within the cave environment so data is not included for this period (Figure 5.11). A new monitor was installed in April 2012. Continuously logged cave pCO_2 data is not corrected to standard atmospheric pressure due to the extremely high resolution logging intervals; corrected values have been calculated to be within 50 ppm of the presented values. If quoted in ppmv, monthly values are corrected using average monthly pressure data from the in-situ (within the same chamber) CTD Diver and the calculations of Spötl et al., (2005) (Equation 3.1).

pCO_2 measurements taken in Asiul (averaged daily) begin to reveal a pattern of seasonality during 2012 and 2013 (Figure 5.11). Values show a similar range as other cave sites, including Ernesto (Frisia et al., 2011) and Obir Cave (Spötl et al., 2005) with pCO_2 maxima in July – August 2013 (2090 ppm) and minima corresponding to external atmospheric (≈ 400 ppm) values during late autumn, early winter 2012. Peak CO_2 values occur during spring and early summer when cave ventilation is under a summer regime, as indicated by gradually increasing air temperatures within the cave. Air drawn through the soil and karst during the

spring and early summer has a high CO_2 concentration, derived from the biogenically active soil zone and possibly a high pCO_2 ground air source. Towards the peak of the summer season cave air CO_2 concentrations decrease, possibly related to reductions in vegetation productivity which is limited by water availability. Cave air pCO_2 minima are observed by October each year.

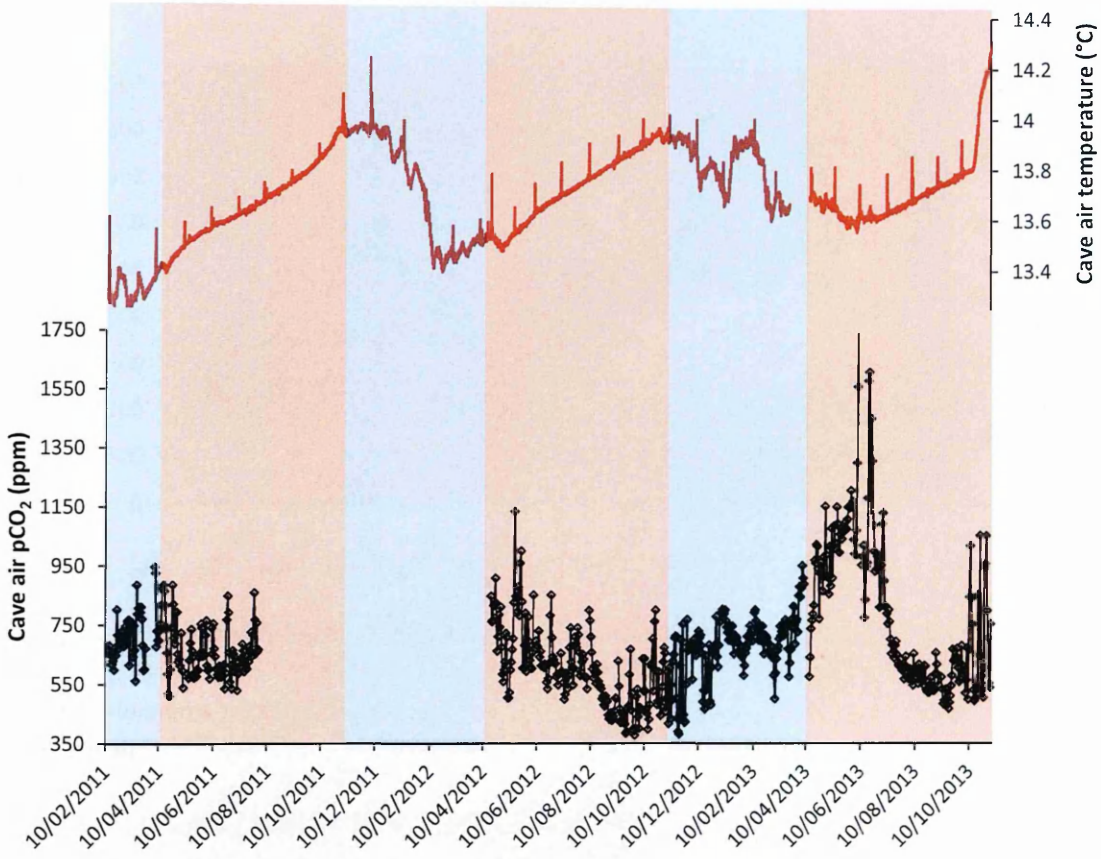

Figure 5.11: Cave air temperature (red line) and pCO_2 (daily averages; black diamonds) values over a 2.5 year logging period. Gap in CO_2 data is due to logger malfunction. Coloured background represents the seasonal cycles with the summer season between March and November.

This is unlike many other cave sites. Reductions in cave air pCO_2 (July 2012 and again in 2013) occur before cave ventilation switch over in Asiul, which is indicated by cave air temperature as occurring in November (beginning of the blue shaded area on Figure 5.11). The reduction in cave air pCO_2 therefore occurs before the inflow of low pCO_2 external air, indicating that cave air pCO_2 values may not be completely coupled with ventilation regime. It is possible that in Asiul, cave air pCO_2 is driven predominantly by CO_2 ingress through the karst from the soil zone. To assess this hypothesis, seasonality in cave air pCO_2 is compared

with soil air pCO_2, to identify peak periods of interconnectivity between the soil and cave zones (Figure 5.12).

Peak soil and cave air CO_2 concentrations coincide (June-July 2013), suggesting some interconnectivity between soil and cave atmospherics during the summer. This coupling is to be expected during periods of maximum soil air draw down into the cave (under summer ventilation).

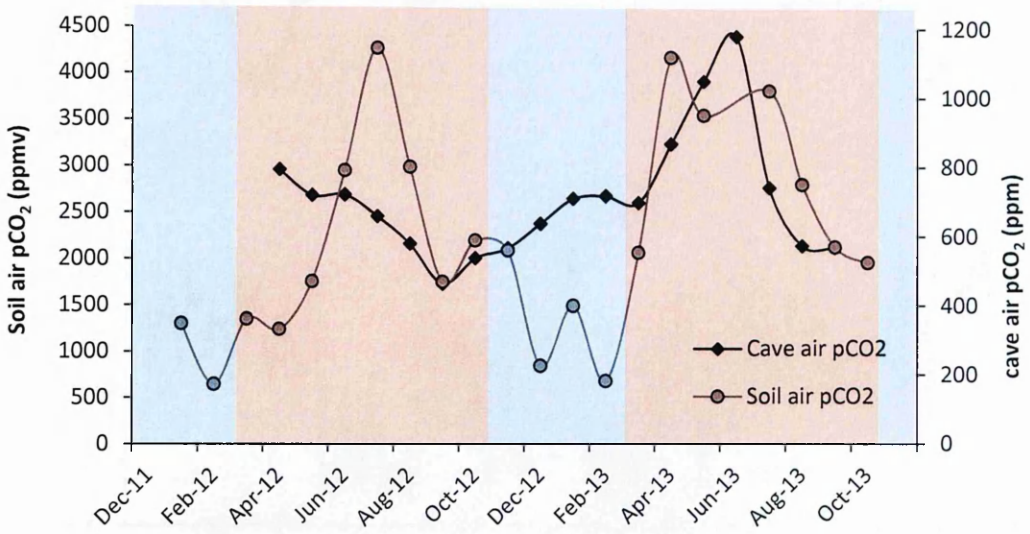

Figure 5.12: Cave air (black circles) and soil air (grey circles) pCO_2 values over a 1.5 year period. Peak values occur in both records during spring and early summer (red shading) and minimums occur at the end of the summer (cave air) or mid-winter (soil air; blue shading).

However, this soil / cave air pCO_2 coupling breaks down in the winter season with cave air pCO_2 minima occurring in September 2012, whilst soil air CO_2 concentrations continue to decrease throughout the winter, only recovering at the onset of the new vegetation growth season, from March 2013 (Figure 5.12).

Unlike summer, winter ventilation promotes diurnal fluctuations in CO_2 concentration, indicating a very strong coupling of cave air with the external atmosphere (Figure 5.13). Diurnal fluctuations of CO_2 of up to 200 ppm are common, even at 65 m into the cave system. CO_2 concentrations rise throughout the day until cold overnight air temperatures external to the cave promote the ingress of low pCO_2 air into the system. Although this ventilation is strong enough to cause considerable pCO_2 variation on a diurnal scale it does not always trigger a concurrent fluctuation in cave temperature (Figure 5.13). The stability of cave temperature during at least some of these large ingresses of external atmospheric air

suggests cave air temperature equilibration occurs rapidly and before 65 m depth into the cave, due to the influence of heat exchange between the cave walls and infiltrating air (Smith et al., 2013).

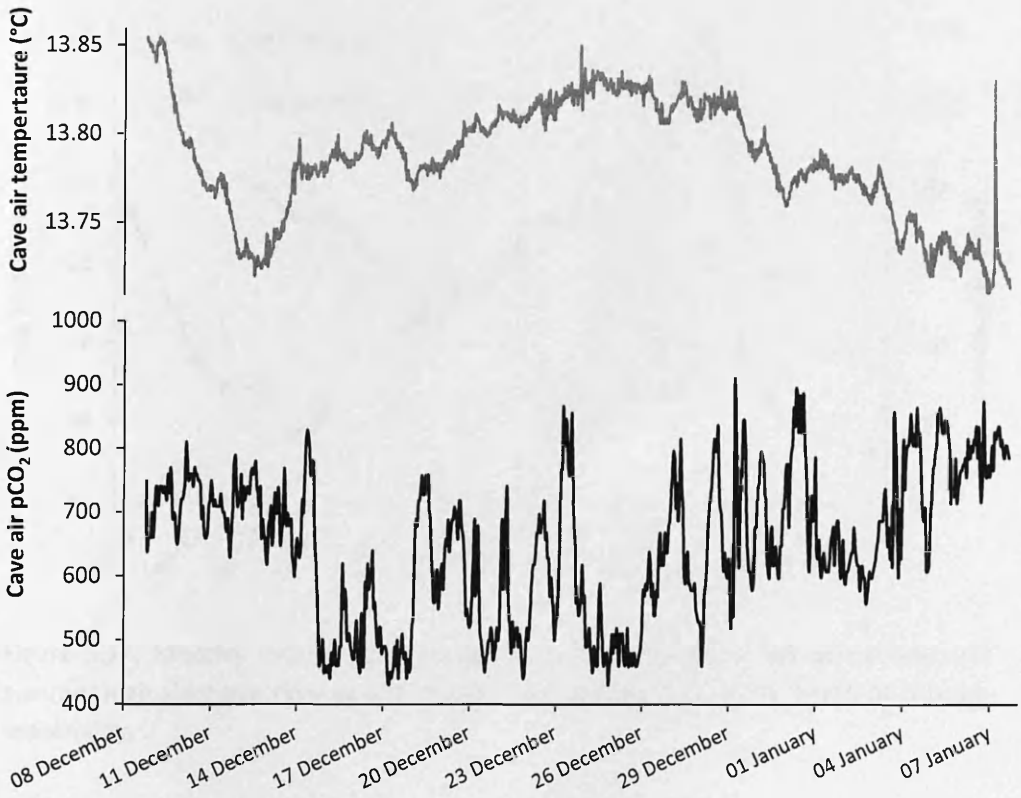

Figure 5.13: Cave air pCO_2 values over a one month period during winter 2012-13 (black line) alongside cave temperatures (grey line). Diurnal fluctuations in pCO_2 are not always mimicked by cave temperature at 65 m depth due to heat exchange between the cave walls and infiltrating air.

Over short time scales, significant diurnal variation in cave air pCO_2 may control the deposition efficiency of $CaCO_3$ and speleothem growth rates during the winter period. Low nightly cave air pCO_2 values would promote the deposition of $CaCO_3$ due to enhanced degassing from drip waters. Monthly average values of cave air pCO_2 may not therefore accurately resolve the complex atmospheric environment, which is apparent throughout the winter at Asiul.

Whilst changes in cave air pCO_2 value and temperature can go some way to characterising the source of cave air on a range of scales, cave air $\delta^{13}C$ can be used as a secondary tracer, to try and accurately identify cave air CO_2 sources throughout the year (Mattey et al., 2013). Cave air $\delta^{13}C$ values are sampled on a monthly basis at 65 m depth into the cave, prior to any

other human sampling within the chamber. Unlike other cave sites the maximum range of cave air $\delta^{13}C$ values is recorded in consecutive months, demonstrating a distinct lack of seasonality in Asiul (Figure 5.14).

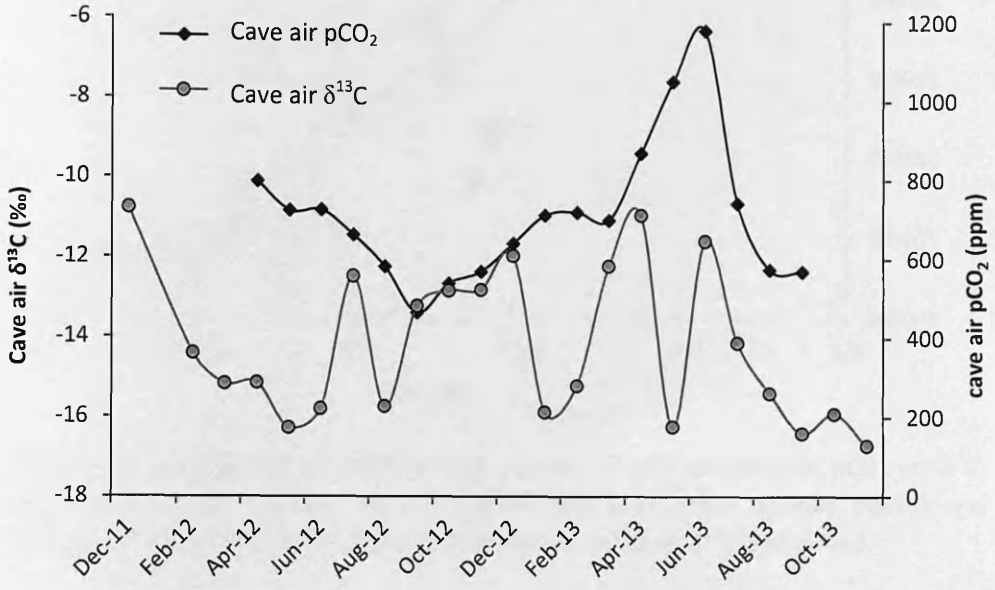

Figure 5.14: Monthly cave air pCO_2 values (grey line) showing a late winter low and summer high alongside cave air $\delta^{13}C$ values (black dashed line) which exhibit no obvious seasonality.

No clear link between monthly cave air CO_2 concentration and carbon isotope value can be established (linear regression; r^2 = 0.00) and no direct co-variance is observed between monthly soil air $\delta^{13}C$ and that of cave air (linear regression ; r^2 = 0.1). However, the pCO_2 and $\delta^{13}C$ values of cave air are clearly a function of soil and atmospheric values (average atmospheric $\delta^{13}C$ = -8 ‰, CO_2 = 400 ppmv). The Keeling plot of $1/pCO_2$ verses $\delta^{13}C$ in Figure 5.15 indicates both summer and winter values are derived by a mixture of soil and atmospheric air. For the most part, soil air pCO_2 and $\delta^{13}C$ are clearly separate from cave air and atmospheric values; even though some mixing would be expected between the soil zone and external atmosphere, especially during summer (Frisia et al., 2011). At this site a complex interaction of soil air and external atmospheric end members accounts for both the CO_2 concentration and isotopic makeup of cave air. The dominance of either end member does not appear to be straightforwardly linked to either soil productivity, cave ventilation regime or season as at other cave sites. The apparent lack of seasonality in CO_2 regime may cause a similar lack of seasonality in speleothem deposition rates, explaining the lack of annual lamina recorded in Asiul speleothems.

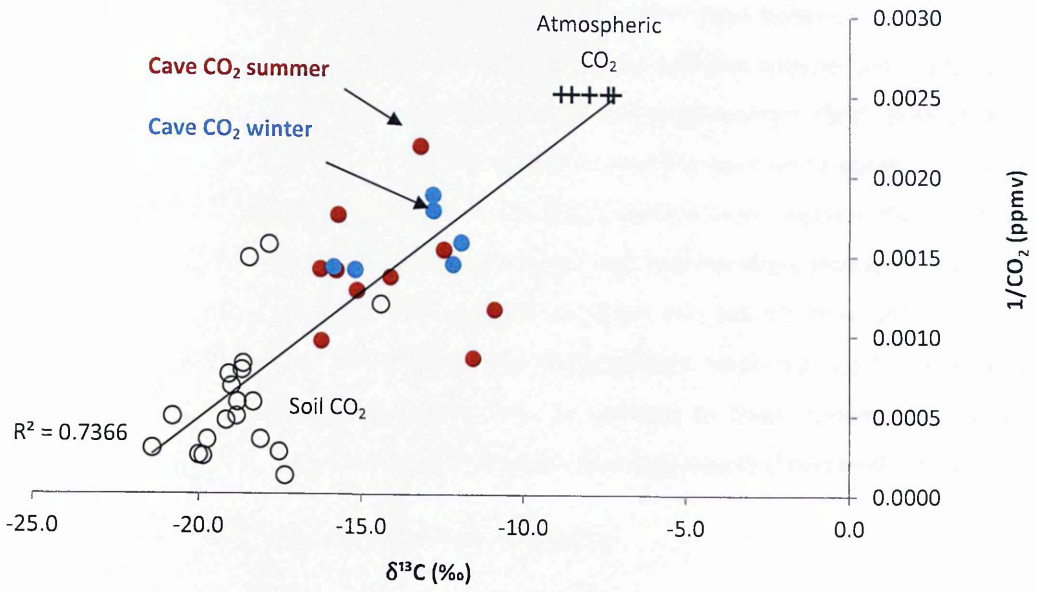

Figure 5.15: Keeling plot of monthly cave air, soil air and atmospheric pCO_2 vs. $\delta^{13}C$. Whilst soil air and the external atmosphere appear to make up two distinct end members for this system little seasonality in cave air pCO2 vs. $\delta^{13}C$ is observed.

To try and more clearly establish the sources of cave air, cave air $\delta^{13}C$ end members are calculated in Figure 5.16, using the same data as presented in Figure 5.15.

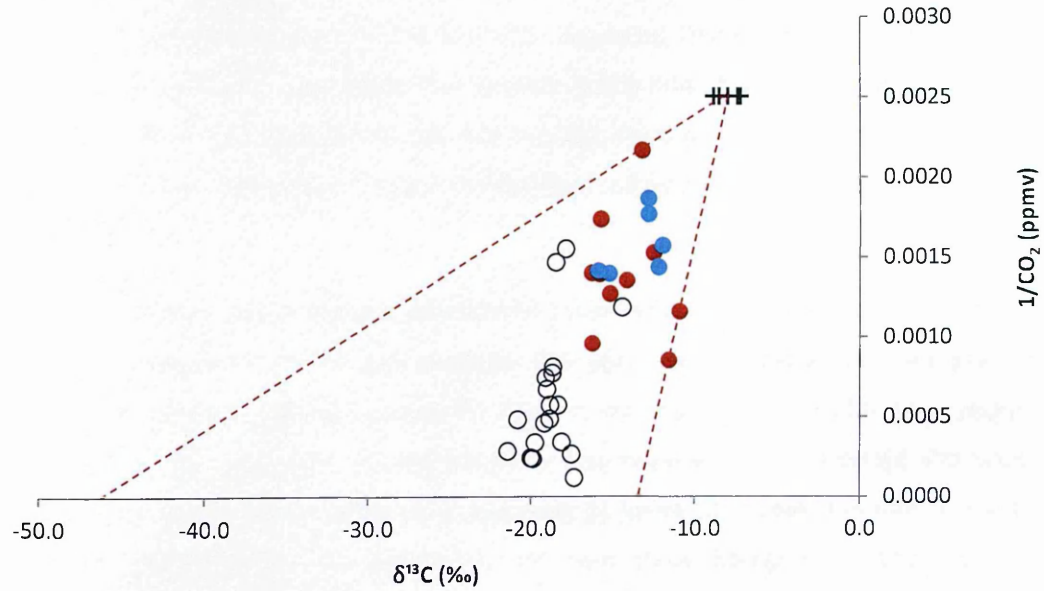

Figure 5.16: Equivalent diagram to Figure 5.9 using cave air sample data. The isotopically light end members incorporate all samples within analysis errors, and lie between -13 and -46 ‰ in composition. Cave air end members incorporate the whole range of soil samples collected at this site, and one summer sample appears to require a CO_2 end member with a more negative isotopic composition than any found within the soil zone.

Figure 5.16 shows that cave air $\delta^{13}C$ has light CO_2 $\delta^{13}C$ end members between -13 and -46 ‰ in composition. Whilst there appears to be little difference between summer and winter end member values, Figure 5.16 does demonstrate that the most extreme (both positive and negative) isotopic end member values are linked to summer cave air samples. The most negative isotopic end members require a source of CO_2 which is more negative than anything previously observed in the soil zone, whilst the heaviest end members indicate a CO2 end member which may be sourced from external air. Cave and soil air monitoring in Asiul indicates that the CO_2 system is driven by two end members. Firstly high pCO_2 soil air and secondly a low pCO_2 external air component. In addition to these sources drip water degassing may add CO_2 into the cave air during high discharge events (Frisia et al., 2011).

5.3.2.1 CO_2 Release from Drip Water Degassing

Cave air CO_2 concentration can be augmented during periods of heightened drip water input due to a greater volume of CO_2 degassing from drip waters within the cave void (Frisia et al., 2011). As shown in a previous chapter, cave air pCO_2 increase in Asiul is often related to an increase in speleothem drip rates; although the timing of CO_2 rise in relation to drip rate rise is seasonally dependent. Calculation of this CO_2 emission can be undertaken assuming CO_2 which is introduced by dripwater is dispersed equally throughout the cave atmosphere. Drip water increase events during summer (24^{th}-29^{th} July) and winter (21^{st} – 24^{th} February) were assessed to establish the CO_2 flux from drip water degassing. Under summer conditions, CO_2 increases are known to occur before any increase in drip rate (due to soil air flushing). For the calculation of CO_2 input due to drip rate increase, the whole CO_2 and drip rise event is considered rather than trying to dissect the flux from soil air and that from direct degassing from water.

Before the summer event, drip rate was close to a summer background average (1.7 D/min) and CO_2 concentrations were approximately 650 ppm. Peak discharge (an increase in background drip rate of 40 %) occurs within 12 hours and drip rates returned to background levels within another 12 hours. CO_2 rise and decay occurred over a 72 hour period with peak CO_2 values (440 ppm above background) occurring 11 hours after peak drip rate; average pCO_2 increase throughout the period was 220 ppm above background. Assuming the complete dispersal of CO_2 throughout the cave a rise in atmospheric pCO_2 of 220 ppm equates to 0.43 g CO_2 per hour for 72 hours; equating to an influx of 0.03 kg of CO_2 during the drip increase event. This value is slightly higher than values reported in Frisia et al., (2011) (0.005 – 0.01 kg), possibly related to the duration of the event.

Under winter conditions, a larger rise in drip rate (60 % increase from background) over a 48 hour period triggered an average increase in atmospheric CO_2 concentration of 180 ppm over a 54 hour period. The calculated CO_2 influx of 0.36 g CO_2 per hour for 54 hours corresponds to a CO_2 rise of 0.02 kg of CO_2 during this winter drip event. Under winter conditions a smaller rise in CO_2 is experienced during the event; which is the opposite from results found in Ernesto cave (Frisia et al., 2011). It is possible that more rapid cave air exchange times and increased ventilation expected to be experienced in Asiul during the winter act to offset atmospheric CO_2 build up and reduce apparent degassed CO_2 volumes. Whilst large drip water increase events only act to add a small amount of CO_2 into the cave atmosphere and these increases are limited to the duration of the drip event a change in cave air CO_2 concentration can be important for the uptake of trace elements into speleothem carbonate (Wynn et al., 2014). Further work aimed at producing extremely high resolution speleothem records from well monitored cave sites such as Asiul may help us to understand the exact event based mechanisms for elemental incorporation into carbonate.

Monitoring of cave air has demonstrated a CO_2 source derived from soil (ground) air which infiltrates into the system as well as external air entering through the caves main entrance and the degassing of CO_2 from drip waters. Drip increase events cause small discrete increases in cave air pCO_2. Effective cave ventilation however, appears to rapidly disperse or flush this CO_2 out of the cave system, so CO_2 from drip water degassing can be considered to have a minor influence on cave air CO_2 concentration. Cave ventilation rates will be considered in the next section but the rapid dispersal of degassed CO_2 suggests cave air turnover may be rapid at this small cave site. The major source of cave air CO_2 appears to be the soil zone, especially during the summer season where a strong coupling between soil air pCO_2 and cave air pCO_2 can be observed. An annual cycle in cave air pCO_2 is seen in Asiul as values reach minimums during the winter, suggesting some decoupling of the soil air – cave air relationship. Under winter conditions cave air concentration can vary diurnally indicating a rapid, daily change in cave ventilation.

5.4 Cave Volume

During a single group visit (10 individuals) lasting approximately one hour in 2012, CO_2 concentrations were measured during and after visitors were present in the cave site (Figure 5.17). Based on the exponential decay of CO_2 concentration (from peak during the tourist visit) to background level, the rate of cave atmospheric exchange was calculated as 6.25 hours, as described in Equation 5.6 by Frisia et al., (2011). This calculation is based on one such experiment undertaken in April 2012, further calculations were not undertaken as the cave is not normally the site of tourist visits.

$$C_t = C_i e^{-\lambda t} \quad (5.6)$$

Where C_t is the cave air concentration of CO_2 above the background level at time (t) after visitors have left, C_i is the initial peak value above background and $e^{-\lambda t}$ is the decay constant. The cave air relaxation time $1/\lambda$ relates to the exchange time of cave air.

The calculated period of 6.25 hours represents the time taken for the exchange of equal volumes of air between the cave and external atmospheres. This atmospheric recovery rate can be used as an analogue value of daily air exchange under natural conditions of pCO_2 rise and recovery to base levels.

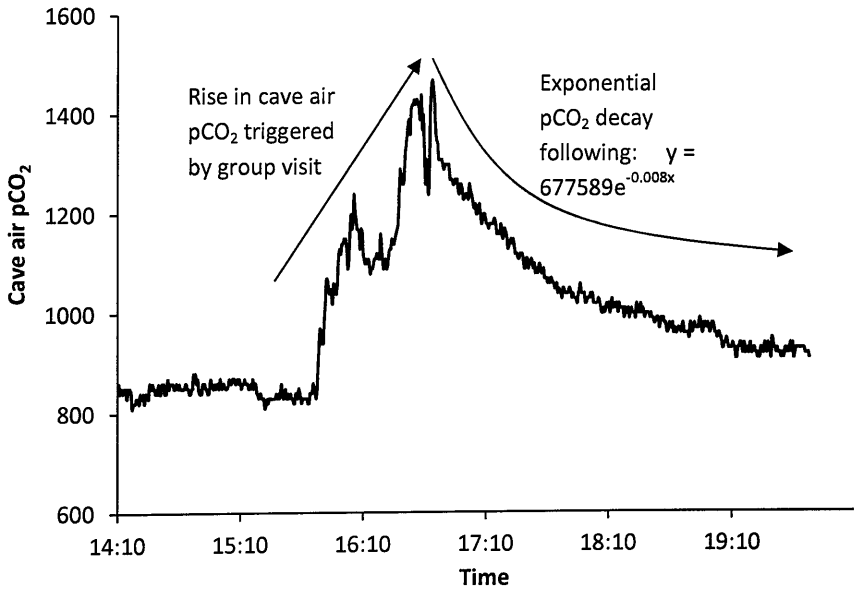

Figure 5.17: Cave air pCO_2 rise and exponential decay following a tourist group visit into Asiul cave in April 2012.

Following the calculation of cave air exchange; cave volume (V_c) was calculated following the methodology of Frisia et al., 2011 (Equation 5.7).

$$V_c = (480/R)*(C_b - C_4) \quad (5.7)$$

Where R is an average CO_2 increase in ppm per person, per hour in the cave system (Equation 5.8).

$$R = (\text{Peak } CO_2 - \text{background } CO_2) / \text{visitor number (10)} \quad (5.8)$$

Peak CO_2 during this event was 1470 ppm from a background value of 850 ppm. C_b is the concentration of human breath, calculated as 480 litres of exhaled breath per hour at a concentration of 36000 ppm (Kivastik 1998), C_4 is the base level cave CO_2 concentration in ppm at the time of the experiment (850 ppm).

Assuming an equal dispersion of CO_2 throughout the cave system, the effective cave volume at Asiul is calculated as V_c = 272129 litres or approximately 2.7 x 10^6. Frisia et al., (2011) suggest this technique of cave volume calculation yield results within 30 % of the values given by estimating the cave's cylindrical volume.

The calculation of cave volume and flushing rates helps to characterise other processes occurring within the cave system. Large increases in drip water infiltration and associated CO_2 degassing must be equally transmitted through the full volume of the cave system and will only start to decay as air flushing occurs. Cave air flushing is calculated as only taking 6.25 hours but may increase or decrease dependent upon seasonality and cave ventilation regime. Understanding the role and quantifying the process of cave ventilation may be important to understand speleothem growth dynamics under variable ventilation regimes.

5.5 Speleothem Growth Rates

Monitoring has indicated that speleothem growth in Asiul may be controlled by a range of processes both hydrological and atmospheric, all of which may vary throughout the year. Previous studies have identified drip rate, temperature, drip water Ca^{2+} concentration, thickness of the thin film covering the stalagmite and cave air pCO_2 as the major controls on speleothem growth rate (Dreybrodt 1999, Genty et al., 2001, Baldini 2010). Using monitoring data from Asiul, a calculation of monthly speleothem growth rates can be undertaken throughout the year to identify points of maximum and minimum growth. These calculations may also help to identify key process of speleothem growth and by doing so the nature of the palaeorecords from these speleothems.

Theoretical speleothem growth can be calculated using the equation of Baldini (2010) which is derived from equations in papers by Dreybrodt (1999) and Baker et al., (1998) (Equation 5.9).

$$R_o = 1.174 * 10^3 (Ca - Ca_{eq}) * (\delta * \Delta T\text{-}1) [1 - e^{(-\alpha * \Delta T * \delta^{-1})}] \quad (5.9)$$

Where: R_o is the speleothem extension rate (mm yr^{-1})

$1.174 * 10^3$ is a conversion constant which changes molecular accumulation (mmol mm^{-2} s^{-1}) into growth rates (mm yr^{-1})

Ca_{eq} is drip water [Ca^{2+}] at equilibrium with a stated atmospheric pCO_2

Ca is the initial drip water [Ca^{2+}] (mmol L^{-1})

δ is the thin film thickness (mm) (0.1 in this study)

ΔT is the time between successive drips (s)

α is a kinetic constant (mm s^{-1}) that is dependent upon δ and temperature (10°C)

Ca_{eq} is derived from Equation 5.10 and is dependent upon cave air pCO_2 measured each month.

$$Ca_{eq} = 7.611 * P_{CO2}^{0.275} \quad (5.10)$$

This relationship is derived from previous work by Dreybrodt (1999) and Baldini et al., (2008) and is derived for a temperature of 10 degrees °C. The kinetic constant α (cm s^{-1}) is derived from Equation 5.11 and is dependent upon temperature and thin film thickness, which are encapsulated in the term β (Dreybrodt 1999). Dreybrodt (1999) give values of β at different temperatures and film thicknesses; at 10 °C and 0.1 mm this component yields the α value of 0.0001275 which is used in this study following Baldini (2010).

$$\alpha = 8.5 * 10^{-4} * \beta \quad (5.11)$$

	ASF Ca drip (mmol L^{-1})	Temp	pCO_2 (atm)	Ca_{eq}	Film thickness (mm)	Time between drips (s)	α (mm s^{-1})	β	R_o (mm/year - 1)	ASF (microns/ $year^{-1}$)
Average ASF	1.03	13.70	0.0007	1.014	0.1	39	0.00013	0.024	0.002	2.31
Average ASM	0.99	13.70	0.0007	1.014	0.1	260	0.00013	0.024	-0.003	-3.32
Average ASR	1.10	13.70	0.0007	1.014	0.1	128	0.00013	0.024	0.011	11.45

Table 5.2: Components of speleothem growth rate calculations undertaken following Baldini (2010). Speleothems ASF and ASR show small positive annual growth rates whilst ASM indicates negative growth.

Using average cave conditions, a theoretical growth rate per year can be calculated for the major speleothems (Table 5.2). Speleothems ASR and ASF indicate small positive annual growth rates of a few microns/ year whilst ASM indicates slight negative growth or corrosion under measured atmospheric and hydrological components. However, detailed assessment of speleothem ASM before palaeoclimate analysis discovered no evidence of carbonate dissolution possibly suggesting slight inaccuracies with the growth rate model at such low growth rates. One other possible problem is the use of bulk water samples for the initial Ca concentration of the drip water; these samples may have undergone some prior (on speleothem or equipment) Ca precipitation. When measured, these samples would therefore have lower Ca concentrations than expected from instantaneously collected samples, leading to an underestimation of speleothem growth rate. Whilst this consideration is noted, no instantaneous drip water chemistry is available for these sample sites so growth rate reconstructions should be considered as minimal speleothem growth rates.

Whilst average yearly growth rates may give a broad overview of calcite deposition volumes, this calculation does not indicate when speleothem growth rates are at maximum or minimum rates throughout the annual cycle. Calculations of monthly growth rate were undertaken for each speleothem where data was available; aiming to give a higher resolution overview of speleothem growth dynamics (Figure 5.18). Monthly calculations are presented as a yearly value of calcite thickness (μm) which would have deposited if the atmospheric and hydrological conditions of any individual month were to persist for a full year.

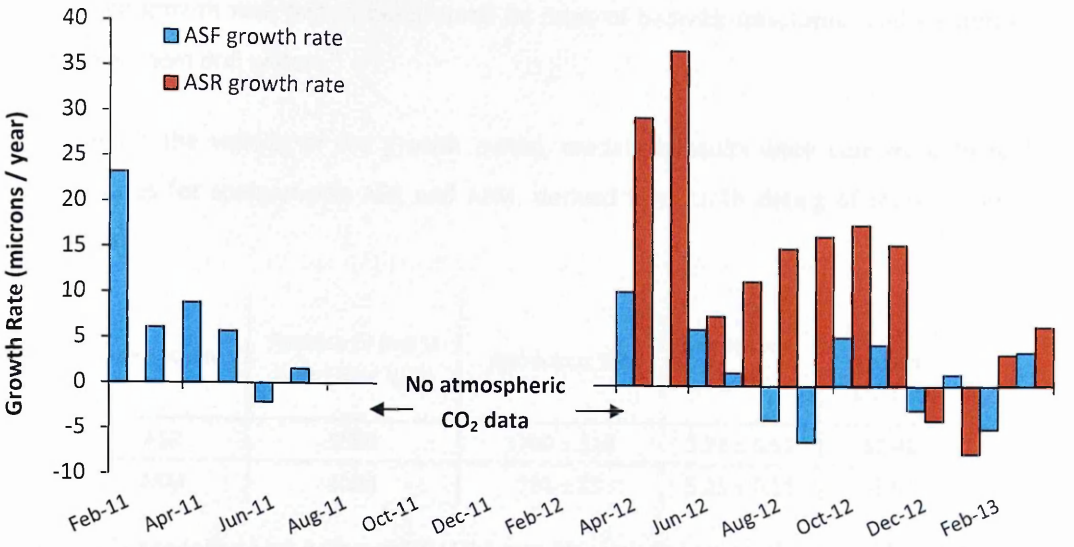

Figure 5.18: Speleothem growth rates (microns/ year) in the main monitoring chamber, Asiul Cave. Both speleothems exhibit phases of positive and negative growth, meaning it is possible for some speleothem degradation to occur.

Figure 5.18 shows growth rates for two of the major speleothems used for monitoring and palaeoclimate reconstructions. These speleothems exhibit slow growth rates in comparison to other cave sites (Baldini 2010). Highest growth rates are observed at speleothem ASR during the spring / summer (37 µm / year in May 2012). This speleothem displays continuity in growth phases, with February – November in positive mode and December and January in a slightly negative growth mode. The ASF record indicates phases of slight positive and negative growth throughout the year, but does not indicate a stable seasonality in growth dynamics. This irregularity in the records possibly suggests that seasonally variant components of the cave system (primarily atmospheric pCO_2) are not the principle control on speleothem deposition at this site.

Growth rate modelling is dependent upon the relationship between two independent factors: drip water Ca concentration and cave air pCO_2 concentration. In Asiul, peak atmospheric pCO_2 values are lower than those regularly found in other cave systems, especially during the summer months. A lack of seasonal growth rate structure (lamina) in many of the speleothems at this site and growth rate modelling suggests seasonal variations in cave air pCO_2 are not a driver for speleothem growth. Speleothem growth rate and cave air pCO_2 values exhibit only a weak linear relationship (linear regression; $r^2 = 0.2$) under conditions modelled in Asiul; by implication, the lack of a control by pCO_2 leaves Ca as the

controlling growth rate factor, determined by rates of bedrock dissolution and Ca uptake into speleothem drip waters.

To establish the validity of the growth model, modelled results were compared to real growth rates for speleothems ASR and ASM, derived from U/Th dating of these samples (Table 5.3).

Speleothem	Position of first U series date (μm)	Age (years BP)	Growth rate (μm)	Modelled growth rate (μm)
ASR	5500	1702 ± 319	3.23 ± 0.51	11.48
ASM	4150	791 ± 15	5.25 ± 0.11	-3.51

Table 5.3: Modelled and measured (U/Th) growth rates for speleothems ASM and ASR, both of which are used for palaeoenvironmental reconstructions. Measure growth rates are based upon distance growth / year over a time slice constrained by U/Th dating positions.

Modelled and observed growth rates for these two speleothems seem relatively consistent. Any offset between the modelled and observed growth rates can be explained by a 2 ppm change in Ca concentration within drip waters (only 20% of the observed seasonal variation in drip water Ca concentration). The close affinity between modelled and observed growth rates adds confidence to both methodologies and confirms these speleothems are both extremely slow growing in the modern day.

Under the most rapid growth rates observed in either speleothem record (ASR record between 9.2 and 9.6 ka) an estimated growth rate of 47 μm / year is observed. If atmospheric conditions within the cave remain as under modern conditions, this growth rate change would equate to an increase in drip water Ca of 11 ppm; from a modern average of 38.1 ppm (Table 4.7) to 49.5 ppm at 9.2 ka. The most extreme modern drip water values (43.8 ppm) do not quite reach 49.5 ppm, but this value does not far exceed measured modern hydrological conditions at the height of the contemporary hydrological cycle for this speleothem core.

The calculation of speleothem growth rates at this site has shown drip water Ca concentration to be the major control over speleothem growth dynamics in Asiul. The cave's year round, low atmospheric pCO_2 means seasonal cycles in cave ventilation are not of a magnitude to drastically change the extent of speleothem deposition. Modelling of modern

growth and measured growth based on U/Th decay, both suggest the main monitoring speleothems exhibit very slow growth rates. Back calculation of drip water Ca concentration based upon measured (U/Th) growth rates indicates that a relatively minor shift in drip water chemistry can drastically alter speleothem growth rates and can explain all growth rates observed in these Holocene age speleothems. Growth rate modelling indicates that the hydrochemical cycle at this cave site has remained relatively stable throughout the Holocene.

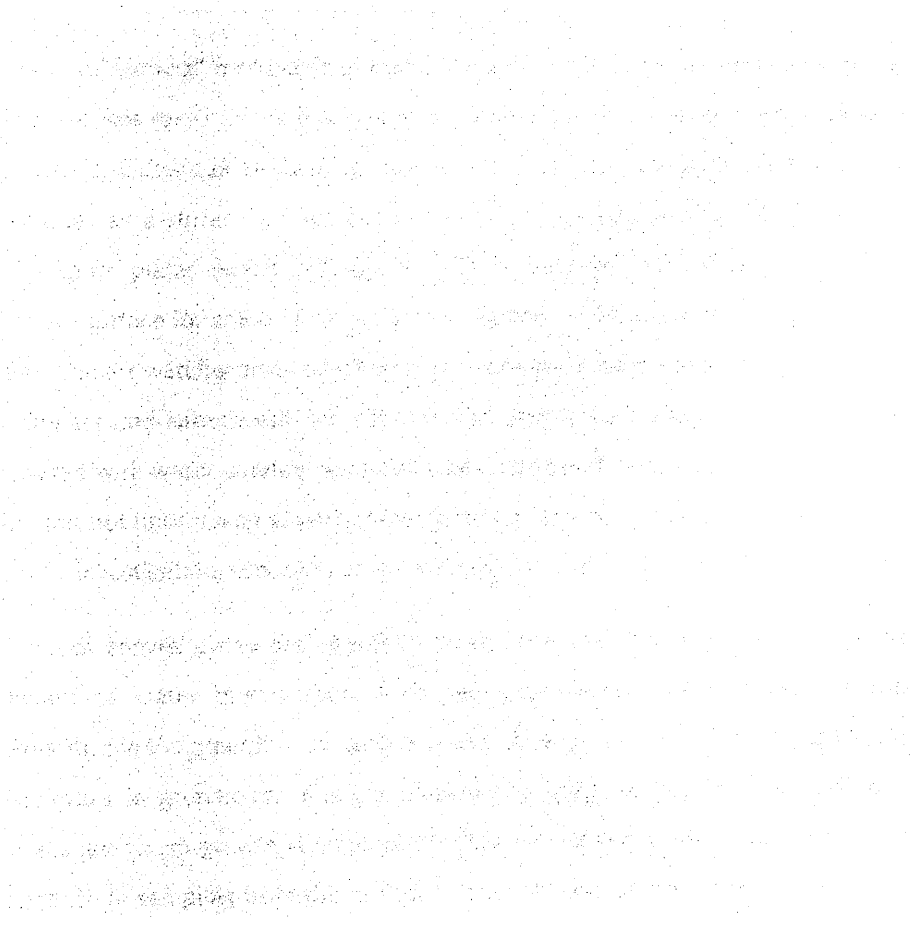

5.6 Calcite Growth Plates

Hydrological and atmospheric components of the Asiul system as well as speleothem growth dynamics have been reviewed in previous sections. Parallel to the constant monitoring of these fundamental components of the cave system, glass plates were placed on top of actively growing speleothems to collect or "farm" calcite under monitored modern conditions. Calcite farming was intended to offer the last piece of information regarding the growth of speleothems in Asiul Cave, aiding our interpretation of how speleothems incorporate drip water chemistry and respond to changing cave atmospherics. One fundamental question addresses how faithfully speleothems incorporate the stable isotope signature of drip waters (derived from rainfall) and therefore how accurately they may record changes in palaeoenvironmental conditions.

5.6.1 Farming Methodology

The calcite "farming" methodology implemented in Asiul aimed to collect enough calcite to enable analysis for O and C isotopes and trace elements, allowing direct comparison with drip waters. Other calcite farming studies which used glass microscope slides fixed atop stalagmites as a surface for speleothem growth (Tremaine et al., 2011). This study used convex glass plates (watch glasses) which we believed may offer a more appropriate surrogate surface for speleothem growth by replicating the shape of the speleothem (Figure 5.19a). Convex watch glasses may therefore facilitate a more accurate replication of natural drip impact and subsequent run off than flat plates, and remove problems that may be associated with water ponding upon flat slides. Quantitative analysis of both convex and flat slides was not undertaken as part of this study but maybe a valuable addition to speleothem scientific investigation, especially as more studies are using calcite growth experiments.

The use of convex plates has identified preferential water flow and carbonate deposition pathways as water moves away from the drip impact point; leading to small scale irregularities in the growth of carbonate across the watch glass surface (Figure 5.19b). These irregularities in growth are thought to replicate irregularities which would occur under natural speleothem growth conditions. Modern monitoring in Asiul therefore reiterates the importance of sampling from the central portion of speleothems collected for palaeoclimate analysis and for U/Th dating; both due to chemical fractionations which may occur as CO_2 degassing progresses (Hendy 1971, Fairchild et al., 2005) but also because of small scale irregularities in water runoff and calcite deposition away from the central growth axis.

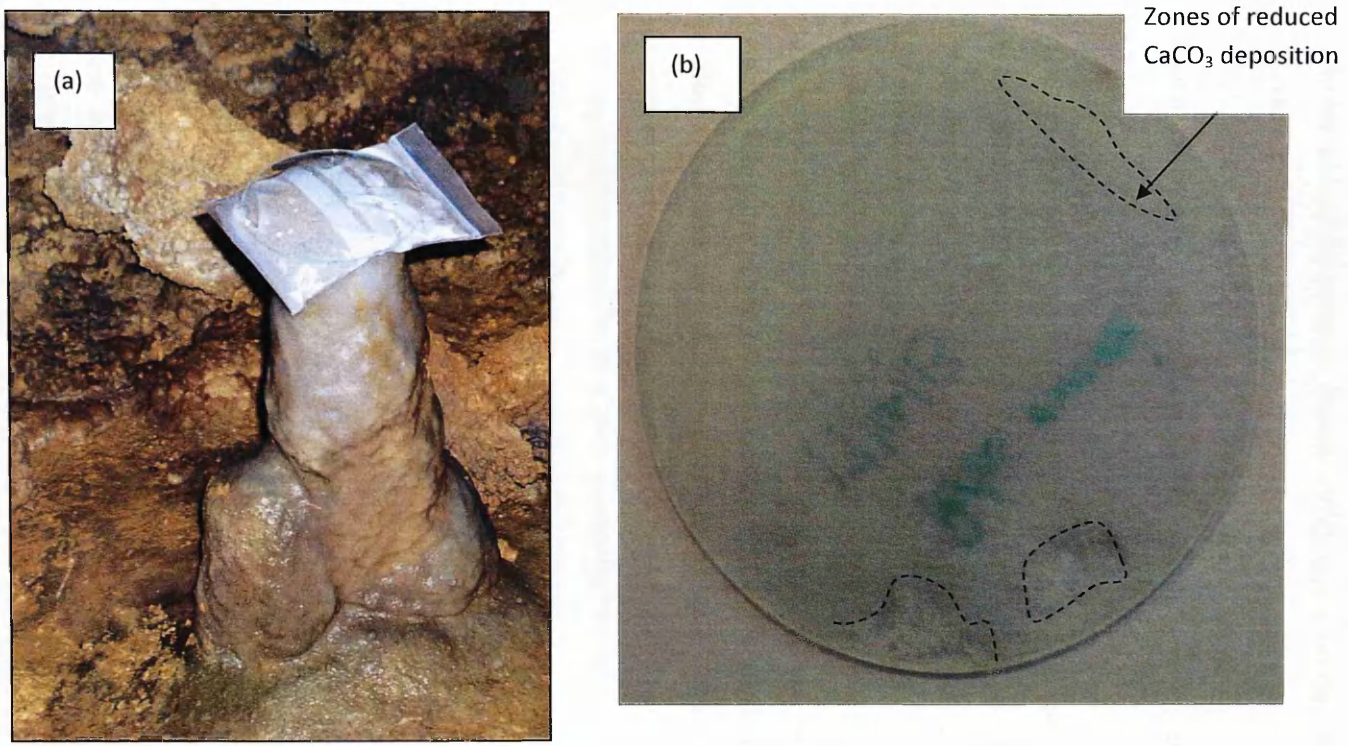

Figure 5.19: (a) Convex calcite growth plates in-situ in Asiul Cave, due to the shape of the plates they can easily be securely positioned on top of the speleothem deposit using a small sand bag. (b) Calcite plate showing 1 year's $CaCO_3$ deposition, zones of reduced calcite growth have been highlighted away from the central axis.

5.6.2 O and C Isotope Equilibrium

The growth and collection of calcite under modern conditions allows for the assessment of isotopic temperature dependence (Kim and O'Neil 1997, Coplen 2007, Tremaine et al., 2011) and cross-lamina isotopic co-variation (Hendy 1971), under natural growth conditions. A thorough review of $\delta^{18}O$ temperature dependence in speleothems is undertaken by Tremaine et al., (2011), who assume that only evaporation, temperature and drip water $\delta^{18}O$ hold any significant influence over carbonate $\delta^{18}O$, if calcite grows at near equilibrium with drip waters.

The calcite plate analysed in this experiment grew between Feb 2010 and March 2011, presenting approximately 1 years growth (13 months) on top of speleothem ASR. During this time the main monitoring chamber of Asiul cave has a continuously high relative humidity, between 97 and 100 % minimising the effects of evaporation; while constant air temperature monitoring allows for the accurate estimation of growth temperatures as 13.7 ± 0.4 °C (similar to longer term averages at this site). Due to equipment restrictions cave air CO_2 and speleothem drip rate were not monitored at the same time as calcite was deposited upon the plate. However, subsequent monitoring undertaken from 2011 indicates a relatively stable speleothem drip rate and relatively minimal amplitude in cave air CO_2. The longer term monitoring program started in 2011 gives an average cave air CO_2 content of 693 ppm and an average speleothem drip rate for ASR as 0.5 drips /min equating to a discharge of 0.053 l /day.

Average calcite plate carbonate $\delta^{18}O$ at site ASR ($\delta^{18}O$ = -5.13 ± 0.32 ‰) should therefore be a function of drip water $\delta^{18}O$ ($\delta^{18}O$ = -6.08 ‰) and formation temperature (T). It should be noted that average $\delta^{18}O$ drip water values are those from the year after calcite growth experiments, although minimal variation would be expected under the relatively homogeneous karst conditions in Asiul.

Following equations from the experiments of Kim and O'Neil (1997) (Equation 5.12) and "natural cave laboratory" results compiled by Tremaine et al., (2011) (Equation 5.13) theoretical carbonate $\delta^{18}O$ values can be established for Asiul cave drip waters and compared to modern calcite growth. $1000\ln\alpha$ represents the theoretical fractionation factor between drip water and calcite.

$$1000\ln\alpha = 18.03(10^3) / T - 32.17 \quad \text{Kim and O'Neil (1997)} \quad (5.12)$$

$$1000\ln\alpha = [16.1 \pm 0.65]\ (10^3 T^{-1}) - [24.6 \pm 2.2] \quad \text{Tremaine et al., (2011)} \quad (5.13)$$

Equation 5.12 indicates that modern average drip water values should deposit calcite with an oxygen isotopic value of -6.28 ‰ whilst Equation 5.13 yields a value of -5.45 ‰; the actual measured calcite value was -5.13 ± 0.32‰.

Modern calcite shows a $\delta^{18}O$ enrichment of 1.15 ± 0.35 ‰ in comparison with that expected under equilibrium conditions following the Kim and O'Neil (1997) equilibrium equation. Asiul cave calcite is more closely replicated by the experimental results and equation of Tremaine et al., (2011). Modern Asiul (ASR growth plate) calcite $\delta^{18}O$ is only offset by 0.32 ± 0.2 ‰ from the Tremaine et al., (2011) equation and falls within the quoted error of this line.

The close relationship modern carbonate has with the Tremaine et al., (2011) isotope fractionation line suggests speleothem development in Asiul is similar to many other cave sites. Oxygen isotope chemistry from modern carbonate deposits indicate near isotopic equilibrium in Asiul, meaning speleothems from this site should be as suitable for palaeoclimate reconstruction as those from many other caves where successful climate reconstructions have previously been undertaken (Tremaine et al., 2011). Due to the possibility of disequilibrium deposition, isotope records from Asiul speleothems will not be used to try and quantify change in any climatic parameter but rather be used to establish long term trends in the climate and environmental systems operating at this site. Further assessment of isotopic equilibrium during the formation of cave calcite was undertaken, using simple techniques laid down by Hendy (1971). These techniques aim to enable an assessment of isotopic equilibrium at any point in the speleothem record; we test these techniques using modern farmed carbonate.

5.6.3 O and C Isotope Co-variance

Characterisation of equilibrium growth conditions within a cave site has been routine to establish the validity of palaeoclimate reconstructions based upon both O and C isotopes. Many studies follow the methodology of Hendy (1971) who suggested sampling speleothems both vertically (down the central growth axis) and horizontally (across one growth layer) to assess the co-variation of O and C isotopes. Under equilibrium deposition conditions within a cave, the processes which drive O and C isotopic values are thought to be different, therefore no co-variation should be observed. However, due to the compact nature of many speleothems, accurate single lamina analysis to complete a routine Hendy isotope co-variation test (Hendy 1971) is often impossible, as is the case in the very slow growing speleothems of Asiul.

Although, the validity of this method of testing for isotopic equilibrium has been called into question over recent years (Dorale and Liu, 2009) one simple way of ensuring single, annual lamina analysis, is to assess modern annual carbonate growth from a calcite plate. In Asiul Cave, a single calcite growth plate from speleothem ASR was analysed for isotopic co-variation in two horizontal directions for O and C isotopes as outlined by Hendy (1971) (Figure 5.20 and Table 5.4).

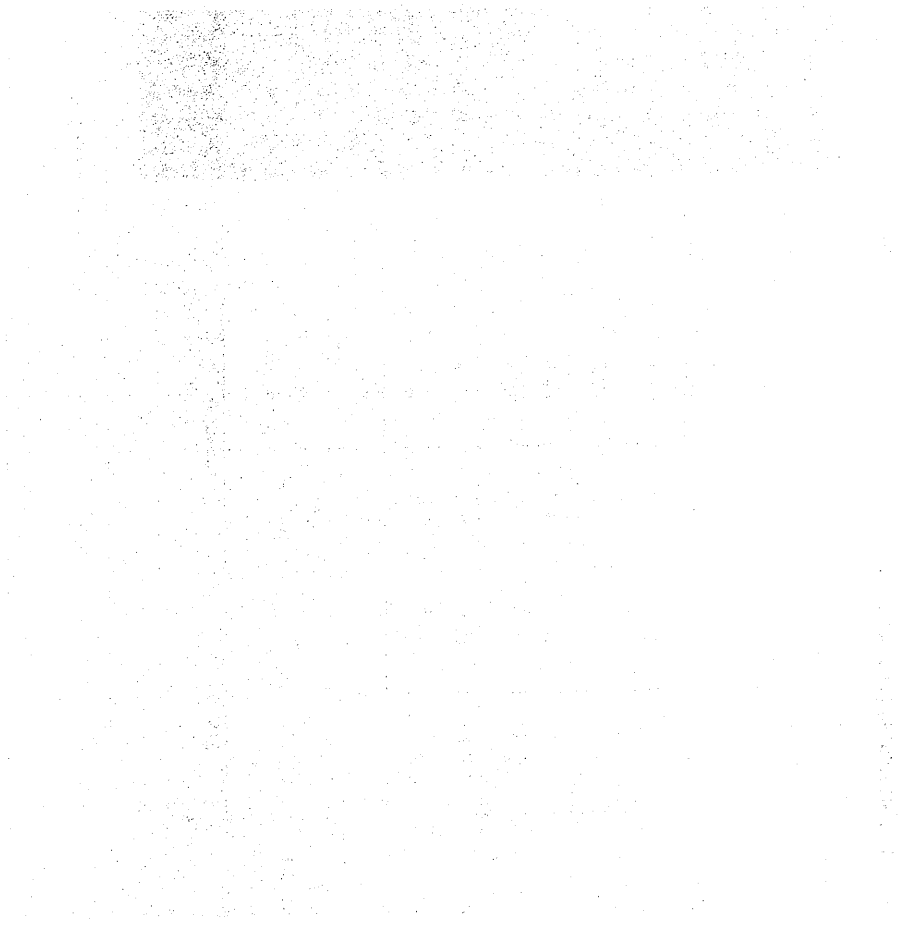

	Transect A		Transect B	
Distance from plate centre (mm)	O isotope (‰)	C isotope (‰)	O isotope (‰)	C isotope (‰)
40			-4.8	-9.2
30	-5.1	-10.2	-5.1	-10.0
20	-5.1	-10.6	-5.1	-10.4
10	-5.3	-10.8	-5.3	-10.7
0	-5.1	-10.9	-5.1	-10.9
10	-5.1	-10.7	-5.2	-11.0
20	-5.2	-10.6	-5.1	-10.7
30	-5.3	-10.1	-4.9	-10.2

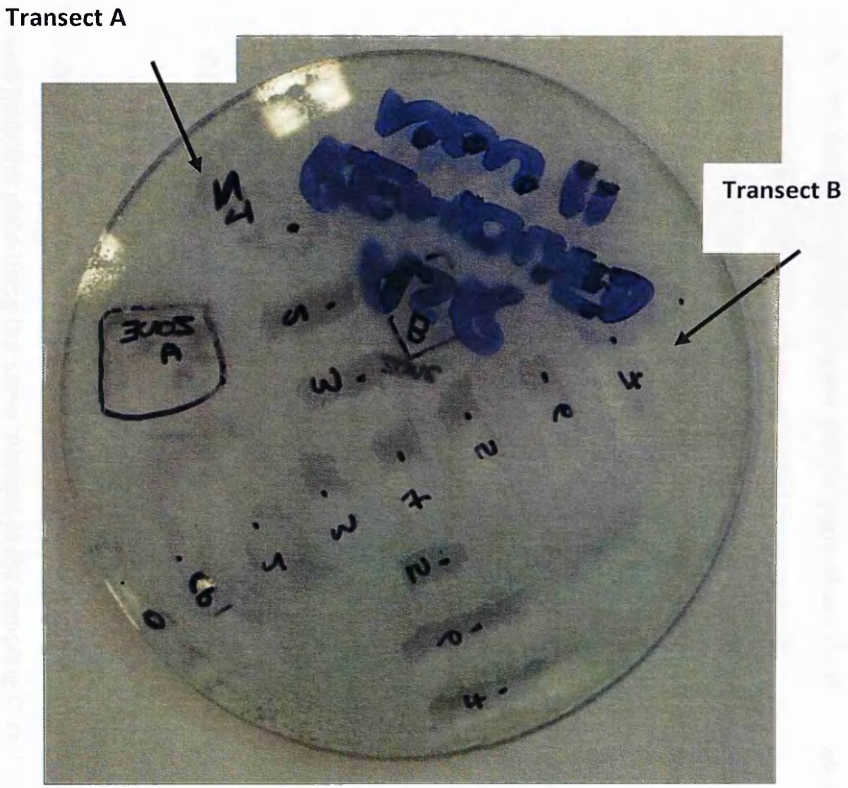

Table 5.4: O and C isotopic values for both transects A and B across the calcite plate at 1 cm intervals.

Figure 5.20: Transects A and B, showing the sampling squares for isotopic and trace element analysis and un-uniform growth across the plate.

Transect A shows no O and C co-variation (linear regression; r^2= 0.04) whilst transect B indicates a relatively high level of linear co-variance (linear regression; r^2 = 0.68). This lack of clear agreement between two transects from the same calcite growth plate calls into question the validity of this cross lamina test, both for modern deposits and ancient speleothem samples.

Calcite plate analyses suggest Hendy (1971) test results may be as dependent upon the direction of speleothem dissection and therefore the direction of cross lamina analysis as upon equilibrium or non-equilibrium growth conditions. Further validation of this finding is required, but modern growth samples from Asiul indicate alternative methods are needed to establish equilibrium isotopic incorporation into actively growing speleothem carbonate, over both short and long time periods. We would suggest, following Dorale and Liu (2009) the best insurance of isotopic equilibrium deposition within a cave is accurate stable isotope replication of several speleothems from the same cave chamber.

5.6.4 Trace Elements

Two calcite plates from speleothem ASR were sampled for trace elements. 4 mg samples were removed from the plate using the same method as for sampling O and C isotopes. The sample was dissolved using 0.1 M nitric acid solution for 24 hours, until no residue was visible. Calcite plate trace element concentrations were calculated by converting measured (by ICP-OES) Ca concentrations in solution to a stochastic distribution of 400,000 ppm (mg/kg) in calcite, all other calcite and rock trace element concentrations were then calculated to this stochastic Ca concentration, these values are shown in Table 5.5.

	Ca (ppm)	Na (ppm)	Mg (ppm)	Sr (ppm)
Plate 2010 – 2011	400,000	110572	5647	11.4
Plate 2011 – 2012	400,000	10096	-	7.1
Average Holocene core	400,000	-	4697	16.5
Modern ASR core	400,000	-	5548	13.3

Table 5.5: Concentrations of trace elements on two calcite plates removed from speleothem ASR during the study period (missing data due to analysis problems). Ca concentrations are based upon the dissolved solution whilst Na, Mg and Sr are converted to a concentration in $CaCO_3$. Where available this dissolution data is compared to trace element analysis of the ASR speleothem core, using average Holocene values.

Mg and Sr display similar concentrations in modern carbonate as displayed throughout the rest of the Holocene speleothem sample. When calcite plate carbonate is compared with just the youngest carbonate samples from the ASR core, Mg is offset by 99 ppm and Sr by 1.9 ppm. The minimal offset between Mg and Sr in the speleothem and calcite growth plates adds confidence our interpretation of longer Holocene age data sets and to our modern calcite farming techniques, using the previously untested convex watch glasses.

Whilst Mg or Sr concentrations in modern carbonate are similar to those of old carbonate from the same speleothem; the existence of modern carbonate also enables a comparison between drip water values and those in modern $CaCO_3$. For both Mg and Sr partitioning coefficients have been experimentally calculated (Huang and Fairchild 2001), which enable the calculation of expected trace element concentration in carbonate based upon drip water trace element values (Fairchild et al., 2006). These partitioning coefficients are tested using measured drip water trace element values and measured carbonate plate trace element values. Equations 4.4 and 4.5 show that the partition coefficient (K) of Mg is 0.02 (Fairchild et al., 2000); for Sr K = 0.15 (Tooth and Fairchild 2003) or 0.3 (Mattey et al., 2010). In Asiul average measured drip water trace element values are 40.22 ppm Ca, 17.41 ppm Mg and 0.009 ppm Sr.

Average Mg/Ca in drip waters is 0.44 meaning that following Equation 5.14 with a K value = 0.02 the Mg/Ca content of modern carbonate should be 0.0088.

$$(Mg/Ca)CaCO_3 = 0.02*0.44 = 0.0088 \quad (5.14)$$

However, modern carbonate values show an Mg/Ca value of 0.0014, lower than that expected from drip water values. For Asiul carbonate, a Mg partition coefficient of K = 0.003 is required to accurately calculate modern carbonate Mg/Ca values based upon monitored drip water concentrations. Whilst Asiul cave temperatures (13°C) are slightly lower than those used in Huang and Fairchild's (2001) study (15°C) this cannot explain the large offset between the experimentally derived partition coefficient of Huang and Fairchild (2001) and that observed in Asiul.

For Sr partitioning, Equation 5.15 uses the measured drip water Sr/Ca value of 0.0002 and the partition coefficient of K = 0.15 (Tooth and Fairchild 2003) to calculate a theoretical $CaCO_3$ Sr/Ca composition of $3.6*10^{-5}$. However, this Sr/Ca ratio in $CaCO_3$ is once again larger than the measured modern carbonate Sr/Ca composition of $2.3*10^{-6}$.

$$(Sr/Ca)CaCO_3 = 0.15*0.0002 = 0.000036 \quad (5.15)$$

For Asiul a Sr partition coefficient of close to 0.01 is required to accurately calculate modern $CaCO_3$ Sr/Ca values from the measured drip water Sr/Ca composition. The exact mechanism that drives Mg/Ca and Sr/Ca values to be lower than expected following experimentally derived partition coefficients (Huang and Fairchild 2001) in Asiul carbonate is unclear, although it must be related to speleothem growth dynamics and in the case of Sr possibly controlled by slow speleothem growth rates (Huang and Fairchild 2001).

Section 5.6 has demonstrated through the analysis of calcite removed from modern growth plates, that Asiul cave speleothems are depositing calcite at near isotopic equilibrium conditions, similar to those found at other cave sites from which successful palaeoclimatic reconstructions form speleothem carbonate have been undertaken. This adds confidence to our palaeoenvironmental interpretation of the isotopic records in subsequent chapters, but these chapters refrain from attempting any quantification of climatic change, instead they use speleothem isotope records to infer longer term trends in climate and environmental evolution in northern Iberia. Trace element analysis of carbonate from the same plates records very similar modern day elemental concentrations as those during the Holocene and extremely similar values to those in the youngest section of the ASR core. Partition coefficients calculated from modern carbonate and drip water monitoring indicate that both Sr and Mg incorporation into $CaCO_3$ is lower than expected following experimentally derived data (Huang and Fairchild 2001). Partition coefficients for the Asiul system are calculated as 0.003 for Mg and 0.01 for Sr. Modern calcite plate analysis has enabled the development of accurate partition coefficients for this cave site as well as adding confidence to our interpretation of trace element and stable isotope records in Chapters 6 and 7.

5.7 Asiul Cave as a Repository for Climate Archives

Palaeoenvironmental reconstructions from speleothem deposits are becoming increasingly important for understanding past climates. Speleothem deposits have been used to reconstruct changes in regional aridity (McMillan et al., 2005), atmospheric systems (McDermott et al., 2001), biogeochemical cycling (Rudzka et al., 2011) and numerous other processes (Fairchild and Baker 2012). The major proxies used for such palaeoclimate reconstructions include stable isotopes of oxygen and carbon, speleothem growth rates and trace element concentrations. Individually, these proxies have numerous valid interpretations which are often relevant to only a select group of cave sites. Therefore, accurate interpretation of speleothem chemical proxies requires both a detailed understanding of the cave system from which the samples were extracted and ideally a combination of proxies which all indicate the occurrence of a similar climate process.

Monitoring in Asiul cave has been undertaken to allow such a classification of palaeoclimate proxies in ancient speleothem deposits. This final section will review cave monitoring, to present the most accurate available interpretations of popular chemical proxies analysed in speleothem deposits. Modern monitoring will therefore lay the ground work for all palaeoclimate interpretations based upon speleothems extracted from this cave.

5.7.1 $CaCO_3$ Deposition and Speleothem Growth Phases

The incorporation of chemical proxies into the speleothem crystal lattice is driven by speleothem growth dynamics. The rate and timing of calcite deposition therefore offers a major physical control over the uptake of drip water chemistry and could alter our interpretation of palaeoclimate proxies derived from speleothem chemistry. Modern carbonate deposits and ancient speleothems have been shown to grow slowly in Asiul, from constantly saturated (with respect to Ca) drip waters. Variations in cave air CO_2 concentration holds a minimal control over the growth of speleothem deposits due to minor fluctuations in the relatively low concentrations observed on seasonal scales. Over shorter time scales, changes in atmospheric pCO_2 may act to regulate the prior deposition of $CaCO_3$ leaving drip waters relatively enriched or devoid of Ca for deposition onto stalagmite deposits. However, these short lived Ca-controlling fluctuations in cave air pCO_2 (indicated by changes in EC) do not account for the majority of speleothem deposition conditions and are therefore discounted on the millennial timescales important for palaeoclimatic reconstruction.

Due to the low seasonal variation in cave air CO_2 concentration, the overriding long term control on speleothem growth rate at this site appears to be the concentration of Ca within drip water and the extent of supersaturation. Ca concentrations vary slightly between speleothem deposits collected for palaeoclimate analysis, meaning that speleothems from the same chamber may be deposited at different rates throughout the year. Peak summer drip water Ca concentrations which may be related to enhanced rock water contact times, cause peak summer speleothem growth rates, in contrast to many other cave sites which highlight the winter season as the time of maximum carbonate deposition.

A summer speleothem deposition maxima still incorporates a winter rainfall isotopic signal due to the relative homogeneity of karst waters. Drip water chemistry suggests this winter rainfall slowly drains through the aquifer feeding speleothem drip sites year round. Therefore, in Asiul the sub-annual timing and rate of speleothem deposition is not important, as all speleothem deposits grow from a mixed winter sourced karst aquifer. Speleothems from this cave site would therefore be expected to accurately represent the isotopic chemistry of winter rainfall, over scales greater than one year. Slight homogeneity in karst water chemistry such as that found in Asiul can be important for long duration palaeoclimate reconstructions. Under such conditions, palaeo changes in speleothem chemistry should only result from real, bulk changes in karst water chemistry (and therefore winter rainfall chemistry) rather than sub-annual variations in speleothem growth dynamics, karst water incorporation or cave atmospherics.

5.7.2 Carbonate Oxygen Isotopes

The oxygen isotope composition of modern carbonate grown during 2010-11 on speleothem ASR has been shown to accurately reflect the composition of drip waters, based upon an empirical equilibrium fractionation factor, which was derived from the analysis of speleothems from a number of other cave sites (Tremaine et al., 2011). Variations in the oxygen isotope value of ancient speleothem deposits are therefore expected to reflect a change in bulk karst water oxygen isotope composition. Under modern conditions, this aquifer water is sourced predominately from winter rainfall derived from a North Atlantic Ocean source region. The strong amount effect exhibited in modern rainfall is thought to be the major control over palaeo changes in rainfall oxygen isotope value and any changes in speleothem carbonate value. Speleothems from Asiul cave are therefore expected to preserve a palaeo rainfall amount effect which can be used to identify changes in winter precipitation delivery to the region. Due to the homogeneity of modern $\delta^{18}O$ values in karst

water above all the major speleothems in Asiul, it is hoped that speleothem archives may produce covariant records of rainfall variation.

5.7.3 Carbonate Carbon Isotopes

The carbon isotopic composition of Asiul drip waters and CO_2 concentrations are complex to interpret, influenced by a range of within karst processes. Unlike oxygen isotopes, the carbon isotopic composition of instantly collected drip waters does not directly reflect the expected (equilibrium) value derived from soil air measurements. Drip waters appear to be offset from the calculated equilibrium value derived from an average soil air composition by ≈ 3 ‰. This positive offset indicates either prior degassing of ^{12}C within the karst zone (with accompanied PCP) or the decoupling of karst water from the soil air $\delta^{13}C$ reservoir, under closed system conditions and the significant introduction of a bedrock $\delta^{13}C$ component. This offset means that speleothem $\delta^{13}C$ values cannot be used directly to interpret changes in vegetation or soil productivity as in other studies. Speleothem carbon isotopes may be more correctly used in conjunction with other proxies to indicate periods of enhanced calcite-water interaction within the karst during process such as PCP or ICD.

5.7.4 Trace elements

Trace element concentrations in drip waters exhibit minimal seasonality, suggesting speleothems growing from these waters would incorporate a similar trace element signal year round. Summer season peaks in Ca concentration drive enhanced speleothem deposition during this period but the homogeneity of drip waters would mean that for many trace elements carbonate deposition rates are not critical. However, seasonal variations in elements such as Sr and Mg in ratio to Ca are often used as palaeo aridity indicators, or more simply indicators of calcite - water interactions within the karst. At the Asiul site ratios of Mg and Sr to Ca are shown to relate to enhanced calcite - water interactions, either PCP or ICD; unusually these processes are identified year round. Modern monitoring suggests increases in Mg/Ca or Sr/Ca ratios within speleothem carbonate may indicate enhanced aridity over palaeo timescales. However, the existence of calcite - water interactions year round and the slow growth rate of speleothem deposits make it impossible to resolve an annual cycle using carbonate Mg or Sr/ Ca concentrations alone.

Annual drip monitoring of Y and Mn suggests these trace metals identify periods of peak water deficit; either linked to enhanced microbial decomposition of organic matter or the release of colloidally bound substances at low soil water pH values. Importantly for climatic

reconstruction, these trace metals may offer a valuable aridity indicator, which offer insight into both karst conditions and microbial activity within the overlying soil zone.

Trace metals within speleothem carbonate from this cave site offer a range of useful palaeoenvironmental proxies especially for identifying periods of peak water deficit. Trace elements will therefore be compared to oxygen isotope values to try and highlight important periods of wetting and drying in Northern Spain throughout the Holocene.

6. STABLE ISOTOPE AND TRACE ELEMENT RECORDS FROM ASIUL CAVE SPELEOTHEMS

6.1 Introduction

Cave speleothem deposits are now one of the major sedimentary archives used to reconstruct past climatic conditions. Whilst speleothem growth dynamics can vary between cave sites, speleothems have the capacity to identify event scale changes in climatic and environmental systems (Wynn et al., 2014), a resolution rarely achieved by more traditional palaeoclimate archives. Speleothems also offer a good option when trying to identify late Holocene climatic changes from terrestrial environments, especially when human activity may have significantly altered records from lake sediments as can be the case in northern Iberia (Moreno et al., 2012).

The previous two chapters of this thesis have dealt with the assessment of within cave conditions, specifically to identify if Asiul cave is suitable for the preservation of speleothem records which may contain a climatic signature and what the various proxies stored with speleothem carbonate may tell us about past climatic conditions. Whilst this monitoring can only truly inform about modern karst, cave and carbonate growth conditions the conclusions drawn in the previous two chapters offer a starting point for subsequent proxy interpretation. Over longer, Holocene time periods proxies maybe re-interpreted due to changes which can be identified within the karst hydrological system or have been identified by other work within the climate system. However, it is thought that initially the most robust method of palaeoclimate reconstruction is one which uses known (modern) relationships between speleothem proxies and climate. Two speleothems were therefore removed from Asiul for palaeoclimate analysis.

Speleothems ASR and ASM (Figures 3.5 and 3.7) from Asiul Cave have been analysed for stable oxygen and carbon isotopes and a number of trace elements, all of which can offer important information regarding climatic change over a range of temporal and spatial scales. Speleothem ASR has the single longest stable isotope record from the cave site, spanning 12500 to 250 years BP and a trace element record which extends from 8000 to 250 years BP; whilst the rapidly growing speleothem ASM produced a higher resolution, shorter stable isotope record from 7900 – 0 years BP and a trace element record which extends from 6600 to 50 years BP.

6.2 Speleothem Chronologies

Chronologies have been developed for both speleothem deposits ASR and ASM using Uranium/ Thorium decay dating. This technique is routinely used on carbonate deposits up to the age of 500,000 years, with many samples only exhibiting minimal U and Th concentrations. This dating technique has rapidly become the standard technique for dating speleothem deposits.

Dates and the associated errors produced using the U/Th dating method are shown for both speleothems (Table 6.1).

Name	Distance from core top (mm)	Weight (mg)	U (ppm)	232Th (ppm)	230/232 Activity Ratio	Age (ka)	Error (ka)
ASR							
ASR 3 64-3	5.5	109.6	0.07442	0.00162	4.0	1.70	0.32
ASR 9 43-9	7	90.5	0.06279	0.00060	8.6	1.97	0.16
ASR 8 43-8	22	84.1	0.19130	0.00078	35.3	4.06	0.10
ASR 7 43-7	28.5	88.5	0.06318	0.00017	113.4	7.84	0.15
ASR 6 43-6	41	106.1	0.08038	0.00024	119.9	9.20	0.24
ASR 5 43-5	62	88.6	0.08499	0.00024	139.5	9.65	0.18
ASR 4 43-4	80	144.1	0.07875	0.00014	225.1	9.93	0.15
ASR 3 43-3	103	165.5	0.07891	0.00017	203.0	10.95	0.21
ASR 2 43-2	124	88.9	0.07294	0.00023	143.4	10.90	0.22
ASR 1 43-1	152	95.3	0.15020	0.00033	224.6	12.39	0.26
ASM							
ASM 23 67-7	12.5	383.5	0.0928	0.00005	10.6	0.17	0.02
ASM 5 61-4	41.5	106.2	0.1024	0.00005	45.6	0.79	0.01
ASM 6 61-5	55.5	117.6	0.0763	0.00005	43.0	0.94	0.02
ASM 7 61-6	69.5	91.7	0.0571	0.00007	39.9	1.48	0.03
ASM 8 61-7	81.5	101.5	0.0670	0.00034	11.9	1.86	0.10
ASM 11 61-8	99.5	120.0	0.0638	0.00008	53.0	2.07	0.03
ASM 12 61-9	110.5	110.5	0.0791	0.00009	59.7	2.15	0.03
ASM 16 64-15	138	97.2	0.1080	0.00042	35.8	4.23	0.08
ASM 13 61-10	168.5	101.3	0.0566	0.00007	114.2	4.78	0.06
ASM 22 61-21	269.5	132.4	0.0376	0.00034	22.1	6.71	0.20
ASM 27 67-7	306	481.5	0.0536	0.00004	321.5	7.61	0.10
ASM 28	329		0.0623	0.00004	354.1	8.70	0.05

Table 6.1: U/Th sample information, including position within the core and final age and error. These samples were used to produce the two final speleothem age models (Figure 4.

For each speleothem deposit a series of U/Th analyses were undertaken. As prior to this analysis the age of the speleothems was unknown, initial U/Th samples were equally spaced along the speleothem length, to produce an age model with equidistant sample spacing. For speleothem ASR where a distinct dark band could be visually identified (Section 3.1.2.1), U/Th samples were taken either side of this textural change, with the aim of characterising as closely as possible the temporal extent of this change in speleothem growth structure. Using the U/Th dates a chronology is then developed for both speleothem using the StalAge algorithm (Scholz and Hoffmann 2011); apart from during a significant change in growth rate, where linear fitting was assumed to be more accurate. StalAge is an automated statistical algorithm, run in the open access statistical package "R". This age model is based upon a three step process explained in detail by Scholz and Hoffmann (2011).

1) The positioning of known U/Th ages (and errors) vs. distance from the top of the speleothem sample (mm) is calculated.
2) Major and minor outliers are identified, to ensure the data set has no age inversions which would affect the modelling (Figure 6.1). The uncertainty on identified outliers can be expanded at this point by the user (Scholz and Hoffmann 2011), although error expansion was not needed for either the ASR or ASM chronologies.

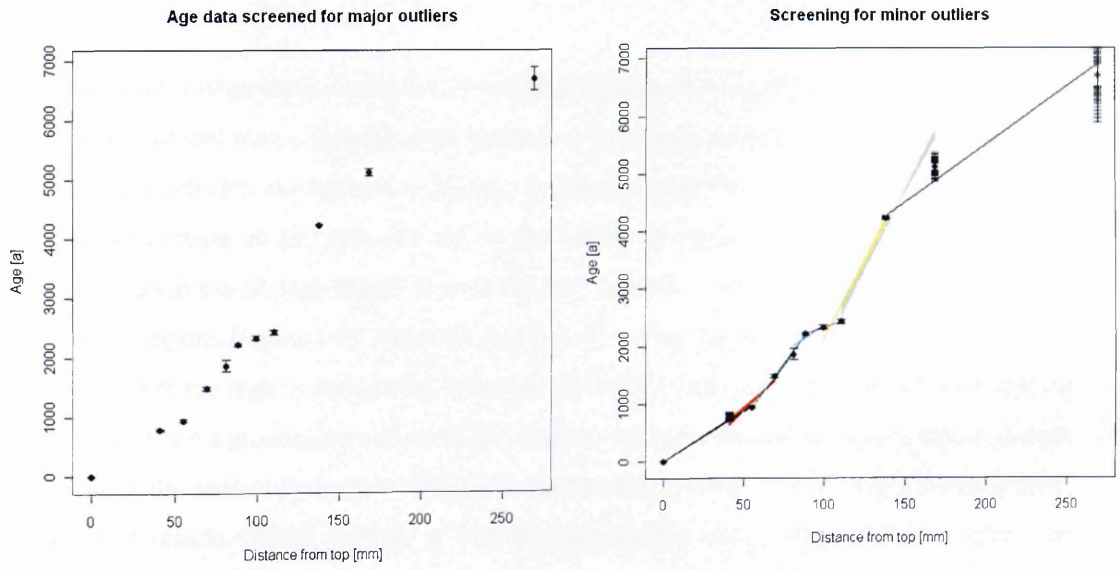

Figure 6.1: StalAge modelling to screen for outliers and age reversals from the raw U/Th data and associated errors.

3) The age model is then created with corresponding 95 % confidence age limits using a Monte-Carlo simulation which fits a series of straight lines through the data set (Figure 6.2a and 6.2b).

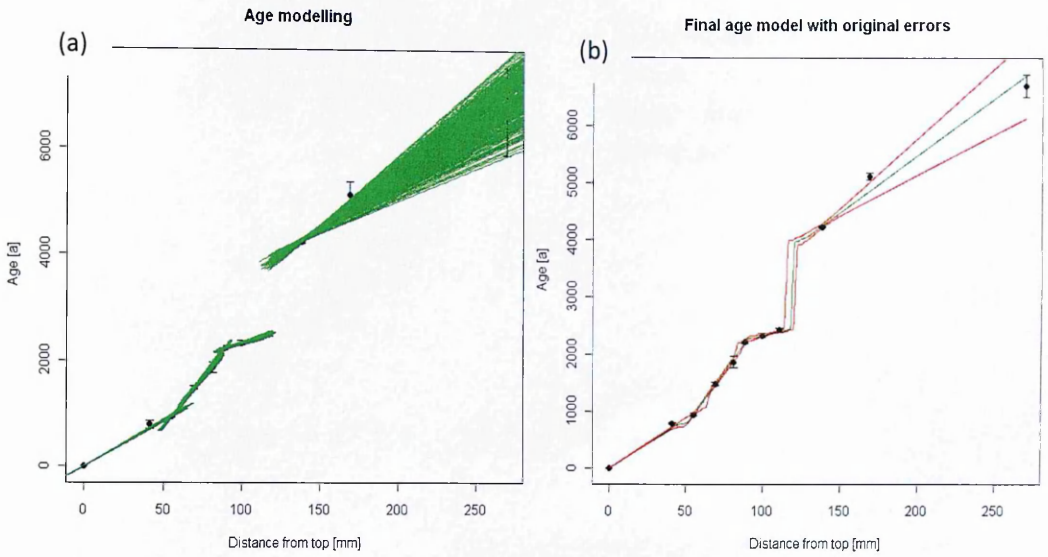

Figure 6.2a and 6.2b: StalAge modelling to create a speleothem chronology. The figures show both the use of a Monte-Carlo simulation to fit straight lines to the data set and also the final chronology (green line) with 95 % error limits (red lines).

Once final StalAge chronologies are developed these were manually appraised to assess how the age model may influence data presentation. During periods of constant growth the StalAge model fits the discrete U/Th data points and uses the errors associated with these points to create an accurate and logical age model. However, during periods of extremely slow growth the StalAge model often artificially extends rapid growth conditions into slow growth regions (Figure 6.3). Although this extension may be valid, without additional U/Th dating in these regions (which was often not possible) this growth rate extension cannot be tested. When a growth rate extension occurs, the StalAge model often causes data to bunch towards the second (youngest) U/Th date, giving an unrealistic spread of geochemical data. For this reason and as no new U/Th dating is possible during these periods, regions of extremely slow growth are modelled using a simple straight line fit, rather than the StalAge interpretation (Figure 6.3). This technique does not suggest the StalAge model is inaccurate or that a break in growth has occurred, but without validation we do not believe variable growth rates should be assumed between very temporally different U/Th dates, during extremely slow growth phases.

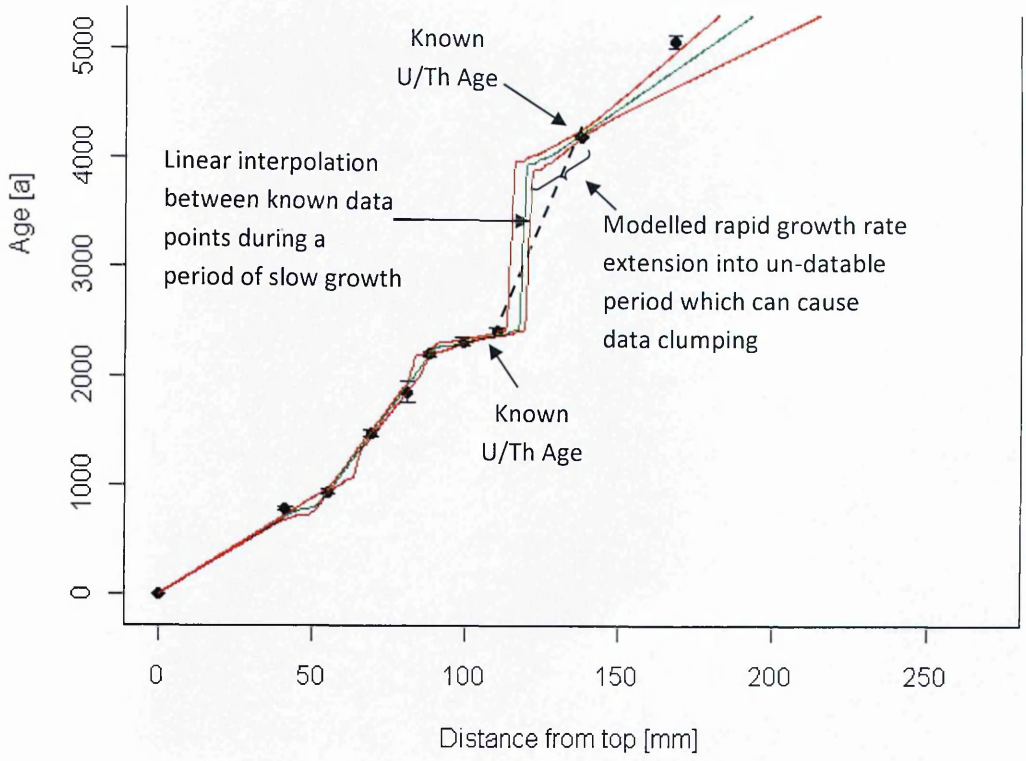

Figure 6.3: StalAge model output showing the known dates and errors (black dots) and the modelled chronology (green line) with 95 % confidence limits (red lines). A clear extension of growth rate occurs beyond the last known U/Th age before slow growth is modelled. The real extent and timing of any slowdown in growth cannot be known, so we use a straight line fit between the known U/Th ages during periods of slow growth.

The final growth chronologies for both speleothem are shown below (Figure 6.4). Speleothem ASR has grown slowly throughout the last 12,500 years with one major slowdown in growth ca. 5500 years BP. Speleothem ASM grows continuously through the last 7900 years encompassing the slow growth period in speleothem ASR, thereby providing not only an important replication of the youngest section of ASR but also helping to extend our high resolution oxygen isotope data set through 4000 – 7900 years BP. The dashed section in the ASM record is a linear interpolation of constant growth rather than a growth rate over extension indicated by the StalAge model. The combined oxygen isotope record from these two speleothems therefore offers a complete, Holocene duration reconstruction of regional climate and environmental change.

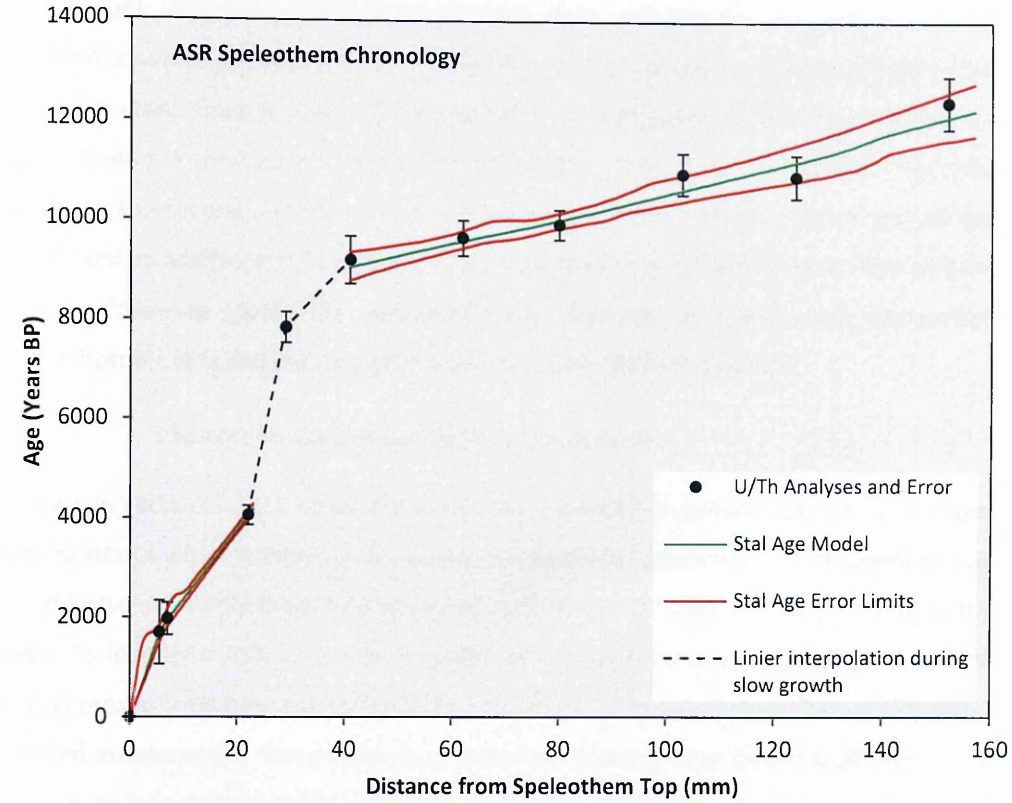

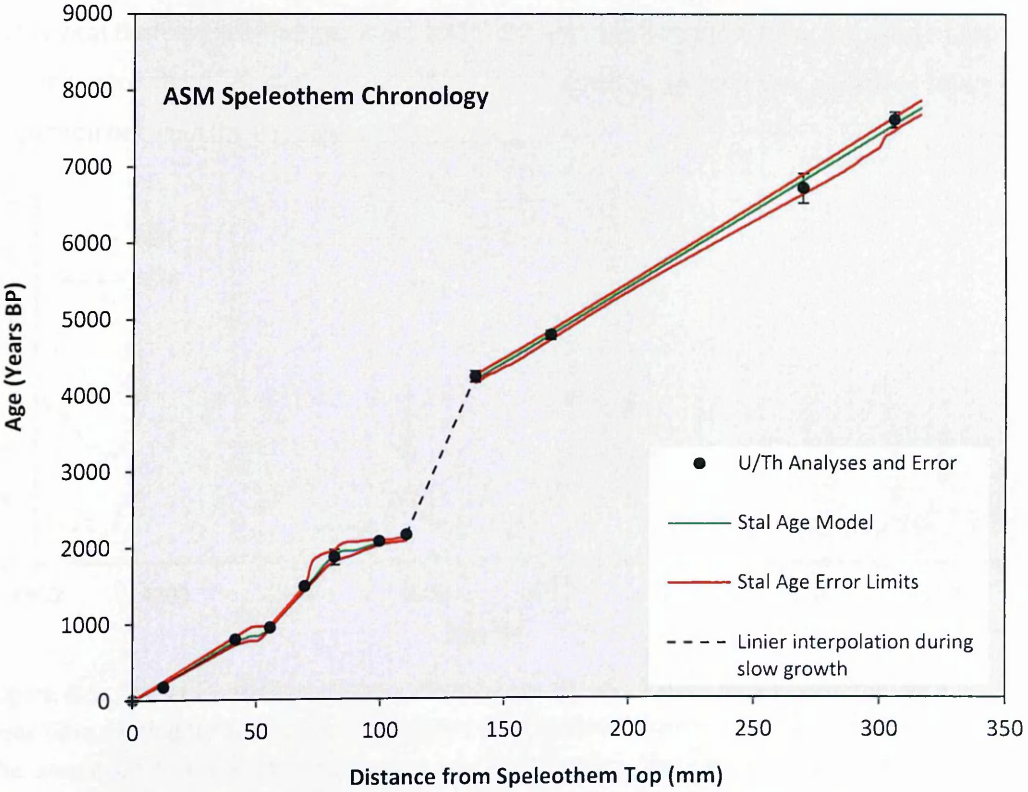

Figure 6.4: Speleothem growth chronologies using both StalAge and linier interpolation techniques.

High resolution U/Th dating of speleothems from Asiul cave enables two separate sets of speleothem chemical proxies to be considered based upon independent chronologies; each of which is made from at least 10 independent U/Th analyses. These chronologies are developed using a combination of the StalAge algorithm and linear interpolation between data points. This second technique was used only where a slowdown or break in growth has occurred and no additional U/Th dating was possible. These chronologies are used to present all of the following speleothem elemental data, allowing for direct cross comparison between isotopic data and the very high resolution trace element data sets.

6.2.1 Evidence for Continuous Speleothem Growth

As shown in section 3.1.2.1 speleothem ASR has a significant textural and colour change, which co-insides with extremely slow growth or a hiatus in speleothem development during the mid Holocene; speleothem ASM shows no such textural change and rapid mid Holocene growth. To identify if ASR accurately recorded any palaeoclimate signal during this period chemical proxies from both speleothems are compared, using the independent chronologies presented in Section 6.2. The proxies used include a series of trace elements (P, Mn, Y and Zn) which are transported to speleothem growth sites attached to colloidal particles during hydrological flush events (Borsato et al., 2007). For each speleothem a stack has been made from the normalised (Borsato et al., 2007) concentrations of elements to allow direct comparison between the two speleothems (Figure 6.5).

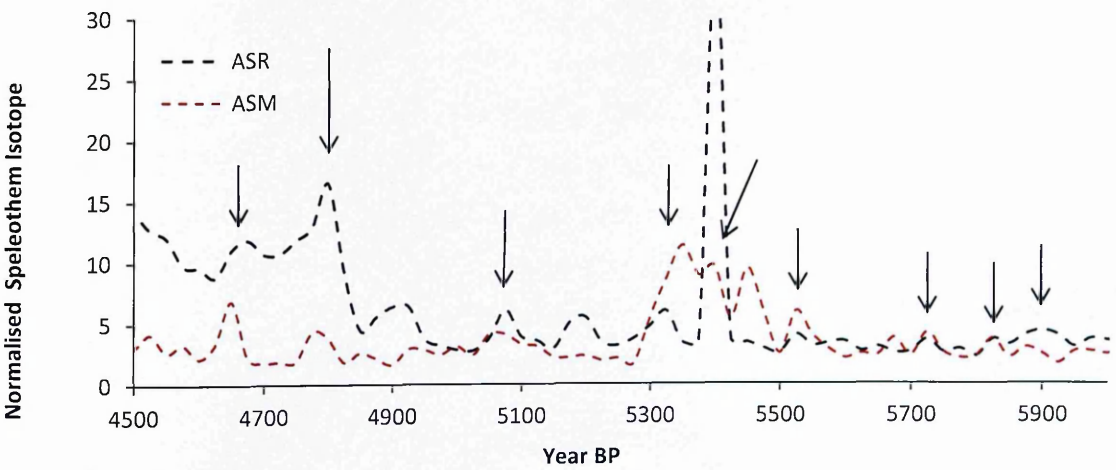

Figure 6.5: Stacked normalised trace element (Zn, P, Mn and Y) concentrations on a 25 year time spacing for speleothem ASR (black line) and ASM (red line). Whilst differences in the amplitude of trace element change can be observed, the timing of elemental peaks appears similar throughout the records (arrows), indicating that speleothem ASR was recording changes in trace elements sourced within the vegetation zone and transported via a hydrological mechanism into the cave in the same manner as ASM.

Figure 6.5 shows that even with a ±200 year error, the ASR speleothem chronology accurately replicates periods of maximum trace element incorporation from speleothem ASM, based on the ASM StalAge chronology with a lower ±60 year dating error. As P, Zn, Y and Mn are known to be hydrologically delivered to speleothem growth sites (Borsato et al., 2007) the similarity in the trace element stacks suggests that speleothem ASR grew, albeit very slowly during the mid Holocene and accurately replicated the record of the much faster growing ASM sample. ASR is therefore used as a source of palaeoclimate information for this period in the remainder of the thesis.

However, due to the slow growth rate of speleothem ASR, the lower resolution stable isotope records from this speleothem, lack the detail of those from ASM. There is also a possibility that $\delta^{18}O$ and $\delta^{13}C$ of ASR are more influenced by slow carbonate deposition rates and dry cave conditions than trace elements. The stable isotope records from ASR must therefore be treated with caution during the mid Holocene.

6.3 Oxygen Isotope Profiles

The two chronologies presented in Section 6.2 are used to develop the stable isotope profiles for speleothems ASR and ASM (Figure 6.6). Sample spacing was 100 μm for the 156 mm long ASR sample; whilst the ASM record which grew more rapidly was sampled at 300 μm for the first 195 mm and then at 500 μm resolution for the remaining 121.5 mm. The lowest resolution sections of either speleothem equate to one sample every 55 years and at highest resolution one sample every 2 years. When combined, the two oxygen isotope profiles comprise over 2150 oxygen isotope analyses.

Three distinct phases of oxygen isotope change can be observed in the speleothem records (Figure 6.6), being especially evident in ASR. Firstly, from the Younger Dryas (YD) to 8700 years BP; this phase is denoted by decreasing oxygen isotope values, with lowest values (-6.2 ‰) occurring at 8500 years BP. The second growth phase (7000 to 4800 BP) is denoted by a rapid and unprecedented transition to higher values (-4.3 ‰) and much slower growth rates in ASR. This period can be clearly identified in speleothem ASR by both a change in colour and crystal morphology. Under such slow growth, only a low resolution oxygen isotope record can be developed. Therefore, during this mid Holocene period, the faster growing speleothem ASM offers a higher resolution record of palaeorainfall change than speleothem ASR, as explained in Section 6.2.1. Whilst ASM also exhibits an increase in isotopic values during this second development stage, from an isotopic low around 6000 years BP, the mid Holocene oxygen isotope records from the two speleothems do not show a high level of replication. This is possibly due to the observed change in speleothem ASR's growth dynamics and crystal structure. The third growth phase shows ASR and ASM records continuing from 4800 BP until the ASR record ends at 250 years BP, periods of possible isotopic co-variation are highlighted in Figure 6.6 (black dashed lines). The very top of speleothem ASR is thought to have been damaged during collection, removing the top 250 years of carbonate deposition. This damage explains why this speleothem which is known to actively deposit calcite under modern conditions does not replicate the ASM record for the last 250 years.

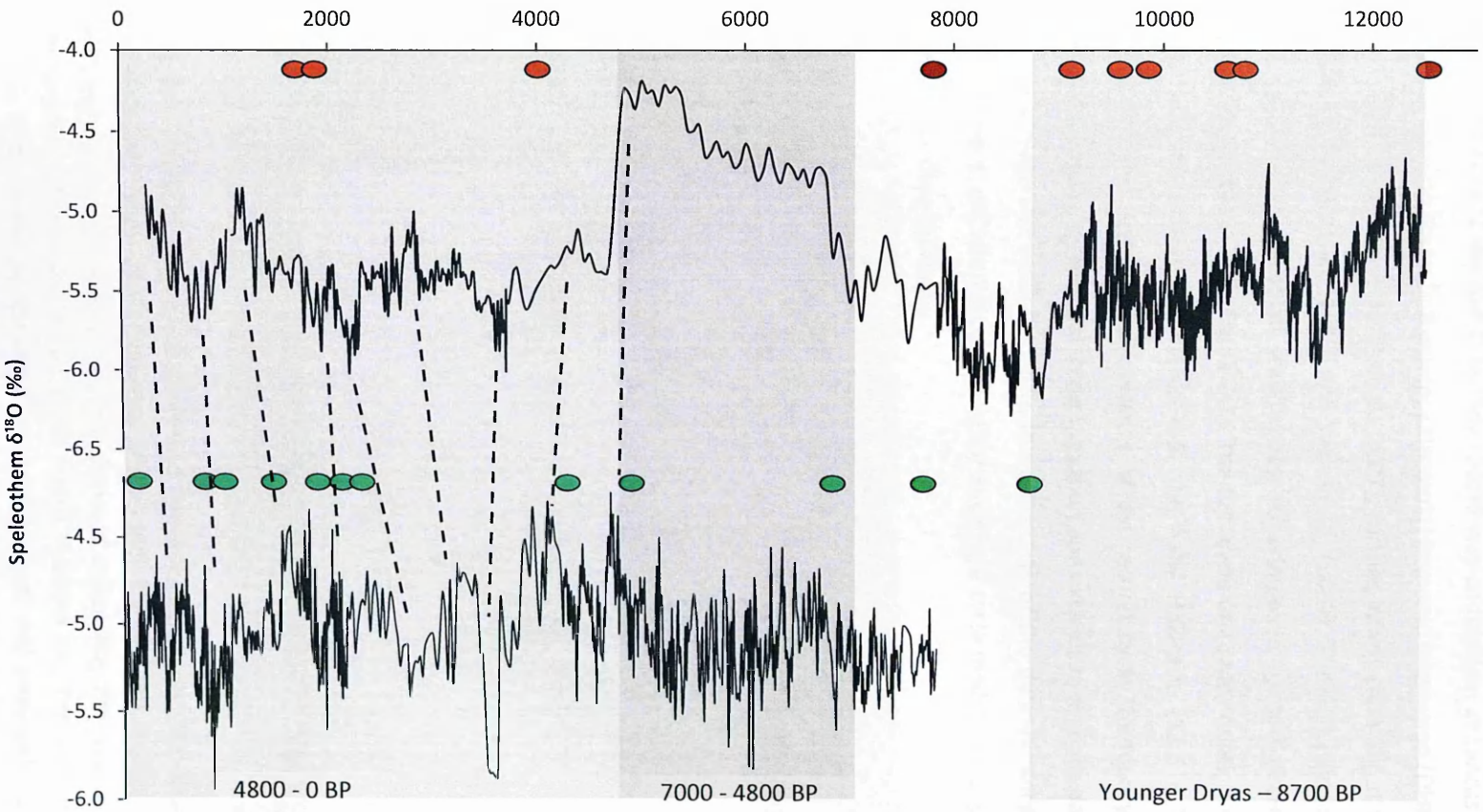

Figure 6.6: Speleothem ASR and speleothem ASM oxygen isotope profiles. The red circles represent the position of U/Th dates for speleothem ASR and the green circles those for speleothem ASM. Grey boxes indicate the three periods of isotopic change Younger Dryas to 8700 BP, 7000-4800 BP and 4800-0 BP, black dashed lines indicate how the two records may co-vary in the late Holocene.

6.3.1 Timeseries Analysis of Oxygen Isotope Records

Time series analysis of the ASR O isotope record was undertaken at Lancaster University by Dr. Wlodek Tych using a multi frequency Dynamic Harmonic Regression (DHR) model and the MATLAB Captains toolbox (Taylor et al., 2007); further information about this technique is presented by Young et al., (1999) and Tych et al., (2002). The ASR oxygen isotope record exhibits two distinct millennial scale cycles, superimposed upon a decreasing and then increasing trend component (Figure 6.7). The first cycle originates during the YD period and extends, with decreasing dominance into the early Holocene (12.5 – 10 ka), with an amplitude of 1350 years. The dominance of the second cycle (frequency of 1575 years) appears during the late - mid Holocene transition and extends to modern day (Figure 6.8). In combination these two models explain three quarters of the data variance over the active periods (YD, early and late Holocene); whilst any single cycle model only explains up to 50 % of the observed data variance.

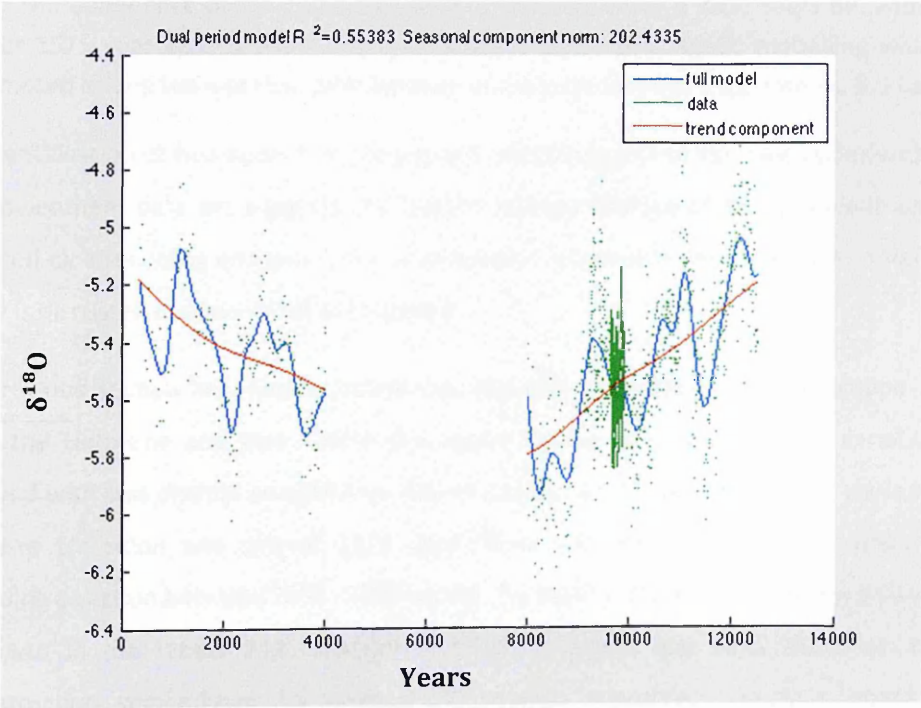

Figure 6.7: The ASR oxygen isotope record (green circles) alongside cycles which have been identified using a multi frequency DHR model. For ASR this model is comprised of two cycles which best describe this data shown as a blue line. The DHR model describes three quarters of the variance observed within the data set. The overarching trend of this data is described by the red line. Modelling was not attempted during the mid Holocene because of the large isotopic excursion ca. 5.5 ka which unbalanced the data set.

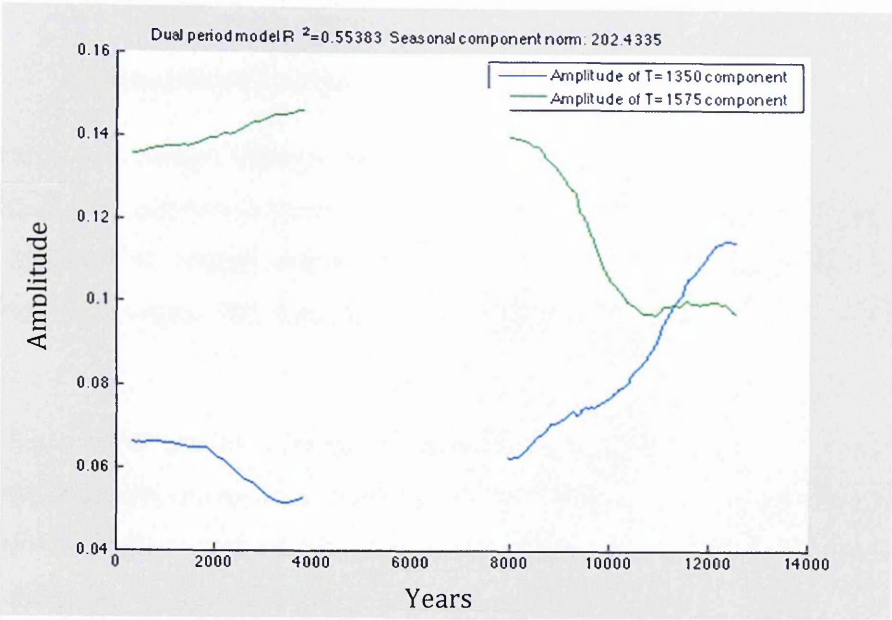

Figure 6.8: Amplitude vs. time plot of the ASR oxygen isotope record. The two part model which best describes the isotope data set is displayed as two distinct cyclical components one with a 1350 year frequency (blue line), the other with a 1575 year frequency (green line). The dominance of the 1350 year cycle is replaced around 9500 years BP, with the longer 1575 year cycle predominating until the modern day. Again, modelling was not attempted during the mid Holocene because of the large isotopic excursion ca. 5.5 ka.

The identification of two distinct, repeating and interacting millennial scale cycles within the ASR speleothem data set suggests the oxygen isotope profiles of these speleothems are governed by a recurring environmental phenomenon external to the cave environment; this theory is discussed in more detail in Chapter 7.

The previous section has demonstrated that the ASR speleothem oxygen isotope record spans the Holocene and that within this record cycles of oxygen isotope variation are observed with two distinct periodicities, one of 1350 years during the YD time period – late Holocene transition and one of 1575 years from the early Holocene to modern day (excluding a section between 7800 - 4000 years). During the mid Holocene when a slowdown in growth in the longer ASR speleothem record prevents any high resolution climate reconstruction, speleothem ASM offers a more rapidly depositing, complete record which can be used to interpret this period. What may have caused such a difference in speleothem deposition rates between ASR and ASM during the mid Holocene is unknown. However, this period is characterised by higher speleothem $\delta^{18}O$, which indicates significant aridity as seen elsewhere in northern Spain (Stoll et al., 2013), it is therefore possible that high levels of karst drying caused the re-routing of aquifer water away from speleothem ASR, causing a reduction in drip rates and extremely slow speleothem deposition during this period.

6.4 Carbon Isotope Profiles

Speleothem carbon isotopic analysis was undertaken in conjunction with the analysis of oxygen isotopes, therefore the sampling resolution and frequency of carbon isotopes are the same as described for oxygen isotope profiles. Figure 6.9 presents the carbon isotope profiles from speleothems ASR and ASM and highlights the different periods discussed below.

These carbon isotope profiles overlap throughout the last 7900 years and whilst they demonstrate little high resolution co-variance, similar trends can be distinguished. During the earliest part of the record only displayed in ASR (12.5 – 8.0 ka), carbon isotopes show gradually decreasing values until a low at approximately 8 ka. Although some fluctuation is observed in the early Holocene, values remain relatively stable only varying from the observed trend by ±0.5 ‰. The mid Holocene is characterised (as with the oxygen isotopes) by a return to much higher isotopic values in both speleothem samples. From 5.8 to 4.4 ka carbon isotope values within ASR increase by 3.3 ‰ and in ASM by 2.5 ‰. This transition to higher values co-insides with the dark band in ASR. A rapid and dramatic return to lower isotopic values is recorded in ASR at the end of this growth period where isotopic values fall by 3.9 ‰ in ASR. This fall in isotopic values appears to be replicated in ASM where values fall from -7.65 to -10.48 ‰ during this period. The late Holocene in both samples is characterised by a gradual transition towards high isotopic values, with significant, but not co-varying carbon isotope fluctuations observed in both samples.

Carbon isotope records from Asiul cave speleothems indicate similar isotopic trends without replicating high resolution changes in isotopic values. The only period of obvious consistency in the high resolution records occurs at ca. 4700 BP, where both records indicate a rapid fall in isotopic values. In ASR this phase is associated with an abrupt end to the dark coloured calcite which is characterised by low growth rates and distinct crystal fabrics. No such dramatic reduction in growth rate or textural change is observed in ASM. Co-variation of carbon isotope trends at the end of the dark band in ASR indicates that although obvious physical growth changes can be observed within this speleothem, the ASR record appears to accurately record changes in the chemistry of incoming drip waters, allowing for a replication of the ASM record.

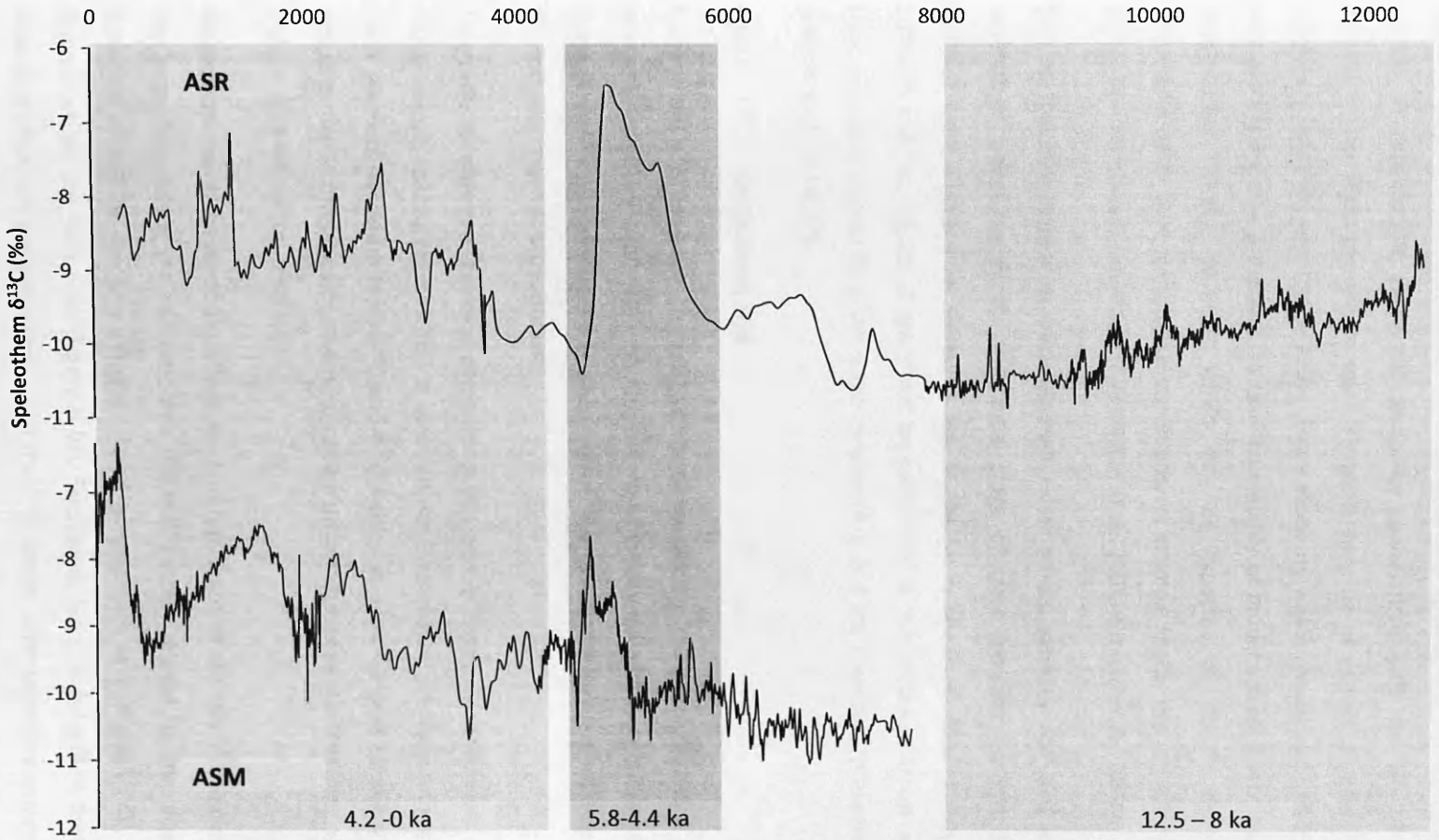

Figure 6.9: Speleothem ASR and ASM carbon isotope profiles. Grey shading indicates the three different periods of growth identified within the text Section 6.4, 12.5 -8 ka, 5.8 -4.4 ka and the late Holocene 4.2 -0 ka.

6.5 Trace Element Profiles

Relationships between trace element species from each speleothem are assessed to identify periods of considerable elemental change or co-variation; with the aim of highlighting periods of the Holocene where trace elements may be of use as palaeoenvironmental indicators (Fairchild and Treble 2009). Trace elements which are strongly coupled in Asiul cave waters are also presented, to test the stability of modern karst water trace element relationships. Finally, elements which may be expected to co-vary during variable environmental or karst hydrological conditions, for example Mg/Sr and $\delta^{13}C$ are compared to assess periods of karst water deficit (McMillan et al., 2005, Borsato et al., 2007).

Due to the complexities of trace element relationships, samples ASR and ASM will be considered independently for this initial stage of trace element analysis. Speleothem samples were analysed for elements Mg, Sr, Ba, U, P, Zn, Al, V, Mn, Fe, Co, Y and Ce; although only Sr, Mg, Ba, U and P will be considered in this section. Carbon isotopes and trace elements appear to show some co-variation, and are therefore presented together (Figures 6.10 and 6.12).

6.5.1 Speleothem ASR

Speleothem ASR has trace element data between 8000 - 250 years BP and a $\delta^{13}C$ record which spans 12500 - 250 years BP. Obvious co-variations exist between different elements throughout this period. Figure 6.10 shows raw $\delta^{13}C$ and major trace element data sets during the last 8000 years of the Holocene.

To enable an effective statistical comparison between $\delta^{13}C$ and trace element data sets, a single sample spacing (chronology) is required. An Excel macro program is used to identify trace element concentrations, $\delta^{13}C$ and $\delta^{18}O$ values at a set 25 year sampling resolution, meaning direct correlation comparisons can be undertaken between the trace element and isotope data sets at this resolution.

Magnesium values appear to show high levels of replication of the ASR $\delta^{13}C$ record with peak concentrations during the mid Holocene (4800 BP) either related to the variable growth dynamics of ASR or due to a climate related process such as enhanced PCP, a result of dryness within the karst zone (Figure 6.10). Fluctuating Mg concentrations during the late Holocene often correspond to changes in the $\delta^{13}C$ record. Strontium concentrations appear variable but high (20-40 ppm) during the early – mid Holocene transition (8000 – 5500 BP), at which point a sharp reduction in average Sr concentration can be observed. From 5500 BP

to 250 BP Sr concentrations vary between 7 and 22 ppm indicating a significant reduction in Sr incorporation into speleothem carbonate in the latter part of the Holocene, occurring at the same time as the change in speleothem ASR texture and colour. The large reduction in Sr (and Ba and U) concentration ca. 800 BP is related to a reduction in Ca concentration in the sample. As all other element concentrations are calculated in relation to Ca this reduction becomes apparent in elements with relatively low initial concentrations (Figure 6.10).

Barium exhibits a very similar architecture as Sr during the late Holocene but has a relatively stable concentration between 1 and 6 ppm throughout the record, indicating that Ba incorporation was not influenced by any growth or climate based changes which occurred during the mid Holocene. Uranium concentrations remain low throughout the speleothem record with a district low during the mid Holocene (6000 – 4000 BP), low U levels during this period make the speleothem too difficult to date during this period, leading to problems identifying continuous mid Holocene growth using the StalAge chronology. Phosphorus concentrations are relatively stable for the early and late Holocene with major increases in P incorporation only occurring during the mid Holocene (Figure 6.10). The change in P during this period may indicate a change in the vegetation and climate system above the cave site, this is discussed in more detail in Section 7. Although these elements may hold important information about Holocene climate change when assessed in isolation (Treble et al., 2003), it is also important to assess the strength of inter element relationships, which can be used to produce more conclusive evidence of major changes to the climate or karst hydrological systems (McMillan et al., 2005).

To establish the strength of variable inter-element relationships on a temporal scale, a running correlation is performed between the 25 year spaced data sets. This moving correlation gives an r value (Pearson correlation) for the relationship between any two elements over a moving 400 year time slice. Figures 6.11a and b show the results of a running (Excel CORREL) Pearson correlation between data sets.

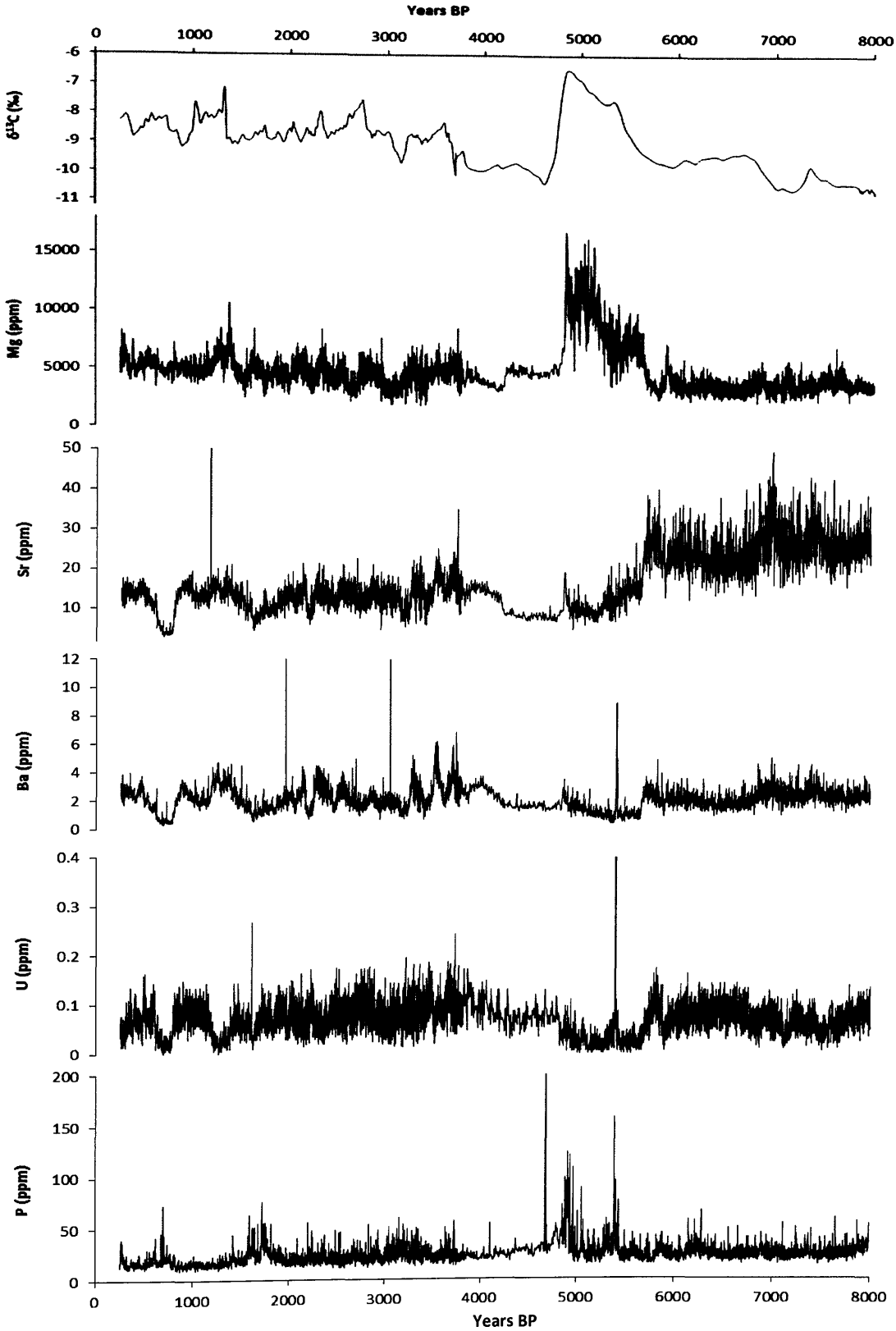

Figure 6.10: Speleothem ASR trace element and $\delta^{13}C$ data for the time period 0 – 8000 years BP.

Analysis in Chapter 4 identified relationships between $\delta^{13}C$ and Sr, Mg as well as Mn with Y in cave drip waters feeding speleothem ASR, often driven by changes in karst hydrology. By implication, it may be expected that these relationships should be transferred into the speleothem calcite (McMillan et al., 2005). Figure 6.11a therefore tests for periods of co-variation between these elements within speleothem carbonate; whilst Figure 6.11b compares additional trace element relationships observed within the speleothem but not in modern drip waters. Relationships within carbonate which are not observed within drip waters may be driven by speleothem growth dynamics (Treble et al., 2003) and the preferential uptake of specific elements into the crystal lattice. These 'growth' effects are considered in more detail in Chapter 7, when they offer evidence for climatic or environmental change.

Correlations displayed in Figure 6.11a demonstrate that elemental relationships which are observed to be annually stable in modern cave drip waters are actually variable when preserved within the speleothem record, on a Holocene timescale. Elemental relationships regularly change between statistically significant positive and negative r values (Pearson corrilation); meaning that whilst modern monitoring gives us a good understanding of the modern karst and cave hydrogeochemical system, this system is open to change over longer time periods. It must also be considered that elemental relationships observed in drip waters may not be directly transferred to speleothem carbonate, due to elemental partitioning co-efficients (Huang and Fairchild 2001), changes in speleothem growth rate, temperature variations (Roberts et al., 1998) and the incorporation of other elements (Fairchild and Treble 2009, Boch et al., 2011). Figure 6.11b displays additional trace element relationships which are observed exclusively in speleothem carbonate, giving a full picture of trace element dynamics in speleothem ASR.

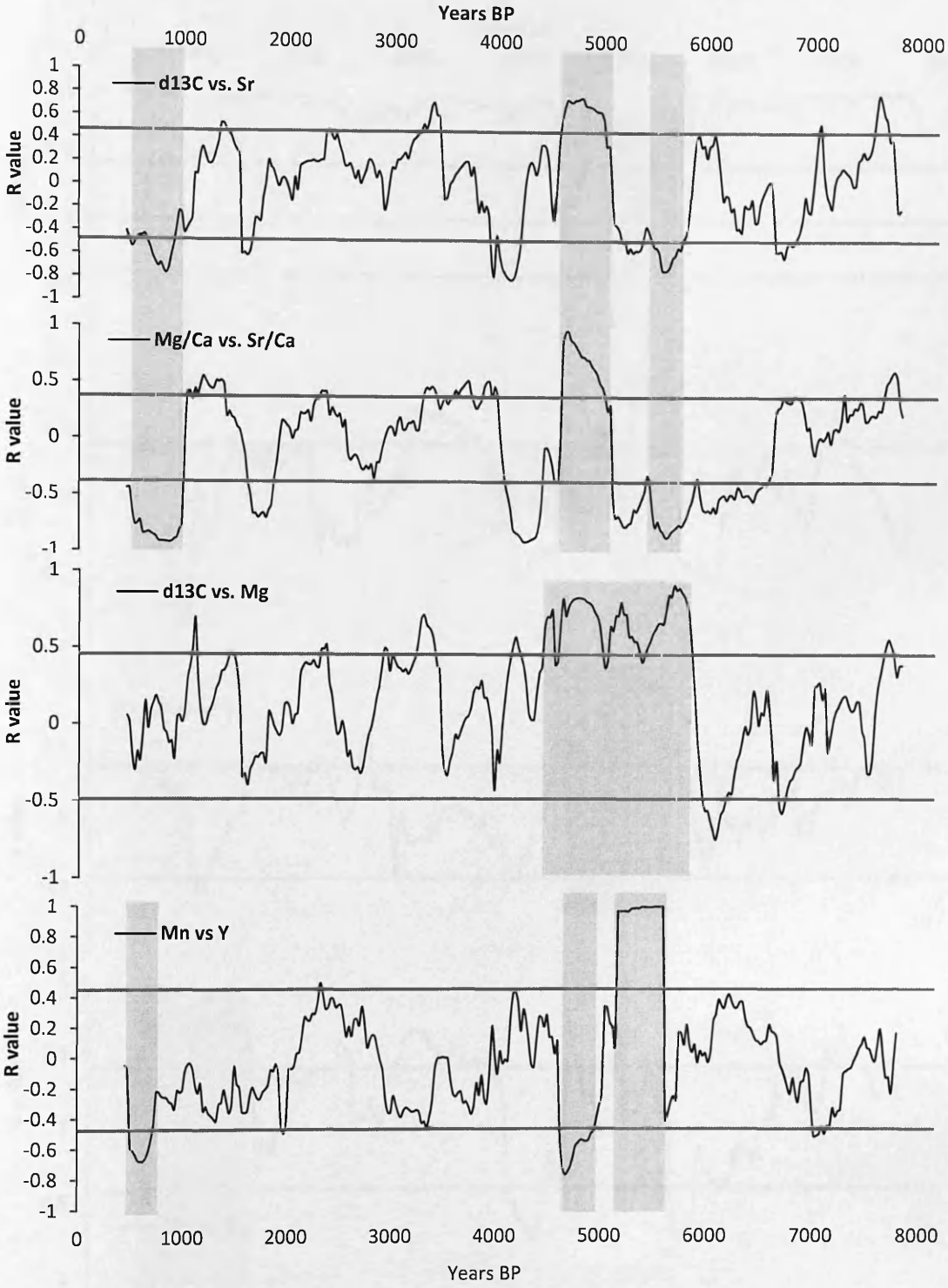

Figure 6.11a: Running elemental relationships observed in cave drip waters and tested for in speleothem ASR carbonate (Spearman correlation). Statistical significance levels are shown with blue lines representing a 95% confidence level; calculated using a spearman two tailed z table, where n-2 = 17 (95% confidence = r of 0.456 and 99% confidence = r of 0.528). Grey boxes indicate periods of the Holocene where several sets of elements are shown to statistically co-vary; possibly indicating significant changes to the karst hydrogeochemical system, driven by climatic change.

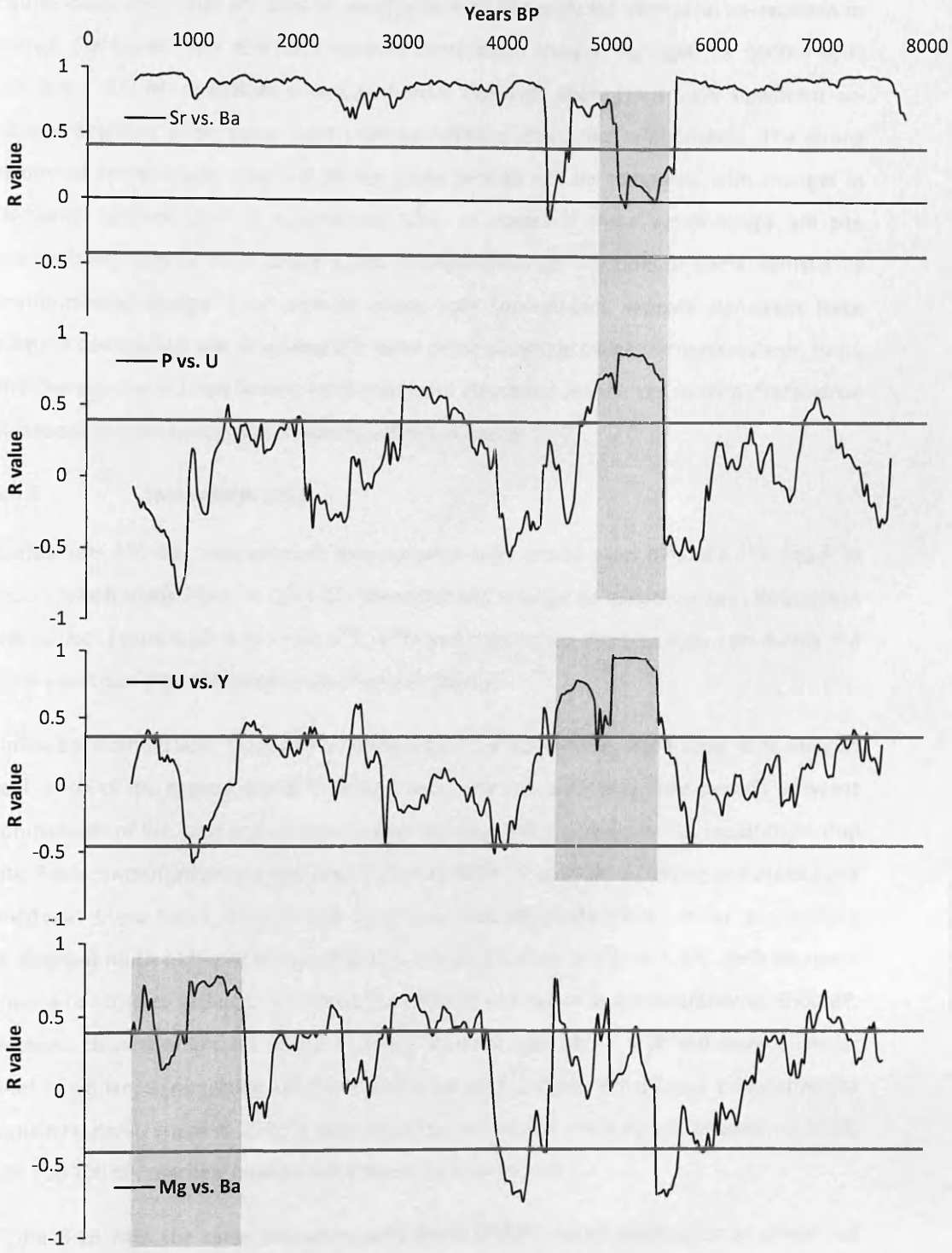

Figure 6.11b: Running elemental relationships observed in speleothem ASR carbonate. Statistical significance levels (spearman correlation) are the same as Figure 6.10a and displayed are by blue lines. Grey boxes indicate periods of the Holocene where several sets of elements are shown to statistically co-vary or in the case of Sr and Ba show no co-variation which is abnormal in comparison with the rest of the Holocene Sr/ Ba sequence.

Figures 6.10a and 6.10b are used to identify periods of significant elemental co-variation or change. For speleothem ASR trace element co-variation analysis highlights ca. 6000 – 4600 and 900 - 500 BP as periods where numerous elements show statistically significant co-variations and in some cases rapid changes between elemental relationships. The strong elemental co-variations observed during these periods will be compared with changes in elemental concentration in speleothem ASM, to assess if these relationships are site (speleothem) specific or a larger scale hydrogeochemical reaction to some climatic or environmental change. Time periods where both speleothems indicate significant trace element co-variation will be assessed in more detail alongside oxygen isotope records, to try and characterise possible forcing mechanisms for elemental change and to help characterise palaeoenvironmental changes in northern Spain (Chapter 7).

6.5.2 Speleothem ASM

Speleothem ASM has trace element data between 6600 and 50 years BP and a $\delta^{13}C$ and $\delta^{18}O$ record which spans 7900 - 0 years BP. Elemental and isotopic co-variations exist throughout this period. Figure 6.12 shows raw $\delta^{13}C$, $\delta^{18}O$ and major trace element data sets during the 6600 year trace element record from this speleothem.

Unlike speleothem ASR, Magnesium concentrations in speleothem ASM show little obvious replication of the speleothem $\delta^{13}C$ record, indicating that over long time periods different components of the karst and climate system influence these proxies at this speleothem drip site. Peak concentrations are recorded 5500 and 2000 BP possibly indicating enhanced karst aridity at these times. Barium and Strontium concentrations show similar architecture throughout much of the ASM record (this is assessed further in Figure 6.13). Both elements show a rise toward higher concentrations at 800 BP and spikes in concentration at 5500 BP. Uranium concentrations are similar to those found in speleothem ASR and show a similar level of variance, remaining relatively stable up to 0.2 ppm. Phosphorus concentrations remain relatively stable at 20 ppm apart from discrete spikes which occur frequently at 5500, 800 and 100 BP, reaching peak concentrations of over 140 ppm.

Figure 6.13 uses the same smoothing and Excel CORREL trend techniques as presented previously (section 6.5.1) to display the inter-element relationships and periods of significant co-variation for speleothem ASM. As less drip water data is available for speleothem ASM, Figure 6.13 only shows inter-element relationships observed within speleothem carbonate, which may be a function of drip water elemental relationships or speleothem growth dynamics (Fairchild and Treble 2009).

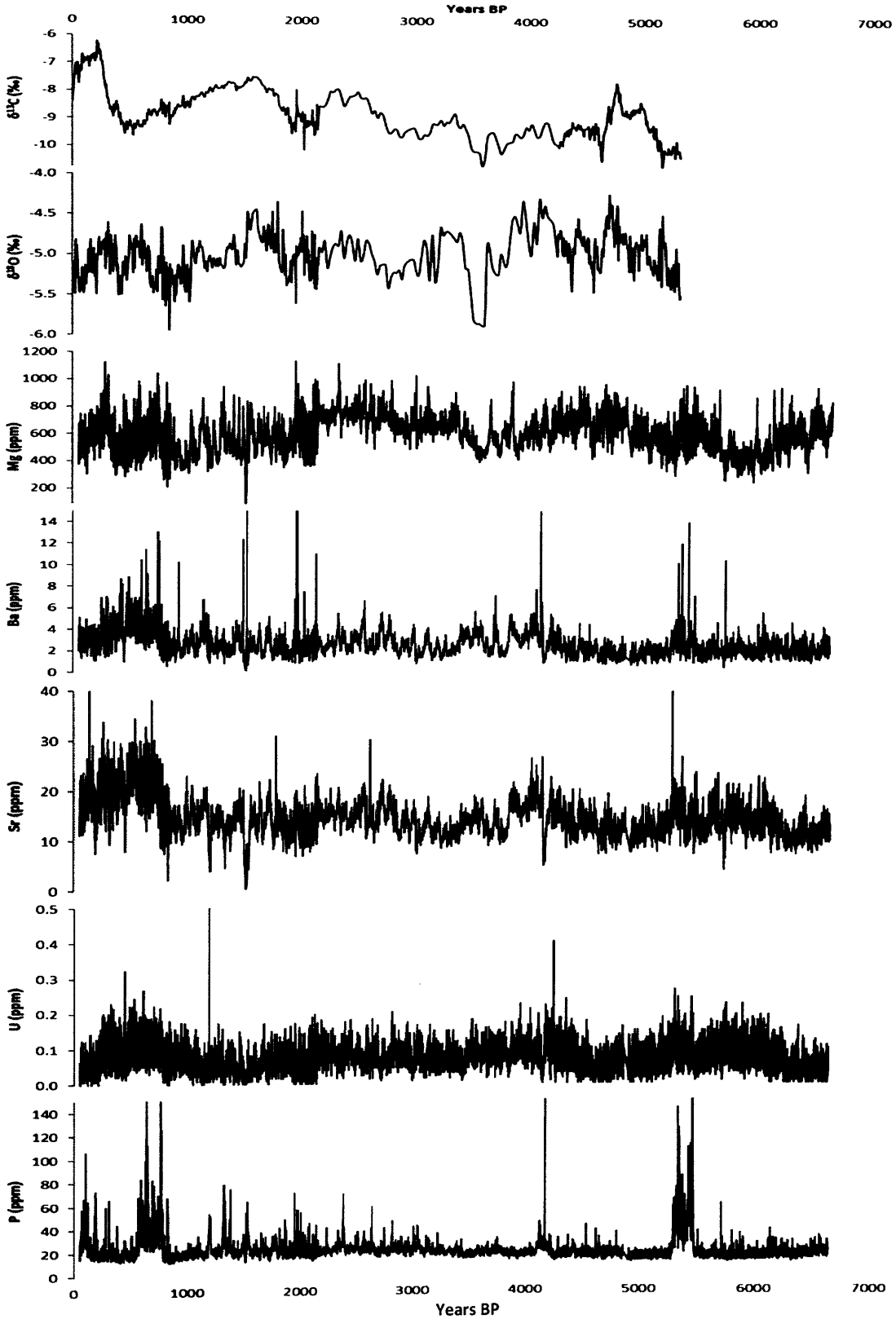

Figure 6.12: Oxygen and carbon isotope data alongside trace element data from speleothem ASM.

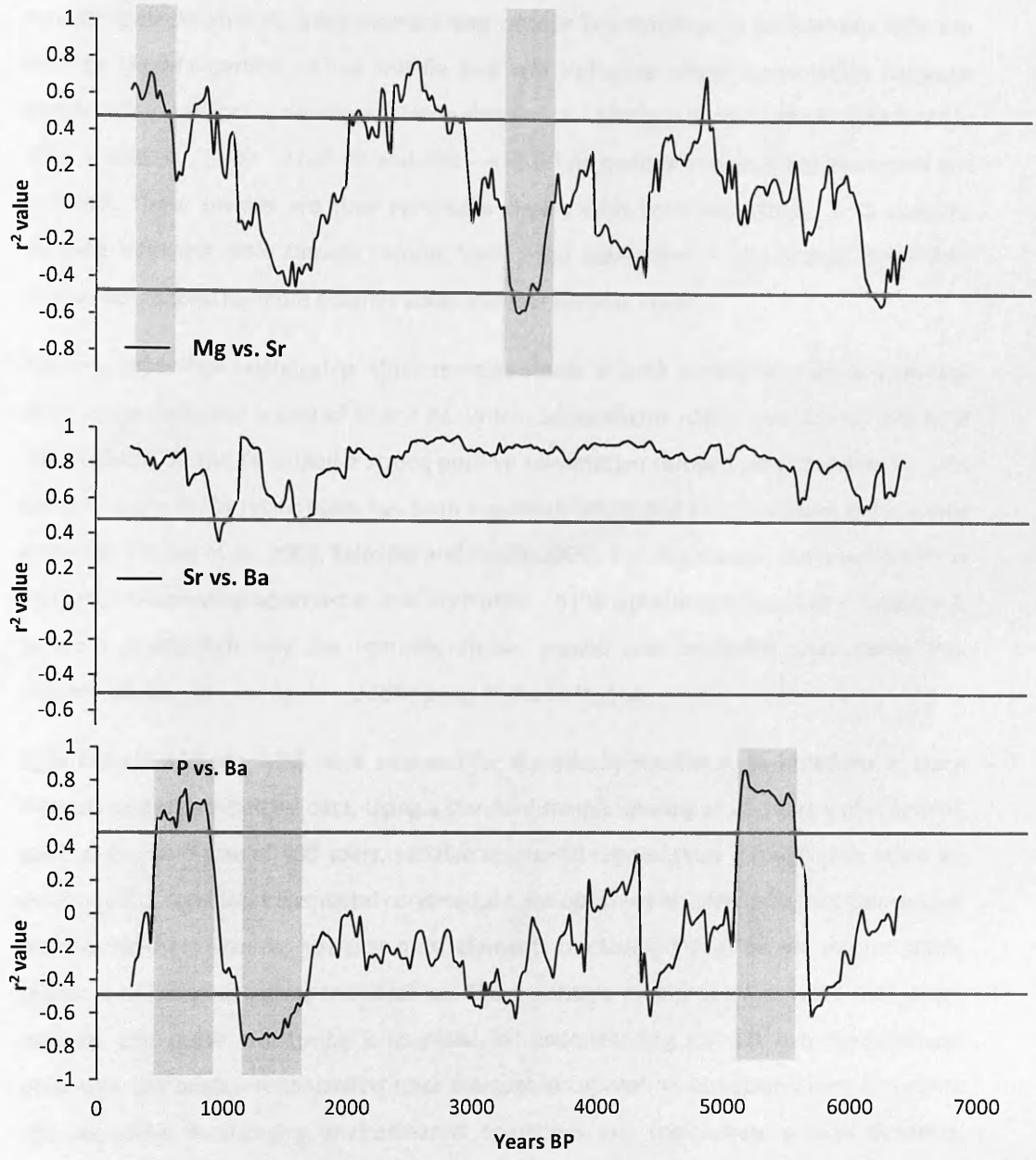

Figure 6.13: Elemental relationships observed in speleothem ASR carbonate. Statistical significance levels are shown with blue lines representing a 95% confidence level; calculated using a spearman two tailed z table, where n-2 = 15 (95% confidence = r of 0.48 and 99% confidence = r of 0.56). Grey boxes indicate periods of the Holocene where several sets of elements are shown to statistically co-vary.

As with speleothem ASR, trace element and isotope relationships in speleothem ASM are used to identify periods of the middle and late Holocene where co-variation between elements are statistically significant. Trace element co-variations in speleothem ASM identify 5500 – 5100 BP, 3500 - 3100 BP and 850 - 450 BP as periods of significant elemental co-variation. These periods are then compared closely with both speleothem $\delta^{18}O$ records; allowing Holocene scale climate records from these speleothem to be broken down into shorter time slices, for more detailed palaeoclimate reconstruction.

The only elemental relationship which remains stable in both speleothem deposits during most of the Holocene is that of Sr and Ba. Within speleothems ASR (Figure 6.11b) and ASM (Figure 6.13), Sr and Ba exhibit a strong positive co-variation throughout the Holocene. This stability in the Sr/Ba relationship has been previously attributed to speleothem growth rate dynamics (Treble et al., 2003, Fairchild and Treble 2009). For this reason, the break down in this Sr/Ba relationship observed in ASR from 6000 – 5100 will also be discussed in Chapter 7, to try and establish why this normally stable, growth rate indicating relationship may become de-coupled during this specific point of the Holocene.

Speleothems ASR and ASM were analysed for statistically significant co-variations in trace element and stable isotope data. Using a standard sample spacing of 25 years and a running analysis time window of 400 years, variable elemental relationships through time could be deconvolved. Significant elemental co-variations are observed at different times throughout both speleothem records; however most elements (excluding Sr/Ba) do not display stable (either positive or negative) relationships. These variable relationships indicate that whilst modern drip water monitoring is essential for understanding current hydrogeochemical processes, the processes controlling trace element incorporation into speleothem carbonate are susceptive to changing environmental conditions and speleothem growth dynamics (Fairchild and Treble 2009). Speleothem palaeoclimate proxies must therefore be interpreted based upon both known, modern controls over elemental or isotopic composition but also as part of a wider understanding of climatic evolution at any given time. To better understand the controls over any single chemical proxy the following section compares all the speleothem proxy data from Asiul cave for the Holocene, with the aim of characterising more generally when changes to the climate or karst system may have taken place. Section 7 develops this by considering other climate archives from northern Spain and southern Europe allowing for a re-interpretation of Asiul cave proxies where appropriate and in the light of previously published work on the controls over chemical proxies in speleothems.

6.6 A High Resolution Assessment of Climate Change during Five Discrete Periods of the Holocene

The following section presents in more detail periods of the Holocene where significant changes in oxygen and carbon isotope as well as trace element records have been identified, using the analytical techniques presented previously in this chapter. A closer assessment of these sections aims to characterise climatic and environmental changes which have shaped Northern Iberia through the Holocene.

The time periods presented in the following section are the Younger Dryas period (12.9 – 11.5 ka), the YD period to Early Holocene transition (11.5 – 8 ka), the Mid-Holocene (7.0 – 4.6 ka), the Medieval Climate Anomaly (1260 – 760 BP) and the Little Ice Age (510 – 250 BP). These periods are identified on the oxygen isotope records from Asiul (Figure 6.14).

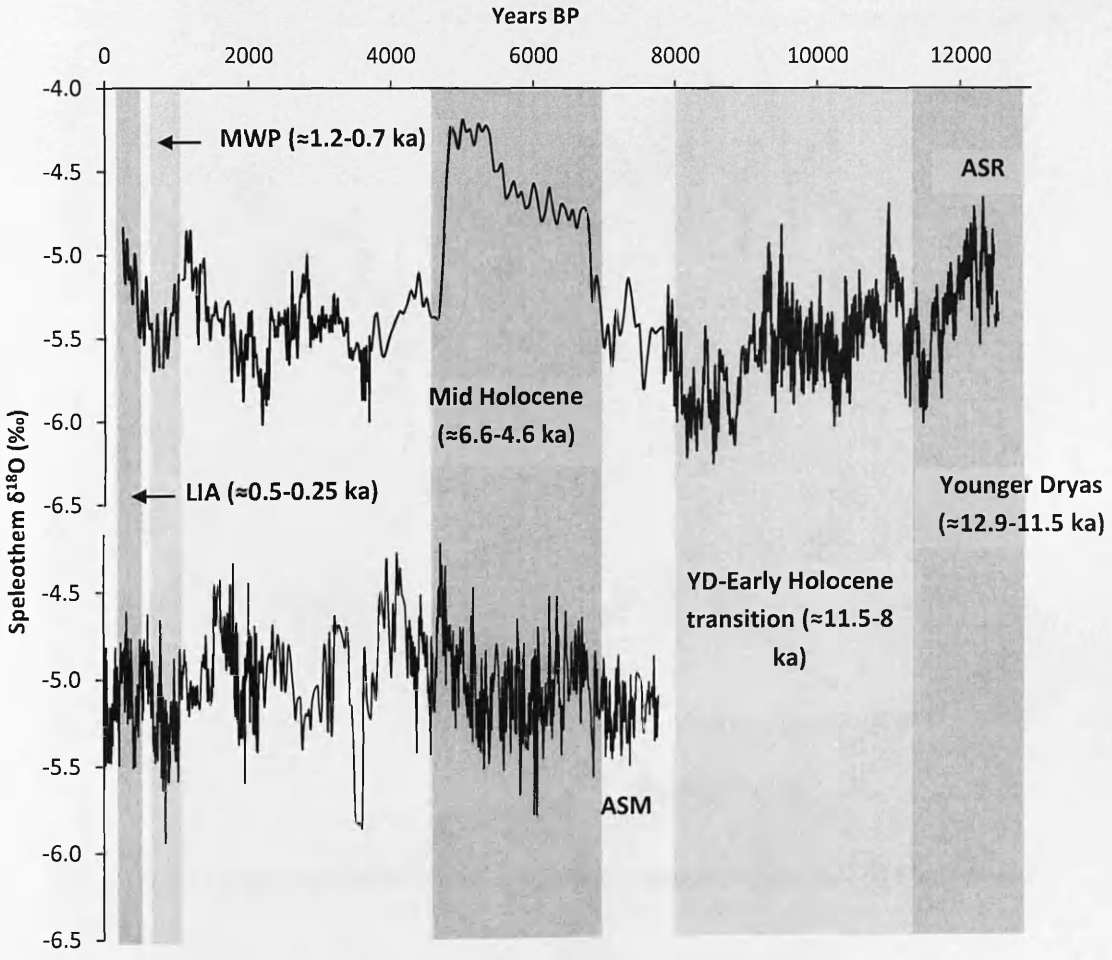

Figure 6.14: Asiul cave speleothem oxygen isotope profiles. Major Holocene events are shaded in grey, including the Younger Dryas (YD) The Medieval warm period (MWP) and the Little Ice Age (LIA).

6.6.1 The Younger Dryas (12.9 – 11.5 ka)

The Younger Dryas period is encapsulated in the oldest section of the ASR speleothem record. Although major climate and environmental changes are known to have occurred in northern Iberia during the YD, speleothem ASR grows continuously throughout this period (Figure 6.15). The oxygen isotope profile indicates a period of high isotopic values characterised by two peaks at 12.3 and 12.1 ka. After the final peak, isotopic values begin to decrease until 11.5 ka. A similar reduction in carbon isotope value is also observed during the YD with the highest isotopic values at 12.5 ka and the lowest values at 11.5 ka. No trace element data is available from either speleothem for this period of the Holocene so discussions in Chapter 7.2.1 focus on the stable isotope records from speleothem ASR only.

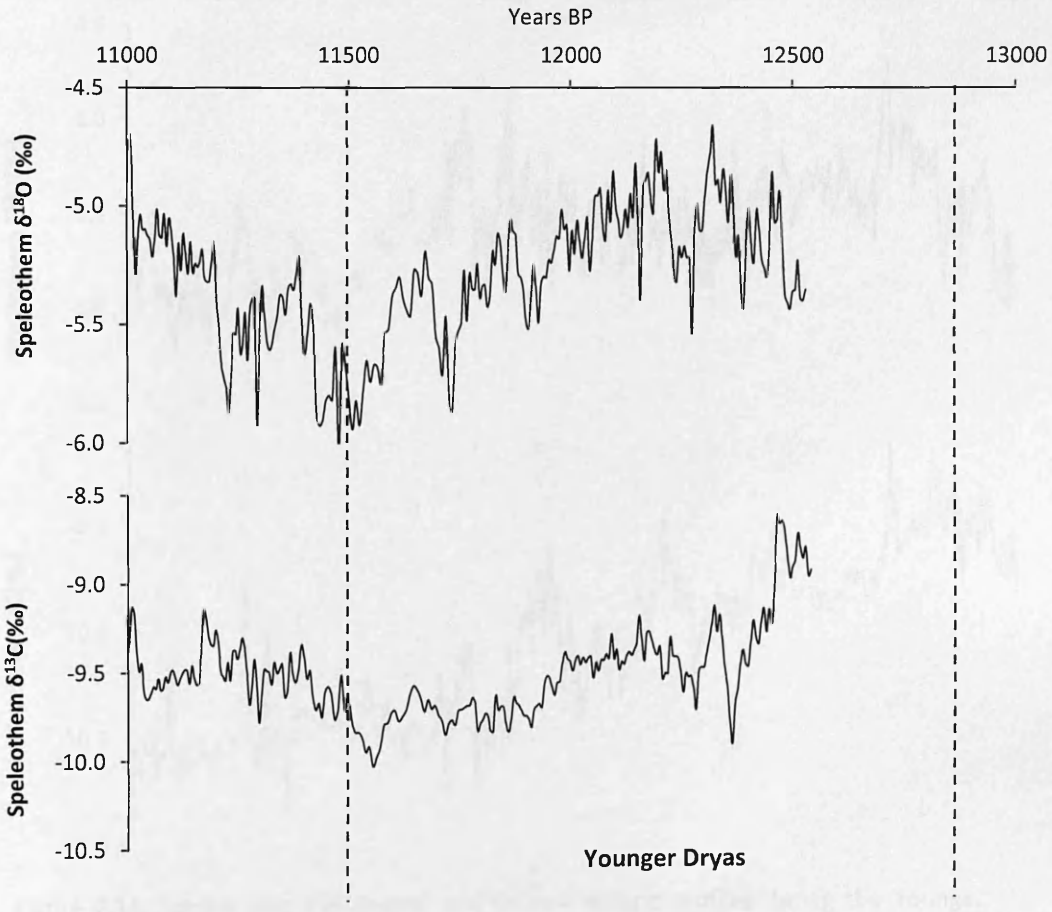

Figure 6.15: Speleothem ASR oxygen and carbon isotope profiles during the Younger Dryas.

6.6.2 YD to Early Holocene Transition (11.5 – 8.0 ka)

The Asiul speleothem record offers a regionally unique high resolution assessment of climatic and environmental change during the transition into the early Holocene (Chapter 7.2.2). This period is one of great global significance as it marks the end of our most recent glacial to interglacial transition. Asiul speleothem records during this period are limited to the ASR stable isotope records. Oxygen isotopes show periods of higher (11.0 and 9.5 ka) and lower (11.5, 10.25 and 8.5 ka) isotopic values, part of the distinctive isotopic cycling discussed previously (Figure 6.16). Carbon isotopic values however, exhibit a trend of gradually decreasing values throughout this period reaching minimum levels at 8.6 ka.

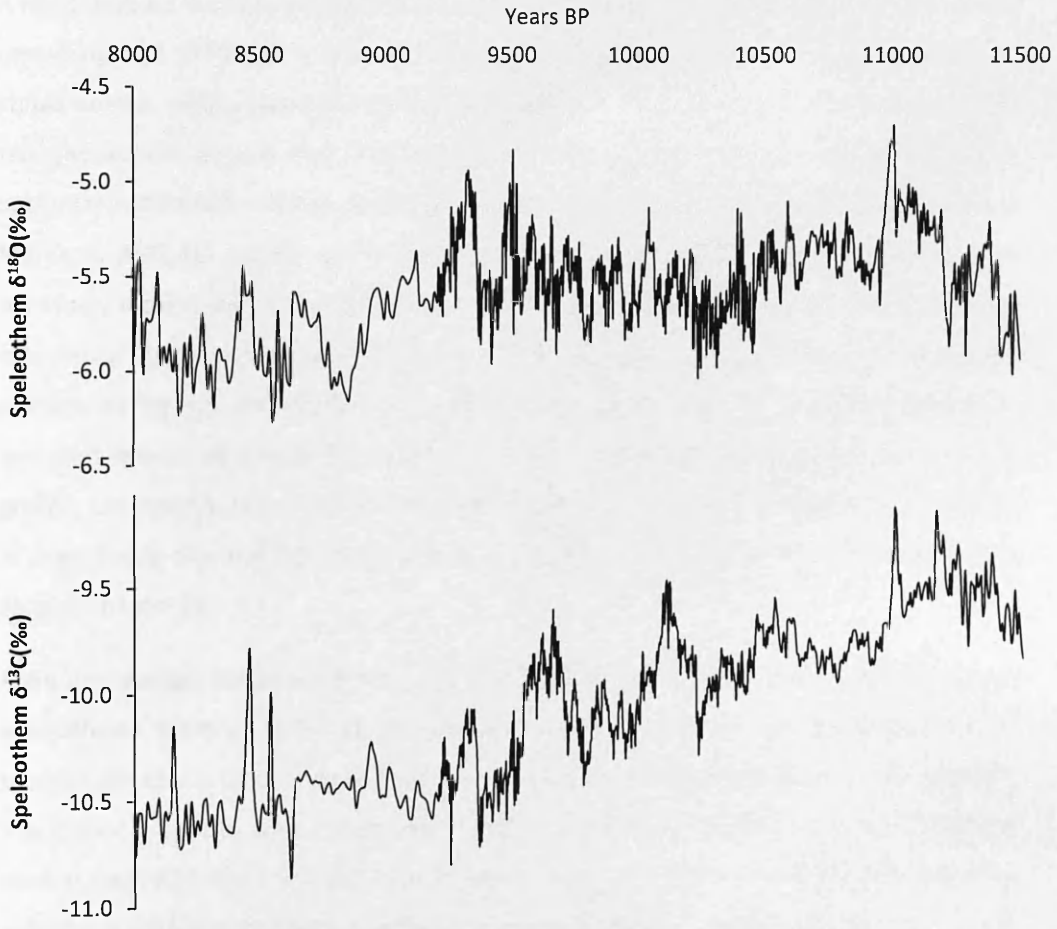

Figure 6.16: Speleothem ASR oxygen and carbon isotope profiles during the Younger Dryas to early Holocene transition.

6.6.3 Mid Holocene Aridity (7.0 – 4.8 ka)

The mid Holocene is one of the most interesting sections of the Asiul speleothem record, with significant changes identified in both speleothem trace element and stable isotope archives. During this period speleothem ASR exhibits extremely slow carbonate deposition rates and significant physical changes in the speleothem. Interpretations regarding environmental conditions at this time may not therefore be as reliable as the rest of the ASR oxygen isotope record, so other proxies and speleothems are considered. Trace element concentrations are presented alongside oxygen and carbon isotope records from both speleothems (Figure 6.17).

A rapid increase in stable isotopes can be observed in speleothem ASR from 7 ka with values remaining high ($\delta^{18}O$ max = -4.19 ‰, $\delta^{13}C$ max = -6.52 ‰) until 4.8 ka. These increases in stable isotope values, especially the carbon profile are mimicked by the Mg/Ca record from this speleothem deposit from 5.8 ka (Figure 6.17) and by O and C isotope records in speleothem ASM from ~5.5 ka. After 4.8 ka stable isotope values from both speleothem (and Mg/Ca in ASR) fall rapidly within only 200 years, reaching lower values by 4.6 ka. This extremely rapid reduction in isotopic and Mg/Ca values coincides with the end of the dark colouration in speleothem ASR. Whilst the ASR record is characterised by physiological changes during this period which may reflect a significant change in carbonate deposition dynamics, the strong isotopic co-variation between ASR and ASM (which shows no change in growth physiology) indicates that speleothem ASR still accurately incorporated elemental proxies during the mid Holocene; adding confidence to our wider interpretation of this record (Chapter 7).

Alongside changes in stable isotopes, is a significant phase of trace element change in both speleothems. From 5.5 to 5.3 ka in speleothem ASM and for a shorter period ca. 5.4 ka in speleothem ASR numerous trace elements concentrations rise, including U, P, Zn and Mn. This period coincides with a slight dip in Mg/Ca ratio and a plateau in O and C isotope records from ASR. Simultaneous trace element changes in both speleothem ASR and ASM indicates a change to the hydrogeochemical or environmental system operating throughout the cave site and once again indicates that speleothem ASR grew sufficiently during this period to accurately record changes in environmental proxies; regardless of speleothem growth dynamics.

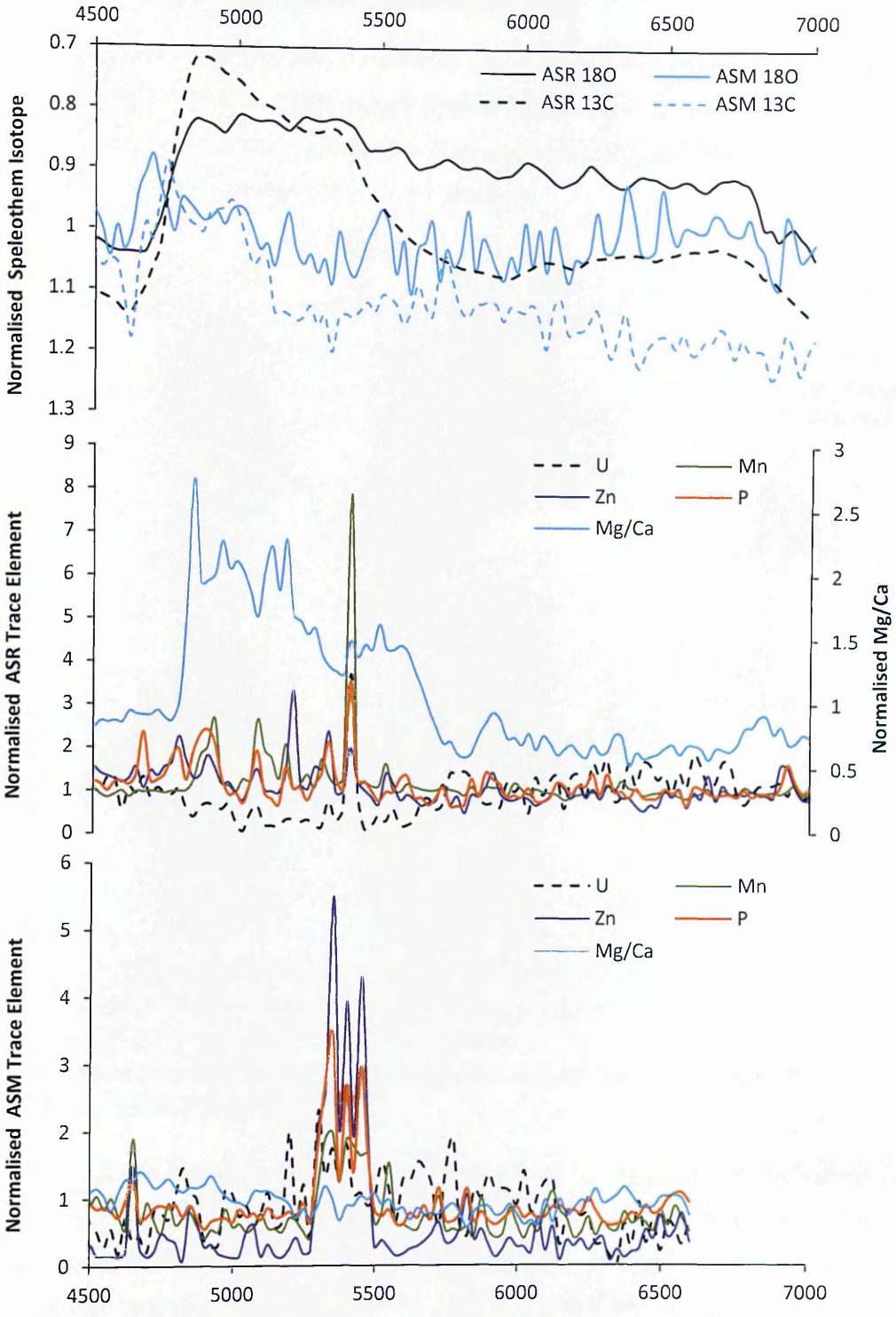

Figure 6.17: Normalised following the protocol of Borsato et al., (2007); $\delta^{18}O$, $\delta^{13}C$ (note reverse axis) and trace element data from speleothems ASR and ASM during the period 7.0 – 4.5 ka.

6.6.4 Medieval Climate Anomaly and Little Ice Age

The Medieval Climate Anomaly and the Little Ice Age are two of the most well documented climatic periods of the late Holocene and are shown to be of interest in the Asiul speleothem archives. Stable oxygen isotope records from Asiul speleothem are presented in Figure 6.18 and again alongside trace element records in Figure 6.19.

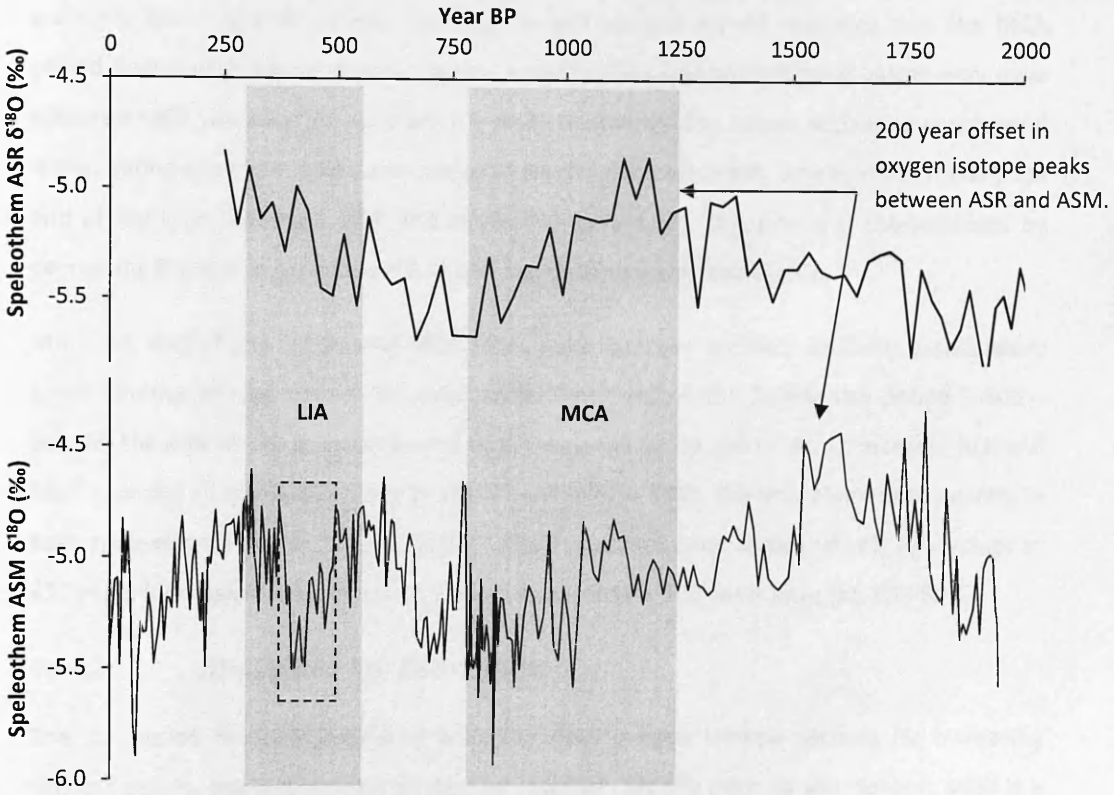

Figure 6.18: Stable oxygen isotope records from speleothems ASR and ASM during the last 2000 years of the Holocene. Grey boxes indicate the traditionally agreed timing of the MCA and LIA throughout Europe. The small dashed box indicates a period where isotopic values show a significant reduction, possibly reflecting the true timing of the LIA or Maunder Minimum in northern Iberia.

Whilst the MCA and LIA are known to be significant periods of climatic change throughout Europe, these periods are regularly characterised by a lack of temporal homogeneity across proxy archives and both phases are relatively short lived; occurring within only a few hundred years in many records. This lack of wide scale agreement as to the timing and consequence of the MCA and LIA coupled with a dating error of ±200 years for the ASR chronology and ±60 years for that of ASM means that palaeoclimate reconstruction of the MCA and LIA push the boundaries of what is possible using Asiul cave stable isotope archives, especially for inter-speleothem comparison. However, Figure 6.18 presents the

Asiul stable isotope archives and shows, using grey boxes an approximate timing and duration for the MCA and LIA.

6.6.4.1 Medieval Climate Anomaly (1250 - 760 BP)

Rather than recording a major climate event during the traditional MCA, speleothem $\delta^{18}O$ values in the ASM and ASR speleothem records define this as a transitional period, toward gradually lower isotopic values. The ASR oxygen isotope record indicates that the MCA period begins with higher isotopic values, where ASM suggests that peak values may have occurred ≈200 years earlier (Figure 6.18). Peak oxygen isotope values appear to correspond within dating error to a significant change in several trace elements, which occurs toward the end of the MCA, between 1400 and 1200 BP (Figure 6.19). This period is characterised by decreasing P and U in speleothem ASR and increases in Ba, Sr and Mg/Ca.

After the end of the traditional MCA Asiul trace element archives indicate a secondary environmental change before the onset of the LIA (Figure 6.19). During this period (~800 – 600 BP) the ASR record is characterised by decreases in Sr, Ba and U and an increase in P and Mg/Ca, whilst all elements appear to rise in speleothem ASM. The only element to co-vary in both speleothems during this period is P, which increases from comparatively low values at 825 years BP to peak concentrations in both speleothems 200 years later (ca. 650 BP).

6.6.4.2 The Little Ice Age (510 - 250 BP)

The LIA period is characterised in both the Asiul oxygen isotope records by increasing isotopic values, peaking approximately 250 years BP. Slightly prior to this isotopic peak is a marked, short lived (~150 yr) reduction observed only in the higher resolution ASM isotope curve, indicated by the dashed grey box in Figure 6.18. This rapid and significant reduction in oxygen isotope values and a concurrent but less convincing peak in U concentrations (Figure 6.19) may accurately reflect the timing and extent of the LIA or Maunder Minimum in northern Spain; reflected by a period of rapid isotopic reduction superimposed upon a gradually increasing isotopic curve. It is possible that the lower resolution, slower growing ASR record does not capture this marked return to lower isotopic values.

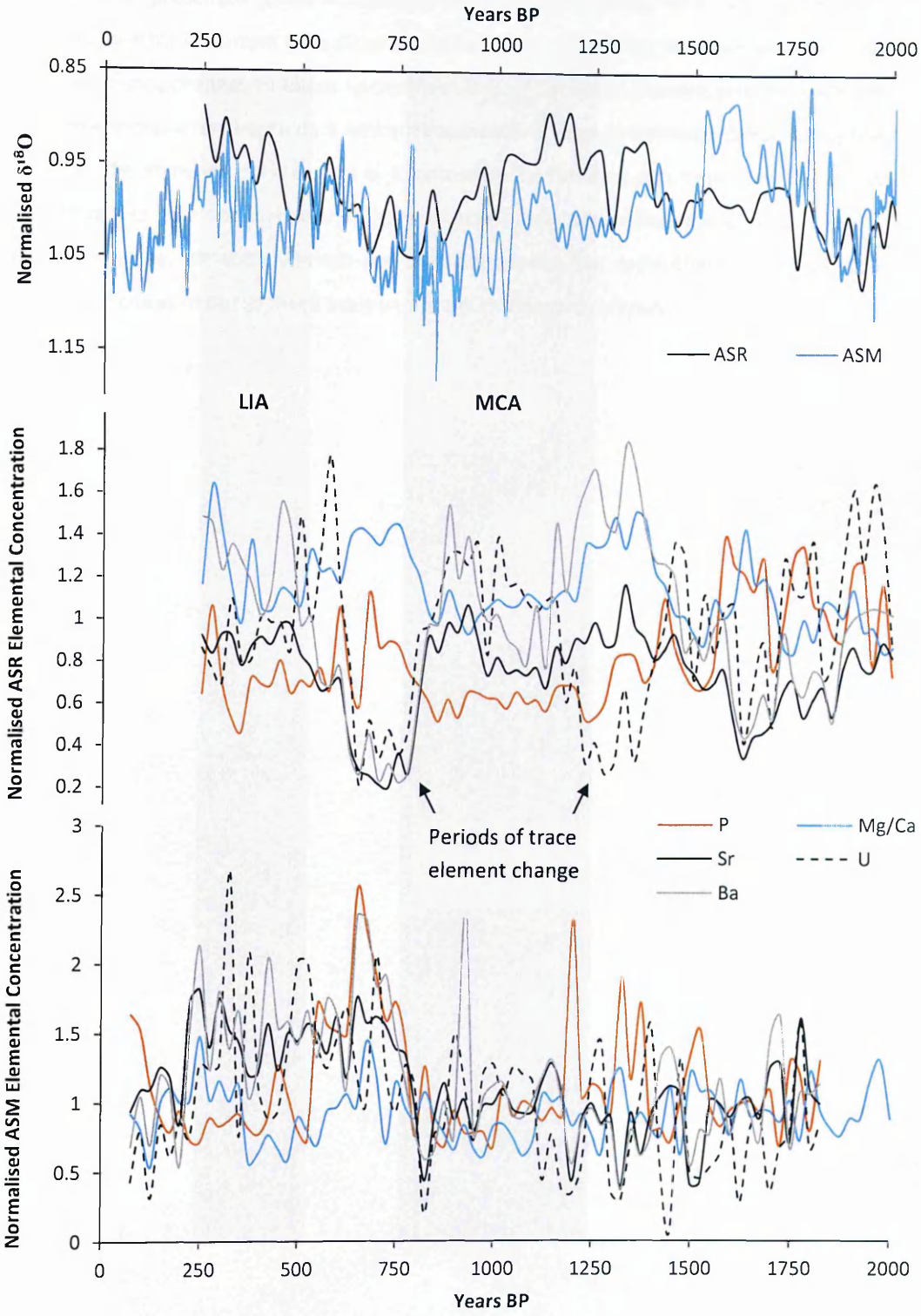

Figure 6.19: Normalised oxygen isotope (note reverse axis) and trace element data from speleothems ASR and ASM between 2000 and 0 years BP. The grey boxes indicate the traditional timing of the MCA and the LIA, whilst periods of significant change in the Asiul trace element archives are also identified.

Section 6.5 has presented stable isotope and trace element profiles from two speleothems from Asiul Cave for important time slices of the Holocene. These time intervals were selected due to significant changes to either speleothem isotopic or trace element profiles; with the aim of better characterising climate and environmental change in northern Iberia during the Holocene. The following chapter acts as a discussion for the data sets presented here; first considering the identified Holocene time intervals and comparing these to previously identified regional climatic variations and then considering the speleothem oxygen isotope records as archives of hemispheric scale variations in moisture delivery.

7. ASIUL CAVE SPELEOTHEMS: ARCHIVES OF LOCAL AND GLOBAL CLIMATE CHANGES THROUGHOUT THE HOLOCENE

7.1 Introduction

Asiul speleothem deposits have been shown (Chapter 6) to record high resolution changes in carbonate chemical composition, throughout the Holocene period. The observed changes in speleothem chemistry are a direct result of fluctuations within the climate, karst or cave systems and can therefore act as proxies for these systems. However, any palaeoclimate interpretation from these speleothem deposits requires a modern day understanding of carbonate chemical proxies. This introductory section briefly reviews our modern understanding of the Asiul cave system (Chapters 4 and 5) to enable the accurate interpretation of ancient speleothem chemistry.

7.1.1 Oxygen Isotopes

Cave and climate monitoring in Matienzo identifies a specific set of controls over the oxygen isotope composition of modern cave drip waters and therefore modern speleothem deposits. During 2011, 80 % of rainfall originated from the North Atlantic Ocean, clearly identifying this region as an almost unidirectional, seasonally invariant source of moisture for Matienzo. Changes in the oxygen isotopic composition of rainfall are shown instead to be driven by a strong regional "amount" effect. This effect is caused by intense rainfall events which originate from the upper atmosphere, where water vapour undergoes numerous cycles of condensation and evaporation (Dansgaard 1964). These processes cause the isotopic makeup of this water to fractionate, becoming increasingly negative in value with continued rainfall. During intense storms, water sourced in the upper atmosphere gives resultant rainfall a more negative isotopic signature (Dansgaard 1964, Lachniet 2009). Seasonal monitoring identifies winter rainfall as the dominant source of karst and cave water recharge, due to high evapotranspiration rates and lower rainfall volumes during the summer. Karst waters above Asiul Cave are therefore thought to accurately encapsulate a winter rainfall oxygen isotope signature, which varies dependent upon the amount of rainfall.

Flow routing within the karst system above Asiul has been shown to cause water mixing over an annual scale, meaning speleothem drip waters reflect a bulk winter isotopic signature for the preceding year; independent of the time of drip water collection. Carbonate deposition

appears to occur with a degree of disequilibrium that is constant with other cave sites, meaning speleothems from this cave site are thought to accurately reflect the oxygen isotope value of the drip waters from which they form. Speleothem oxygen isotope records from Asiul cave are therefore interpreted as showing variations in the precipitation amount effect (Figure 4.5) in water that penetrates into the karst system, manly comprised of winter rainfall (Figure 4.2), this rainfall is in turn driven by changes in the North Atlantic Ocean.

Under this regime, increases in speleothem $\delta^{18}O$ are associated with reductions in rainfall intensity and drier conditions, whilst lower $\delta^{18}O$ values indicate enhanced winter rainfall and wetter conditions.

7.1.2 Trace Elements

Modern drip water trace element data indicates two interesting processes occurring at the cave site. Firstly, the impact of calcite - water interaction, which causes strong co-variations between Mg/Ca and Sr/Ca (Sinclair 2011). Periods of water deficit are reflected as an increase in Sr and Mg in ratio to Ca. This intensification of Mg and Sr is expected during periods of reduced water flow where processes of calcite – water interaction cause the preferential uptake of Ca into precipitates, leaving Sr and Mg enriched in the drip waters collected in the cave environment (Fairchild et al., 2006b). Where drip water enrichments in Mg/Ca and Sr/Ca are preserved in speleothem deposits, these relationships can be used as a tracer for calcite – water interactions and karst dryness, throughout the Holocene (Sinclair et al., 2012). Secondly, more minor elements including Y and Mn are known to peak in Asiul cave drip waters during the summer season. Measured enrichments in these elements during periods of monthly water deficit indicate that at this site, occasional summer rainfall events must flow directly through into the cave; transporting Mn and Y to speleothem drip sites. Mn and Y have previously been identified as proxies of a productive soil zone and enhanced breakdown of soil organic matter during the summer (Baldini et al., 2012), and may therefore offer just such a proxy in Asiul speleothem archives.

7.1.3 Carbon Isotopes

Unlike the stable oxygen isotope records which are a direct proxy of external climate change, modern drip water carbon isotope data indicates a within karst driver for changes in the isotopic composition of waters reaching the speleothem drip site. Speleothem drip waters reflect a carbon isotopic value which has been modified from its source in the soil zone, where it is influenced by vegetation and soil respiration. Modern cave drip waters however,

appear depleted in ^{12}C from expected equilibrium partitioning values (Clarke and Fritz 1997). Cave drip waters enriched in ^{13}C indicate either, closed system karst dissolution (McDermott 2004), within karst PCP or lower cave air pCO_2 conditions which causes rapid CO_2 degassing. Although none of these processes could be definitively characterised as the cause of apparent ^{13}C enrichment in cave drip waters, trace element data indicates calcite – water interaction (possibly PCP) within the karst. PCP concentrates ^{13}C in solution and may therefore be the cause of high $\delta^{13}C$ values measured in Asiul drip waters. For this reason, speleothem $\delta^{13}C$ values are thought to reflect variable rates of PCP and therefore karst dryness, and only offer a secondary record of changes in vegetation makeup or productivity.

The following discussion of palaeoclimate and environmental change in northern Iberia focuses on discrete time intervals during the Holocene. These intervals are identified in Chapter 6 as periods of the Holocene within which significant variations in stable isotope or trace element records can be identified. The Asiul speleothem records are discussed in relation to other local and regional climate archives to build a high resolution picture of climatic variation and environmental evolution. The Asiul Cave records are shown to considerably add to our current knowledge of northern Iberian climate change through the Holocene.

In addition to understanding local changes during the Holocene, the Asiul speleothem oxygen isotope archives have the capacity to aid our interpretation of global climate systems and their forcing mechanisms. Close coupling of the ASR speleothem oxygen isotope archive and records of North Atlantic Ocean temperature (Bond et al., 1997, Bond et al., 2001) is identified and linked through an atmospheric mechanism. These speleothem records offer comprehensive evidence of Holocene scale linkages between global atmospheric and oceanic systems and add to a growing body of literature which aims to explain millennial scale shifts in the global climate system.

7.2 Holocene Palaeoenvironmental Reconstruction

This section considers stable isotope and trace element data from Asiul speleothems as proxies of climatic and environmental change throughout discrete time periods during the Holocene. This assessment of local climate change is important both to understand and interpret the wealth of archaeological archives which are found in the Cantabrian region of northern Spain (Straus 2011). Understanding regional environmental and climatic change may help to unravel when and why large cultural upheavals took place in this region.

Where possible, data sets from both speleothems (ASR and ASM) are considered for each time period. Cross speleothem analysis is undertaken for a number of reasons: firstly, to identify if changes to the isotopic and trace element systems are speleothem specific or homogenous throughout the karst; secondly to robustly characterise the hydrogeochemical system in the cave and karst at any given time period and thirdly, to interpret the environmental conditions which may have driven changes in the trace element and stable isotope systems. The time intervals which will be considered in the following sections are the Younger Dryas period (12.9 – 11.5 ka), the YD period to Early Holocene transition (11.5 – 8 ka), the Mid-Holocene (7.0 – 4.6 ka), the Medieval Climate Anomaly (1260 – 760 BP) and the Little Ice Age (510 – 250 BP).

7.2.1 The Younger Dryas Period (12.9 – 11.5 ka)

Throughout the Northern Hemisphere the YD event represents the most dramatic return to cold conditions experienced since deglaciation began, at the end of the last glacial maximum (LGM ≈ 21 ka) (McManus et al., 2004, Anderson et al., 2007). This period of rapid cooling is thought to have been driven by a massive influx of cold fresh water into the North Atlantic Ocean, which interrupted ocean and atmospheric circulation patterns (Alley 2000, Broecker et al., 2010). Many proxy records from Europe show reductions in rainfall, occurring simultaneously with decreases in temperature; a direct result of atmospheric restructuring (Anderson et al., 2007). In northern Spain, rainfall records are often contradictory (Carrión et al., 2010). Some records indicate significant cooling and drying (Moreno et al., 2010, Moreno et al., 2011a, Yanes et al., 2012), whilst others show the YD as a relatively cold but humid period (Straus 2011); what does remain clear from all records is that the YD was characterised by significant changes in vegetation type (Allen et al., 1996, Sobrino et al., 2005). Abrupt decreases in arboreal pollen percentages are observed as forest cover declined throughout northern Spain and a return to open shrubland communities was common (Garcia et al., 2002, Straus 2011).

Unlike many other regional records, speleothem ASR enables a high resolution appraisal of moisture delivery and karst aquifer conditions throughout the YD period (Figure 6.14). Oxygen isotopes show two episodes of peak dryness at 12.3 and 12.1 ka, reflecting serious regional aridity; the only section of the Asiul record which indicates higher levels of aridity is the mid Holocene. Oxygen isotope values during these periods are best considered as a representing a minimum level of dryness, as extreme cold conditions may have acted to drive oxygen values to more negative values, partially obscuring the amount effect. However, arid conditions rapidly subside and rainfall levels increase throughout the remainder of the YD period, with relatively high levels of winter rainfall by 11.5 ka. Carbon isotopic values demonstrate a sharp reduction in $\delta^{13}C$ values from 12.5 ka, reaching a peak low at approximately 11.5 ka (Figure 6.14). This decrease in carbon isotopic values indicates a reduction of calcite – water interaction within the karst overlying Asiul, suggestive of wetter karst conditions and a reduction in karst air space; correlating well with oxygen isotope records of enhanced moisture delivery toward the end of the YD period.

Asiul speleothem records therefore indicate that rather than being characterised as a single major event, the YD is best viewed as a transitional period; from initial dryness at the beginning of the speleothem record to relatively humid conditions by 11.5 ka. Increases in effective winter rainfall amount may have been driven by a gradual, southerly shift in the Atlantic Westerly Jet, which is believed to have occurred during the YD period; enhancing southern European rainfall delivery (Magny and Bégeot 2004).

Alongside climatic change, major cultural upheavals were occurring in the region around the timing of the YD period. The transition from Magdalenian to Azilian cultural complexes is thought to have occurred towards the end of the Allerød warm period (≈14 - 13 ka) (Straus and Morales 2012). This cultural change is characterised by a decline in lithic and osseous artefacts, thought to be linked to a reduced dependence on hunting game and the start of very simple cultivation activities (Barbaza 2011, Straus 2011). Climatic change during the YD appears to have had little impact upon these newly dominant Azilian cultures, and no evidence of a return to Magdalenian (cultural complex which dominated during the last glacial) belief systems is found in the region (Barbaza 2011, Bicho et al., 2011). Archaeological evidence therefore indicates that human populations were robust enough to endure the YD in northern Iberia; probably because the YD did not, at least in this region, represent a major reversal to glacial like conditions and therefore a significant problem for the continued development of human populations (Straus 2011, Bicho et al., 2011).

7.2.2 YD to Early Holocene Transition (11.5 – 8.0 ka)

One of the most important sections of the Holocene is the return to favourable (warm and wet) conditions after the YD (Moreno et al 2011a). In northern Spain, this period is marked by a return to dominance of pre YD vegetation species, including the increase of deciduous forests (Allen et al., 1996, Magny et al., 2002, Anton et al., 2006, Kaal et al., 2011). However, records of lake level rise from NE Spain offer contradictory evidence for the timing of increases in moisture delivery. Several lake cores indicate a rapid increase in moisture availability originating at the termination of the YD (Perez-Obiol and Julia 1994, Gonzalez-Samperiz et al., 2006, Davis and Stevenson 2007), whilst cores from Lake Estanya point towards a delayed atmospheric response, where lake levels remain low until 9.4 ka (Morellón et al., 2009). These inconsistencies can be attributed to differences in local basin dynamics and the influence of summer temperatures (Morellón et al., 2009). The low resolution and often inconsistent records of moisture availability from lake cores means that the production of high resolution, reliable proxy records is fundamental for understanding centennial and even millennial scale changes to moisture delivery during this period. For this reason cave speleothem archives are becoming ever more popular, especially from northern Spain where these archives are numerous.

Speleothem growth rate records from across northern Spain have identified this period (9 - 6 ka), as the Holocene's speleothem growth optimum (Stoll et al., 2013). Increases in speleothem growth rate indicate climatic amelioration, associated in this case with an increase in moisture delivery. Rainfall increases were at times so severe that cave archives from Cueva Major are interrupted during this period due to extreme flood events within the cave (Martinez-Pillado et al., 2014). Although the early Holocene is identified as a period of enhanced humidity by these speleothem records, only a limited understanding as to the exact timing and relative scale of this change can be drawn from records of speleothem growth rate.

Where other regional records are at times patchy or inconsistent (Perez-Obiol and Julia 1994, Gonzalez-Samperiz et al., 2006, Morellón et al., 2009, Stoll et al., 2013), the Asiul cave record offers a high resolution archive of winter moisture delivery to northern Spain during the entire YD to early Holocene transition (Figure 6.15).

The Asiul speleothem record indicates a return to higher oxygen and carbon isotope values after the end of the YD (11 ka), indicating a significant reduction in moisture availability; possibly linked to the delayed onset (ca. 9.4 ka) of humid conditions identified by Morellón

et al., (2009) in Lake Estanya. The high resolution Asiul speleothem sequence indicates that drier early Holocene conditions occur as two discrete events, the first at 11 and the second 9.5 ka (also seen by Jalut et al., 2000) split by a return to wet conditions at 10.25 ka. These reductions in moisture delivery represent part of the millennial cycle of moisture availability preserved within this record and it is possible that other regional records lack the resolution to accurately portray drying as two discrete events.

These two periods of drying observed in the Asiul speleothem are not always recorded in other regional archives of moisture availability; most of which indicate increases in rainfall in the early Holocene (Gonzalez-Samperiz et al., 2008, Perez-Obiol et al., 2010, Höbig et al., 2012). Whilst drying events are observed in the high resolution Asiul record, the overall trend for this period is one of decreasing oxygen and carbon isotopic values. Reductions in speleothem $\delta^{18}O$ from -4.75 (11 ka) to -6.27 ‰ (8.5 ka) occur within 2500 years, representing one of the most dramatic increases in moisture availability throughout the Asiul record. Carbon isotopic values are also seen to decrease steadily throughout this period, indicating an increase in aquifer water storage and possible enhancements in vegetation productivity. Stable isotope values identify 8.5 ka as the wettest section of the Holocene, agreeing with local in lake levels and speleothem growth archives (Morellón et al., 2009, Stoll et al., 2013).

One significant absence from the Asiul speleothem archive during the early Holocene is any evidence of a major return to dry conditions around 8.2 ka. The "8.2 ka event" represents a significant Holocene climate event throughout Europe (Alley et al., 1997), linked to a large outburst of cold fresh water into the North Atlantic Ocean, in a similar manner to the YD (Barber et al., 1999). Evidence of the 8.2 ka event is once again contradictory within northern Spanish proxy records, mainly due to the often broken nature of regional pollen records or poor proxy chronologies at this time (Allen et al., 1996, Sobrino et al., 2005, Morellón et al., 2009). One coherent record of the 8.2 ka event in this region is that from Kaite Cave, this speleothem archive indicates a significant reduction in isotopic values during this event (Dominguez-Villar et al., 2009). Whilst the rest of the $\delta^{18}O$ record from Kaite Cave is interpreted in the same manner as the Asiul isotope record, an archive of precipitation amount; Dominguez-Villar et al., (2009) re-interpret the record around 8.2 ka, suggesting that low speleothem $\delta^{18}O$ values are a result of significant reductions in North Atlantic Ocean water isotope values, a result of fresh water entering the North Atlantic Ocean. This re-interpretation is undertaken due to relatively low speleothem (LV5) growth rates during the 8.2 ka event and significant reductions in speleothem $\delta^{18}O$. Dominguez-Villar et al., rule out other factors which may influence the $\delta^{18}O$ of speleothem carbonate at this time, including

the effects of seasonality and changes to the moisture source, leaving only a change in the isotopic composition of the North Atlantic as a control over the isotopic composition of rainwater and therefore speleothem carbonate. Changes in this record indicate that large scale variations in the isotopic composition of ocean water can overprint smaller scale changes in rainfall isotope composition due to the amount effect, although the amount effect is thought to still have influenced the $\delta^{18}O$ of rainfall during the 8.2 ka event, producing the high frequency variability seen in the record (Dominguez-Villar et al., 2009).

The Asiul speleothem record indicates no such reduction in speleothem isotope composition; instead the record indicates a cyclical shift in oxygen isotopes toward slightly drier (less negative isotope valeus) conditions between 8.5 and 7.3 ka. This positive shift fits with existing oxygen isotope cycles in the speleothem and does not reflect any major "anomalous" 8.2 ka event. It is however, possible that the Asiul speleothem (ASR), records a change in the isotopic composition of North Atlantic source waters which is somewhat masked by a transition to dryer conditions at the same time. Where the Dominguez-Villar et al., (2009) archive used laminar thickness as a proxy for the amount of rainfall during the 8.2 ka event (allowing for an independent check on rainfall amount) the Asiul moisture record can only be assed using the carbonate $\delta^{18}O$ value. Under extremely dry conditions such as those experienced during the 8.2 ka event (Domingeuz-Villar et al., 2009) it would be expected that the Asiul speleothem would record less negative isotope values. If however, there was a synchronous reduction in North Atlantic Ocean water $\delta^{18}O$ this would cause a transition to more negative isotope values in Matienzo rainfall. These two processes may counteract each other in the Asiul record to produce a muted or almost non-existent 8.2 ka event. To confirm this theory however, an independent archive of rainfall amount would be required for the Asiul site, which is not currently available.

7.2.3 The Mid Holocene (7.0 – 4.8 ka)

The mid Holocene is the first time period of the Holocene where both Asiul speleothem records can be compared, to produce a combined archive of climatic and environmental change via a range of proxies. This overlap in the records is fundamental, especially as this period of the Holocene is characterised in speleothem ASR by a change in speleothem colour and a reduction in growth rate (Chapters 3 and 6). The mid Holocene is discussed in terms of three separate events or trend components.

7.2.3.1 *Mid Holocene Aridity (ca. 5.5 ka)*

Many studies have identified the early - mid Holocene as a period of Climatic Optimum (normally associated with hot and humid conditions), not just in Spain but throughout Europe and Northern Africa (Magny et al., 2003, Lopez-Merino et al., 2010, Martinez-Pillado et al., 2014). This period of climatic amelioration led to the stabilisation of arboreal and mesophytic vegetation communities in northern Spain (Carrión 2002, Carrión et al., 2007) and is marked by important changes in human populations. Agricultural practices and forest clearances (normally using fire) have been observed from ≈7300 years BP and cultivated cereal pollen appears around 6700 years BP (Lopez-Merino et al., 2010). It is thought that improved climatic conditions during the early – mid Holocene may have triggered the uptake of agricultural practices; practices which continued through climatic deteriorations during the remainder of the mid Holocene (Lopez-Merino et al., 2010, Kaal et al., 2011).

As the mid Holocene progressed, intense aridification is recorded in regional lake records, (Valero-Garces et al., 2000, Gonzalez-Samperiz et al., 2008) and cave speleothems (Stoll et al., 2013, Martinez-Pillado et al., 2014) although the exact timing of aridity is often contradictory between records. Global climatic optimum conditions are also thought to end during the mid Holocene ca. 6000 years BP. Changes to atmospheric circulation (Mojtahid et al., 2013) and a decline in Northern Hemisphere insolation at this time contributed to the end of the tropical period in North Africa (Gasse 2000, Barker et al., 2001, Gasse 2001). This phase is linked to a northward migration in westerly trade winds, glacial advances in Scandinavia and positive NAO style conditions, which cause significant reductions in moisture availability in southern Europe (Mayewski et al., 2004, Davis and Stevenson 2007, Mojtahid et al., 2013).

In contrast to other climate archives which indicate a rapid change toward dry conditions during the mid Holocene, from 6 ka onward (Mayewski et al., 2004, Perez-Sanz et al., 2013); the ASR speleothem oxygen isotope record identifies this transition to enhanced aridity as a relatively gradual process, starting in northern Iberia at 7 ka and peaking at 4.8 ka (similar to Moreno et al., 2011a). However, oxygen isotope records from ASM and carbon isotope and Mg/Ca records from ASR indicate that this transition to drier conditions occurred later between 6 and 5.5 ka, but still reached peak values at 4.8 ka. Speleothem records are therefore slightly contradictory, possibly related to the extreme change in speleothem ASR growth rate. During this period of the Holocene the more rapidly growing speleothem ASM

may prove more reliable. It therefore appears that the change toward more arid conditions in northern Spain occurred at the end of the mid-Holocene climate optimum at ~6 ka.

Coupled to records of decreasing rainfall from ~6 ka in both speleothems, are significant reductions in speleothem ASR Sr concentrations (Figure 7.1) and a change in the normally stable Sr/Ba relationship.

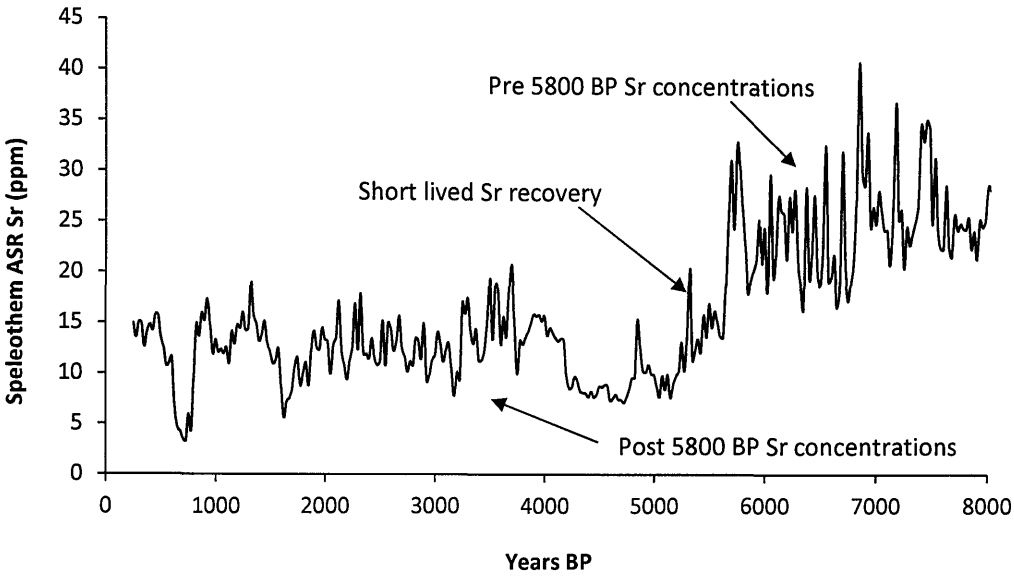

Figure 7.1: ASR Holocene Sr concentration record, showing a significant reduction in Sr concentrations during the mid Holocene period and a short lived recovery in Sr ca. 5300 BP.

As discussed in Chapter 6, the close coupling of Sr and Ba in Asiul speleothems is thought to indicate a growth rate control over these elements (Treble et al., 2003, Fairchild and Treble 2009). However, other studies have used speleothem Sr concentration as a proxy for drying (via PCP) (Fairchild et al., 2000) and under certain conditions as a proxy for vegetation and soil productivity (Hellstrom and McColloch 2000, van Beynen et al., 2008). Strong de-coupling of the Sr and Ba relationship in ASR at 5800 BP is thought to be driven by such a change in the overlying vegetation system.

Sr records from speleothem ASR indicate a rapid decrease in Sr concentration which may indicate a reduction in vegetation productivity from 5700 BP; a result of deteriorating environmental conditions linked to concurrent reductions in moisture availability. During this decrease in Sr concentration (5700 – 5100 BP) a brief return to higher concentrations is observed ca. 5300 BP, indicating a recovery in vegetation growth for a relatively short lived

period. After this recovery, Sr concentrations continue to decrease, establishing a new base level (≈ 20 ppm) and relationship with Ba at 5100 BP.

7.2.3.2 5.5 – 5.3 ka – A Short Lived Return to Wet Conditions

The second significant event recorded in speleothem trace element records during the mid Holocene is a peak in P, Zn, Mn and U concentrations in both speleothems at approximately 5400 BP, coinciding with the peak like recovery of Sr concentrations discussed previously (Figure 6.16). This phase is short lived in the slow growing ASR sample but ASM indicates a 300 year period (5500 – 5200 BP) of enhanced trace element uptake during the mid Holocene.

Increases in P, Sr and Zn all indicate an escalation of organic colloidal transport into the cave system. Enhanced colloid transport indicates an improvement in vegetation growth conditions and the enhanced breakdown of organic matter through microbial cycling in the soil, and an increase in the effective mobilisation and transport of organic colloids by the hydrological regime (Treble et al., 2003, Borsato et al., 2007, Fairchild et al., 2010, Hartland et al., 2011, Baldini et al., 2012, Hartland et al., 2012). Both production and mobilisation of colloids requires an increase in moisture delivery to promote vegetation and soil productivity as well as effective colloidal flushing (Borsato et al., 2007). Whilst no definite increase in winter rainfall amount is indicated by either speleothem $\delta^{18}O$ record, speleothem ASR's oxygen, carbon and Mg/Ca records all appear to plateau or decrease slightly just after 5400 years BP (Figure 6.16). The lack of clear evidence for a return to wet conditions in the stable oxygen records may be due to the courser resolution of sampling, in relation to the trace element analysis. However, a combination of stable isotope and trace element records during this period offers strong evidence for a short lived, but significant return to less arid conditions; increasing karst aquifer storage and vegetation productivity between 5.5 and 5.3 ka.

7.2.3.3 An End of Mid Holocene Aridity at 4.8 ka

At the end of this mid Holocene period is an extremely rapid decrease in stable isotope and Mg/Ca records from both speleothem archives (Figure 6.16). This reduction in stable isotopic and Mg/Ca values indicates a rapid increase in moisture availability within 200 years, and a greater retention of karst aquifer waters, indicated by a reduction of $\delta^{13}C$ values indicative of within karst calcite-water interactions. This rapid change in moisture availability is possibly related to a concurrent change in atmospheric moisture delivery patterns; resulting from a

positive to negative NAO transition, recorded by Olsen et al., (2012). This 200 year phase represents the most dramatic change in isotopic values recorded in the ASR speleothem record and coincides with a change in speleothem ASR's colour and growth rate.

7.2.4 Medieval Climate Anomaly and Little Ice Age

The medieval climate anomaly (MCA) and little ice age (LIA) are well-documented global climatic events. The MCA is importantly the most recent period of pre-industrial climatic warming and as such offers an ideal time period for comparison with modern global climate change (Trouet et al., 2009, Diaz et al., 2011). The LIA is one of the most major returns to cold conditions observed during the Holocene.

7.2.4.1 The Medieval Climate Anomaly (1250 - 760 BP)

Lake records from NE Iberia show a general trend towards wetter conditions from 1200 years BP. These records however, display a major interruption of this wetting trend between 1000 – 750 BP, linked to intense aridification and the MCA (Morellón et al., 2009, Morellón et al., 2012). Recent work by Trouet et al., (2009) and Mojtahid et al., (2013) suggests that reductions in moisture seen in palaeoclimate archives from throughout Iberia and southern Europe (Gil Garcia et al., 2007, Martin-Puertas et al., 2008, Moreno et al., 2011b, Morellón et al., 2012, Perez-Sanz et al., 2013) are driven by stable positive NAO conditions, which dominated during the MCA.

Although a generally arid MCA characterises many proxy records from eastern and southern Iberia; Moreno et al., (2012) present shallow marine cores from the west coast (Ria de Vigo and Ria de Muros), which indicate enhanced moisture delivery (Libreiro et al., 2006, Lopez-Merino et al., 2010). These records of enhanced MCA moisture availability coincide with peripheral lake records from the NE of Iberia, which indicate the period between 880 – 730 years BP as wet, with no obvious return to aridity as previously suggested (Riera et al., 2004, Morellón et al., 2008). This conflict in palaeoclimatic evidence highlights the requirement for the production of more high resolution proxy records, ideally those which have not been influenced by human activity.

In Asiul speleothems, the MCA is associated with gradually decreasing $\delta^{18}O$ values; defining this as a transitional period, which represents a gradual return to wetter conditions in a similar manner to records from Moreno et al., (2012). The ASR speleothem indicates that the MCA begins (1250 BP) with heightened aridity, where speleothem ASM suggests that peak aridity occurred approximately 200 years earlier (Figures 6.17 and 6.18). The offset between

the two speleothem records may be a result of chronological error based upon a 200 year dating uncertainty in the ASR data set. Both speleothem however, present low oxygen isotope values associated with peak wetness between 800 – 600 BP, at the end of the MCA. This period is also one of significant change in the speleothem trace element records.

7.2.4.2 Wet conditions during the Medieval Climate Anomaly 800 – 600 BP

At the end of the traditional MCA speleothems ASR and ASM exhibits significant P increases (Figure 6.18), occurring concurrently to heightened rainfall amounts indicated in the oxygen isotope records. Phosphorus was not measured within Asiul cave drip waters, but previous studies have identified P as a potentially important palaeoclimate indicator (Fairchild et al., 2001, Treble et al., 2003, Borsato et al., 2007, Baldini et al., 2012). Unlike many elements which are sourced within the karst zone, P concentration is controlled by changes in the soil nutrient cycle (Treble et al., 2003, Baldini et al., 2012) and the efficiency of organic colloid transport (Borsato et al., 2007, Hartland and Fairchild 2012); therefore offering a detailed proxy for vegetation change.

The fact that increases in P are observed in both speleothem records between 800 and 600 years BP indicates that a single forcing mechanism controls P concentration during this time period. For P to be actively released from the soil zone, vegetation decay and effective organic colloid transport are both required (Borsato et al., 2007, Baldini et al., 2012), resulting in a positive covariation between P and moisture availability (Treble et al., 2003). Increased P in both Asiul records therefore indicates higher rainfall levels, enhanced vegetation productivity and the leaching of organic colloids from the soil zone (Baldini et al., 2012). Speleothem P records indicate that between 800 and 600 BP the Matienzo valley experienced high levels of vegetation productivity and wetter conditions, in agreement with the $\delta^{18}O$ archive.

Whilst the Asiul records agree with some Iberian data sets (Riera et al., 2004, Morellón et al., 2008), there is obvious disparity with many others (Morellón et al., 2012, Perez-Sanz et al., 2013), indicating that distinctly different moisture regimes were operating throughout Iberia during the MCA. Moreno et al., (2012) hypothesises that the northern and western coasts of Spain may receive enhanced moisture delivery under positive NAO conditions, such as those believed to dominate during the MCA (Trouet et al., 2009). Under positive NAO phase central and southern Iberia receive reductions in moisture availability; explaining spatial differences between moisture archives. As will be discussed in subsequent sections, the Asiul speleothem records dispute this idea for the majority of the Holocene sequence. It is

however, possible that a weak or fluctuating NAO conditions would enhance moisture delivery to northern regions of Iberia and leave central and southern areas with a higher moisture deficit. Further atmospheric modelling and the production of more well dated high resolution proxy records may be the only way to resolve exactly how climate varied throughout Iberia during the MCA.

7.2.4.3 The Little Ice Age (510 - 250 BP)

In a similar manner to the MCA the LIA record preserved in the Asiul speleothems does not appear to completely agree with all other local records. Many local and European archives indicate that stable wet conditions characterise the LIA in southern Europe, driven by either a negative phase NAO or a reduction in Atlantic overturning (Dezileau et al., 2011, Palastanga et al., 2011, Moreno et al., 2012).

In contrast, the Asiul records suggest a transition to enhanced aridity, originating from a humid peak between the MCA and LIA at approximately 800 years BP. Asiul speleothem records of the LIA agree closely with records from southern Spain and the Mediterranean, which indicate peak humidity before the LIA (750 – 600 years BP); although the cause of enhanced moisture delivery remains unclear (Lamb 1977, Gil et al., 2006). From 650 years BP drying is observed in southern Spanish and Mediterranean records (Lamb et al., 1999, Martin-Puertas et al., 2008), as well as those from Asiul.

During the transition toward arid conditions at the height of the LIA, the higher resolution ASM speleothem record indicates a significant return to wet conditions (480 -360 years BP), seen slightly later (350 years BP) in southern Spain by Martin-Puertas et al., (2008). It may be that this short lived dramatic change in atmospheric conditions truly reflects the extent of the "wet" LIA or indeed the Maunder Minimum (ca. 360 BP) in northern Iberia, possibly driven by a rapid fluctuation in dominant NAO phase (Shindell et al., 2001).

Using data presented in Chapter 6 stable isotope and trace element records from Asiul speleothems have been reviewed over discrete Holocene time intervals and compared to other existing climate archives. These records identify periods of palaeomoisture and vegetation change, both of which are fundamental in regulating environmental and human evolution in the region. Whilst during the early Holocene, Asiul speleothems replicate and often improve upon existing archives of climatic change; records from the late Holocene appear at times to be slightly decoupled from other local climate archives. This decoupling either indicates spatially variable moisture delivery in N. Iberia during the late Holocene or is

more likely a function of the speleothem dating error and the difficulty of high resolution analysis of short lived events such as the MCA and LIA. Regardless, the Asiul speleothem records represent an important addition to our understanding of Iberian climate and environmental change; constraining Holocene climatic variation at a higher resolution than has previously been achieved.

The following section of discussion will focus on the mechanisms which force changes in moisture delivery to northern Spain and will consider in detail the cyclical nature of Asiul speleothem oxygen isotope records. These archives show a strong interconnection with existing oceanic and atmospheric records and preserve a now well-established ≈1500 year Holocene climate cycle (Bond et al., 1997). Asiul speleothem archives are finally used to help establish how oceanic and atmospheric records can become so closely interconnected, offering a possible atmospheric forcing mechanism for changes in North Atlantic Ocean temperatures throughout the Holocene.

7.3 Speleothem Records of Holocene Rainfall Intensity

Whilst Asiul speleothem archives have presented unique insights into regional environmental and climatic change, their long duration oxygen isotope records (Figure 6.5) also offer an opportunity to assess the role of global climate systems in controlling moisture delivery to southern Europe. As discussed in previous sections, Asiul speleothems preserve archives of winter rainfall amount through the incorporation of an oxygen isotope signature from cave drip waters (Chapter 4).

Speleothem $\delta^{18}O$ exhibits a series of distinct palaeo winter rainfall minima and maxima, which exhibit millennial scale cycles and are strongly coupled to records of North Atlantic Ocean temperature (Bond et al., 1997, Bond et al., 2001) (Figure 7.2).

During the YD - Holocene transition, speleothem oxygen isotope minima and maxima occur with a cycle length of 1350 years; the length of this cycle extends during the early Holocene, remaining at 1575 years until the modern day (Figure 6.7); within dating error of frequencies observed by Clemens (2005), 1190 and 1667 years. Closely coupled ocean and atmospheric cycles, show that millennial scale variations in northern Iberian moisture delivery and North Atlantic Ocean temperatures must be paced by the same components of the global climate system. To understand how an ocean temperature record from the North Atlantic and an atmospheric record of moisture delivery in northern Iberia become coupled, the modern controls over Iberian winter rainfall are considered.

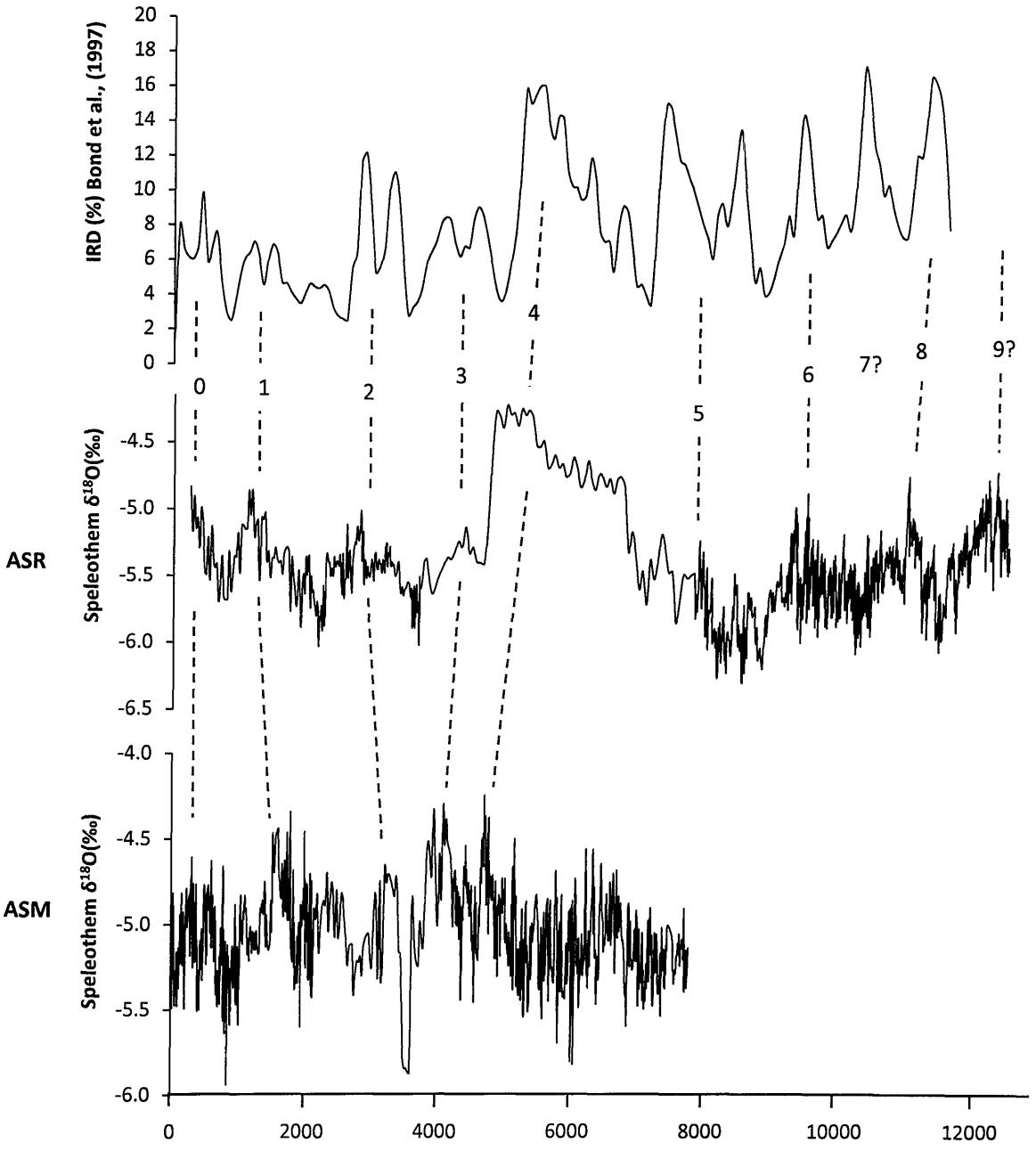

Figure 7.2: Asiul speleothem oxygen isotope profiles alongside records of North Atlantic drift ice index (IRD %) from Bond et al., (1997). Numbers refer to "Bond Events" and speleothem ASR and the Bond record show peaks which are within dating error of the speleothem samples, ASR ±200 years, ASM dating error is = ±60 years.

7.3.1 Modern Day Controls on Winter Storm Activity

Under modern conditions, the frequency and intensity of winter storms over northern Iberia is driven by the latitudinal position of westerly storm tracks, which bring moisture from the North Atlantic Ocean to continental Europe (Hurrell et al., 2001). The positioning of these westerly storm tracks are in turn determined by an atmospheric pressure dipole, which exists between Tropical (centred on the Azores) and Polar Regions (centred over Iceland). This pressure differential is known as the North Atlantic Oscillation (NAO), which can be described as being in positive or negative phase (Figure 7.3a and b) (Hurrell 2003, Hurrell and Deser 2009).

Positive phases occur during periods of high pressure over the Azores and low pressure centred over Iceland; westerly winds are driven northwards, creating warm wet winters in the north of Europe and dry cold winters in the south (Figure 7.3a). In contrast, negative phases occur when weak pressure systems develop over each dipole; westerly winds weaken and move south, resulting in southern Europe receiving a greater number of winter storms (Figure 7.3b).

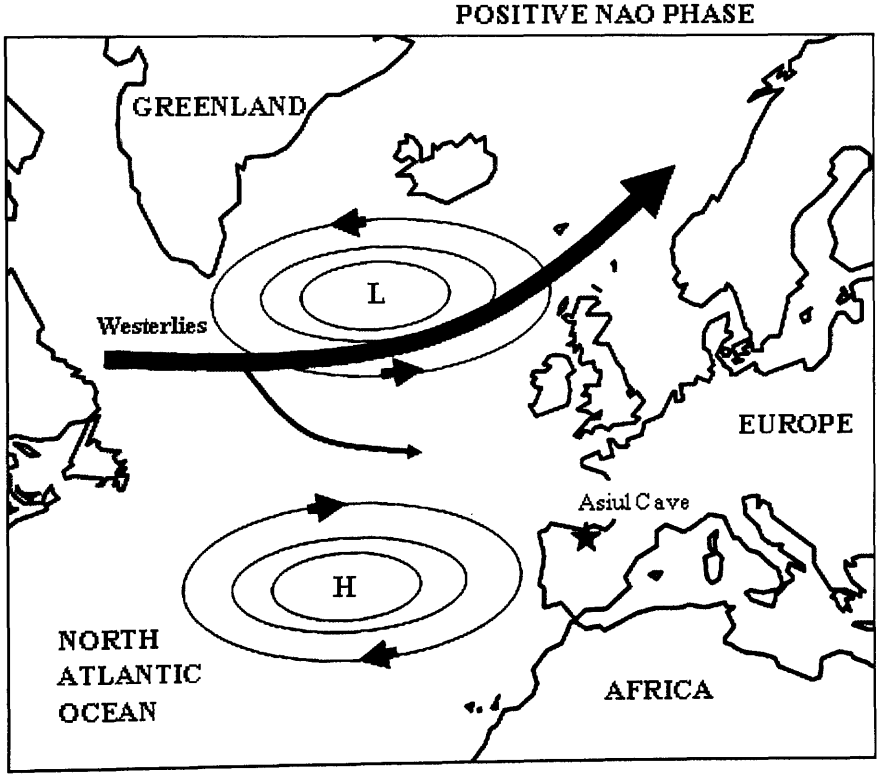

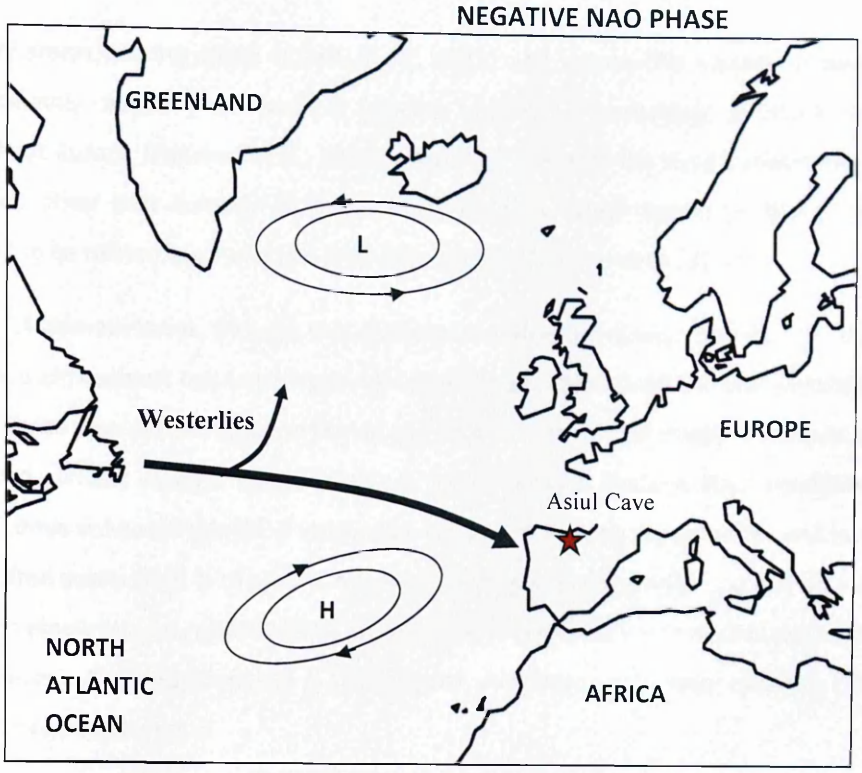

Figure 7.3a and b: Positioning of westerly, moisture bearing air masses over Europe during positive and negative phases NAO conditions.

Although the NAO controls modern rainfall delivery throughout Europe, this dipole is annually sensitive and can change phase on monthly scales. Records such as those from Asiul cannot resolve these sub-annual variations in the isotopic signature of rainfall, mainly due to water homogenisation within the karst but also because of slow growth rates found in speleothem deposits from this cave. Even though sub-annual changes in the NAO cannot be resolved, millennial scale cycles in speleothem oxygen isotopes must be derived from a change in the atmospheric system, which delivers Iberia's moisture. The following section presents several climate records, including that from Asiul and explains cycles in these archives as a product of a fluctuating, millennial scale NAO cycle.

7.3.2 A Holocene Record of the North Atlantic Oscillation

Oxygen isotope cycles in Asiul speleothems indicate that atmospheric conditions over northern Iberia are controlled by a millennial scale cycle. Persistent NAO style atmospheric phases have previously been observed over millennial scales during the Holocene (Olsen et al., 2012, Fletcher et al., 2013, Mojtahid et al., 2013); meaning annual fluctuations currently observed in the modern NAO may in fact be a high resolution harmonic, superimposed upon a longer millennial cycle. It is this long duration NAO cycle, which drives the positioning of

westerly storm bearing winds (Olsen et al., 2012) and causes the system to develop a predominately negative or positive phase; ultimately controlling moisture delivery throughout Europe (Fletcher et al., 2013). Figure 7.4 presents the Asiul speleothem record alongside other long duration Holocene scale archives, which preserve climate changes believed to be related to a Holocene NAO style system (Fletcher et al., 2013).

Figure 7.4 demonstrates, through the coalition of numerous proxy records, the ability of NAO style atmospheric restructuring to influence climate throughout Europe (Fletcher et al., 2013). These proxies have been combined by Fletcher et al., (2013) showing archives of NAO controlled climatic change. Within northern dipole regions, positive NAO conditions (7.4 graph f) drive enhanced rainfall, a northerly transport of Atlantic Water inflow and increases in ice rafted debris (IRD) in the North Atlantic (7.4 grey boxes in graphs e, d and b); whilst in southern dipole regions, positive NAO conditions are related to forest decline and enhanced aridification in the Mediterranean as well as drier conditions at the Asiul cave site (7.4 grey boxes in graphs g, h and a).

Whilst the NAO is shown to have varying regional impacts dependent upon the location of the proxy records; Figure 7.4 also shows a strong millennial scale NAO cycle, manifest in all the proxy records during the mid - late Holocene (8 – 0 ka). However, all records of the NAO (except that of Asiul) fail to identify this millennial cycle during the early Holocene and the YD time period (12.5 – 8 ka). The Asiul speleothem archive therefore extends our record of the NAO record back into the YD period (12.5 ka). Whilst doing so the Asiul record also shows how changing NAO style atmospheric conditions are strongly coupled with changes in IRD and therefore the SST temperature of the North Atlantic Ocean (Figure 7.4).

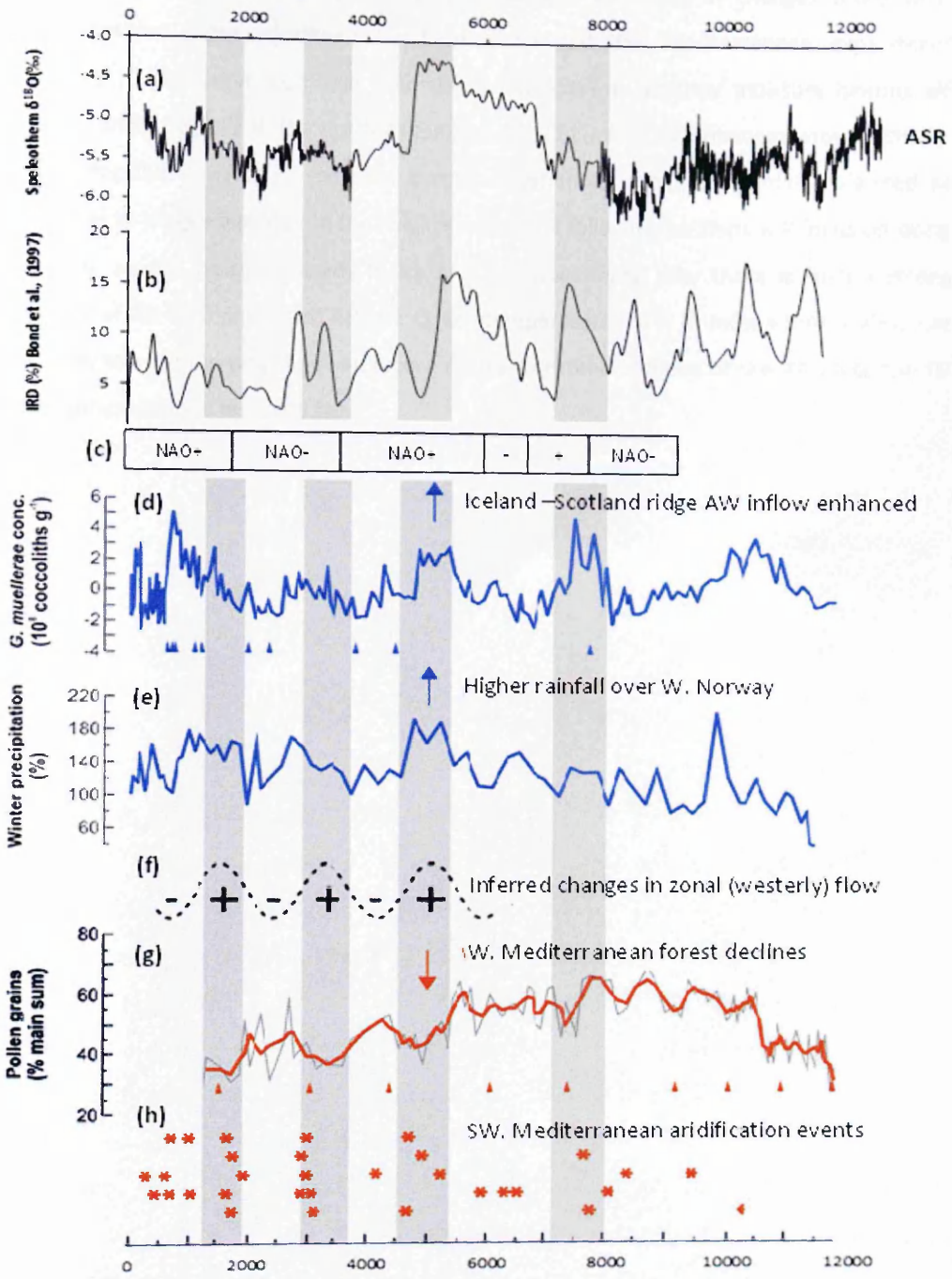

Figure 7.4: (a) Asiul cave ASR oxygen isotope record. (b) Stacked Bond et al., (1997) IRD record. (c) NAO indices from the Bay of Biscay (Mojtahid et al., 2013). (d) Concentrations of coccolith species *Gephyrocapsa muellerae* in marine core MD95-2011 (Giraudeau et al., 2010). (e) Winter precipitation reconstruction, % of present value in Norway (Bjune et al., 2005). (f) Inferred 1750 year oscillation of westerly wind flow from the MD95-2043 pollen record. (g) MD95-2043 temperate and Mediterranean forest record. (h) Western Mediterranean aridification events (Fletcher et al., 2013).

The Asiul speleothem oxygen isotope records appear to be driven by changes in the NAO. Under positive phase conditions northern Iberia and the Mediterranean experiences enhanced aridity, associated with a northerly migration in westerly moisture bearing air masses; whilst regions in the north of Europe are dominated by enhanced storm activity. Under negative conditions, southern Europe experiences enhanced rainfall, reflected as decreases in oxygen isotopes in the Asiul records. The following sections will focus on using the Asiul oxygen isotope records to try and establish firstly, why there is such a strong coupling of the NAO and North Atlantic Ocean temperatures over Holocene time scales; and secondly to establish why the Asiul record is able to extend archives of the NAO into the YD when other archives fail to do so.

7.4 Ocean – Atmosphere Coupling on Millennial Timescales

The strong millennial scale coupling of the Asiul NAO moisture record and the North Atlantic Ocean temperature records of Bond et al., (1997), indicates a possible cause and effect relationship between the atmosphere and ocean systems. Interactions between these two major components of the climate system are however, complex and in many cases poorly understood. For that reason it is possible to see two distinct pathways for tight coupling between the ocean and atmospheric systems. Firstly, an ocean temperature control over moisture availability, NAO phase and therefore prevailing storm direction (Czaja and Frankignoul 2002, Rosqvist et al., 2007, Sorrel et al., 2012). Secondly an atmospheric control over ocean circulation patterns and therefore ocean temperatures (Curry and McCartney 2001, Marshall et al., 2001, Giraudeau et al., 2004, Giraudeau et al., 2010, Fletcher et al., 2013). Using the Asiul speleothem NAO record and the North Atlantic IRD records of Bond et al., (1997) we attempt to offer an explanation as to why there appears to be a strong ocean – atmosphere interconnection throughout most of the Holocene.

7.4.1 A Possible Oceanic Control

Oceanic control over atmospheric systems is driven by changes in ocean surface temperature, salinity (Thornalley et al., 2009) and modes of circulation (Sorrel et al., 2012). However, the exact mechanisms by which a change in SST would drive NAO style atmospheric restructuring are still unclear on Holocene timescales. Currently, the majority of studies focus on annual to multi-decadal NAO / SST analysis, within the instrumental timeframe (Rodwell et al., 1999, Czaja and Frankingnoul 2002, Peng et al., 2003). General circulation models (GCM's) identify local precipitation, evaporation, wind stress and atmospheric-heating processes to be the major factors which may link sea surface and atmospheric conditions (Rodwell et al., 1999). Under modern conditions Czaja and Frankingnoul (2002) suggest the development of a North Atlantic Ocean SST tri-pole may be linked to positive NAO conditions, whilst negative NAO phases are possibly triggered by tropical SST warming (20°S - 20°N) (Czaja and Frankingnoul 2002).

However, if on Holocene timescales the NAO is controlled by changes in the North Atlantic Ocean (specifically temperature) then we would expect to observe two components within the Asiul NAO moisture record. Firstly, the preservation of the ~1500 year cycle in ocean temperature record by Bond et al., (1997); which is observed in Asiul speleothems. The second component should show evidence of significant fresh water outbursts into the North Atlantic, which are known to have changed oceanic temperature and should therefore cause

a change in moisture delivery, recorded in the Asiul speleothem oxygen isotope record. Asiul speleothems fail to record any evidence of significant climatic or atmospheric change (outside of that expected from millennial cycles in moisture delivery) during the Holocene freshwater outburst events, including the YD and 8.2 ka climate events (Mayewski et al., 2004).

The fact that Asiul speleothems do not identify any Holocene fresh water outburst events indicates that the record is not primarily influenced by oceanic conditions, but instead is controlled independently by atmospheric circulation patterns, under NAO style conditions. This finding implies that millennial cycles in the NAO may control both the Asiul speleothem record and changes in IRD in the western Nordic Sea (Bond et al., 1997). The following section explores a mechanism which can explain an NAO driven atmospheric control over ocean circulation, and therefore explain the strong coupling of the atmospheric Asiul record and the ocean temperature records of Bond et al., (1997).

7.4.2 An Atmospheric Control

Recent work undertaken by Giraudeau et al., (2010) in the northern North Atlantic, suggests increases in northern storm activity (Sorrel et al., 2012) and drift ice in the western parts of the Nordic Sea are driven by positive style NAO atmospheric conditions (Jennings et al., 2002, Moros et al., 2004, Dylmer et al., 2013). Intense westerly winds over the northern North Atlantic act to increase the depth of the ocean mixed layer and strengthen the Sub-Polar Gyre (SPG), causing a southward shift in the Sub-Polar Front (SF) and a strengthening of the North Atlantic Current (NAC) (Moros et al., 2004, Solignac et al., 2006, Sarafanov et al., 2010, Staines-Urias et al., 2013). An increase in northerly Atlantic Water (AW) flow in response to changing SPG and SF positioning, forces a concurrent convective outflow (southerly) of ice-baring polar waters into the Greenland and western Nordic Seas and a general cooling of the eastern North Atlantic (Moros et al., 2004, Giraudeau et al., 2010, Staines-Urias et al., 2013).

The Asiul speleothem record offers an excellent NAO dipole record to those presented by Giraudeau et al., (2010) (Figure 7.5). Under positive phase NAO conditions, heightened AW flow, storm conditions and drift ice are observed in the western Nordic Sea and northern North Atlantic Ocean (O'Brien et al., 1995, Bond et al., 1997, Moros et al., 2004, Bjune et al., 2005, Turney et al., 2005) where the Asiul speleothem records show increased aridity, similar to other Mediterranean (Fletcher et al., 2013), southern European and North African records (Lamb et al., 1999, Bout-Roumazeilles et al., 2007). Unlike many other Holocene archives,

Asiul speleothems directly record changes in westerly wind positioning (NAO phase), and therefore become closely coupled with changes in oceanic SST conditions, which are driven by the same atmospheric process (Turney et al., 2005).

Such a "top down" NAO style atmospheric control over North Atlantic SSTs would firstly explain the strong coupling of these systems throughout the Holocene and secondly why Asiul speleothems record no evidence melt water outburst events from Lake Agassiz (Clarke et al., 2001, Teller et al., 2002, Dormoy et al., 2009). Whilst outburst events influence North Atlantic Ocean circulation and in some regions atmospheric circulation, the Asiul records indicate that they should be considered as a product of general Holocene climate warming; semi-independent from Holocene climate cycles which are controlled by NAO style atmospheric conditions.

This represents a significant finding. Numerous previous records have identified each of, or a combination of solar (Bond et al., 2001), oceanic (deMenocal et al., 2000, Thornalley et al., 2009, Sorrel et al., 2012) and atmospheric (Shindell et al., 2001, Hu et al., 2003) changes, as the driving force for Holocene climate cycles. However, until the production of the Asiul record it has been almost impossible to distinguish whether the global oceans or atmosphere drives this ~1500 year Holocene climate cycle (Hu et al., 2003). The Asiul speleothem directly identify large, millennial scale cyclical changes in the atmosphere, as the driving force behind Holocene climate cycles in both oceanic and atmospheric proxies. The Asiul record indicates that cyclical changes in the latitudinal positioning of westerly moisture bearing air masses occurs with distinct periodicities of 1350 and 1575 years through the Holocene (Fletcher et al., 2013). The strong secondary relationship the speleothem record exhibits with ocean cooling indicates that atmospheric cycles, have dictated the timing of North Atlantic Ocean cooling events (Giraudeau et al., 2010).

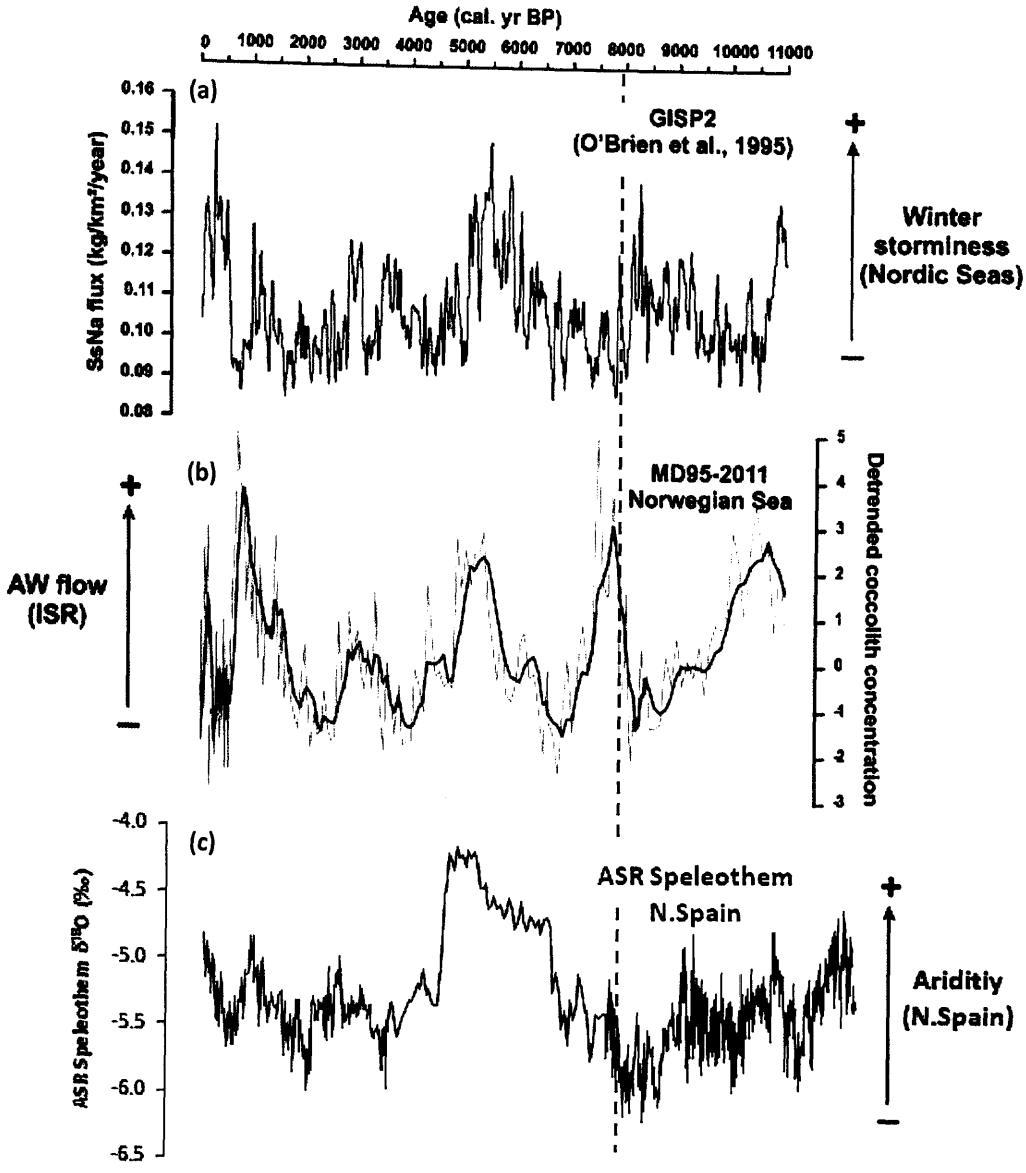

Figure 7.5: Comparison of the ASR speleothem oxygen isotope record (c) with North Atlantic Ocean and atmosphere proxy records. (a) Sea salt sodium flux over central Greenland (O'Brian et al., 2005). (b) Smoothed and detrended flow record of AW into the Nordic Seas (Giraudeau et al., 2010). Decoupling of North Atlantic ice core and ocean core records can be observed before 8 ka due to the existence of the Laurentide Ice shelf (dashed vertical black line).

7.4.3 Extending the NAO Record through the Holocene

Whilst existing archives of the NAO exhibit millennial scale cycles throughout the mid to late Holocene (Giraudeau et al., 2010, Fletcher et al., 2013), none of these records extend into the early Holocene or YD periods (Giraudeau et al., 2010). This absence in existing records has been interpreted to represent a complete absence of any millennial scale NAO-style signal before 8 ka (Figure 7.5). Figure 7.5 shows the timing of NAO development in two northern climate records which are both linked to the NAO. Under positive NAO phases enhanced westerly wind flow over the Nordic Sea and Greenland acts to simultaneously enhance rainfall levels (Figure 7.5 graph a) and cause an increase in Atlantic water inflow (due to wind stress on the ocean surface) (Figure 7.5 graph b). These two climate records exhibit a millennial cyclicity in the NAO from approximately 8 ka to the modern day; however, before 8 ka no such coupling in these records exist (Figure 7.5 dashed line), indicating that NAO style conditions did not develop in extreme northern regions until 8 ka.

The lack of NAO development before 8 ka has been attributed to the existence of the Laurentide ice sheet which caused a southward shift in the westerly atmospheric jet stream (Carlson et al., 2008) and interrupted the positioning of westerly storm tracks over Europe (Giraudeau et al., 2010, Fletcher et al., 2013). However, such a southerly shift in the jet stream may actually mean that proxy records from the current northern NAO dipoles are not ideally positioned to record the NAO during the YD period to early Holocene transition (Giraudeau et al., 2010).

The Asiul speleothem record which is situated in a mid-latitude location appears not to be as influenced by the existence of the Laurentide Ice shelf, continuing to record changes in both NAO style atmospheric conditions and associated oceanic cooling. Both northerly (Giraudeau et al., 2010) and southerly (Fletcher et al., 2013) palaeo NAO records indicate that the approx. 1500 year cycle only developed after the breakup of the Laurentide Ice shelf; with a shorter 900 year (possibly solar) cycle leading changes in moisture during the early Holocene. However, the Asiul record only records a 200 year difference between the timing of NAO driven cycles in precipitation delivery between the early and late Holocene, suggesting a relatively stable control over moisture availability.

The lack of evidence for NAO forcing during the early Holocene in current day NAO dipole proxies and the stable NAO signal in the Asiul speleothem record, indicates a significant latitudinal contraction in the NAO during the early Holocene and YD (Figure 7.6).

The Asiul speleothem record therefore demonstrates the first complete YD to modern day record of NAO style atmospheric conditions and the resultant coupling with oceanic temperature. These speleothem archives extend our understanding of both ocean cooling processes and NAO style atmospheric conditions into the YD, unaffected by deglaciation processes which interfere with proxy records in modern day NAO dipole regions.

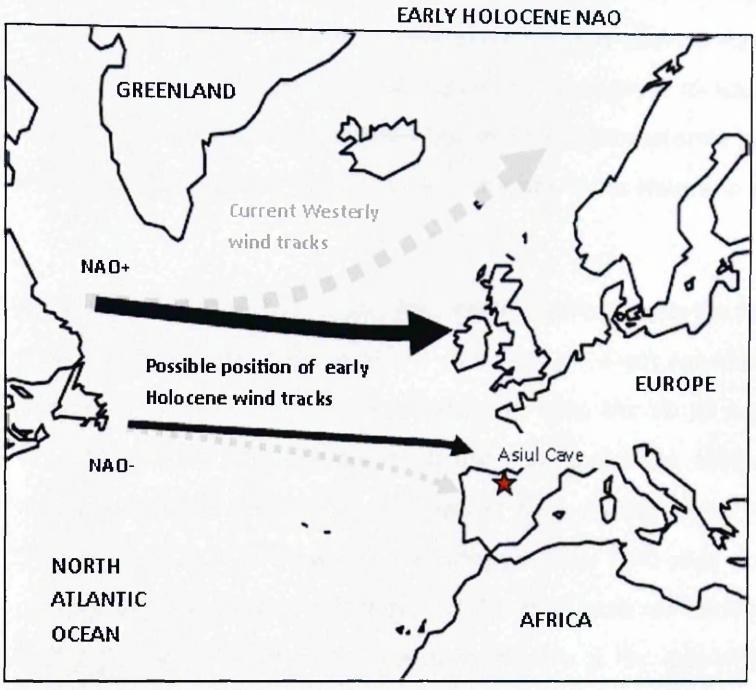

Figure 7.6: Possible positioning of westerly winds under positive and negative NAO style conditions during the YD and early Holocene (black arrows), in comparison with current positioning for NAO storm track trajectories (grey arrows). The Asiul Cave site records an accurate southern dipole record of NAO conditions under both styles of NAO positioning.

Asiul speleothem archives preserve a Holocene to YD duration record of NAO conditions. Positive NAO phases cause an increase in storminess in the northern north Atlantic, which in turn forces a change in oceanic circulation patterns and enhances the delivery of IRD to the western Nordic Sea (Giraudeau et al., 2010). The Asiul dipole archive records positive NAO conditions as an increase in aridity. Under negative NAO conditions westerly storm tracks migrate southwards, enhancing moisture delivery to northern Iberia. The Asiul NAO record extends beyond existing archives of the NAO into the YD; possibly related to a latitudinal contraction of NAO style atmospheric conditions away from current dipole regions, driven by the existence of the Laurentide ice shelf (Giraudeau et al., 2010). Asiul speleothems therefore offer a hemispherically important archive, of both the NAO and oceanic circulation from the YD to the modern day.

7.5 Summary

Asiul speleothem deposits, through the analysis of stable isotopes and trace elements have been shown to accurately preserve variations in winter moisture delivery to northern Iberia throughout the Holocene. Precipitation for this region is sourced from the North Atlantic Ocean and is known under modern conditions to be strongly controlled by hemispheric scale atmospheric processes, namely the NAO. Asiul speleothem deposits offer perhaps the best long duration, high resolution and accurately dated archive of changes in moisture delivery to this region. Speleothem oxygen isotopes exhibit two distinct millennial scale cycles (1350 and 1575 years) of moisture delivery, approximately reflecting other Holocene archives of the NAO.

Where other proxies, sourced from modern day NAO dipole regions suggest the NAO to be a phenomena existing only since the breakup of the Laurentide ice shelf; Asiul speleothems indicate that NAO style atmospheric cycles have persisted from the YD to modern day. Records sourced from modern day NAO dipole regions may have been affected by the existence of the Laurentide Ice shelf, which is known to have caused westerly winds to contract southward, retarding the formation of a European-wide NAO style atmospheric system. It is possible that a latitudinal contraction of the NAO occurred during the early Holocene, and that the NAO only regulated moisture delivery in the mid-latitudes. The discovery of a stable early Holocene atmospheric system operating at a frequency of ≈ 1350 years in the Asiul records is regionally important as it indicates that a version of the NAO operated throughout Holocene and YD.

Whilst the Asiul speleothem record accurately reflects changes in atmospheric systems and moisture delivery regimes to northern Iberia, it also exhibits a strong coupling with North Atlantic ice rafting events. This coupling indicates a close atmosphere – ocean relationship throughout the Holocene. The lack of evidence for major, ocean sourced climatic events (YD, 8.2) in the Asiul record indicates that atmospheric processes operate independently from the ocean system. Atmosphere - ocean coupling preserved in the Asiul record, therefore suggests that NAO style atmospheric conditions have at least partly controlled the timing of North Atlantic Ocean cooling events for the duration of the Holocene. Further work is still required to extend this archive further, with the aim of understanding atmospheric systems during the last de-glacial transition and possibly establishing a timing for the onset of NAO control over European climate.

Whilst preserving archives of major Holocene climate systems, Asiul speleothems have also been shown to offer high resolution local environmental and climate archives through the analysis of a range of chemical proxies. During the early Holocene, Asiul speleothem archives help to improve upon our understanding of regional climate dynamics, corresponding well to other local records. During the late Holocene, Asiul records become slightly de-coupled from other local palaeoclimate archives, possibly related to errors associated with U/Th dating of younger carbonate samples. Regardless of these discrepancies, the Asiul records offer a complete Holocene archive of climate and vegetation change which helps to build upon and improve existing climate records. In combination, these archives begin to give a clear picture of environmental and climatic change in northern Iberia throughout the last 12.5 ka and can help to shed light upon the conditions within which human populations developed.

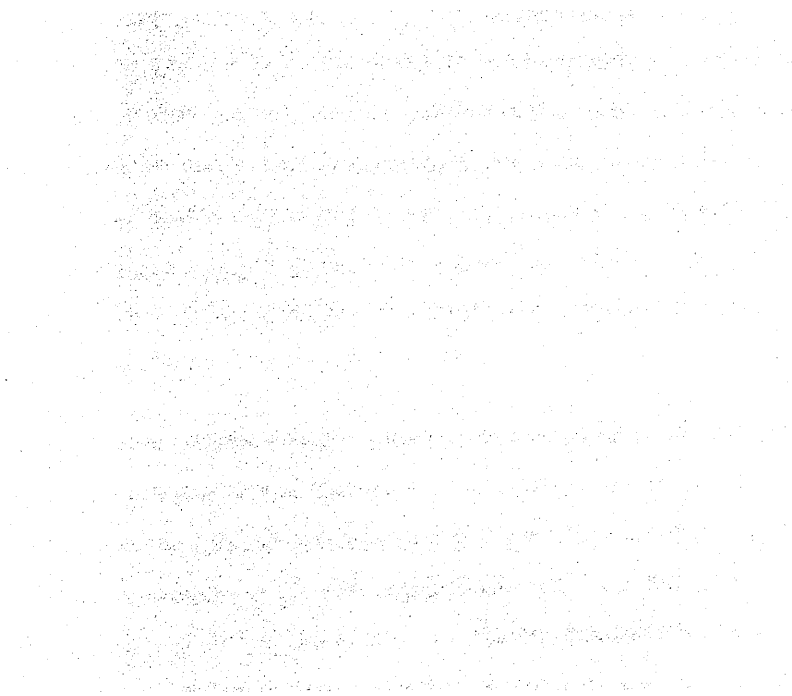

8.0 PROJECT IMPACTS AND SUGGESTIONS FOR FURTHER RESEARCH

This final section will act as a conclusion for the thesis; highlighting the major findings from cave monitoring and palaeoclimate reconstruction undertaken in Asiul Cave. Within each of the major project areas suggestions for further research will be laid out. The inclusion of this section aims to spark interest in new research projects surrounding specifically, the Matienzo karst depression but also the wider Cantabrian region, which has been shown to house globally significant climate records.

8.0.1 The Matienzo Depression

Before the initiation of this project the Matienzo valley had only received a minimal amount of research interest, predominantly from geomorphologists and archaeologists. Whilst it was widely known that the valley housed thousands of cave systems of varying ages, the potential use of this region for cave monitoring studies had to a large extent been overlooked. The initiation of climate and cave monitoring in 2010 as part of this project has hopefully marked a new era for scientific research within the valley.

Monitoring in Matienzo during the last 4 years has highlighted the importance of climate seasonality in this region, both for the preservation of speleothem deposits but also for the wider evolution of valley ecology. Like the majority of the northern Iberian coastline, rainfall has been shown to be sourced predominately from the North Atlantic Ocean and the amount of winter rainfall determined by the modern day North Atlantic Oscillation. More locally, calculations of water excess have shown that winter rainfall is critical for the recharging of karst aquifers, which are depended upon as a major water source for modern day agricultural practices.

Whilst external climate monitoring in Matienzo shows broad similarities with more costal research sites, including that of Santander; the valley is known to have a very specific microclimate. It is the detailed understanding of this microclimate that is essential to future palaeoclimate reconstructions from this region, especially those that aim to characterise the most recent periods of our climate history. It is therefore hoped that climate monitoring in Matienzo will continue, to help characterise this regionally unique valley and the dynamics of its climate.

8.0.2 Asiul Cave

High-resolution cave monitoring in Asiul has expanded our knowledge of this important cave, helped to interpret palaeoclimatic records from speleothem deposits and develop our understanding with regards to processes ubiquitous throughout cave sites.

Whilst atmospheric dynamics in Asiul are strongly controlled by seasonal variations in external air temperature, seasonal cave ventilation is not obviously recorded within cave air CO_2 and $d^{13}C$ records. This disparity between traditional techniques for identifying cave ventilation is one area that requires further research at this site. Ideally this work would continue to develop high resolution temperature and CO_2 records alongside a multi-annual cave air $d^{13}C$ record, to try and more accurately characterise atmospheric end members. As the most negative CO_2 end members currently identified within cave air samples reach values as low as -60 ‰, it is therefore possible that ground air has a methane component. A program of cave and soil air sampling for methane would therefore help to fully characterise the cave atmospheric system over a range of temporal scales.

Regardless of the complex atmospherics that are apparent in Asiul, speleothem growth can be observed throughout this cave. In-cave carbonate growth experiments indicate that speleothem development occurs relatively rapidly after nucleation. Further, high resolution (sub-annual) carbonate collection with pre-weighed glass slides may help to define the rate and timing of peak speleothem deposition. If expanded to other speleothem drip sites, modern carbonate growth experiments may help to identify ideal speleothems for further palaeoclimate reconstructions.

8.0.2.1 Controls over Drip Water EC

One of the most significant findings from the cave monitoring program in Asiul was the identification of a high resolution cave air pCO_2 control over drip water EC at event scales. Previously, our understanding of drip water EC indicated that karst water values controlled drip water EC and that once water entered the cave chamber EC values remained relatively stable. However, high resolution monitoring using a previously untested (within caves) CTD Diver probe shows a strong EC and cave air pCO_2 relationship; where changes in cave air pCO_2 are shown to be the only control necessary to explain changes in measured drip water EC.

Whist this cave air pCO_2 – EC relationship remained stable, increases in cave air pCO_2 are shown to be controlled by two seasonally variant, drip rate related processes. Under winter conditions heightened karst water percolation and an increase in drip water degassing causes an increase in cave air pCO_2 and a delayed increase in measured EC values. Whilst during the summer, the flushing of high pCO_2 soil and karst air in front of percolating water causes a concurrent rise in cave air pCO_2 and drip water EC, before any change in drip rate is observed. Whilst in Asiul, such a high resolution coupling may offer little control over the chemical makeup or growth of speleothem deposits over Holocene timescales, this relationship may be fundamental for understanding speleothem chemistry when assessing monthly or event scale carbonate deposition. These findings from Asiul highlight the important role that continuous, high resolution monitoring has to play in future cave research, both at this site and others.

8.0.3 Holocene Climate Change in Iberia

Speleothem deposits from Asiul cave span the entire Holocene period from the end of the YD at 12.5 ka to the modern day. On a regional scale, oxygen isotope archives offer a uniquely high resolution record of moisture delivery throughout the Holocene, whilst trace element records offer an unprecedented local archive of environmental change. During the majority of the Holocene the Asiul speleothem archive agrees closely with other palaeoenvironmental records from northern Iberia, often improving upon the current resolution of palaeoclimate reconstruction.

However, during specific sections of the Holocene including the 8.2 ka event, the Medieval Climate Anomaly and the Little Ice Age there are important disparities between the Asiul records and other northern Iberian archives. Although this is not uncommon, with conflict between climate records being observed throughout northern Iberia, it is important that all climate records are where possible duplicated. Future speleothem extraction from the caves of Matienzo may therefore wish to focus attention upon these specific time periods, to produce very high resolution proxy records that may begin to explain why we observe a level of conflict between regional archives.

Alongside the production of further high resolution Holocene age records, caves within Matienzo offer a fantastic opportunity to source much older speleothem deposits. Future analysis may wish to focus on extracting speleothem that developed during two important periods of human evolution in Iberia. The first, approximately 50 thousand years BP is characterised by Neanderthal population extinction; whilst the second period of interest is

the last glacial maximum (LGM). Speleothem climate records from these time periods could work alongside current and future archaeological archives to help explain driving forces behind human population change and cultural evolution.

8.0.4 An Extended Record of the North Atlantic Oscillation

Oxygen isotope records from Asiul show significant replication throughout the Holocene, lending confidence in our modern interpretation of these archives as palaeo-rainfall amount indicators. These speleothem suggest that significant periods of wetting and drying have been experienced in this region during the last 12.5 ka, leading to changes in vegetation productivity and therefore possible changes in human subsistence. Variations in long term moisture availability in northern Iberia is dependent on the direction and intensity of westerly storm baring winds from the North Atlantic Ocean, which is in turn controlled by the NAO.

Palaeorecords from Asiul cave have shown this NAO system to operate over millennial timescales, strongly influencing Holocene winter moisture availability. Unlike many existing archives, which indicate the emergence of the NAO at approximately 8 ka, the Asiul record indicates that this atmospheric system had already developed by the middle of the YD; possibly becoming established prior to this. Our extension of the NAO record using speleothems from Asiul may only have been possible due to the central European location of the Matienzo valley and its extreme sensitivity to changes in the NAO. Currently most other archives of the NAO are sourced from modern dipole regions, which are thought to have been influenced by the existence of the Laurentide Ice shelf up until 8 ka. Records from Asiul therefore indicate that although NAO style conditions existed through the YD and early Holocene there was a possible latitudinal contraction of dipole regions, toward the centre of Europe. A major area of future interest would be to extend the Asiul cave records, searching for an NAO signal to try and establish when this atmospheric system began to dominate European winter climate and how it may have been influenced by periods of climate variation, related to glacial conditions.

8.0.5 Millennial Climate Cycles and Their Origins

Whilst Asiul oxygen isotope records act to extend currently existing archives of the NAO they also exhibit a strong relationship with cycles of ocean temperature variability, first identified by Bond et al., (1997). The connection of atmospherically driven records from Asiul Cave and ocean sediment records from the North Atlantic indicates a significant ocean – atmosphere

coupling, on millennial scales. One possible explanation developed using the Asiul records and an excellent northern dipole record of ocean circulation presented by Giraudeau et al., (2010) is an NAO derived, atmospheric control over oceanic circulation patterns. Such a control leads to a strong coupling of positive phase NAO and enhanced levels of ice rafted debris in ocean sediments. Using the records of Bond et al (1997) and those developed from Asiul we can observe this millennial coupling of atmospherics and ocean circulation throughout the Holocene.

However, whilst Bond et al., (1997) and numerous others have identified a 1500 ±500 year cycle, the Asiul records indicate that millennial variability in the North Atlantic region is more precisely controlled by two distinct cycles. The first has a period of 1350 years and is observed in the YD and early Holocene and the second a period of 1575 years, which continues to the modern day. The existence of such strong and repeating cycles within numerous northern hemisphere archives requires future research both to establish a forcing mechanism for these cycles and to understand how they may control future climate change in the light of modern anthropogenic influences. We hope that the two distinct cycles identified in Asiul may help to better characterise Holocene climate change, aiding in our search for a comprehensive explanation of millennial climate cycles.

8.0.6 Summary

This project has focused upon two distinct areas of scientific scrutiny, cave monitoring and palaeoclimate reconstruction. We hope that the project, through this thesis and future publications will further our understanding of both areas of research and that conclusions drawn here will spark a new interest in research within the Cantabrian region.

BIBLIOGRAPHY

Adkins, J., DeMenocal, P. and Eshel, G. (2006) The "African humid period" and the record of marine upwelling from excess (230)Th in Ocean Drilling Program Hole 658C. *Paleoceanography*, 21, 14.

Allegre, C.J. (2008) *Isotope Geology*, Cambridge, Cambridge University Press.

Allen, J.R.M., Huntley, B. and Watts, W.A. (1996) The vegetation and climate of northwest Iberia over the last 14000 yr. *Journal of Quaternary Science*, 11, 125-147.

Alley, R. B., Mayewski, P.A., Sowers, T., Stuiver, M., Taylor, K.C. and Clark, P.U. (1997) Holocene climatic instability: A prominent, widespread event 8200 yr ago. *Geology*, 25, 483-486.

Alley, R.B. (2000) The Younger Dryas cold interval as viewed from central Greenland. *Quaternary Science Reviews*, 19, 213-226.

Alley, R.B. and Ágústsdóttir, A.M. (2005) The 8k event: cause and consequences of a major Holocene abrupt climate change. Quaternary Science Reviews, 24, 1123-1149.

Anderson, D.E., Goudie, A.S. and Parker, A.G. (2007). *Global environments through the Quaternary*. New York, Oxford University Press.

Andreo, B., Liñán, C., Carrasco, F., de Cisneros, C.J., Caballero, F. and Mudry, J. (2004) Influence of rainfall quantity on the isotopic composition (^{18}O and ^{2}H) of water in mountainous areas. Application for groundwater research in the Yunquera-Nieves karst aquifers (S Spain). *Applied Geochemistry*, 19, 561-574.

Anton, M.G., Romera, G.G., Pages, J.L. and Millan, A.A. (2006) The Holocene pollen record in the Villaviciosa Estuary (Asturias, North Spain). *Palaeogeography Palaeoclimatology Palaeoecology*, 237, 280-292.

Appenzeller, C., Stocker, T.F. and Ankiln, M. (1998) North Atlantic Oscillation dynamics recorded in Greenland ice cores. *Science*, 282, 446-449.

Arz, H.W., Lamy, F. and Pätzold, J. (2006) A pronounced dry event recorded around 4.2 ka in brine sediments from the northern Red Sea. *Quaternary Research*, 66, 432-441.

Asrat, A., Baker, A., Mohammed, M.U., Leng, M.J., van Calsteren, P. and Smith, C. (2007) A high-resolution multi-proxy stalagmite record from Mechara, Southeastern Ethiopia:

palaeohydrological implications for speleothem palaeoclimate reconstruction. *Journal of Quaternary Science*, 22(1), 53-63.

Ayalon, A., Bar-Matthews, M. and Sass, E. (1998) Rainfall-recharge relationships within a karstic terrain in the eastern Mediterranean semi-arid region, Israel: $\delta^{18}O$ and δD characteristics. *Journal of Hydrology*, 207, 18-31.

Ayalon, A., Bar-Matthews, M. and Kaufman, A. (1999) Petrography, strontium, barium and uranium concentrations, and strontium and uranium isotope ratios in speleothems as palaeoclimatic proxies: Soreq Cave, Israel. *The Holocene*, 9, 715-722.

Baker, A., Barnes, W.L. and Smart, P.L. (1997a) Variations in the discharge and organic matter content of stalagmite drip waters in Lower Cave, Bristol. *Hydrological Processes*, 11, 1541-1555.

Baker, A., Ito, E., Smart, P.L. and McEwan, R.F. (1997b) Elevated and variable values of ^{13}C in speleothems in a British cave system. *Chemical Geology*, 136, 263-270.

Baker, A., Genty, D., Drybrodt, W., Grapes, J. and Mockler, N.J. (1998) Testing theoretically predicted stalagmite growth rates with recent annually laminated samples: implications for past stalagmite deposition. *Geochimica et Cosmochimica Acta*, 62, 393-404.

Baker, A., Mockler, N.J. and Barnes, W.L. (1999) Fluorescence intensity variations of speleothem-forming groundwaters: Implications for palaeoclimate reconstruction. *Water Resources Research*, 35, 407-413.

Baker, A., Genty, D. and Fairchild, I.J. (2000) Hydrological characterisation of stalagmite dripwaters at Grotte de Villars, Dordogne, by the analysis of inorganic species and luminescent organic matter. *Hydrology and Earth System Sciences*, 4(3), 439-449.

Baker, A. and Brunsdon, C. (2003) Non-linearities in drip water hydrology: an example from Stump Cross Caverns, Yorkshire. *Journal of Hydrology*, 227, 151-163.

Baker, A., Asrat, A., Fairchild, I.J., Leng, M.J., Wynn, P.M., Bryant, C., Genty, D. & Umer, M. (2007) Analysis of the climate signal contained within $\delta^{18}O$ and growth rate parameters in two Ethiopian stalagmites. *Geochimica et Cosmochimica Acta*, 71, 2975-2988.

Baker, A., Smith, C.L., Jex, C., Fairchild, I.J., Genty, D. and Fuller, L. (2008) Annually Laminated Speleothems: a Review. *International Journal of Speleology*, 37(3), 193-206.

Baker, A., Asrat, A., Fairchild, I.J., Leng, M.J., Thomas, L., Widmann, M., Jex, C.N., Dong, B.W., van Calsteren, P. and Bryant, C. (2010) Decadal-scale rainfall variability in Ethiopia recorded in an annually laminated, Holocene-age, stalagmite. *The Holocene*, 20(6), 827-836.

Bakke, J., Lie, O., Heegaard, E., Dokken, T., Haug, G.H., Birks, H.H., Dulski, P. and Nilsen, T. (2009) Rapid oceanic and atmospheric changes during the Younger Dryas cold period. *Nature Geoscience*, 2, 202-205.

Baldini, J.U.L., McDermott, F., Baker, A., Baldini, L.M., Mattey, D.P. and Railsback, L.B. (2005) Biomass effects on stalagmite growth and isotope ratios: A 20th century analogue from Wiltshire, England. *Earth and Planetary Science Letters*, 240, 486-494.

Baldini, J.U.L., McDermott, F. and Fairchild, I.J. (2006a). Spatial variability in cave drip water hydrochemistry: Implications for stalagmite paleoclimate records. *Chemical Geology*, 235, 390-404.

Baldini, J.U.L., McDermott, F., Hoffmann, D.L., Richards, D.A. and Clipson, N. (2008) Very high-frequency and seasonal cave atmosphere PCO_2 variability: Implications for stalagmite growth and oxygen isotope-based paleoclimate records. *Earth and Planetary Science Letters*, 272, 118-129.

Baldini, J.U.L. (2010) Cave atmospheric controls on stalagmite growth rate and palaeoclimate records. In Pedley, H.M. and Rogerson, M. (eds) Tufas and Speleothems: Unravelling the microbial and physical controls. *Geological Society, London*, Special Publications, 336, 283-294.

Baldini, J.U.L., McDermott, F., Baldini, L.M., Ottley, C.J., Linge, K.L., Clipson, N. and Jarvis, K.E. (2012) Identifying short-term and seasonal trends in cave drip water trace element concentrations based on a daily-scale automatically collected drip water dataset. *Chemical Geology*, 330-331, 1-16.

Baldini, L.M., McDermott, F. and Baldini, J.U.L. (2006b) Detecting NAO-mode variability in high-resolution speleothem isotope records. Presented at the 16th V.M. Goldschmidt Conference *Geochimica et Cosmochimica Acta*, 70, A31-A31.

Baldini, L. M., McDermott, F., Foley, A.M. and Baldini. J.U.L. (2008) Spatial variability in the European winter precipitation $\delta^{18}O$-NAO relationship: Implications for reconstructing NAO-mode climate variability in the Holocene. Geophysical Research Letters, 35, L04709.

Baldini, L.M., McDermott, F., Baldini, J.U.L., Fischer, M.J. and Möllhoff, M. (2010) An investigation of the controls on Irish precipitation $\delta^{18}O$ values on monthly and event timescales. *Climate Dynamics*, 35, 977-993.

Bar-Matthews, M., Ayalon, A., Kaufman, A. and Wasserburg, G.J. (1999) The Eastern Mediterranean paleoclimate as a reflection of regional events: Soreq cave, Israel. *Earth and Planetary Science Letters*, 166, 85-95.

Barbaza, M. (2011) Environmental changes and cultural dynamics along the northern slope of the Pyrenees during the Younger Dryas. *Quaternary International*, 242, 313-327.

Barber, D.C., Dyke, A., Hillaire-Marcel, C., Jennings, A.E., Andrews, J.T., Kerwin, M.W., Bilodeau, G., McNeely, R., Southon, J., Morehead, M.D. and Gagnon, J.-M. (1999) Forcing of the cold event of 8,200 years ago by catastrophic drainage of Laurentide lakes. *Nature*, 400, 344-348.

Barker, P.A., Street-Perrott, F.A., Leng, M.J., Greenwood, P.B., Swain, D.L., Perrott, R.A., Telford, R.J. and Ficken, K.J. (2001) A 14,000 year old oxygen isotope record from diatom silica in two Alpine lakes on Mt. Kenya. *Science*, 292, 2307-2310.

Barlow, L.K., White, J.W.C., Barry, R.G., Rogers, J.C. and Grootes, P.M. (1993) The North Atlantic Oscillation signature in Deuterium and Deuterium excess signals in the Greenland Ice Sheet Project 2 ice core, 1840-1970. *Geophysical Research Letters*, 20(24), 2901-2904.

Bauer, S., Liedl, R. and Sauter, M. (2005) Modelling the influence of epikarst evolution on karst aquifer genesis: A time-variant recharge boundary condition for joint karst-epikarst development. *Water Resources Research*, 41, 12.

Bicho, N., Haws, J. and Almeida, F. (2011) Hunter-gatherer adaptations and the Younger Dryas in central and southern Portugal. *Quaternary International*, 242, 336-347.

Björck, S., Rittenour, T., Rosén, P., França, Z., Möller, P., Snowball, I., Wastegård, S., Bennike, O. and Kromer, B. (2006) A Holocene lacustrine record in the central North Atlantic: proxies from volcanic activity, short term NAO mode variability, and long-term precipitation changes. *Quaternary Science Reviews*, 25, 9-32.

Bjune, A.E., Bakke, J., Nesje, A. and Birks, H.J.G. (2005) Holocene mean July temperature and winter precipitation in western Norway inferred from palynological and glaciological lake-sediment proxies. The Holocene, 15(2), 177-189.

Black, D.E., Peterson, L.C., Overpeck, J.T., Kaplan, A., Evans, M.N. and Kashgarian, M. (1999) Eight centuries of North Atlantic Ocean atmosphere variability. *Science*, 286, 1709-1713.

Boch, R., Spotl, C. and Kramers, J. (2009) High-resolution isotope records of early Holocene rapid climate change from two coeval stalagmites of Katerloch Cave, Austria. *Quaternary Science Reviews*, 28, 2527-2538.

Boch, R., Spotl, C. and Frisia, S. (2011) Origin and palaeoenvironmental significance of lamination in stalagmites from Katerloch Cave, Austria. *Sedimentology*, 58, 508-531.

Bond, G., Showers, W., Cheseby, M., Lotti, R., Almasi, P., deMonocal, P., Priore, P., Cullen, H., Hajdas, I. and Bonani, G. (1997) A pervasive millennial-scale cycle in North Atlantic Holocene and glacial climates. *Science,* 278, 1257-1266.

Bond , G., Kromer, B., Beer, J., Muscheler, R., Evans, M.N., Showers, W., Hoffmann, S., Lotti-Bond, R., Hajdas, I. and Bonani, G. (2001) Persistent solar influence on North Atlantic climate during the Holocene. *Science*, 294, 2130-2136.

Borsato, A. (1997) Dripwater monitoring at Grotta di Ernesto (NE-Italy): a contribution to the understanding of karst hydrology and the kinetics of carbonate dissolution. Proceedings of the 12th International Congress of Speleology, 2, 57-59.

Borsato, A., Frisia, S., Fairchild, I.J., Somogyi, A. and Susini, J. (2007) Trace element distribution in annual stalagmite laminae mapped by micrometer-resolution X-ray fluorescence: Implications for incorporation of environmentally significant species. *Geochimica et Cosmochimica Acta*, 71, 1494-1512.

Bout-Rounazeilles, V., Combouriew Nebout, N., Peyron, O., Cortijo, E., Landais, A. and Masson-Delmotte, V. (2007) Connection between South Mediterranean climate and North African atmospheric circulation during the last 50,000 yr BP North Atlantic cold events. *Quaternary Science Reviews*, 26, 3197-3215.

Bradley, C., Baker, A., Jex, C.N. and Leng, M.J. (2010) Hydrological uncertainties in the modelling of cave drip-water delta O-18 and the implications for stalagmite palaeoclimate reconstructions. *Quaternary Science Reviews*, 29, 2201-2214.

Broecker, W.S., Denton, G.H., Edwards, R.L., Cheng, H., Alley, R.B., and Putnam, A.E. (2010) Putting the Younger Dryas cold event into context: *Quaternary Science Reviews*, 29, 1078-1081,

Brunet, M., Sigro, J., Saladie, O., Aguilar, E., Jones, P.D., Moberg, A., Walther, A., and López, D. (2005) Spatial patterns of long-term Spanish temperature change. *Geophysical Research Abstracts*, 7, 04007, European Geosciences Union 2005.

Carlson, A.E. (2008) Why there was not a Younger Dryas-like event during the Penultimate Deglaciation. *Quaternary Science Reviews*, 27, 882-887.

Carrasco, F., Aandreo, B., Liñán, C. and Mudry, J. (2006) Contribution of stable isotopes to the understanding of the unsaturated zone of a carbonate aquifer (Nerja Cave, southern Spain). *Comptes Rendus Geoscience*, 338, 1203-1212.

Carrión, J.S. (2002) Patterns and processes of Late Quaternary environmental change in a montane region of southwest Europe. *Quaternary science Reviews*, 21, 2047-2066.

Carrión, J.S., Fuentes, N., González-Sampériz, P., Sánchez Quirante, L., Finlayson, J.C., Fernández, S. and Andrade, A. (2007) Holocene environmental change in a montane region of southern Europe with a long history of human settlement. *Quaternary Science Reviews*, 26, 1455-1475.

Carrión, J.S., Fernández, S., González-Sampériz, P., Gil-Romera, G., Badal, E., Carrión-Marco, Y., López-Merino, L., López-Sáez, J., Fierro, E. and Burjachs, F. (2010) Expected trends and surprises in the Lateglacial and Holocene vegetation history of the Iberian Peninsula and Balearic Islands. *Review of Palaeobotany and Palynology*, 162, 458-475.

Chu, G.Q., Liu, J.Q., Sun, Q., Lu, H.Y., Gu, Z.Y., Wang, W.Y. and Liu, T.S. (2002) The 'Mediaeval Warm Period' drought recorded in Lake Huguangyan, tropical South China. *The Holocene*, 12(5), 511-516.

Clark, I. and Fritz, P. (1997) *Environmental isotopes in hydrogeology*. CRC Press/Lewis Publishers, Florida.

Clarke, P.U., Marshall, S.J., Clarke, G.K.C., Holetler, S.W., Licciardi, J.M. and teller, J.T. (2001) Freshwater forcing of abrupt climate change during the last glaciation. *Science*, 293, 283-287.

Clemens, S.C. (2005) Millennial-band climate spectrum resolved and linked to centennial-scale solar cycles, *Quaternary Science Reviews*, 24, 521-531.

Collister, C. and Mattey, D. (2008) Controls on water drop volume at speleothem drip sites: An experimental study. *Journal of Hydrology*, 358, 259-267.

Coplen, T.B. (2007) Calibration of the calcite-water oxygen-isotope geothermometer at Devils Hole, Nevada, a natural laboratory. *Geochimica et Cosmochimica Acta*, 71, 3948-3957.

Cosford, J., Qing, H.R., Mattey, D., Eglington, B. and Zhang, M.L. (2009) Climatic and local effects on stalagmite $\delta^{13}C$ values at Lianhua Cave, China. *Palaeogeography Palaeoclimatology Palaeoecology*, 280, 235-244.

Craig, H. (1961) Standard for reporting concentrations of deuterium and oxygen-18 in natural water. *Science*, 133, 1702-1703.

Cronin, T.M., Hayo, K., Thunell, R.C., Dwyer, G.S., Saenger, C. and Willard, D.A. (2010) The Medieval Climate Anomaly and Little Ice Age in Chesapeake Bay and the North Atlantic Ocean. *Palaeogeography Palaeoclimatology Palaeoecology*, 297, 299-310.

Cruz, F.W., Burns, S.J., Jercinovic, M., Karmann, I., Sharp, W.D. and Vuille, M. (2007) Evidence of rainfall variations in Southern Brazil from trace element ratios (Mg/Ca and Sr/Ca) in a Late Pleistocene stalagmite. *Geochimica et Cosmochimica Acta*, 71, 2250-2263.

Curry, R.G. and McCartney, S. (2001) Ocean gyre circulation changes associated with the North Atlantic Oscillation. *Journal of Physical Oceanography*, 31, 3374-3400.

Czaja, A. and Frankignoul, C. (2002) Observed impact of Atlantic SST anomalies on the North Atlantic Oscillation. Journal of Climate,15, 606-623.

Dansgaard, W. (1964) Stable isotopes in precipitation. *Tellus*, 16, 436-468.

Dandgaard, W., Johnsen, S.J., Clausen, H.B., Dahl-Jensen, D., Gundestrup, N.S., Hammer, C.U., Hvidberg, C.S., Steffensen, J.P., Sveinbjöornsdottir, A.E., Jouzel, J. and Bond, G. (1993) Evidence for general instability of past climate from a 250-kry ice-core record. *Nature*, 364, 218-220.

Davis, B. A. S. and Stevenson, A. C. (2007) The 8.2ka event and Early-Mid Holocene forests, fires and flooding in the central Ebro Desert, NE Spain. *Quaternary Science Reviews*, 26, 1695-1712.

Debret, M., Bout-Roumazeilles, V., Grousset, F., Desmet, M., McManum, J.F., Massei, N., Sebag, D., Petit, J.-R., Copard, Y. and Trentesaux, A. (2007) The origin of the 1500-year climate cycles in Holocene North-Atlantic records. *Climate of the Past*, 3, 569-575.

Debret, M., Sebag, D., Crosta, X., Massei, N., Petit, J.-R., Chapron, E. and Bout-Roumazeilles, V. (2009) Evidence from wavelet analysis for a mid-Holocene transition in global climate forcing. *Quaternary Science Reviews*, 28, 2675-2688.

DeMenocal, P., Ortiz, J., Guilderson, T., Adkins, J., Sarnthein, M., Baker, L. and Yarusinsky, M. (2000a) Abrupt onset and termination of the African Humid Period: rapid climate responses to gradual insolation forcing. *Quaternary Science Reviews*, 19, 347-361.

DeMenocal, P., Ortiz, J., Guilderson, T. and Sarnthein, M. (2000b) Coherent high- and low-latitude climate variability during the Holocene Warm Period. *Science*, 288, 2198-2202.

DeMenocal, P.B. (2001). Cultural responses to climate change during the Late Holocene. *Science*, 292(5517), 667-673.

DeMenocal, P B. (2011) Climate and Human Evolution. *Science*, 331, 540-542.

Desprat, S., Goñi, M.F.S. and Loutre, M. F. (2003) Revealing climatic variability of the last three millennia in northwestern Iberia using pollen influx data. *Earth and Planetary Science Letters*, 213, 63-78.

Dezileau, L., Sabatier, P., Blanchmanche, P., Joly, B., Swingedouw, D., Cassou, C., Castaings, J., Matrinez, P. and Von Grafenstein, U. (2011) Intence storm activity during the Little Ice Age on the French Mediterranean coast. *Palaeogeography Palaeoclimatology Palaeoecology*, 299, 289-297.

Diaz, H.F., Trigo, R., Hughes, M.K., Mann, M.E., Xoplaki, E. and Barriopedro, D. (2011) Spatial and temporal characteristics of climate in medieval times revisited. *Bulletin of the American Meteorological Society*, 92, 1487-1500.

Dickinson, S.R., Henderson, G.E. and McGrath, K.M. (2002) Controlling the kinetic versus thermodynamic crystallisation of calcium carbonate. *Journal of Crystal Growth*, 244, 369-378.

Dima, M. and Lohmann, G. (2009) Conceptual model for millennial climate variability: a possible combined solar-thermohaline circulation origin for the ~1500-year cycle. *Climate Dynamics*, 32, 301-311.

Dominguez-Villar, D., Wang, X.F., Cheng, H., Martin-Chivelet, J. and Edwards, R.L. (2008) A high-resolution late Holocene speleothem record from Kaite Cave, northern Spain: $\delta^{18}O$ variability and possible causes. *Quaternary International*, 187, 40-51.

Dominguez-Villar, D., Fairchild, I.J., Baker, A., Wang, X., Edwards, L.R. and Cheng, H. (2009) Oxygen isotope precipitation anomaly in the North Atlantic region during the 8.2 ka event. *Geology*, 37, 1095-1098.

Dorale, J.A. and Liu, Z.H. (2009) Limitations of the Hendy test criteria in judging the palaeoclimatic suitability of speleothems and the need for replication. *Journal of Cave and Karst Studies*, 71, 73-80.

Dormoy, I., Peyron, O., Combourieu Nebout, N., Goring, S., Kotthoff, U., Magny, M. and Pross, J. (2009) Terrestrial climate variability and seasonality changes in the Mediterranean region between 15 000 and 4000 years BP deduced from marine pollen records. *Climate of the Past*, 5, 615-632.

Dracler, R.R. and Rolph, G.D. (2014) HYSPLIT (HYbrid Single-Particle Lagrangian Integrated Trajectory) model access via NOAA website (http://ready.arl.noaa.gov/HYSPLIT.php). NOAA Air Resources Laboratory, Silver Spring, MD.

Dredge, J., Fairchild, I.J., Harrison, R.M., Fernandez-Cortes, A., Sanchez-Moral, S., Jurado, V., Gunn, J., Smith, A.C., Spötl, C., Mattey, D., Wynn, P. and Grassineau. (2013) Cave aerosols: distribution and contribution to speleothem geochemistry. *Quaternary Science Reviews*, 63, 23-41.

Dreybrodt, W. (1999) Chemical kinetics, speleothem growth and climate. *Boreas*, 28, 347-356.

Drysdale, R.N., Zanchetta, G., Hellstrom, J.C., Fallick, A.E., McDonald, J. and Cartwright, I. (2007) Stalagmite evidence for the precise timing of North Atlantic cold events during the early last glacial. *Geology*, 35, 77-80.

Dulinski, M. and Rozanski, K. (1990) Formation of ^{13}C / ^{12}C isotope ratios in speleothems: a semi-dynamic model. *Radiocarbon*, 32, 7-16.

Dylmer, C.V., Giraudeau, J., Eynaud, F., Husum, K. and De Vernal, A. (2013) Northward advection of Atlantic water in the eastern Nordic Seas over the last 3000 yr. *Climate of the Past*, 9, 1505-1518.

Eiriksson, J., Bartels-Jónsdóttir, H.B., Cage, A.G., Gudmundsdóttir, E.R., Klitgaard-Kristensen, D., Marret, F., Rodrigues, T., Abrantes, F., Austin, W.E.N., Jiang, H., Knudsen, K.L. and Sejrup, H.P. (2006) Variability of the North Atlantic Current during the last 2000 years based on shelf

bottom water and sea surface temperatures along an open ocean/shallow marine transect in western Europe. *The Holocene,* 16, 1017-1029.

Elkibbi, M. and Rial, J.A. (2001) An outsider's review of the astronomical theory of the climate: is the eccentricity-driven insolation the main driver of the ice ages? *Earth-Science Reviews*, 56, 161-177.

Fairchild, I.J., Borsato, A., Tooth, A.F., Frisia, S., Hawkesworth, C.J., Huang, Y., McDermott, F. and Spiro, B. (2000) Controls on trace element (Sr-Mg) compositions of carbonate cave waters: implications for speleothem climatic records. *Chemical Geology*, 166, 255-269.

Fairchild, I.J., Baker, A., Borsato, A., Frisia, S., Hinton, R.W., McDermott, F. and Tooth, A.F. (2001) Annual to sub-annual resolution of multiple trace-element trends in speleothems. *Journal of the Geological Society, London*, 158, 831-841.

Fairchild, I.J., Frisia, S., Borsato, A. and Tooth, A.F. 2005 Speleothems in their geomorphic, hydrogeological and climatological context. In: Nash, D.J. and McLaren, S.J. (eds.) *Geochemical Sediments and Landscapes.* Blackwells, Oxford.

Fairchild, I.J., Smith, C.L., Baker, A., Fuller, L., Spotl, C., Mattey, D., McDermott, F. and EIMP (2006a) Modification and preservation of environmental signals in speleothems. *Earth-Science Reviews*, 75, 105-153.

Fairchild, I.J., Tuckwell, G.W., Baker, A. and Tooth, A.F. (2006b) Modelling of dripwater hydrology and hydrogeochemistry in a weakly karstified aquifer (Bath, UK): Implications for climate change studies. *Journal of Hydrology*, 321, 213-231.

Fairchild, I.J. and McMillan, E.A. (2007) Speleothems as indicators of wet and dry periods. *International Journal of Speleology*, 36(2), 69-74.

Fairchild, I.J. and Treble, P.C. (2009) Trace elements in speleothems as recorders of environmental change. *Quaternary Science Reviews*, 28, 449-468.

Fairchild, I.J., Spotl, C., Frisia, S., Borsato, A., Susini, J., Wynn, P. M., Cauzid, J. and EIMF. (2010) Petrology and geochemistry of annually laminated stalagmites from an Alpine cave (Obir, Austria): seasonal and cave physiology. In: Pedley, H.M. & Rogerson, M. (eds.) *Tufas and Speleothems: Unravelling the Microbial and Physical Controls.* The Geological Society, Special Publications, London.

Fairchild, I.J. and Baker, A. (2012) *Speleothem Science*. Wiley-Blackwell, Sussex, UK.

Fawcett, P.J., Ágústsdóttir, A.M., Alley, R.B. and Shuman, C.A. (1997) The Younger Dryas termination and North Atlantic Deep Water Formation: Insights from climate model simulations and Greenland ice cores. *Paleoceanography*, 12(1), 23-38.

Fernández-Cortés, A., Calaforra, J.M., Sánchez-Martos, F. and Gisbert, J. (2007) Stalactite drip rate variations controlled by air pressure changes: an example of non-linear infiltration processes in the 'Cueva del Agua' (Spain). *Hydrological Processes*, 21, 920-930.

Fletcher, W.J., Debret, M., Sanchez Goñi, M.F. (2013) Mid-Holocene emergence of a low-frequency millennial oscillation in western Mediterranean climate: Implications for past dynamics of the North Atlantic atmospheric westerlies. *The Holocene*, 23(2), 153-166.

Ford, D.C. (1997) Dating and Paleo-Environmental studies of Speleothems. In: Hill, C.A. and Forti, P. (eds.) Cave Minerals of the World. Huntsville: National Speleological Society, Huntsville.

Ford, D.C. and Williams, P.W. (2007) *Karst Hydrogeology and Geomorphology*. Wiley and Sons Ltd, Chichester.

Frisia, S. and Borsato, A. (2010) Karst. In Alonso-Zarza, A.M. and Tanner, L.H. (eds) Carbonates in Continental Settings: Facies, Environments, and Processes. *Developments in Sedimentology*, 61, Elsevier. B. V.

Frisia, S., Borsato, A., Fairchild, I.J. and McDermott, F. (2000) Calcite fabrics, growth mechanisms, and environments of formation in speleothems from the Italian Alps and southwestern Ireland. *Journal of Sedimentary Research*, 70(5), 1183-1196.

Frisia, S., Borsato, A., Fairchild, I.J., McDermott, F. and Selmo, E.M. (2002) Aragonite-calcite relationships in speleothems (Grotte de Clamouse, France): Environment, fabrics, and carbonate geochemistry. *Journal of Sedimentary Research*, 72, 687-699.

Frisia, S., Borsato, A., Fairchild, I.J. and Susini, J. (2005) Variations in atmospheric sulphate recorded in stalagmites by synchrotron micro-XU and XANES analyses. *Earth and Planetary Science Letters*, 235, 729-740.

Frisia, S., Fairchild, I.J., Fohlmeister, J., Miorandil, R., Spotl, C. and Borsato, A. (2011) Carbon mass-balance modelling and carbon isotope exchange processes in dynamic caves. *Geochimica et Cosmochimica Acta*, 75, 380-400.

Fritz, P. and Fontes, J.C. (1980) *Handbook of Environmental Isotope Geochemistry*. Elsevier Scientific Publishing Company, Amsterdam.

Fuller, L., Baker, A., Fairchild, I.J., Spotl, C., Marca-Bell, A., Rowe, P. and Dennis, P.F. (2008) Isotope hydrology of dripwaters in a Scottish cave and implications for stalagmite palaeoclimate research. *Hydrology and Earth System Sciences*, 12, 1065-1074.

Gallego, M.C., Garcia, J.A. and Vaquero, M.J. (2005) The NAO signal in daily rainfall series over the Iberian Peninsula. *Climate Research*, 29, 103-109.

Garcia, M.J.G, Valiño, M.D., Rodriguez, A.V. and Zapata, M.B.R. (2002) Late-glacial and Holocene palaeoclimate record from Sierra de Cebollera (Northern Iberian Range, Spain). *Quaternary International*, 93-94, 13-18.

Gascoyne, M. (1983) Trace-element partition-coefficients in the calcite water-system and their palaeoclimatic significance. *Journal of Hydrology*, 61, 213-222.

Gasse, F. (2000) Hydrological changes in the African tropics since the Last Glacial Maximum. *Quaternary Science Reviews*, 19, 189-211.

Gasse, F. (2001) Hydrological changes in Africa. *Science*, 22 (5525), 2259-2260.

Genty, D. and Deflandre, G. (1998) Drip flow variations under a stalactite of the Père Noël cave (Belgium). Evidence of seasonal variations and air pressure constraints. *Journal of Hydrology*, 211, 208-232.

Genty, D., Baker, A., Massault, M., Proctor, C., Gilmour, M., Pons-Branchu, E. and Hamelin, B. (2001) Dead carbon in stalagmites: Carbonate bedrock paleodissolution vs. ageing of soil organic matter. Implications for ^{13}C variations in speleothems. *Geochimica et Cosmochimica Acta*,65(20), 3443-3457.

Genty, D., Balmart, D., Ouahdi, R., Gilmour, M., Baker, A., Jouzel, J. and Van-Exter, S. (2003) Precise dating of Dansgaard-Oeschger climate oscillations in western Europe from stalagmite data. *Nature*, 421, 833-837.

Gil, I.M., Abrantes, F. and Hebbeln, D. (2006) The North Atlantic Oscillation forcing through the last 2000 years: Spatial variability as revealed by high-resolution marine diatom records from N and SW Europe. *Marine Micropaleontology*, 60, 113-129.

Giraudeau, J., Jennings, A.E. and Andrews, J.T. (2004) Timing and mechanisms of surface and intermediate water circulation changes in the Nordic Seas over the last 10,000 cal years: a view from the North Iceland shelf. *Quaternary Science Reviews*. 23, 2127-2139.

Giraudeau, J., Grelaud, M., Solignac, S., Andrews, T.J., Moros, M. and Jansen, E. (2010) Millennial-scale variability in Atlantic water advection to the Nordic Seas derived from Holocene coccolith concentration records. *Quaternary Science Reviews*, 29, 1276-1287.

Goede, A., McCulloch, M., McDermott, F. and Hawkesworth, C. (1998) Aeolian contribution to strontium and strontium isotope variations in a Tasmanian speleothem. *Chemical Geology*, 149, 37-50.

Gonzalez, L.A., Carpenter, S.J. and Lohmann, K.C. (1993) Columnar calcite in speleothems - reply. *Journal of Sedimentary Petrology*, 63, 553-556.

González-Sampériz, P., Valero-Garcés, B.L., Moreno, A., Jalut, G., Garcia-Ruiz, J.M., Marti-Bono, C., Delgardo-Huertas, A., Navas, A., Otto, T. and Dedoubat, J.J. (2006) Climate variability in the Spanish Pyrenees during the last 30,000 yr revealed by the El Portalet sequence. *Quaternary Research*, 66, 38-52.

González-Sampériz, P., Valero-Garcés, B.L., Moreno, A., Morellón, M., Navas, A., Machin, J. and Delgardo-Huertas, A, (2008) Vegetation changes and hydrological fluctuations in the Central Ebro Basin(NE Spain) since the Late Glacial period: Saline lake records. *Palaeogeography Palaeoclimatology Palaeoecology*, 259, 157-181.

Goodess, C.M. and Jones, P.D. (2002) Links between circulation and changes in the characteristics of Iberian rainfall. *International Journal of Climatology*, 22, 1593-1615.

Griffiths, M.L., Drysdale, R.N., Vonhof, H.B., Gagan, M.K., Zhao, J.X., Ayliffe, L.K., Hantoro, W.S., Hellstrom, J.C., Cartwright, I., Frisa, S. and Suwargadi, B.W. (2010) Younger Dryas - Holocene temperature and rainfall history of southern Indonesia from $\delta^{18}O$ in speleothem calcite and fluid inclusions. *Earth and Planetary Science Letters*, 295, 30-36.

Guo W. (2008) Carbonate clumped isotope thermometry: application to carbonaceous chondrites and effects of kinetic isotope fractionation. Ph. D. thesis, Caltech. Available at: <http://resolver.caltech.edu/CaltechETD:etd-12182008-115035>.

Gutiérrez, J.C.F. (2010) The geology around Matienzo. In: Corrin, J. and Smith, P. (eds) *Matienzo 50 years of speleology*. Matienzo caves, Lancashire.

Hammarlund, D. and Edwards, T.W.D. (2008) Stable isotope variations in stalagmites from northwestern Sweden document changes in temperature and vegetation during the early Holocene: a comment on Sundqvist et al. 2007a. *The Holocene*, 18, 1007-1008.

Hardt, B., Rowe, H.D., Springer, G.S., Cheng, H. and Edwards, R.L. (2010) The seasonality of east central North American precipitation based on three coeval Holocene speleothems from southern West Virginia. *Earth and Planetary Science Letters*, 295, 342-348.

Hartland, A., Fairchild, I.J. and Lead, J.R. (2009) Colloids in karstic percolation waters: Implications for the interpretation of trace element variations in speleothems. Presented at the 19th V.M. Goldschmidt Conference, *Geochimica et Cosmochimica Acta*, 73(13), A498-A498.

Hartland, A., Fairchild, I.J., Lead, J.R., Zhang, H. and Baalousha, M. (2011) Size, speciation and lability of NOM-metal complexes in hyperalkaline cave dripwater. *Geochimica et Cosmochimica Acta*, 75, 7533-7551.

Hartland, A., Fairchild, I.J., Lead, J.R., Borsato, A., Baker, A., Frisia, S. and Baalousha, M. (2012) From soil to cave: Transport of trace metals by natural organic matter in karst dripwaters. *Chemical Geology*, 304-305, 68-82.

Heiri, O., Tinner, W. and Lotter, A.F. (2004) Evidence for cooler European summers during periods of changing meltwater flux to the North Atlantic. *Proceedings of the National Academy of Sciences of the United States of America,* 101(43), 15285-15288.

Hellstrom, J.C. and McCulloch, M.T. (2000) Multi-proxy constraints on the climatic significance of trace element records from a New Zealand speleothem. *Earth and Planetary Science Letters*, 179, 287-297.

Hellstrom, J. (2006) U-Th dating of speleothems with high initial Th-230 using stratigraphical constraint. *Quaternary Geochronology*, 1, 289-295.

Hendy, C.H. (1971) The isotopic geochemistry of speleothems - 1. The calculation of the effects of different modes of formation on the isotopic composition of speleothems and their applicability as palaeoclimatic indicators. *Geochimica et Cosmochimica Acta*, 35, 801-824.

Höbig, N., Weber, M.E., Kehl, M., Weniger, G-C., Juliá, R., Melles, M., Fűlöp, R-H., Vogel, H. and Reicherter, K. (2012) Lake Banyoles (northeastern Spain):A Last Glacial to Holocene

multi-proxy study with regard to environmental variability and human occupation. *Quaternary International*, 274, 205-218.

Hodge, E.J., Richards, D.A., Smart, P.L., Andreo, B., Hoffmann, D.L., Mattey, D.P. and González-Ramón, A. (2008) Effective precipitation in southern Spain (~266 to 46 ka) based on a speleothem stable carbon isotope record. *Quaternary Research*, 69, 447-457.

Hoefs, J. (1973) Stable isotope Geochemistry. In: Von Englehardt, W., Hahn, T. and Roy, R. (eds.) *Minerals, Rocks and Inorganic Materials*. Springer-Verlag Berlin, New York.

Hu, C.Y., Huang, J.H., Fang, N.Q., Xie, S.C., Henderson, G.M. and Cai, Y.J. (2005) Adsorbed silica in stalagmite carbonate and its relationship to past rainfall. *Geochimica et Cosmochimica Acta*, 69(9), 2285-2292.

Hu, F.S., Kaufman, D., Yoneji, S., Nelson, D., Shemesh, A., Huang, Y., Tian, J., Bond, G., Clegg, B. and Brown, T. (2003) Cyclic variation and solar forcing of Holocene climate in the Alaskan subarctic. *Science*, 301, 1890-1893.

Huang, C.C., Pang, J.L., Zha, X.C., Zhou, Y.L., Su, H.X. and Li, Y.G. (2010) Extraordinary Floods of 4100-4000 a BP recorded at the Late Neolithic Ruins in the Jinghe River Gorges, Middle Reach of the Yellow River, China. *Palaeogeography Palaeoclimatology Palaeoecology*, 289, 1-9.

Huang, H.M., Fairchild, I.J., Borsato, A., Frisia, S., Cassidy, N. J., Mcdermott, F. and Hawkesworth, C.J. (2001) Seasonal variations in Sr, Mg and P in modern speleothems (Grotta di Ernesto, Italy). *Chemical Geology*, 175, 429-448.

Huang, Y.M. and Fairchild, I.J. (2001) Partitioning of Sr^{2+} and Mg^{2+} into calcite under karst-analogue experimental conditions. *Geochimica et Cosmochimica Acta*, 65(1), 47-62.

Hughes, M.K. and Diaz, H.F. (1994) Was there a 'Medieval Warm Period' and if so, where and when? *Climatic Change*, 26, 109-142.

Hulme, M., Barrow, E.M., Arnell, N.W., Harrison, P.A., Johns, T.C. and Downing, T.E. (1999) Relative impacts of human-induced climate change and natural climate variability. *Nature*, 397, 688-691.

Hulme, M. (2003) Abrupt climate change: can society cope? *Philosophical Transactions of the Royal Society of London Series a-Mathematical Physical and Engineering Sciences*, 361, 2001-2019.

Hurrell, J.W. (1995) Decadal trends in the North Atlantic Oscillation: Regional temperatures and precipitation. *Science*, 269(5224), 676-679.

Hurrell, J.W. and Van Loon, H. (1997) Decadal variations in climate associated with the North Atlantic Oscillation. *Climatic Change*, 36, 301-326.

Hurrell, J.W., Kushnir, Y. and Visbeck, M. (2001) Climate - The North Atlantic oscillation. *Science*, 291, 603-605.

Hurrell, J.W., Kushnir, Y., Ottersen, G. and Visbeck, M. (2003) An overview of the North Atlantic Oscillation. *Geophysical Monograph*, 134.

Hurrell, J.W. and Deser, C. (2009) North Atlantic climate variability: The role of the North Atlantic Oscillation. *Journal of Marine Systems*, 78, 28-41.

IAEA/WMO (2014). Global Network of Isotopes in Precipitation. The GNIP Database. Accessible at: http://www.iaea.org/water.

Ivanovich, M. and Harmon, R.S. (1992) *Uranium-series Disequlibrium: Applications to earth, marine and environmental sciences*. Oxford University Press, New York.

Jackson, A.S., McDermott, F. and Mangini, A. (2008) Late Holocene climate oscillations and solar fluctuations from speleothem STAL-AH-1, Sauerland, Germany: A numerical perspective. *Geophysical Research Letters*, 35, 5.

Jalut, G., Amat, A.E., Bonnet, L., Gauquelin, T. and Fontugne, M. (2000) Holocene climatic changes in the Western Mediterranean, from south-east France to south-east Spain. *Palaeogeography Palaeoclimatology Palaeoecology*, 160, 255-290.

Jex, C.N., Baker, A., Fairchild, I.J., Eastwood, W.J., Leng, M.J., Sloane, H.J., Thomas, L. and Bekaroglu, E. (2010) Calibration of speleothem $\delta^{18}O$ with instrumental climate records from Turkey. *Global and Planetary Change*, 71, 207-217.

Jiménez de Cisneros, C., Caballero, E., Vera, J.A., Durán, J.J. and Juliá, R. (2003) A record of Pleistocene climate from a stalactite, Nerja Cave, southern Spain. *Palaeogeography, Palaeoclimatology, Palaeoecology,* 189, 1-10.

Jochum, K.P., Weis, U., Stoll, B., Kuzmin, D., Yang, Q., Raczek, I., Jacob, D.E., Stracke, A., Birbaum, K., Frick, D.A., Gűnther, D. and Enzweiler, J. (2011) Determination of reference

values for NIST SRM 610-617 glasses following ISO guidelines. *Geostandards and Geoanalytical Research*, 35(4), 397-429.

Johnson K.R., Chaoyong H., Belshaw N.S., and Henderson G.M. 2006 Seasonal trace-element and stable-isotope variations in a Chinese speleothem: The potential for high resolution palaeomonsoon reconstruction. *Earth and Planetary Science Letters*, 244: 394-407.

Jones, P.D., Jonsson, T. and Wheeler, D. (1997) Extension to the North Atlantic Oscillation using early instrumental pressure observations from Gibraltar and south-west Iceland. *International Journal of Climatology*, 17, 1433-1450.

Kaal, J., Marco, Y.C., Asouti, E., Seijo, M.M., Cortizas, A.M., Casais, M.C. and Boado, F.C. (2011) Long-term deforestation in NW Spain: linking the Holocene fire history to vegetation change and human activities. *Quaternary Science Reviews*, 30, 161-175.

Kendall, A.C. (1993) Columnar calcite in speleothems: Discussion. *Journal of Sedimentary Petrology*, 63, 550-552.

Kendall, A.C. and Broughton, P.L. (1978) Origin of fabrics in speleothems composed of columnar calcite crystals. *Journal of Sedimentary Petrology*, 48, 519-538.

Kim, S.T. & O'Neil, J.R. (1997) Equilibrium and nonequilibrium oxygen isotope effects in synthetic carbonates. *Geochimica et Cosmochimica Acta*, 61(16), 3461-3475.

Kivastik, J. (1998) Paediatric reference values for spirometry. *Clinical Physiology*, 18, 489-497.

Kluge, T., Riechelmann, D.F.C., Wieser, M., Spotl, C., Sűltenfuß, J., Schröder-Ritzru, A., Niggemann, S. and Aeschbach-Hertig, W. (2010) Dating cave drip water by tritium. *Journal of Hydrology*, 394, 396-406.

Lachniet, M.S. (2009) Climatic and environmental controls on speleothem oxygen-isotope values. *Quaternary Science Reviews*, 28, 412-432.

Lamb, H., Roberts, N., Leng, M., Barker, P., Benkaddour, A. and van der Kaars, S. (1999) Lake evolution in a semi-arid montane environment: responses to catchment change and hydroclimatic variation. *Journal of Paleolimnology*, 21, 325-343.

Lange, J., Arbel, Y., Grodek, T. and Greenbaum, N. (2010) Water percolation process studies in a Mediterranean karst area. *Hydrological Processes*, 24, 1866-1879.

Lebreiro, S.M., Frances, G., Abrantes, F.F.G., Diz, P., Bartels-Jónsdóttir, H.B., Strynowski, Z.N., Gil, I.M., Pena, L.D., Rodrigues, T., Jones, P.D., Nombela, M.A., Alejo, I., Briffa, K.R., Harris, I. and Grimalt, J.O. (2006) Climate change and coastal hydrographic response along the Atlantic Iberian margin (Tagus Prodelta and Muros Ria) during the last two millennia. *The Holocene*, 16(7), 1003-1015.

Li, X.Y., Contreras, S. and Sole-Benet, A. (2008) Unsaturated hydraulic conductivity in limestone dolines: Influence of vegetation and rock fragments. *Geoderma*, 145, 288-294.

Lopez-Merino, L., Cortizas, A.M. and Lopez-Saez, J.A. (2010) Early agriculture and palaeoenvironmental history in the North of the Iberian Peninsula: a multi-proxy analysis of the Monte Areo mire (Asturias, Spain). *Journal of Archaeological Science*, 37, 1978-1988.

Luo, W.J. and Wang, S.J. (2009) Transmission of $\delta^{13}C$ signals and its paleoclimatic implications in Liangfeng Cave system of Guizhou Province, SW China. *Environmental Earth Sciences*, 59, 655-661.

Magny, M., Miramont, C. and Sivan, O. (2002) Assessment of climate and anthropogenic factors on Holocene Mediterranean vegetation in Europe on the basis of palaeohydrological records. *Palaeogeography, Palaeoclimatology, Palaeoecology*, 186, 47-59.

Magny, M., Bégeot, C., Guiot, J. and Peyron, O. (2003) Contrasting patterns of hydrological changes in Europe in response to Holocene climate cooling phases. *Quaternary Science Reviews*, 22, 1589-1596.

Magny, M. and Bégeot, C. (2004) Hydrological changes in European midlatitudes associated with freshwater outburst from Lake Agassiz during the Younger Dryas event and the early Holocene. *Quaternary Research*, 61, 181-192.

Magny, M., Vannière, B., Zanchetta, G., Fouache, E., Touchais, G., Petrika, L., Coussot, C., Walter-Simonnet, A.V. and Arnaud, F. (2009) Possible complexity of the climatic event around 4300-3800 cal. BP in the central and western Mediterranean. *The Holocene*, 19, 823-833.

Maher, B.A. (2008) Holocene variability of the East Asian summer monsoon from Chinese cave records: a re-assessment. *The Holocene*, 18(6), 861-866.

Martin-Chivelet, J., Muños-Garcia, M.B., Edwards, R.L., Turrero, M.J. and Ortega, A.I. (2011) Land surface temperature changes in Northern Iberia since 4000 yr BP, based on $\delta^{13}C$ of speleothems. *Global and Planetary Change*, 77, 1-12.

Martin-Puertas, C., Valero-Garcés, B.L., Mata, M.P., González-Sampériz, P., Bao, R., Moreno, A. and Stefanova, V. (2008) Arid and humid phases in southern Spain during the last 4000 years: the Zoñar Lake record, Córdoba. *The Holocene*, 18(6), 907-921.

Martinez-Pillado, V., Aranburu, A., Arsuaga, J.L., Ruiz-Zapata, B., Gil-Garcia, M.J., Stoll, H., Yusta, I., Iriarte, E., Carretero, J.M., Edwards, R.L. and Cheng, H. (2014) Upper Pleistocene and Holocene palaeoenvironmental records in Cueva Major karst (Atapuerca, Spain) from different proxies: speleothem crystal fabrics, palynology and archaeology. *International Journal of Speleology*, 43(1), 1-14.

Marshall, J., Johnson, H. and Goodman, J. (2001) A study of the interaction of the North Atlantic Oscillation with ocean circulation. *Journal of Climate*, 14, 1399-1421.

Maslin, M., Pike, J., Stickley, C. and Ettwein, V. (2005) Evidence of Holocene climate variability in marine sediments. In: Mackay, A., Battarbee, R., Birks, J. and Oldfield, F. (eds.) *Global Change in the Holocene.* New York: Oxford University Press.

Mattey, D., Lowry, D., Duffet, J., Fisher, R., Hodge, E. and Frisia, S. (2008) A 53 year seasonally resolved oxygen and carbon isotope record from a modem Gibraltar speleothem: Reconstructed drip water and relationship to local precipitation. *Earth and Planetary Science Letters*, 269, 80-95.

Mattey, D., Fairchild, I.J., Atkinson, T.C., Latin, J-P., Ainsworth, M. and Durell, R. (2010) Seasonal microclimate control of calcite fabrics, stable isotopes and trace elements in modern speleothem from St Michaels Cave, Gibraltar. In Pedley, H.M. and Rogerson, M. (eds) Tufas and Speleothems: Unravelling the microbial and physical controls. *Geological Society, London*, Special Publications, 336, 283-294.

Mattey, D.P., Fisher, R., Atkinson, T.C., Latin, J.-P., Durrell, R., Ainsworth, M., Lowry, D. and Fairchild, I.J. (2013) Methane in underground air in Gibraltar karst. *Earth and Planetary Science Letters*, 374, 71-80.

Mayewski, P.A., Rohling, E.E., Stager, J.C., Karlen, W., Maasch, K.A., Meeker, L.D., Meyerson, E.A., Gasse, F., van Kreveld, S., Holmgren, K., Lee-Thorp, J., Rosqvist, G., Rack, F.,

Staubwasser, M., Schneider, R.R. and Steig, E.J. (2004) Holocene climate variability. *Quaternary Research*, 62, 243-255.

McDermott, F., Frisia, S., Huang, Y., Longinelli, A., Spiro, B., Heaton, T.H.E., Hawkesworth, C.J., Borsato, A., Keppens, E., Fairchild, I.J., van der Borg, K., Verheyden, S. and Selmo, E. (1999) Holocene climate variability in Europe: Evidence from $\delta^{18}O$, textural and extension-rate variations in three speleothems. *Quaternary Science Reviews*, 18, 1021-1038.

McDermott, F., Mattey, D.P. and Hawkesworth, C. (2001) Centennial-scale Holocene climate variability revealed by a high resolution speleothem $\delta^{18}O$ record from SW Ireland. *Science*, 294, 1328-1331.

McDermott, F. (2004). Palaeo-climate reconstruction from stable isotope variations in speleothems: a review. *Quaternary Science Reviews*, 23, 901-918.

McDonald, J., Drysdale, R., Hill, D., Chisari, R. and Wong, H. (2007) The hydrochemical response of cave drip waters to sub-annual and inter-annual climate variability, Wombeyan Caves, SE Australia. *Chemical Geology*, 244, 605-623.

McGillen, M. and Fairchild, I.J. (2005) An experimental study of the controls on incongruent dissolution of $CaCO_3$ under analogue glacial conditions. *Journal of Glaciology*, 51, 383-390.

McManus, J.F., Francois, R., Gherardil, J.M., Keigwin, L.D. and Brown-Leger, S. (2004) Collapse and rapid resumption of Atlantic meridional circulation linked to deglacial climate changes. *Nature*, 428, 834-837.

McMillan, E.A., Fairchild, I.J., Frisia, S., Borsato, A. and McDermott, F. (2005) Annual trace element cycles in calcite-aragonite speleothems: evidence of drought in the western Mediterranean 1200-1100 yr BP. *Journal of Quaternary Science*, 20(5), 423-433.

Meyer, H., Schirrmeister, L., Yoshikawa, K., Opel, T., Wetterich, S., Hubberten, H.W. and Brown, J. (2010) Permafrost evidence for severe winter cooling during the Younger Dryas in northern Alaska. *Geophysical Research Letters*, 37, 5.

Mickler, P.J., Banner, J.L., Stern, L., Asmerom, Y., Edwards, R.L. and Ito, E. (2004) Stable isotope variations in modern tropical speleothems: Evaluating equilibrium vs. kinetic isotope effects. *Geochimica et Cosmochimica Acta*, 68, 4381-4393.

Mickler, P.J., Stern, L.A. and BANNER, J.L. (2006) Large kinetic isotope effects in modern speleothems. *Geological Society of America Bulletin*, 118, 65-81.

Miorandi, R., Borsato, A., Frisia, S., Fairchild, I.j. and Richter, D.K. (2010) Epikarst hydrology and implications for stalagmite capture of climate changes at Grotta di Ernesto (NE Italy): results from long-term monitoring. *Hydrological Processes*, 24, 3101-3114.

Moberg, A., Sonechkin, D.M., Hlomgren, K., Datsenko, N.M. and Karlen, W. (2005) Highly variable Northern Hemisphere temperatures reconstructed from low- and high-resolution proxy data. *Nature*, 433, 613-617.

Mojtahid, M., Jorissen, F.j., Schiebel, R., Michel, E., Eynaud, F., Gillet, H., Cremer, M., Ferreiro, P.D, Siccha, M. and Howa, H. (2013) High resolution Holocene record in the southeastern Bay of Biscay: Global versus regional climate signals. *Palaeogeography, Palaeoclimatology, Palaeoecology*, 377, 28-44.

Moreno, A., Stoll, H., Jiménez-Sánchez, M., Cacho, I., Valero-Garcés, B.L., Ito, E. and Edwards, R.L. (2010) A speleothem record of glacial (25-11.6 kry BP) rapid climatic changes from northern Iberian Peninsula. *Global and Planetary Change*, 71, 218-231.

Moreno, A., López-Merino, L., Leira, M., Marco-Barba, J., González-Sampériz, P., Valero-Garcés, B.L., López-Sáez, J.A., Santos, L., Mata, P. and Ito, E. (2011a) Revealing the last 13,500 years of environmental history from the multiproxy record of a mountain lake (Lago Enol, northern Iberian Peninsula). *Journal of Palaeolimnology*, 46, 327-349.

Moreno, A., Morellón, C., Martin-Puertas, C., Frigola, J., Canals, M., Cacho, I., Corella, J.P., Perez, A., Belmonte, A., Vegas-Vilarrŭbia, T., González-Sampériz, P. and Valero-Garcés, B.L. (2011b) Was there a common hydrological pattern in the Iberian Peninsula region during the Medieval Climate Anomaly? *PAGES News*, 19(1), 16-18.

Moreno, A., Pérez, A., Frigola, J., Nieto-Moreno, V., Rodrigo-Gámiz, m., Martrat, B., González-Sampériz, P., Morellón, M., Martin-Puertas, C., Corella, J.P., Belmonte, A., Sancho, C., Cacho, I., Herrera, G., Canals, M., Grinalt, J.O., Jiménez-Espejo, Martinez-Ruiz, F., Vegas-Vilarrŭbia, T. and Valero-Garcés, B.L. (2012) The medieval Cliamte Anomoly in the Iberian Peninsula reconstructed from marine and lake records. *Quaternary Science Reviews*, 43, 16-32.

Morellón, M., Valero-Garcés, B.L., Moreno, A., González-Sampériz, P., Mata, P., Romero, O., Maestro, M. and Navas, A. (2008) Holocene palaeohydrological and climate variability in northeastern Spain: The sedimentary record of Lake Estanya (Pre-Pyrenean range). *Quaternary International*, 181, 15-31.

Morellón, M., Valero-Garcés, B.L., Vegas-Vilarrŭbia, T., González-Sampériz, P., Romero, O., Delgado-Huertas, A., Mata, P., Moreno, A., Rico, M. and Corella, J.P. (2009) Lateglacial and Holocene palaeohydrology in the western Mediterranean region: the Lake Estanya record (NE Spain). *Quaternary Science Reviews*, 28, 2582-2599.

Morellón, M., Pérez-Sanz, A., Corella, J.P., Bűntgen, U., Catalán, J., González-Sampériz, P., González-Trueba, J.J., López-Sáez, J.A., Moreno, A., Pla-Rabes, S., Saz-Sánchez, M.A., Scussolini, P., Serrano, E., Steinhilber, F., Stefanova, V., Vegas-Vilarrŭbia, T. and Valero-Garcés, B.L. (2012) A multi-proxy perspective on millennium-long climate variability in the Southern Pyrenees. *Climate of the Past*, 8, 683-700.

Morley, M., Schulz, Y., Rosenthal, S., Mulitza, A.P. and Ruhlemann, C. (2011) Solar modulation of North Atlantic central water formation at multidecadal timescales during the late Holocene. *Earth and Planetary Science Letters,* 308, 161-171.

Moros, M., Emeis, K., Risebrobakken, B., Snowball, I., Kuilpers, A., McManus, J. and Jansen, E. (2004) Sea surface temperatures and ice rafting in the Holocene North Atlantic: climate influences on northern Europe and Greenland. *Quaternary Science Reviews*, 23, 2113-2126.

Műller, W., Shelley, M., Miller, p. and Broude, S. (2009) Initial performance metrics of a new custom-designed ArF excimer LA-ICPMS system coupled to a two-volume laser-ablation cell. *Journal of Analytical Spectrometry,* 24, 209-214.

O'Brien, S.R., Mayewski, P.A., Meeker, L.D., Meese, D.A., Twickler, M.S. and Whitlow, S.I. (1995) Complexity of Holocene climate reconstruction from a Greenland ice core. *Science*, 270 (5244), 1962-1964.

Olsen, J., Anderson, J.N. and Knudsen, M.F. (2012) Variability of the North Atlantic Oscillation over the past 5,200 years. *Nature Geoscience*, 5, 808-812.

O'Neill, J.R., Clayton, R.N. & Mayeda, T.K. (1969) Oxygen isotope fractionation in divalent metal carbonates. *Journal of Chemical Physics*, 51, 5547-5558.

Onac, B.P. (1997) Crystallography of Speleothems. In: Hill, C.A. and Forti, P. (eds.) *Cave Minerals of the World*. National Speleological Scociety, Inc, Huntsville.

Oster, J.L., Montañez, I.P., Guilderson, T.P., Sharp, W.D. and Banner, J.L. (2010) Modelling speleothem $\delta^{13}C$ variability in a central Sierra Nevada cave using ^{14}C and $^{87}Sr/^{86}Sr$. *Geochimica et Cosmochimica Acta*, 74, 5228-5242.

Palastanga, V., van der Schrier, G., Weber, S.L., Kleinen, T., Briffa, K.R. and Osborn, T.J. (2011) Atmosphere and ocean dynamics: contributors to the European Little Ice Age? *Climate Dynamics*, 36, 973-987.

Palmer, A.N. (2010) Understanding the hydrology of karst. *Geologia Croatica*, 63, 143-148.

Pape, J.R., Banner, J.L., Mack, L.E., Musgrove, M. and Guilfoyle, A. (2010) Controls on oxygen isotope variability in precipitation and cave drip waters, central Texas, USA. *Journal of Hydrology*, 385, 203-215.

Pauling, A., Luterbacher, J., Casty, C. and Wanner, H. (2006) Five hundred years of gridded high-resolution precipitation reconstructions over Europe and the connection to large-scale circulation. *Climate Dynamics*, 26, 387-405.

Pena, L.D., Francés, G., Diz, P., Esparza, M., Grimalt, J.O., Nombela, M.A. and Alejo, I. (2010) Climate fluctuations during the Holocene in NW Iberia: High and low latitude linkages. *Continental Shelf Research*, 30, 1487-1496.

Peña-Chocarro, L., Zapata, L., Iriarte, M.J., Morales, M.G. and Straus, L.G. (2005) The oldest agriculture in northern Atlantic Spain: new evidence from El Miron Cave (Ramales de la Victoria, Cantabria). *Journal of Archaeological Science*, 32, 579-587.

Peng, S., Robinson, W.A. and Li, S. (2003) Mechanisms for the NAO responses to the North Atlantic SST tripole. *American Meteorological Society*, 16, 1987-2004.

Pérez-Obiol, R. and Juliá, R. (1994) Claiatic change on the Iberian Peninsula recorded in a 30,000-yr pollen record from Lake Banyoles. *Quaternary Research*, 41, 91-98.

Pérez-Obiol,R., Jalut, G., Juliá, R., Pèlachs, A., Iriarte, M.J., Otto, T. and Hernández-Beloqui, B. (2010) Mid-Holocene vegetation and climatic history of the Iberian Peninsula. *The Holocene*, 21(1), 75-93.

Pérez-Sanz, A., González-Sampériz, P., Moreno, A., Valero-Garcés, B., Gil-Romera, G., Rieradevall, M., Tarrats, P., Lasheras-Alverez, I., Morellón, M., Belmonte, A., Sancho, C., Sevilla-Callejo, M. and Navas, A. (2013) Holocene climate variability, vegetation dynamics and fire regime in the central Pyrenees: the Basa de la Mora sequence (NE Spain). *Quaternary Science Reviews*, 73, 149-169.

Plummer, L.N., Parkhurst, D.L. and Kosiur, D.R. (1975) MIX2, a computer program for modelling chemical reactions in natural waters. *U.S. Geological Survey, Water Resources Investigations Report 61*.

Proctor, C.J., Baker, A., Barnes, W.L. and Gilmour, R.A. (2000) A thousand year speleothem proxy record of North Atlantic climate from Scotland. *Climate Dynamics*, 16, 815-820.

Proctor, C.J., Baker, A. and Barnes, W.L. (2002) A three thousand year record of North Atlantic climate. *Climate Dynamics*, 19, 449-454.

Pronk, M., Goldscheider, N., Zopfi, J. and Zwahlen, F. (2009) Percolation and particle transport in the unsaturated zone of a karst aquifer. *Ground Water*, 47(3), 361-369.

Riera, S., Wansard, G. and Juliá, R. (2004) 2000-year environmental history of a karstic lake in the Mediterranean Pre-Pyrenees: the Estanya lakes (Spain). *Catena*, 55, 293-324.

Roberts, M.S., Smart, P.L. and Baker, A. (1998) Annual trace element variations in a Holocene speleothem. *Earth and Planetary Science Letters*, 154, 237-246.

Roberts, M.S., Smart, P.L., Hawkesworth, C.J., Perkins, W.T. and Pearce, N.J.G. (1999) Trace element variations in coeval Holocene speleothems from GB cave, southwest England. *The Holocene*, 9, 707-713.

Rodríguez-Puebla C, García-Casado LA, Frías MD. (2001) Trend and interannual variations in air temperature over Iberian Peninsula. In 13th symposium on global change and climate variations, *13-17 January 2002, Orlando, Florida, American Meteorological Society*, Boston, USA, 106-108.

Rodwell, M.J., Rowell, D.P. and Folland, C.K. (1999) Oceanic forcing of the wintertime North Atlantic Oscillation and European climate. *Nature*, 398, 320-323.

Roig, F.A., Barriopedro, D., Herrera, R.G., Dominguez, D.P. and Monge, S. (2009) North Atlantic Oscillation signatures in western Iberian tree-rings. *Geografiska Annaler Series a-Physical Geography*, 91A, 141-157.

Rosenzweig, C., Karoly, D., Vicarelli, M., Neofotis, P., Wu, Q.G., Casassa, G., Menzel, A., Root, T.L., Estrella, N., Seguin, B., Tryjanowski, P., Liu, C.Z., Rawlins, S. and Imeson, A. (2008) Attributing physical and biological impacts to anthropogenic climate change. *Nature*, 453, 353-357.

Rosqvist, G.C., Leng, M.J. and Jonsson, C. (2007) North Atlantic region atmospheric circulation dynamics inferred from a late-Holocene lacustrine carbonate isotope record, northern Swedish Lapland. *The Holocene*, 17(7), 867-873.

Rossum, J.R. (1975) Checking the accuracy of water analysis through the use of conductivity. *Journal of the Water Works Association*, 67, 204-205.

Ruddiman, W.F. and McIntyre, A. (1981) The North Atlantic Ocean during the last deglaciation. *Palaeogeography, Palaeoclimatology, Palaeoecology*, 35, 145-214.

Rudzka, D., McDermott, F., Baldini, L.M., Fleitmann, D., Moreno, A. and Stoll, H. (2011) The coupled $\delta^{13}C$-radiocarbon systematics of three Late Glacial/early Holocene speleothems; insights into soil and cave processes at climatic transitions. *Geochimica et Cosmochimica Acta*, 75, 4321-4339.

Sarafanov, A., Mercier, H., Falina, A., Sokov, A. and Lherminier, P. (2010) Cessation and partial reversal of deep water freshening in the northern North Atlantic: observation-based estimates and attribution. *Tellus*, 62A, 80-90.

Scholz, D., Műhlinghaus, C. and Mangini, A. (2009) Modelling $\delta^{13}C$ and $\delta^{18}O$ in the solution layer on stalagmite surfaces. *Geochimica et Cosmochimica Acta*, 73, 2592-2602.

Scholz, D. and Hoffmann, D. L. 2011. StalAge - An algorithm designed for construction of speleothem age models. *Quaternary Geochronology*, 6, 369-382.

Schwarz, K., Barth, J.A.C., Postigo-Rebollo, C. and Grathwohl, P. (2009) Mixing and transport of water in a karst catchment: a case study from precipitation via seepage to the spring. *Hydrology and Earth System Sciences*, 13, 285-292.

Sejrup, H.P., Haflidason, H. and Andrews, J.T. (2011) A Holocene North Atlantic SST record and regional climate variability. *Quaternary Science Reviews*, 30, 3181-3195.

Semenov, V.A., Latif, M., Jungclaus, J.H. and Park, W. (2008) Is the observed NAO variability during the instrumental record unusual? *Geophysical Research Letters*, 35.

Shindell, D.T., Schmidt, D.A., Mann, M.E., Ring, D. and Waple, A. (2001) Solar forcing of regional climate change during the Maunder Minimum. *Science*, 294, 2149-2152.

Sinclair, D.J. (2011) Two mathematical models of Mg and Sr partitioning into solution during incongruent calcite dissolution. Implications for dripwater and speleothem studies. *Chemical Geology*, 283, 119-133.

Sinclair, D.J., Banner, J.L., Taylor, F.W., Partin, J., Jenson, J., Mylroie, J., Goddard, E., Quinn, T., Jocson, J. and Miklavič. (2012) Magnesium and strontium systematics in tropical speleothems from the Western Pacific. *Chemical Geology*, 2940295, 1-17.

Smart, P.L. and Friedrich, H. (1987) Water movement and storage in the unsaturated zone of a maturely karstified aquifer, Mendip Hills, England. Conference on Environmental Problems in Karst Terrains and their Solution, Bowling Green, Kentucky. National Water Well Association, 57-87.

Smith, A.C., Wynn, P.M. and Barker, P.A. (2013) Natural and anthropogenic factors which influence aerosol distribution in Ingleborough Show Cave, UK. *International Journal of Speleology*, 42(1), 49-56.

Sobrino, C.M., Ramil-Rego, P., Gomez-Orellana, L. and Varela, R.A.D. (2005) Palynological data on major Holocene climatic events in NW Iberia. *Boreas*, 34, 381-400.

Solignac, S., Giraudeau, J. and de Vernal, A. (2006) Holocene sea surface conditions in the western North Atlantic: Spatial and temporal heterogeneities. *Paleoceanography*, 21.

Sorrel, P., Debret, M., Billeaud, I., Jaccard, S.L., McManus, J.F. and Tessier, B. (2012) Persistant non-solar forcing of Holocene storm dynamics in costal sediment archives. *Nature Geoscience*, 5, 892-896.

Spötl, C., Fairchild, I.J. and Tooth, A.F. (2005) Cave air control on dripwater geochemistry, Obir Caves (Austria): Implications for speleothem deposition in dynamically ventilated caves. *Geochimica et Cosmochimica Acta*, 69(10), 2451-2468.

Spötl, C., Nicolussi, K., Patzelt, G., Boch, R. and Daphne team. (2010) Humid climate during deposition of sapropel 1 in the Mediterranean Sea: Assessing the influence of the Alps. *Global and Planetary Change*, 71, 242-248.

St Pierre, E., Zhao, J.X. and Reed, E. (2009) Expanding the utility of Uranium-series dating of speleothems for archaeological and palaeontological applications. *Journal of Archaeological Science*, 36, 1416-1423.

Staines-Urias, F., Kuijpers, A. and Korte, C. (2013) Evolution of subpolar North Atlantic surface circulation since the early Holocene inferred from planktic foraminifera faunal and stable isotope records. *Quaternary Science Reviews*, 76, 66-81.

Staubwasser, M., Sirocko, F., Grootes, P.M. and Segl, M. (2003) Climate change at the 4.2 ka BP termination of the Indus valley civilization and Holocene south Asian monsoon variability. *Geophysical Research Letters*, 30(8), 4.

Stoll, H.M., Muller, W., Prieto, M. (2012) I-STAL, a model for interpretation of Mg/Ca, Sr/Ca and Ba/Ca variations in speleothems and its forward and inverse application on seasonal to millennial scales. *Geochemistry Geophysics Geosystems*, 13 (1), 27.

Stoll, H.M., Moreno, A., Mendez-Vicente, A., Gonzalez-Lemon, S., Jimenez-Sanchez, M., Dominguez-Cuesta, M.J., Edwards, R.L., Cheng, H. and Wand, X. (2013) Palaeoclimate and growth rates of speleothems in the northwestern Iberian Peninsula over the last two glacial cycles. *Quaternary Research*, 80, 284-290.

Straus, L.G. (2011) Were there human responses to Younger Dryas in Cantabrian Spain? *Quaternary International*, 242, 328-335.

Straus, L.G. and Morales, M.R.G. (2012) The Magdalenian settlement of the Cantabrian region (Northern Spain): The view from El Miron Cave. *Quaternary International*, 272-273, 111-124.

Sundqvist, H.S., Holmgren, K. and Lauritzen, S.E. (2007) Stable isotope variations in stalagmites from northwestern Sweden document climate and environmental changes during the early Holocene. *The Holocene*, 17, 259-267.

Sundqvist, H.S., Holmgren, K. and Lauritzen, S.E. (2008) Stable isotope variations in stalagmites from northwestern Sweden document changes in temperature and vegetation during the early Holocene: a reply to Hammarlund and Edwards. *The Holocene*, 18, 1009-1010.

Taylor, K.C., Mayewski, P.A., Alley, R.B., Brook, E.J., Gow, A.J., Grootes, P.M., Meese, D.A., Saltzman, E.S., Severinghaus, J.P., Twickler, M.S., White, J.W.C., Whitlow, S. and Zielinski, G.A. (1997). The Holocene Younger Dryas transition recorded at Summit, Greenland. *Science*, 278, 825-827.

Taylor, C. J., Pedregal, D. J., Young, P. C., & Tych, W. (2007). Environmental time series analysis and forecasting with the Captain toolbox. *Environmental Modelling & Software*, 22(6), 797-814.

Teller, J.T., Leverington, D.W. and Mann, J.D. (2002) Freshwater outbursts to the oceans from glacial Lake Agassiz and their role in climate change during the last deglaciation. *Quaternary Science Reviews*, 21, 879-887.

Thornalley, D.J.R., Elderfield, H. and McCave, N.I. (2009) Holocene oscillations in temperature and salinity of the surface subpolar North Atlantic. *Nature*, 457, 711-714.

Thornthwaite, C.W. (1948) An approach toward a rational classification of climate. *Geophysical Review*, 38, 55-94.

Tooth, A.F. and Fairchild, I.J. (2003) Soil and karst aquifer hydrological controls on the geochemical evolution of speleothem-forming drip waters, Crag Cave, southwest Ireland. *Journal of Hydrology*, 273, 51-68.

Treble, P., Shelley, J.M.G. and Chappell, J. (2003) Comparison of high resolution sub-annual records of trace elements in a modern (1911-1992) speleothem with instrumental climate data from southwest Australia. *Earth and Planetary Science Letters*, 216, 141-153.

Treble, P.C., Budd, W.F., Hope, P.K. and Rustomji, P.K. (2005) Synoptic-scale climate patterns associated with rainfall $\delta^{18}O$ in southern Australia. *Journal of Hydrology*, 302, 270-282.

Tremaine, D.M., Froelich, P.N and Wang, Y. (2011) Speleothem calcite farmed *in situ*: Modern calibration of $\delta^{18}O$ and $\delta^{13}C$ palaeoclimate proxies in a continuously-monitored natural cave system. *Geochimica et Cosmochimica Acta*, 75, 4929-4950.

Trouet, V., Esper, J., Graham, N.E., Baker, A., Scourse, J.D. and Frank, D.C. (2009) Persistent Positive North Atlantic Oscillation Mode Dominated the Medieval Climate Anomaly. *Science*, 324, 78-80.

Turgeon, S. and Lundberg, J. (2001) Chronology of discontinuities and petrology of speleothems as paleoclimatic indicators of the Klamath Mountains, Southwest Oregon, USA. *Carbonates and Evaporites*, 16, 153-167.

Turney, C., Baillie, M., Clemens, S., Brown, D., Palmer, J., Pilcher, J., Rimer, P. and Leuschner, H.H. (2005) *Journal of Quaternary Science*, 20(6), 511-518.

Tych, W., Pedregal, D. J., Young, P. C., & Davies, J. (2002). An unobserved component model for multi-rate forecasting of telephone call demand: the design of a forecasting support system. *International Journal of forecasting*, 18(4), 673-69.

Valero-Garcés, B.L., González-Sampériz, P., Delgardo-Huertas, A., Navas, A., Machin, J. and Kelts, K. (2000) Lateglacial and Late Holocene environmental and vegetational change in Salada Mediani, central Ebro Basin, Spain. *Quaternary International*, 73-74, 29-46.

van Beynen, P.E., Soto, L. and Pace-Graczyk. (2008) Paleoclimate reconstruction derived from speleothem strontium and $\delta^{13}C$ in Central Florida. *Quaternary International*, 187, 76-83.

van Calsteren, P. and Thomas, L. (2006) Uranium-series dating applications in natural environmental science. *Earth-Science Reviews*, 75, 155-175.

Vicente-Serrano, S.M. and Cuadrat, J.M. (2007) North Atlantic oscillation control of droughts in north-east Spain: evaluation since 1600 A. D. *Climatic Change*, 85, 357-379.

Vogel, J.C., Lerman, J.C. and Mook, W.G. (1975) Natural isotopes in surface and groundwater from Argentina. *Hydrological Sciences Bulletin*, 20, 203-221.

Wanner, H., Brönnimann, S., Casty, C., Gyalistras, D., Luterbacher, J., Schmutz, C., Stepenson, D.B. and Xoplaki, E. (2001) North Atlantic Oscillation - Concepts and studies. *Surveys in Geophysics*, 22, 321-382.

Wanner, H., Beer, J., Bűtikofer, J., Crowley,T.J., Cubasch, U., Flűckiger, J., Goose, H., Grosjean, M., Joos, F., Kaplan, J.O., Kűttel, M., Műller, S.A., Prentice, C.I., Solomina, O., Stocker, T.F., Tarasov, P., Wagner, M. and Widmann, M. (2008) Mid-to late Holocene climate change: and overview. *Quaternary Science Reviews*, 27, 1791-1828.

Wanner, H. and Bűtikofer, J. (2008) Holocene Bond cycles: Real or imaginary? *Geografie*, 4, 338-350.

Watanabe, Y., Matsuoka, H., Sakai, S., Uedu, J., Yamada, M., Ohsawa, S., Kiguchi, M., Satomura, T., Nakai, S., Brahmantyo, B., Maryunanil, K.A., Tagami, T., Takemura, K. and Yoden, S. (2010) Comparison of stable isotope time series of stalagmite and meteorological data from West Java, Indonesia. *Palaeogeography Palaeoclimatology Palaeoecology*, 293, 90-97.

White, W.B. (1988) *Geomorphology and Hydrology of Karst Terrains*. Oxford University Press, New York.

White, W.B. (2002) Karst hydrology: recent developments and open questions. *Engineering Geology*, 65, 85-105.

Whiticar, M.J. (1999) Carbon and hydrogen isotope systematics of bacterial formation and oxidation of methane. *Chemical Geology*, 161, 291-314.

Wigley, T.M.L. (1967) Non-steady flow through a porous medium and cave breathing. *Journal of Geophysical Research*, 72, 3199-3205.

Williams, P.W. (2008) The role of the epikarst in karst and cave hydrogeology: a review. *International Journal of Speleology*, 37(1), 1-10.

Wynn, P.M., Fairchild, I.J., Baker, A., Baldini, J.U.L. and McDermott, F. (2008) Isotopic archives of sulphate in speleothems. *Geochimica et Cosmochimica Acta*, 72, 2465-2477.

Wynn, P.M., Fairchild, I.J., Frisia, S., Spötl, C., Baker, A., Borsato, A. and EIMF (2010) High-resolution sulphur isotope analysis of speleothem carbonate by secondary ionisation mass spectrometry. *Chemical Geology*, 271, 101-107.

Wynn P.M., Fairchild I.J., Spötl C., Hartland A., Mattey D., Fayard B., and Cotte M. 2014 Synchrotron X-ray distinction of seasonal hydrological and temperature patterns in speleothem carbonate. *Environmental Chemistry*, 11, 28-36.

Yanes, Y., Gutiérrez-Zugasti, I. and Delgado, A. (2012) Late-glacial to Holocene transition in northern Spain deduced from land-snail shelly accumulations. *Quaternary Research*, 78, 373-385.

Young, P. C., Pedregal, D. J. and Tych, W. (1999). Dynamic harmonic regression. *Journal of Forecasting*, 18: 369–394.

Zhao, J.X., Yu, K.F. and Feng, Y.X. (2009) High-precision ^{238}U-^{234}U-^{230}Th disequilibrium dating of the recent past: a review. *Quaternary Geochronology*, 4, 423-433.